

---

Electronic Theses and Dissertations, 2004-2019

---

2005

## Structural Condition Assessment Of Prestressed Concrete Transit Guideways

Robert Zachary Shmerling  
*University of Central Florida*



Part of the [Civil Engineering Commons](#)

Find similar works at: <https://stars.library.ucf.edu/etd>

University of Central Florida Libraries <http://library.ucf.edu>

This Masters Thesis (Open Access) is brought to you for free and open access by STARS. It has been accepted for inclusion in Electronic Theses and Dissertations, 2004-2019 by an authorized administrator of STARS. For more information, please contact [STARS@ucf.edu](mailto:STARS@ucf.edu).

---

### STARS Citation

Shmerling, Robert Zachary, "Structural Condition Assessment Of Prestressed Concrete Transit  
Guideways" (2005). *Electronic Theses and Dissertations, 2004-2019*. 503.

<https://stars.library.ucf.edu/etd/503>

STRUCTURAL CONDITION ASSESSMENT OF  
PRESTRESSED CONCRETE TRANSIT GUIDEWAYS

by

ROBERT Z. SHMERLING  
B.S. University of California, Berkeley, 2001

A thesis submitted in partial fulfillment of the requirements  
for the degree of Master of Science  
in the Department of Civil and Environmental Engineering  
in the College of Engineering and Computer Science  
at the University of Central Florida  
Orlando, Florida

Summer Term  
2005

© 2005 Robert Z. Shmerling

## **ABSTRACT**

Objective condition assessment is essential to make better decisions for safety and serviceability of existing civil infrastructure systems. This study explores the condition of an existing transit guideway system that has been in service for thirty-five years. The structural system is composed of six-span continuous prestressed concrete bridge segments. The overall transit system incorporates a number of continuous bridges which share common design details, geometries, and loading conditions. The original analysis is based on certain simplifying assumptions such as rigid behavior over supports and simplified tendon/concrete/steel plate interaction. The current objective is to conduct a representative study for a more accurate understanding of the structural system and its behavior. The scope of the study is to generate finite element models (FEMs) to be used in static and dynamic parameter sensitivity studies, as well load rating and reliability analysis of the structure. The FEMs are used for eigenvalue analysis and simulations. Parameter sensitivity studies consider the effect of changing critical parameters, including material properties, prestress loss, and boundary and continuity conditions, on the static and dynamic structural response. Load ratings are developed using an American Association for State Highway Transportation Officials Load and Resistance Factor Rating (AASHTO LRFR) approach. The reliability of the structural system is evaluated based on the data obtained from various finite element models. Recommendations for experimental validation of the FEM are presented. This study is expected to provide information to make better decisions for operations, maintenance and safety requirements; to be a benchmark for future studies, to establish a procedure and methodology for structural condition assessment, and to contribute to the general research body of knowledge in condition assessment and structural health monitoring.

## ACKNOWLEDGMENTS

I wish to acknowledge and thank Dr. F. Necati Catbas for the research opportunity under his direction and vision, for exposure and involvement in the important fields of structural condition assessment and structural health monitoring, and for his interest in the quality of my graduate experience; my committee members, Dr. Lei Zhao and Dr. Manoj Chopra, for their time and valuable feedback; our student research team, especially Jason Burkett, Mustafa Gul, and Tom Braswell, who contributed important engineering advice and perspective to this study; and Mr. J. Douglas Smith for support of this project and my education, for exceptional mentoring, and for teaching me invaluable lessons about engineering and business.

I want to thank Linden Parchment for mentoring and development as a structural engineer and for advice, feedback, and resources in the present study; Dr. Bruce Butler for sharing engineering principles of the beamway; John Anderson for inspection and maintenance history; Ken Young and Robin Schinina for mentoring and guidance; Kevin Niles for graphic production; and the myriad professionals at Architectural and Facilities Engineering and Ride and Show Engineering who gave time and support to this study.

I want to thank my family for support and encouragement through many months of personal, professional, and academic challenges; my mother, Barbara Halpern, for her constant love, support, and endless stream of cards and letters; my father, Ronald Shmerling, who is always there when I need advice and encouragement on tough issues; my stepfather, Jeff Halpern, who reminded me of the importance of finishing; and my grandparents Vi and Jack Dorfman, who always encourage and believe in my success. I want to thank my friends, especially Dara Glass, Rachel Zaiden, Amy Melin, Pete Mangos, and Shelley Bowles, who helped me survive and succeed in graduate school.

# TABLE OF CONTENTS

LIST OF FIGURES .....	ix
LIST OF TABLES .....	xi
LIST OF ACRONYMS .....	xii
LIST OF VARIABLES.....	xiii
CHAPTER ONE: INTRODUCTION.....	1
Structural Concept .....	2
Post-tensioning.....	3
Continuity .....	4
Design Specifications.....	5
Inspection and Maintenance Practice .....	6
Study Purpose .....	9
Increased Loads and Load Effects .....	9
Service Life and Life-Cycle Cost .....	11
Research Interest.....	14
Methodology, Scope, and Tasks.....	14
Expected Outcomes and Findings.....	16
CHAPTER TWO: LITERATURE REVIEW AND FUNDAMENTAL CONCEPTS .....	18
Condition Assessment.....	18
Structural Identification .....	19
Structural Health Monitoring.....	20
Simulations and Load Rating.....	21
Experimental Verification and Model Updating .....	22

Experimental Data Processing .....	25
Damage Detection from Modal Response .....	26
Finite Element Analysis .....	28
Finite Element Methods for Concrete Structures .....	29
Transit Guideways .....	33
CHAPTER THREE: PRELIMINARY MODEL DEVELOPMENT .....	37
Bridge Segment Selection.....	37
Primary Selection Criteria.....	37
Secondary Criteria .....	39
Software Considerations .....	41
Model Visualization.....	43
Information Sources.....	43
Visualization Tools .....	43
Connection Visualization and Analytical Model.....	45
Preliminary Models and Benchmark Studies.....	49
Benchmark Study: Simple Reinforced Concrete Beam.....	49
Benchmark Study: Concrete Box Girder Bridge .....	51
Steel Crossheads and Concrete Columns.....	54
Post-Tensioning Tendons.....	56
CHAPTER FOUR: SIX-SPAN FINITE ELEMENT MODEL .....	58
Superstructure .....	59
Beams.....	59
Prestressing .....	61

CIP Connections .....	62
Steel Crossheads .....	63
Beam Hanger Plates .....	63
Shear Studs on Crossheads .....	64
Precast Columns .....	65
Model Parameters .....	66
Bounding Parameters for Sensitivity Studies .....	67
Concrete Modulus of Elasticity .....	68
Prestress Loss .....	69
Time-Dependent Behavior of Concrete .....	70
Boundary Conditions .....	71
Continuity Condition .....	74
CHAPTER FIVE: MODAL ANALYSIS AND PARAMETER SENSITIVITY .....	76
Modal Analysis .....	76
Selection of Modes .....	77
Preliminary Moving Load Analysis .....	77
Parameter Sensitivity Studies .....	78
Results .....	78
Discussion .....	81
CHAPTER SIX: SIMULATIONS, LOAD RATING AND RELIABILITY .....	84
Reliability Index and Probability of Failure .....	84
Load Rating .....	86
Live Load Factor .....	87

Design vs. Load Rating.....	89
Relationship between Load Rating and Reliability .....	90
Simulations, Load Rating and Reliability.....	90
Load Distribution.....	92
Verification.....	93
Results.....	95
Discussion.....	96
CONCLUSIONS AND RECOMMENDATIONS .....	106
APPENDIX A: BOUNDING CONCRETE STIFFNESS .....	110
APPENDIX B: BOUNDING PRESTRESS LOSS .....	115
APPENDIX C: FREQUENCIES AND MODE SHAPES .....	122
APPENDIX D: STATIC DEFLECTION RESULTS.....	147
APPENDIX E: TRAIN LOAD ASSUMPTIONS .....	151
APPENDIX F: LOAD RATING AND RELIABILITY ANALYSES.....	154
APPENDIX G: BOX GIRDER BENCHMARK STUDY.....	197
LIST OF REFERENCES.....	216

## LIST OF FIGURES

Figure 1: Prestressed Guideway Structural Concept .....	3
Figure 2: Crosshead Designed to Uncouple Beam End Rotations .....	5
Figure 3: Mark IV Train Axle Loads (1971) .....	10
Figure 4: Mark VI Train Axle Loads (2000) .....	10
Figure 5: Condition Assessment and Life-Cycle Cost Analysis.....	13
Figure 6: High-Visibility Bridge Segment.....	39
Figure 7: Low-Visibility Bridge Segment .....	39
Figure 8: 3D CAD Model of Columns, Crossheads, and Post-tensioning.....	44
Figure 9: 3D CAD Model of CIP Connection (Perspective View) .....	46
Figure 10: Free-Body Diagram (Precast Beam End).....	47
Figure 11: CIP Connection Analytical Model .....	48
Figure 12: Extruded FEM Perspective.....	48
Figure 13: Simple Concrete Beam with Solid Elements .....	50
Figure 14: Solid Element Longitudinal Stress Contours in Bending.....	50
Figure 15: Benchmark Model - Box Girder Bridge.....	52
Figure 16: Benchmark Study Moment Envelope.....	53
Figure 17: Benchmark Study Shear Envelope .....	53
Figure 18: Single-Span Preliminary Model .....	54
Figure 19: Connection and Adjacent Spans.....	55
Figure 20: Early Steel Crosshead Mesh with Maximum Tensile Stress Contours.....	56
Figure 21: Refined Crosshead Mesh with Horizontal Stress Contours .....	56
Figure 22: Bridge Frame Bending Moment under Post-Tension Load .....	57

Figure 23: Six-Span Continuous Bridge FEM (Extruded View).....	58
Figure 24: Beam Cross-Section Definition in SAP2000 .....	60
Figure 25: Parametric Variation of Section Depth .....	60
Figure 26: Shear Studs at CIP Connection .....	64
Figure 27: Tendon Assignments Including Prestress Loss .....	70
Figure 28: U1 Displacement Loading to Generate Stiffness Matrix .....	72
Figure 29: Boundary Condition Definition in SAP2000 .....	74
Figure 30: Free-Body Diagram (Precast Beam End).....	75
Figure 31: Distinct Modal Behaviors.....	79
Figure 32: Modal Analysis Sensitivity Study .....	81
Figure 33: Moving Load Sensitivity Study Results.....	82
Figure 34: Critical Locations for Moment and Shear .....	91
Figure 35: Rating Factor, Negative Bending at First Interior Support .....	99
Figure 36: Reliability Index, Negative Bending at First Interior Support .....	101
Figure 37: Reliability Index, Positive Bending at 0.4L, Span 1 .....	103
Figure 38: Reliability Index, Positive Bending at 0.5L, Span 2 .....	104
Figure 39: Reliability Index, Shear at Critical Section, First Interior Support.....	105
Figure 40: Run #1 Static Deflection Results.....	148
Figure 41: Run #2 Static Deflection Results.....	149
Figure 42: Run #3 Static Deflection Results.....	150

## LIST OF TABLES

Table 1: Gross Vehicle Load Comparison.....	9
Table 2: Objective Rating of Bridge Segment Candidates .....	40
Table 3: Parameter Bounds.....	67
Table 4: Boundary Condition Stiffness Matrix (Opposite End Unrestrained) .....	72
Table 5: Boundary Condition Stiffness Matrix (Opposite End Restrained).....	73
Table 6: Modal and Static Analysis Results .....	80
Table 7: Capacities and Load Effect Comparison .....	94
Table 8: Load Rating and Reliability Analysis Results .....	97
Table 9: Nominal Model Frequencies and Mode Shapes .....	123
Table 10: Lower-Bound Stiffness Model Frequencies and Mode Shapes.....	126
Table 11: Upper-Bound Stiffness Model Frequencies and Mode Shapes .....	129
Table 12: Lower-Bound Prestress Loss Model Frequencies and Mode Shapes.....	132
Table 13: Upper-Bound Prestress Loss Model Frequencies and Mode Shapes .....	135
Table 14: Upper-Bound Boundary Condition Model Frequencies and Mode Shapes .....	138
Table 15: Lower-Bound Continuity Condition Model Frequencies and Mode Shapes.....	141
Table 16: Upper-Bound Continuity Condition Model Frequencies and Mode Shapes .....	144
Table 17: Mark IV Train Loads .....	152
Table 18: Mark VI Train Loads and Loading Assumptions .....	153

## LIST OF ACRONYMS

AASHTO	American Association of State Highway and Transportation Officials
AASHO	American Association of State Highway Officials (predates AASHTO)
ACI	American Concrete Institute
BPR	Bureau of Public Roads
CIP	Cast-In-Place (Concrete)
DOF	Degree of Freedom
FEM	Finite Element Model
FHWA	Federal Highway Administration
FRF	Frequency Response Function
LRFD	Load and Resistance Factor Design (of Highway Bridges)
LRFR	Load and Resistance Factor Rating (of Highway Bridges)
MAC	Modal Assurance Criterion
PC	Personal Computer
PTI	Post-tensioning Institute
RF	Rating Factor

## LIST OF VARIABLES

$A_c$	gross area of concrete member cross-section, in <sup>2</sup> .
$A_{ps}$	area of prestressed reinforcement in tension zone, in <sup>2</sup> .
$A_v$	area of shear reinforcement within a distance, s, in <sup>2</sup> .
a	depth of equivalent uniformly stressed compression zone assumed for concrete in the strength limit state, in.
b	width of compressive face of member, in.
$b_w$	web width, in.
COV	coefficient of variation
c	distance from extreme compression fiber to neutral axis, in.
DC	subscript referring to dead load from structural components and attachments
DW	subscript referring to superimposed dead load (wearing surfaces, utilities)
d	distance from compression face to centroid of tension reinforcement, in.
$d_v$	effective shear depth, in.
$E_c$	modulus of elasticity of concrete (general), ksi; modulus for precast beams, ksi.
$E_{CIP}$	modulus of elasticity of concrete, cast-in-place connection, ksi.
$E_{cLT}$	long-term modulus of elasticity of concrete, ksi.
$E_{cn}$	ultimate effective modulus of elasticity of concrete, ksi.
$E_{COL}$	modulus of elasticity of concrete, precast columns, ksi.

$E_s$	modulus of elasticity of reinforcing bars, ksi.
$E_p$	modulus of elasticity of prestressing reinforcement
$e$	eccentricity of load parallel to axis of member measured from centroid of cross-section, in.
$f'_c$	specified 28-day compressive strength of concrete, psi.
$f_{ps}$	stress in prestressed reinforcement at nominal strength, psi.
$f_{pu}$	specified tensile strength of prestressing tendons, psi.
$f_{py}$	specified yield strength of prestressing tendons, psi.
$f_y$	specified yield strength of nonprestressed reinforcement, ksi.
$h$	overall beam thickness of member, in.
$I_c$	moment of inertia of concrete section, in <sup>4</sup> .
IM	dynamic load allowance (impact factor)
K	prestress loss (wobble) coefficient, 1/ft.
LL	subscript referring to live load
$M_n$	nominal flexural resistance, kip-ft.
$M_u$	factored moment at the section, kip-ft.
$n$	modular ratio of elasticity, $E_{ps}/E_c$ .
$P_f$	probability of failure
RF	load rating factor
S	section modulus of concrete section, in <sup>4</sup> .
s	spacing of shear reinforcement in the direction parallel to longitudinal reinforcement, in.
t	time, days.

$V_c$	nominal shear resistance provided by tensile stresses in the concrete, kip.
$V_n$	nominal shear resistance, kip.
$V_s$	shear resistance provided by shear reinforcement, kip.
$V_u$	factored shear force at section, kip.
$w_c$	unit weight of concrete, pcf.
$\beta$	reliability index
$\beta_1$	ratio of depth of the equivalent uniformly stressed compression zone assumed for concrete in the strength limit state to the depth of the actual compression zone.
$\gamma$	load factor
$\Delta f_{CR}$	prestress loss due to creep, psi.
$\Delta f_{ES}$	prestress loss due to elastic shortening, psi.
$\Delta f_R$	prestress loss due to relaxation of steel, psi.
$\Delta f_{SH}$	prestress loss due to shrinkage, psi.
$\Delta f_T$	total prestress loss, psi.
$\mu$	prestress loss (curvature) coefficient; also mean value.
$\sigma$	standard deviation
$\phi$	resistance factor

## CHAPTER ONE: INTRODUCTION

An existing transit system began service in 1971 and was expanded in 1982. It provides up to 200,000 daily passenger trips with a fleet of monorail trains that travel along 14.7 miles of elevated guideway. The system includes three distinct service lines, six passenger stations, twelve trains, track switches, spur lines, and an indoor maintenance and storage facility. The aerial guideway, or *beamway*, consists of continuous, prestressed concrete beam spans, precast concrete columns, and steel beam-column connections. The beamway system has exhibited excellent strength behavior during its 35 years of service. It is expected to last without major repair or replacement for a long but unspecified period of time.

The primary objective of this research work is to develop a better understanding of the structural behavior and capacity used up in the beamway structural system. The author hopes to provide additional insight into the structural behavior that compliments existing inspection and maintenance programs, which are comprehensive by state-of-practice standards. This study will provide finite element models which may be validated experimentally, with the long-term goal of developing objective information to make better decisions for operations, maintenance, and safety requirements. Additional objectives include establishing a procedure and methodology for structural condition assessment that may be applied in similar studies, and contributing a practical implementation of structural condition assessment methodology to the general practice and academic body of knowledge. The study scope includes modeling and analyzing a significant and representative guideway section with finite element models that incorporate lower-bound and upper-bound structural parameters.

This introductory chapter presents historical background of the existing system, emphasizing structural configuration, as well as the purpose, methodology, scope, and expected

outcomes for this study. A literature review follows, which focuses on state-of-practice approaches to bridge assessment and the related fields. Essential analytical concepts and methods are introduced. The structural modeling process is described, including model visualization and preliminary development of the finite element models. The FEMs are used in eigenvalue analysis, load rating, reliability analysis, and parameter sensitivity studies. Results and discussion are included for the various analyses. The final chapter includes conclusions and recommendations for future research.

### **Structural Concept**

The transit system is composed of aerial guideways which are commonly referred to as the *beamway* or *beamways*. A typical structural section consists of two parallel beamways connected to precast columns with steel hanger plates. Each beamway segment (Figure 1) is composed of six simply-supported precast, prestressed concrete box girders that were post-tensioned together to form a continuous structure. Typical interior straight spans are 110 ft long with end spans of 100 ft. Curved sections have 100-ft interior spans and 90-ft end spans. The beams are hollow to reduce the dead weight and to ease handling during construction (Mast and Dolan 1972).

Individual beams were pre-tensioned for dead load moment and then post-tensioned together in the field, creating a continuous beamway to carry the live load moments. Advantages of beam continuity include increased span length, reduction in the number of expansion joints, and the elimination of bearings. Increasing the span length allows for fewer beams, fewer columns, and less substructure construction. The reduction in the number of expansion joints reduces the number of abrupt angle changes at beam ends. This provides a smoother vehicle ride

for passengers. The hardware required at typical simple-span ends was eliminated. This was intended to reduce maintenance during the system's life cycle (Mast and Dolan 1972).

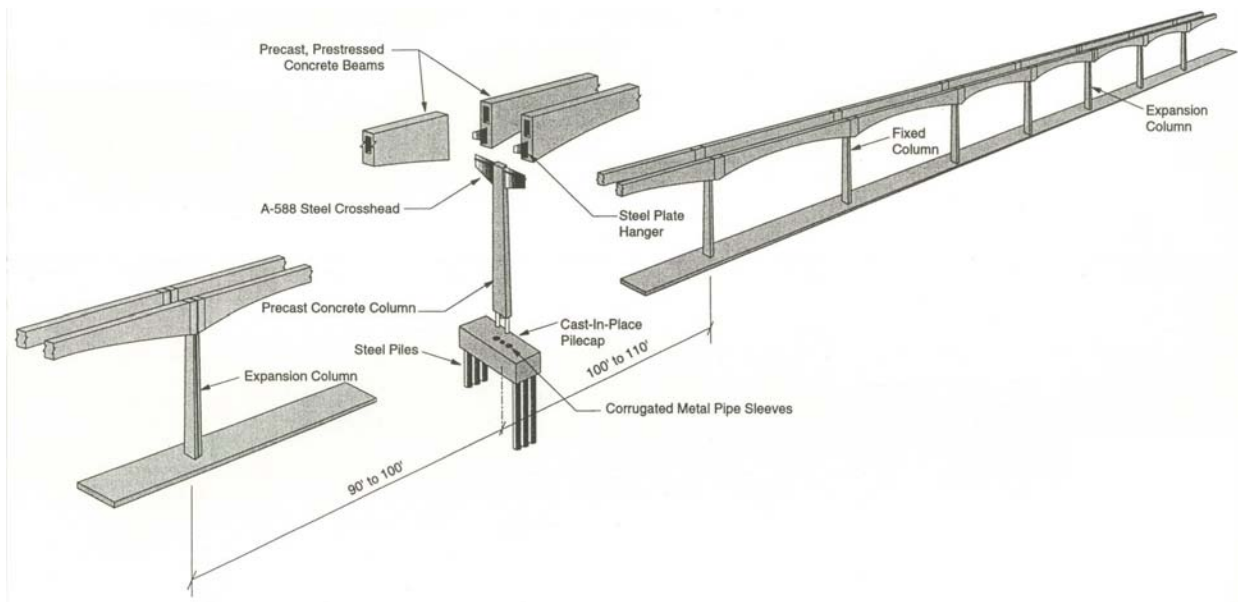


Figure 1: Prestressed Guideway Structural Concept

### Post-tensioning

The post-tensioned beams have a parabolic soffit, or *haunched beam profile*. The haunched beam profile was developed for camber control and to make the field post-tensioning feasible. In typical post-tensioned beams, the tendons are harped or draped to match the dead load moment. Typical post-tensioning strands fluctuate to accommodate positive moment at midspan and negative moment at the supports. Because the continuous spans in this system are so long (up to 640 ft over six supports), the typical undulations in strand profile associated with a prismatic section would result in prohibitive friction losses of the prestress force. Designing the

haunched beam profile allowed pre-tensioning and post-tensioning strands to run straight, with the concrete center of gravity fluctuating to obtain the required eccentricities.

The exact dimensions of the haunched profile were chosen so dead-load moments could be accurately balanced, to provide a zero camber condition with dead load, and so that the resultant beam stress is axial  $P/A$  stress only. Concrete creep would result in axial shortening of the beam with no effect on camber. Post-tensioning in straight sections was accomplished by jacking, from one end, the eight-strand tendons through the 640-ft long duct. A compact rack was designed for use in the six-foot gap between adjacent beam ends. Several pulls were required to obtain 54 in of strand elongation. After the post-tensioning operation was completed, the ducts were grouted and the expansion joints were cast in-place.

### **Continuity**

Continuity on the dual beamway created two major design concerns. These were the accommodation of thermal strain and the release of beam end rotations due to live load. Longitudinal thermal strains in the beams were accommodated by designing slender columns to deflect with longitudinal beam movements. Slender columns, designed in accordance with the proposed 1971 ACI Code, were designed to deflect without significant secondary stresses. One center column in each six-span continuous section was designed to restrain the longitudinal forces resulting from train deceleration or wind forces. Typical columns provide resistance to transverse forces, but do not offer significant longitudinal restraint(Mast and Dolan 1972).

The engineers intended to uncouple live load rotations of parallel beamways by means of the steel plate beam/column connection (Figure 2). The steel plate resists vertical loads and is stiffened for longitudinal forces, while also providing torsional flexibility to uncouple the

parallel beam motions. The plate material is A-588 steel, chosen for high strength and excellent fatigue properties. The 1 3/4-in. plate thickness was optimized to provide adequate resistance to vertical bending (thick plate preferred) while minimizing torsional resistance (thin plate preferred).

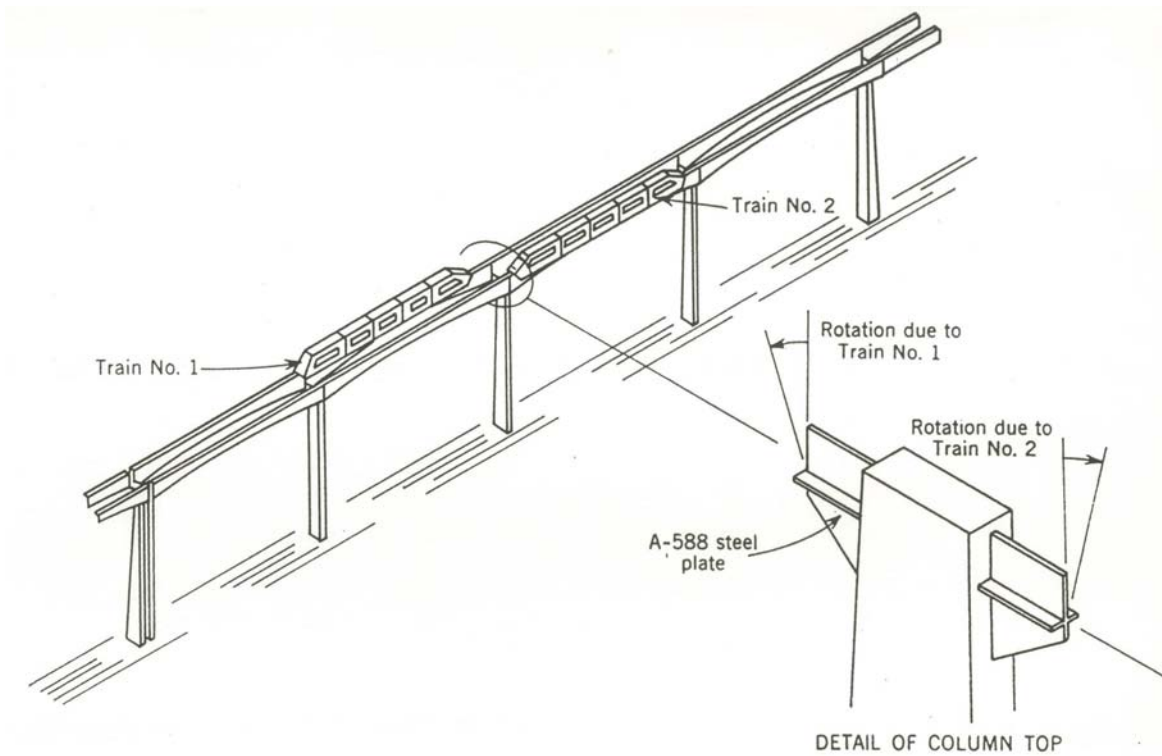


Figure 2: Crosshead Designed to Uncouple Beam End Rotations

### Design Specifications

For determination of loads and load factors, the *AASHTO Standard Specifications for Highway Bridges* (1965) and the *BPR Strength and Serviceability Criteria* (1966) were used as guides. Strength of reinforced concrete members was determined by ultimate strength design, using the 1966 BPR criteria as well as the *ACI 318-63, Building Code Requirements for Reinforced Concrete*. In the original structural calculations, it is noted that these two design

specifications "...are substantially the same." Prestressed members are examined for flexure at service loads and at ultimate loads. Service load analysis follows the AASHTO criteria. Ultimate load analysis follows *ACI 318-63*.

For shear and torsion design, as well as column buckling analysis, principles outlined in the proposed 1971 ACI criteria were used. The specifications at that time presented analysis equations that considered shear and torsion load effects individually, but gave no explicit formulation for combined effects of shear and torsion. The engineers studied shear and torsion interaction, and concluded that a conservative and adequate design assumption would be a linear interaction envelope defined between maximum shear and maximum torsion capacities of a given section (Mast and Dolan 1972).

### **Inspection and Maintenance Practice**

Regular maintenance and inspection is performed on the guideway system. Engineering technicians perform visual inspections on a biennial basis. The beamway bridge fleet is private and, as such, is not required to meet the Federal Highway Administration (FHWA) biennial bridge inspection and rating requirements. However, the rigorous visual inspection program by the owner is modeled after the FHWA standards and exceeds these standards in some respects. Additionally, because of the beamway structure's visibility, ongoing observations are made by system operators, maintenance personnel, and other representatives and employees of the owner. One might consider the high visibility of the structure as a secondary means of inspection and monitoring.

Repairs are made using current state-of-practice techniques. The strength behavior of the beamway has been exceptional over its service life. No flexural or shear cracking has been

observed and no girder has been repaired or replaced because of strength deficiencies. The inspection and maintenance program focuses on identifying and correcting visual indications of serviceability deficiencies. These indications generally appear in predictable locations and fall into one of a few predictable categories. The author hopes to contribute additional knowledge about the structural behavior that may not be readily observed by visual inspection. This includes the development of finite element models that may be validated by experimental studies.

The inspection and maintenance program focuses on identifying and correcting serviceability indications. Many indications appear on a regular basis and fall into one of a few distinct categories. These predictable types of indications are described in subsequent paragraphs.

***Snap Tie/Lift Points:*** Each precast beam was cast with steel snap ties extending out of the beam, providing lift points for a crane to lift and place the beams on the steel crossheads. These ties were cut back below the plane of the beam. Adjacent concrete was chipped away and filled with an epoxy mortar.

One of two situations tends to develop at these lift points; the epoxy delaminates from the surrounding concrete and spalls off the beam or the epoxy patch is ground down by train tire action. The repair procedure is to chip away the epoxy, clean and prepare the concrete surface, and refill the void with high-strength cementitious repair material. Many hundreds of these repairs have been performed.

***Grout Cubes:*** When casting the beams in formwork, grout cubes served as chairs to support the steel stirrups and provide the required cover in the finished beam. These grout cubes, having different stiffness properties than the surrounding concrete, and being located on the

underside of the beams, tend to spall and eventually fall away. The repair involves surface preparation and placement of high-strength cementitious repair material.

***Riding Surface Erosion:*** The load tires have eroded the surface matrix and fine aggregate at certain locations along the beamway. Some locations become rough and deeply pitted. Higher erosion is generally associated with areas of repetitive braking and acceleration. The depth of the top flange is 7 in. The repair involves grinding down the top beam surface to a uniform half-inch U-shaped channel and placing high-strength cementitious surface repair material.

***Lightning:*** Lightning strikes are indicated by a series of spalls along a short span of the beamway. The principal strike is indicated by the largest spall. The repair involves surface preparation and placement of high-strength cementitious repair material as in the cases above.

***Efflorescence:*** Mineral deposits appear on a small set of columns and seem to indicate efflorescence. The scope and effects of water intrusion is not well-known. Repairs have included epoxy material injection of cracks in the columns highlighted by the mineral deposits.

***Pylon Surface Blemishes:*** Incidents involving mowing vehicles bumping the precast concrete columns at or near grade result in minor spalls and surface damage. Repair methods vary.

***Longitudinal Cracks:*** Hairline cracks appear on some beam sections just above the line of the electric bus bar. The cause of these indications is unknown. The cracks align with the bottom corners of the hollow beam core and are not working.

## Study Purpose

There are a number of practical and academic reasons to develop structural condition assessment of the beamway system. Reasons include increasing the present understanding of the structural response to existing or increased loads, planning maintenance activities, evaluating retrofit or improvement alternatives, simulating damage or deterioration, and estimating the structural reliability. The information yielded from the present study may contribute to better decisions for operation, maintenance, and safety requirements, as well as benchmark the structural condition process, contribute a practical implementation example to the civil engineering practice and academic body of knowledge, and identify areas of further research.

## **Increased Loads and Load Effects**

Train loads on the beamway have increased significantly from those assumed in the original design (Figure 3, Figure 4). Table 1 demonstrates that the current gross train load is approximately 150% of the design value.

Table 1: Gross Vehicle Load Comparison

	GRAVITY LIVE LOAD COMPARISON	
	1971 DESIGN VALUES	PRESENT DAY ESTIMATED VALUES
TOTAL TRAIN LOAD	106 KIPS	175 KIPS
# OF PASSENGER CARS	5 CARS	6 CARS

Year 2000 loading information is provided directly from the owner. It should be noted that there is uncertainty associated with the load values measured in 2000. This is explored in subsequent chapters. These values are based on fully loaded trains. The reader should also note that the axle loads are spread over a greater distance (six cars), thus reducing their maximum effects. Still, train loads have significantly increased from the design assumptions.

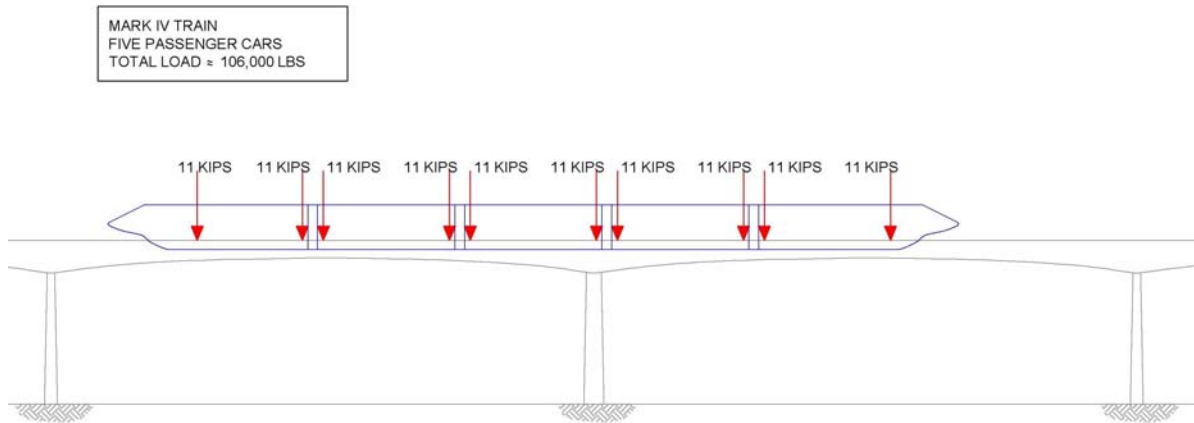


Figure 3: Mark IV Train Axle Loads (1971)

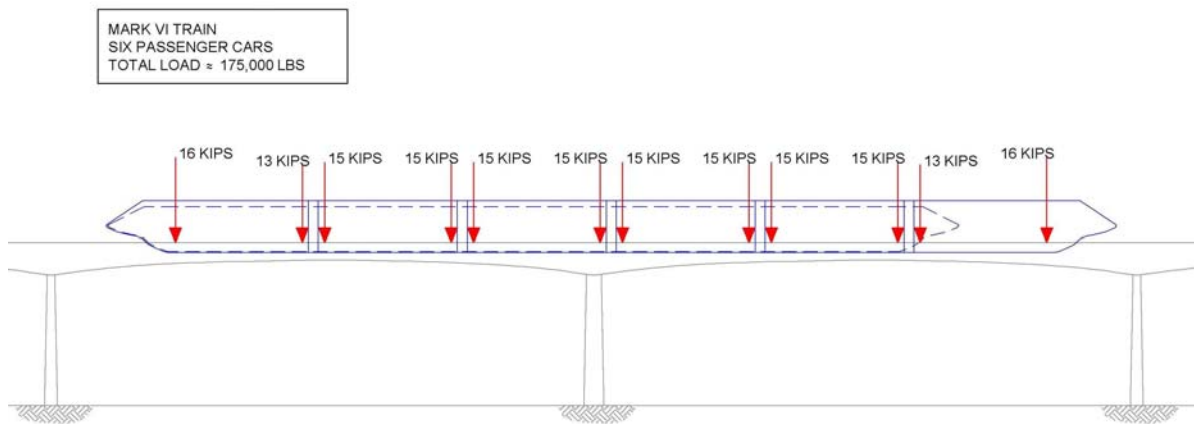


Figure 4: Mark VI Train Axle Loads (2000)

The present study considers the structural response under original (Mark IV) and current (Mark VI) train loads. The finite element models developed may be used to rapidly simulate the effects of additional train loads or axle configurations, increased cycling, or increased passenger capacity.

## Service Life and Life-Cycle Cost

Many design principles from the beamway design were synthesized with standards developed designing other guideway structures. The resultant guidelines have been revised and are presented as *ACI 358.1R-92: Analysis and Design of Reinforced and Prestressed-Concrete Guideway Structures* (American Concrete Institute 1992). The preamble text to this document states the following regarding service life and reliability,

A target reliability index of 4.0 and a service life of 75 years were taken as the basis for safety analysis. The reliability index is higher than the value generally used for highway bridges, in order to provide a lower probability of failure due to the higher consequences of a guideway structure in a public transit system. The 75 year service life is comparable with that adopted by AASHTO for their updated highway bridge design specifications.

Section 4.2 of the same document states that, “The economic life of a transit guideway is taken as 75 years.” Seventy-five years is a nice round number that gives us a sense of the order of magnitude of life to expect from the structure. However, it must be noted that the guideway studied presently was designed before these recommendations were assembled. The design is highly respected as cutting-edge design in post-tensioned concrete bridges. It meets or exceeds ACI 358 with respect to most limit states. One of the two principle designers is a member of ACI Committee 358 and used his knowledge of the beamway to help craft the recommendations (Dolan 2004).

The design is found to be deficient with respect to the fatigue limit state for shear and torsion resistance as defined in *ACI 358-92.1R-92*. The owner used consultants and in-house staff to study the design deficiency. It was determined that there are no *working* (opening and closing) shear cracks. The stress range inferred from strain gauging apparent shear cracks was significantly lower than the code-prescribed stress range limit of 12 ksi. The conclusion of these

studies was that, while ACI 358-92 requires the steel stirrups to resist the entire fatigue load, in reality, the concrete is providing significant shear resistance.

Considering the complexities of the design, the uncertainty associated with the materials including their initial and time-dependent properties, the changes in loading from design values, as well as the comprehensive beamway maintenance and inspection programs, there is no simple answer to the question of how long the beamway will last, or how that service life will be affected by certain maintenance activities or future changes in loading. Yet these are questions the owner would like answered to make better decisions and business plans.

Life-cycle cost analysis (LCCA) is an engineering economic analysis tool used to compare the relative merit of competing project alternatives. The Federal Highway Administration (FHWA) defines five major steps in the LCCA process (Beatty 2002). The steps are ordered so that the analysis builds upon information gathered in prior steps:

1. Establish design alternatives
2. Determine activity time
3. Estimate activity costs
4. Compute the life-cycle costs
5. Analyze the results

By considering all costs to the owner over a finite time period, the LCCA can help the owner make objective business decisions about new construction and maintenance. Transit infrastructure continually ages while population and load demands increase. These events precipitate the need for maintenance or improvement projects coupled with the use of objective information derived from analytical simulations along with experimental data. Objective structural condition assessment can feed information to the first two steps of the process which is outlined by FHWA. Condition assessment may increase knowledge about the effects of

deterioration or increased loads on an existing system, and assist in the formulation of safe and economical design alternatives. Condition assessment may help identify and quantify the effects of existing or increased loads on service life, thereby controlling the required maintenance and improvement activities. The role of the structural condition assessment process in informing the LCCA process may be visualized in Figure 5.

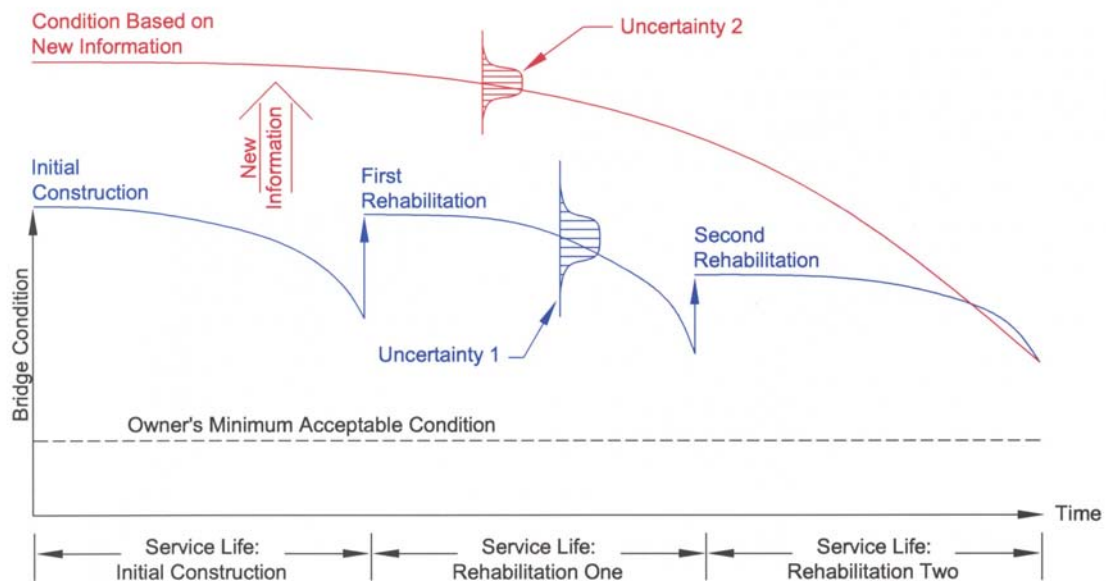


Figure 5: Condition Assessment and Life-Cycle Cost Analysis

Figure 5 shows three maintenance and deterioration cycles in the lower portion. Information used to determine a conventional bridge condition rating comes from visual inspections and load ratings based on design assumptions (AASHTO 2003). Design assumptions are based on simplified models of resistance and load effects. It is widely understood that engineers try to make conservative assumptions when uncertainty in these assumptions exists. Consequently, the first analysis of an aging civil infrastructure system may be based on conservative assumptions to facilitate a rapid design (Beatty 2002). Objective condition

assessment may demonstrate additional capacity, in which case the bridged condition rating would be improved as shown in the upper curve of Figure 5. In any case, structural condition assessment has the potential to provide the owner new information with increased reliability, to make better decisions for operations, maintenance, and safety.

### **Research Interest**

The owner has many facilities and infrastructure assets, some of which are unique designs, as in the case of the beamway. The owner is interested in exploring the condition assessment methodology as a benchmark for this structure and other aging structures. As university researchers, the author and his advisor are interested in contributing to the general body of knowledge related to condition assessment of civil infrastructure systems. The objective for this study is to contribute practical knowledge to the field by applying cutting edge analytical concepts to a new and unique engineering problem.

### **Methodology, Scope, and Tasks**

Structural condition assessment is widely understood as the process of characterizing the physical condition of constructed systems. The process consists of generating a finite element model (FEM), calibrating that model, and using the results from the calibrated model to rate the condition of the bridge or investigate new loadings or retrofit alternatives.

Structural condition assessment begins with structural identification. Structural identification is the process by which the current condition of the structure is investigated and modeled. Identification may be contrasted with structural design in which simple and conservative assumptions are often made to facilitate a rapid design. Design assumptions are

based on simplified models of resistance and load effects. For the structural identification, a detailed FEM is developed. Sensitivity studies are conducted to identify critical parameters. The FEM is verified by comparison with other analyses, experimental data, or long-term monitoring programs. The verification process optimizes the model in terms of the critical parameters.

After structural identification, the FEM may be used for simulation of existing or proposed loads, damage, retrofit, or improvement schemes. Results from the simulations may be combined with resistance calculations to determine load ratings. A reliability analysis can give an objective measure of structural reliability and probability of failure.

The state-of-practice approach to structural condition assessment of bridges commonly involves research teams with each researcher focused on one or more subdivided portions of the study such as FEM development, experimental design and data processing, model calibration, and/or simulations and rating. Many researchers can spend many years on the various aspects of a bridge assessment (Akgul and Frangopol 2003; Catbas and Aktan 2002; Xu et al. 1997).

Clearly it is not possible to perform a comprehensive structural condition assessment of a major bridge fleet within the reasonable scope of a Master's thesis. Consequently, the author proceeds with as many steps of the condition assessment process as possible, in as much depth as possible, within the time and resources allowed.

The scope of the present study is to generate a six-span continuous beamway finite element model that is representative of the fleet. In developing the FEM, complex boundary conditions, indeterminate connections, modal analysis and dynamic behavior are considered. A parameter sensitivity study is performed to understand the effects of changing key model parameters. The FEM is used for simulations of different train loads. AASHTO load ratings are

conducted and a special load factor is developed. Reliability analyses are performed to identify a reliability index and recommendations for experimental verification are presented.

Study tasks include the following:

1. Literature search
2. Bridge segment selection for analysis and testing
3. FEA software evaluation and acquisition
4. Preliminary models and benchmark studies
5. Model visualization
6. Six-span FEM development
7. Critical parameter identification and bounding
8. Eigenvalue analysis and parameter sensitivity studies
9. Simulations, Load ratings, and Reliability Analysis

### **Expected Outcomes and Findings**

The study is expected to provide information to make better business plans and decisions for operations, maintenance, and safety requirements. The author hopes to provide greater insight into structural behavior, system capacity and reliability, and to identify critical parameters and structural components. The FEM will be provided for experimental validation and use in future studies. The key advantage of the FEM is that, once developed, it may be used to simulate different train loads or axle configurations, environmental loads, structural deterioration or damage, as well as improvements or modifications.

A practical implementation of the condition assessment methodology will be useful to the owner, the author, and as a contribution to the structural condition assessment and structural health monitoring fields of research. A successful study will be a benchmark to establish a

procedure and methodology for structural condition assessment and will contribute a practical implementation of the methodology to the general practice and academic body of knowledge.

## **CHAPTER TWO: LITERATURE REVIEW AND FUNDAMENTAL CONCEPTS**

### **Condition Assessment**

The Federal Highway Administration currently maintains an inventory of 593,065 bridges across the U.S. 272,619 of these bridges were built from 1951 to 1980 with a design service life of approximately fifty years. Many of these bridges are experiencing or are starting to experience deterioration as they approach the end of their nominal service life. Approximately 25% of bridges in the U.S. are categorized as either functionally obsolete or structurally deficient (Federal Highway Administration 2004). Efficient and reliable diagnostic methods used to evaluate capacity, reliability, and service life are critical tools being developed to determine how best to allocate limited resources in operating, maintaining, and retrofitting bridges and bridge fleets (Akgul and Frangopol 2003; Catbas and Aktan 2002; Catbas et al. 2004a; Nowak and Collins 2000; Wang et al. 2005).

Objective condition assessment can contribute information to make better decisions for safety and serviceability of existing civil infrastructure systems. Condition assessment begins with structural identification; this includes developing a finite element model of the existing structure and conducting experimental verification and calibration of the model. It is possible to model a structure or its components based on either continuum or discrete analytical methods. Condition assessment of an existing constructed facility is best served by discrete, geometric models that take advantage of any heuristic knowledge base, as opposed to numerical or nonparametric methods that may serve well in the design of new structures (Aktan et al. 1998).

## **Structural Identification**

Condition assessment begins with structural identification. The state-of-practice approach to structural identification is based on practical implementation of discrete finite element analysis methods, using conventional PC hardware and software to generate models that will accurately and completely simulate: (1) 3D geometry of critical regions and elements; (2) boundary and continuity conditions; (3) 3D displacement kinematics at critical regions; (4) stiffness and inertia distribution and connectivity within the structure; and (5) critical mechanisms of external and intrinsic loading (Aktan et al. 1998).

Recent advances in PC hardware and software have made this a feasible and efficient approach. After a nominal 3D FEM of the bridge has been generated, the dynamic response of the bridge is simulated to help define a comprehensive modal test plan. Mode shapes, natural frequencies, and modal contribution coefficients are computed by the preliminary finite element simulation and are used to influence the development of a test plan. The test plan is designed to capture the frequencies and mode shapes of interest. Determining the natural frequencies provides the proper frequency bandwidth for a given bridge. This knowledge is used to configure the bandwidth of the data acquisition system to capture the necessary modes.

The nominal FEM represents the actual structure with limited accuracy because of possible damage, deterioration, or structural details that behave differently than the design assumptions. Thus the nominal model needs to be calibrated to more accurately simulate the experimental results. Experimental techniques include modal testing and truckload testing to measure structural response or known inputs and ambient excitation. The critical parameters of the model are adjusted in a step-by-step process so that the analysis results match the experimentally measured static and dynamic responses. A detailed calibration process is

proposed (Wang et al. 2005). The comparisons of analytical and experimental responses give an indication of the accuracy of the model during calibration.

### **Structural Health Monitoring**

Health monitoring may be defined as the continuous measurement of the loading environment and the critical responses of a system or its components (Catbas et al. 2004b). Health monitoring is typically used to track and evaluate performance, symptoms of operational incidents, anomalies due to deterioration and damage, as well as health during and after an extreme event (Aktan et al. 2000). Structural health monitoring captures long-term structural behavior with continuous or discrete intervals of monitoring, capturing seasonal and environmental changes not readily apparent from a single test. Periodic monitoring of dynamic properties to continually identify the current structural condition of a bridge is an area of active research. The viability of long-term monitoring programs is tied to the accuracy and reliability of the non-destructive test methods used. A successful non-destructive test method has been to identify dynamic properties from ambient excitations of the bridge (Farrar and James 1997).

Health monitoring has gained considerable attention in civil engineering over the last two decades. Although health monitoring is a maturing concept in manufacturing, automotive, and aerospace industries, there are a number of challenges for effective applications on civil infrastructure systems. The challenges include fundamental knowledge and technology needs, implementations, and socio-organizational challenges. Catbas et al. (2004b) outline the main health monitoring components and link them to these challenges, offering promising examples laboratory and field research implementations of structural health monitoring.

## **Simulations and Load Rating**

In most cases, the final deliverable in the condition assessment process is a bridge rating factor (Wang et al. 2005). The calibrated FEM is used to simulate loading conditions and the resulting load effects are recorded and analyzed to arrive at the bridge rating factors. Rating the bridge based on calibrated finite element results offers several advantages over static load testing including. The first is that the FEM can rapidly produce reliable results for rating the bridge under many types of loading. In addition to the truck used for the test, standard AASHTO, FHWA, and state loading conditions can be generated for the rating procedure. A second advantage is that the rating is based on the global response of the entire bridge rather than the local response at strain gauge locations. Ratings based on strain data rely upon the assumption that the strain gauges capture all critical behaviors. A third advantage is that calibrated finite element models can be used in concert with damage identification technology to locate possible localized defects and failures in the bridge that go unnoticed during visual inspections and truck load testing (Catbas and Aktan 2002). A fourth advantage of the using the FEM-based rating is that should an improvement or retrofit of the structure be required, engineers can use the calibrated model to quickly evaluate the alternatives (Wang et al. 2005).

The state-of-practice approach to condition assessment of major bridges commonly involves multiple researchers and even multiple research teams, with different researchers focused on one or more subdivided portions of the study such as FEM development, experimental design and data processing, model correlation, and/or simulations and load rating. Many researchers may spend many years on the various aspects of a bridge assessment (Xu et al. 1997).

## **Experimental Verification and Model Updating**

Finite element modeling gives a detailed description of the physical and modal characteristics of a bridge, while field vibration tests serve as a valuable source of information for evaluating the drawing-based (idealized, nominal) FEM. Discrepancies between the finite element (analytical) prediction and the measured (experimental) bridge response may be caused by the following factors in connection with finite element modeling: (1) inaccuracy in the analytical model discretization; (2) uncertainty in the geometry and boundary conditions; and (3) variations in the material properties of the bridge (Zhang et al. 2001).

It is desirable to measure the dynamic properties of new and existing bridges to better understand their dynamic behavior under normal traffic loads and extreme loads such as those caused by seismic events or high wind. Dynamic properties of interest include resonant frequencies, mode shapes, and modal damping. These measured properties can be used to update numerical models of the bridge so that the models better reflect the actual boundary conditions and as-built structural connectivity. Knowledge of the dynamic properties can be used to assess the effects of traffic loading on the fatigue life of the structure and to determine dynamic load factors for these structures (Farrar and James 1997).

A three-dimensional dynamic FEM was developed for the Tsing Ma long suspension bridge in Hong Kong. Modal analyses were carried out to determine natural frequencies and mode shapes of lateral, vertical, torsional, and longitudinal vibrations of the bridge and to investigate the dynamic interaction between the vibrational modes, between the main span and side span, and between the deck, cables, and towers. The natural frequencies and mode shapes obtained by the numerical analysis were compared with experimental results and found to be in good agreement (Xu et al. 1997).

The combination of numerical modeling and full-scale measurement provides a comprehensive understanding of the behavior and properties of the Tsing Ma Bridge. The validated FEM, computed dynamic characteristics, and the dynamic interactions between bridge elements can serve as topics for future studies on the long-term monitoring or for aerodynamic analysis of the Tsing Ma Bridge.

Model updating is a rapidly developing technology. Zhang et al. (2001) provides an excellent review of literature describing the historical development of model updating methods. For a complex structure with a large number of degrees of indeterminacy, model updating is difficult because it involves uncertainties in many parameters such including material properties, geometric properties, and boundary and continuity conditions. Manual calibration of the FEM should take advantage of existing knowledge from the owner, as well as knowledge of field experiments, analytical modeling, prediction and simulation of bridge response, and uncertainty associated with different types of experimental data. A flowchart that shows a procedure for manual FEM calibration using modal analysis is given in Aktan et al. (1998).

There are generally two approaches for updating the finite element model of a structure, depending on whether the system matrices or the structural parameters are selected for updating (Berman 1998). The method of system matrix updating seeks changes in stiffness and/or mass matrices by solving a system of matrix equations. This approach cannot handle the situation whereby the changes in mass and stiffness matrices are coupled together. The parametric updating method typically involves using the sensitivity of the parameters to find their changes (Friswell and Mottershead 1995). This sensitivity-based parametric updating approach has an advantage of identifying parameters that can directly affect the dynamic characteristics of the structure. Additionally, by employing this method, one may acquire an immediate physical

interpretation of the updated results. For these reasons, the parametric updating method is chosen in the Kap Shui Mun cable-stayed bridge study (Zhang et al. 2001).

Zhang et al. (2001) describe an improved sensitivity-based parameter updating method used for model updating of the Kap Shui Mun cable-stayed bridge. This method is based on the eigenvalue sensitivity to some selected structural parameters that are assumed to be bounded within some prescribed regions according to the degrees of uncertainty and variation existing in the parameters, together with engineering judgment. The changes of the chosen parameters are found by solving a quadratic programming problem. A comprehensive procedure for sensitivity-based model updating is given in the paper referenced.

Assumptions and considerations associated with the Kap Shui Mun bridge study include the following: (1) the structural parameters are grouped into major components of the structural system including the deck, towers, connections, and boundary conditions; (2) the cross section of the composite deck is described by equivalent homogeneous properties and a single spine passing through the shear centers of the deck; (3) the deck/tower connections, deck/pier connections, and boundary conditions are modeled using one elastic spring along each translational and rotational direction. A total of seventeen modes, with a frequency range between 0.4 and 2.2 Hz, are selected for matching between analytical and experimental results. Thirty-one structural parameters were selected for updating based on a comprehensive eigenvalue sensitivity study. It was found that, in general, the frequencies calculated from the updated model are closer to the measured values when compared to those calculated from the initial model. A similar result is seen even for those modes that are not included in the original updating process.

The results seem to suggest that it is possible to update the FEM so that the natural frequencies are reasonably close to the measured ones. However, there is not sufficient evidence to indicate that the updated structural parameters are or are close to the actual values. At best, the updated model can be considered a plausible candidate to represent the real structure. Because the number of structural parameters considered is larger than the number of modes, multiple sets of parameters that satisfy the optimality objectives may exist. The non-unique nature of the solution is an important issue that needs to be addressed in a future study (Zhang et al. 2001).

The modal assurance criterion (MAC) is an objective method to quantify the correlation between mode shapes (Farrar and James 1997). The MAC may be used to compare mode shapes measured during different tests or to compare experimental and analytical results. The MAC makes use of the orthogonality properties of the mode shapes. If the modes are identical, a scalar value of one is calculated by the MAC.

### **Experimental Data Processing**

In conventional vibration testing, analytical forms of frequency response functions (FRF) relating a measured input such as a force to a measured response such as acceleration are fit to measured FRFs to estimate the dynamic properties of the structure. The use of measured input-measured response FRFs to identify a structure's dynamic properties is well-documented. However, when a bridge is subjected to traffic excitation, it is difficult, if not impossible, to measure the input to the structure. The extension of system identification methods to ambient vibration cases, in which an input cannot be measured, is the subject of current research (Farrar and James 1997; Wang et al. 2005). The size of most bridges and the disruption of traffic flow if

they are taken out of service typically make ambient vibration testing the only practical experimental method available for studying their dynamic response.

Farrar and James (1997) present an ambient vibration system identification method, referred to as the Natural Excitation Technique (NExT). The NExT method involves applying time domain curve-fitting algorithms to cross-correlation measurements made between various response measurements on an ambiently excited structure to estimate the resonant frequencies and modal damping. The ambient vibration system identification method was applied to an in-service highway bridge where traffic provided the vibration source. The same bridge was tested with conventional measured-input force vibration procedures. The authors conclude that ambient vibration from traffic provides an adequate source of input for identifying the dynamic properties of the bridge, and that the method presented was able to discern closely spaced modes (0.07 Hz) and the associated modal damping.

### **Damage Detection from Modal Response**

Locating and quantifying damage in large or complex structures is one of the most challenging problems in nondestructive testing (Pothisiri and Hjelmstad 2003). The problem is important because damage in structures is not always apparent from visual inspection methods. Local nondestructive evaluation techniques that require a close proximity of the excitation and measurement to the damage site are not useful for locating damage, but are useful for assessment once damage has been located. Global methods, in which the entire structure is excited and the response is measured at certain places, are more appropriate for locating damage. One such testing method, commonly referred to as *modal testing*, measures the natural frequencies and mode shapes of a structure using resonant forced vibration.

Global damage detection methods based upon measured natural modes and frequencies of a structure have gotten considerable attention in research. In particular, parameter estimation methods have shown promise as tools for detecting damage in structural systems (Pothisiri and Hjelmstad 2003). Damage detection based upon parameter estimation generally requires that the structure be represented by a parameterized FEM and that the values of the system parameters be estimated using a least-squares minimization of either the force residual or displacement residual of the vibration eigenvalue problem.

Generally, the number of elements in the model far exceeds the number of measurements available for parameter estimation. The measurements obtained from a modal test are discrete and sparsely distributed over the spatial domain of the test structure. Only a few natural modes may be accessible through testing. Parameter estimation from measured modal response can have multiple solutions if the data is spatially sparse. Ignoring the possibility of solution multiplicity leads either to erroneous damage locations or else the algorithm fails to converge at all. Additionally, measured data is generally polluted with random measurement errors, dramatically affecting the accuracy of the parameter estimates.

Pothisiri and Hjelmstad (2003) seek to formulate a practical approach for global damage detection from incomplete and noise-polluted modal response of a structure. An element-group updating algorithm is proposed that accounts for the multiplicity of solution to the parameter estimation problem at each step of the damage localization process. The damage detection and assessment procedure was tested with a simulation case study. The numerical simulations were performed on the case where the structural members have only a single stiffness parameter. Evaluation of the statistical distribution of the parameter estimates at the potential damage location proved to be a reliable method for assessing whether damage is detectable above the

noise in measurement data. The authors conclude that their proposed algorithm can detect and assess damage successfully provided that the noise is not too large.

### **Finite Element Analysis**

It is possible to develop a primary finite element model (FEM) for system analysis and use the model to identify critical elements or components. A parallel effort may include the development of secondary, more detailed FEMs at the critical locations, perhaps using different software, to investigate the local behavior further (Kompfner 2004). The present study scope includes the development of a primary FEM to identify global behavior, with sufficient resolution to indicate some local load effects. Secondary FEMs are beyond the scope of this study.

An appropriate dynamic FEM, balancing accuracy and computational effort, is used to determine natural frequencies and mode shapes of a given bridge. Because the sectional properties of the bridge deck have the greatest effect on the natural frequencies and mode shapes of the bridge (as compared with the structural details), the bridge deck in the global analysis of long span bridges is commonly represented by a single equivalent beam, or two and three equivalent beams, or equivalent plates, to avoid prohibitive computational effort (Xu et al. 1997). However, because the owner is interested in a hybrid model that gives global and local effects, and considering great advances in PC computing power in recent years, it is feasible to model the beams not with equivalent 1D frame elements, but with 2D shell elements which give more information about local behavior, allow more detailed development of the connections, and generally provide more resolution to the model.

Before using the FEM, the mechanics and numerical stability of the model should be validated. The mesh size, aspect ratio, and proper connectivity between different analytical elements may be optimized by studying convergence under static loads as well as evaluating the numeric stability of dynamic analyses. The most reliable manner of testing the physical completeness of a calibrated analytical model is to correlate the simulated global and local responses with those measured by a different experiment. To improve the reliability of the model, the simulated dynamic and static properties and behavior should be consistent with the measured experimental counterparts. Once the model is validated by field measurement data, it may be used for static and dynamic analysis of the bridge, as well as in long-term monitoring studies (Xu et al. 1997).

### **Finite Element Methods for Concrete Structures**

Prestressed concrete designs have been widely used for buildings, bridges, tanks, offshore oil platforms, nuclear containment vessels, and many other structures. The design of these structures must satisfy requirements for safety, serviceability, and fatigue. While this can be accomplished with approximate or empirical procedures prescribed in codes, it is desirable to have refined analytical models and methods available which can trace the structural response of these structures throughout their service load history, under increasing loads and through elastic, cracking, inelastic, and ultimate ranges (Scordelis 1984). These refined analytical methods may be used to study the effects of important parameters in a systematic way, to test and improve the design codes, or they may be used directly in the analysis and design of complex structures.

Many advances have occurred in recent decades with respect to the finite element analysis of reinforced and prestressed concrete structures. Three alternative approaches are used for modeling reinforcement. These are the discrete model, embedded model, and smeared model (El-Mezaini and Citipitioglu 1991).

In the discrete model, first suggested by (Ngo and Scordelis 1967), reinforcing bars are modeled using special elements connected to concrete through fictitious springs representing the bond. The boundaries of the concrete elements follow the reinforcing bar to achieve common nodes (DOFs). The discrete representation is the only way to account for bond slip and dowel action directly. The main disadvantage is that the concrete element mesh patterns are restricted by the location of the reinforcement and. Mesh refinement can be difficult. The number of concrete elements and DOFs is increased, thereby increasing computational effort (Arafa and Mehlhorn 1998).

Embedded models allow an independent choice of concrete mesh. The same type of elements with the same number of nodes and DOFs are used for both concrete and steel. The stiffness matrix and internal force vector for the steel element are obtained containing only the contributions of the reinforcing bar. Bond slip and dowel action can only be modeled implicitly by modifying the constitutive relations for concrete or steel. The disadvantages of the embedded model are that additional DOFs increase the computational time and the special reinforcement elements required do not exist in most commonly available finite element analysis computer programs (Arafa and Mehlhorn 1998).

In the smeared model the reinforcement is characterized by smearing the reinforcing bar to thin layers of mechanically equivalent thickness within a particular concrete element. Assuming a perfect bond between concrete and steel, the constitutive relations are derived using

composite theory. The smeared model accurately represents only uniformly distributed reinforcing bars (Arafa and Mehlhorn 1998).

The discrete model is the most general. It is the only model that uses conventional 1D elements to represent reinforcement and the only model which can account for bond slip and dowel action directly. Different material properties for the reinforcement and different bond conditions at different nodes can be directly and independently represented. The disadvantage to the basic discrete model is that the concrete mesh geometry depends on the reinforcement mesh. In order to allow independent choice of the concrete mesh, El-Mezaini and Citipitioglu (1991) propose a special isoparametric element with movable edge nodes. Reinforcing elements are modeled independent of the concrete mesh. Reinforcing bars are commonly modeled as truss or cable elements (Arafa and Mehlhorn 1998). The edge nodes of the concrete elements are moved to the points where the reinforcing layers intersect the edges of concrete elements. The concrete nodes are connected to the steel nodes.

El-Mezaini and Citipitioglu (1991) present a technique for the discrete representation of bonded, unbonded, and partially bonded tendons. The reinforcement nodes are constrained depending upon the bonding assumptions. For the bonded case, the concrete and steel nodes occupy the same location and are assigned the same DOFs. The steel and concrete nodes are fully coupled and no slip is allowed. For the unbonded case, the concrete and steel nodes are coupled in the direction perpendicular to the reinforcement axis, but independent in the direction along the reinforcement axis. The concrete and steel have the same DOFs in the perpendicular direction and different DOFs in the tangent direction. Relative motion can occur and the tangent direction is known as the *slip degree of freedom*. Partial bond is the most general method. The slip DOFs are controlled through the use of a prescribed slip laws such as fictitious springs. The

required bond model is represented by assigning appropriate properties to the fictitious springs. This is the most general case because all bond conditions can be represented by proper selection of spring properties. For example, a very stiff spring may represent perfect bond whereas a very soft spring represents no bond. Any bond in-between can be represented.

In the partially bonded method, linear or nonlinear bond models can be used to represent friction and slip. Linear or nonlinear material properties may be used for concrete and steel. Scordelis (1984) presents a unified numerical procedure for the material and geometric nonlinear analysis of various types of reinforced and prestressed concrete structures including planar or three-dimensional rigid frames composed of 1D elements, panels or slabs composed of 2D triangular or quadrilateral flat finite elements, thin shells composed of 2D flat or curved finite elements or axisymmetric thin shell elements, and solids made up of 3D solid finite elements or axisymmetric solid elements. Time-dependent effects due to load history, temperature, creep, shrinkage and aging of the concrete, and relaxation of the prestressing steel may be included in the analysis. This work (Scordelis 1984) is based on the discrete model for reinforcement.

Arafa and Mehlhorn (1998) present a special discrete and smeared representation of reinforcement to be used in nonlinear analysis of prestressed and reinforced concrete structures. A discrete model is used to represent the main reinforcement bar independent of the concrete finite element mesh, using a an isoparametric Lagrange element with movable side and inner nodes. The secondary reinforcement and/or stirrups are represented by a smeared model. Mapping distortion can occur when mapping unequally spaced node locations on the sides and interior of the physical element to equally spaced nodes of the parent element. A singular Jacobian matrix is obtained if the edge nodes are moved significantly from their normal positions. To allow for flexibility in locating side and interior element nodes, a correction

technique for avoiding or minimizing this distortion is included, based on previous research cited in the paper(Arafa and Mehlhorn 1998). Side nodes are positioned at the same relative distance from corner nodes in both the physical and isoparamteric element.

While it is clear that nonlinear slip models and material properties for prestressed and reinforced concrete structures are available in the literature, the practical implementation of finite element methods may not require these advanced techniques. Elastic behavior is generally accepted as a valid assumption for analysis of prestressed concrete structures under service loads and reinforced concrete elements up to cracking (El-Mezaini and Citipitioglu 1991).

### **Transit Guideways**

The Las Vegas Monorail began operations in 2004. The system provides direct service to eight major resort properties and the convention center. The project has an estimated cost of \$350 million for design, construction, manufacture, installation, testing, and commissioning. The system extends over almost 4 mi (6.5 km), with seven stations and a dedicated operation, maintenance, and storage facility.(Banchik and Jasper 2003)

The elevated guideway consists of 33 linked guideway structural frames and switch structures. A typical guideway structural frame consists of five spans using dual, precast, post-tensioned guide beams. The frame is made continuous through cast-in-place closure pours and continuity post-tensioning. The slender haunched beam section varies in depth from 7 ft (2.1 m) at the supports to 5 ft (1.5 m) at midspan. Spans average 100 ft (30 m), with the longest being about 120 ft (36.6 m). Parallel beams are typically spaced 14 ft (4.2 m) with greater spacing at switch approaches and some stations.

In contrast to the beams used on a typical highway or transit project, the monorail's beams are extremely sensitive to construction defects, since the technology does not allow for second pours. With a side clearance from concrete face to steel reinforcement of approximately 1 in (25 mm), there was not much room to grind or feather concrete. Correcting problems is made all the more difficult because the geometry of the structure depends on such external factors as temperature and position of the sun, which can make repairs to guideway geometry prohibitively expensive. Tight tolerances were specified for construction for the guide beams. Construction tolerances were stricter than those prescribed in *PCI Design Handbook: Precast and Prestressed Concrete*, published by the Precast/Prestressed Concrete Institute, and the publication *Reinforced Concrete Guideway Structures: Analysis and Design*, prepared by American Concrete Institute Committee 311.

A typical cast-in-place column supports two guide beams over transverse supporting members (crossheads) ranging in height from 4 ft (1.2 m) at the end to 6 ft (1.8 m) directly over the column. The crossheads are 17 ft (5.1 m) long. Columns typically vary in height from 25 to 30 ft (7.6 to 9.1 m), but in places where the monorail must span an existing pedestrian bridge the height can reach 60 ft (18.2 m).

The beam-column connection contains a structural steel support and hanger, which, coupled with external supports, make it possible to correctly position each beam during construction. The assembly allows guideway alignment and superelevation to be adjusted before placing the joint closure pour. Longitudinal frame post-tensioning tendons are stressed, and transverse post-tensioning in the intermediate crossheads is then applied. Closure pours in the expansion columns are prepared and poured, including the expansion joint plates that bridge the gap between each two adjacent structures.

During the preliminary design phase, a parametric study was carried out to determine the optimal characteristics for beam and span frame distribution. The optimal configuration was found to be a five-span configuration, with 120 ft (36.5 m) intermediate spans and 100 ft (30.5 m) end spans. The columns at the ends of the frames are hinged in the longitudinal direction so as to minimize moments in the end spans from thermal loading, while maintaining capacity in the transverse direction. The result is a tuning-fork arrangement, the two columns sharing the drilled shaft foundation.

Analysis of the guideway was carried out with the aid of RM2000, structural software developed by Technische Datenverarbeitung, of Graz, Austria. The software made it possible to model structures in three dimensions and to include construction sequences and time-dependent creep and shrinkage. Each monorail car rides on two vertical tires, one at each end of the car. Each vertical tire in turn is guided by two smaller tires in a horizontal position on either side, making for eight guiding tires per monorail car.

Studies were carried out to verify the correlation between theoretical beam deflection and camber and the results obtained in the field. Granite Construction instituted a quality control program that closely tracked the geometry and features of each and every beam.

The contract documents required the contractor to provide infrastructure with a service life of 50 years. The recommendations led to the development of proper concrete mixtures and informed the analysis of creep and shrinkage and of expansion and contraction across joints. The water-cement ratio in the concrete was 0.4, with fly ash admixtures to reduce permeability and increase serviceability. The beam concrete strengths range between 6,000 psi and 7,500 (27.6 and 51.7 MPa), with next-day strengths between 3,500 and 4,200 psi (24.1 and 28.9 MPa). Field

cylinder breaks consistently reported 28-day concrete strengths between 9,000 and 12,000 psi (62.0 and 82.7 MPa).

The precast beams were manufactured in a special yard set up by the contractor in North Las Vegas. Hesler Industries, of Tualatin, Oregon, manufactured the forms used in the project. The forms represent the fourth generation of those developed in 1971 for the monorail at Walt Disney World. Based on experience gathered in constructing the first monorail linking MGM and Bally's, where accelerated curing with gas-fired salamanders caused microcracking of the riding surface, the contractor opted for the Sure-Cure system, developed by Products Engineering, of Boulder, Colorado, which monitors the maturity of the concrete by tracking and controlling the temperature inside the forms.

## **CHAPTER THREE: PRELIMINARY MODEL DEVELOPMENT**

Before developing the full six-span continuous model, consideration was given to which segment to model and what software to use. Additionally, it was important to understand the geometric and analytical details of the beamway system on a smaller scale before attempting the full six-span model. Model visualization included the process of discovering the beamway history through drawings, structural calculations, interviews, observation, and other methods. CAD models were developed and became the geometric basis for the finite element models. Benchmark studies were conducted to acquaint the author with the software, as well as to try different approaches to modeling aspects of the beamway. Special attention was paid to modeling the concrete and prestressing, as well as detailed development of the cast-in-place connection.

### **Bridge Segment Selection**

There are approximately ninety six-span continuous bridge segments in the beamway system. It is important to think critically about which segment to model, to provide maximum benefit at minimum cost and with minimum impact to system operations while useful yet representative information can be obtained. As a result, the following criteria are adapted for the selection of the representative segment.

### **Primary Selection Criteria**

#### ***Significant and Representative Segment***

The segment should be representative and also significant such that it provides an important link in the transit system, it sees significant loads, and it has significant (long) beam

spans. Practically this means we can reduce the entire population considered to long-span 100-ft exterior/110-ft interior span segments, and consider the oldest segments in the system as most significant. Immediately this reduces the number of possible segments to under twenty-five. The segment should be representative in that many other segments in the fleet share the same dimensions, loading, materials, and other design features. This reduces the fleet further to representative curved and straight sections.

The present study is expected to provide insight into the structural behavior of the beamway and to serve as a baseline to establish methodology for system identification and condition assessment. Studying a straight beamway section serves a reasonable baseline, with curved spans recommended for future studies.

### ***Segment Visibility***

A principle operational objective is to provide seamless transit operations to the passengers without the appearance of any maintenance or technical work. All such work is to be minimized or made as invisible as possible so as not to affect the immersive experience of the theme park environment. This means that all noticeable experimental work (equipment installation, lift operations) must be restricted to non-operational hours for the system and that any equipment left in-place (sensors, gages, cables) should not be visible to the typical customer. This criterion rules out a number of segments with outstanding access, because they are in places with unacceptable levels of visibility.

Visibility is a key criterion in the case of the beamway, which makes this application unique when compared with structurally similar highway bridges. Considering the perception of the average user, there is nothing objectionable about seeing engineers or even construction crews on or around a highway bridge. However, in the case of the beamway, such a situation is

significantly damaging to the desired aesthetic and unacceptable to the owner. Figure 6 shows a segment with excellent accessibility for instrumentation and testing, as well as access to electricity and communications. However, because of its high visibility, this segment would be unacceptable should experimental testing be pursued. Figure 7 shows a segment with fewer resources for access, electricity, and communications, but the requirement for minimal visibility is met. Both segments have similar geometries and loading.



Figure 6: High-Visibility Bridge Segment



Figure 7: Low-Visibility Bridge Segment

### **Secondary Criteria**

Considering the above as baseline criteria, secondary criteria may be added to optimize resources. To reduce the cost in collecting experimental data, sections that are low to the ground are preferred for easier access. Other considerations for access are the availability of service or station platforms, adjacent structures, and access for vehicles and lifts. It is also desirable for the segment chosen to have communication hardware and electricity available. Electricity is important to power instruments, lights, and other equipment. The communication hardware (fiber cable) provides an opportunity to feed data to remote computers as part of a real-time structural monitoring program (beyond the scope of this study).

Boundary conditions should be considered. A curved approach will affect behavior on a straight span. Only straight segments with straight approaches are considered.

Existing documentation is a final consideration as the availability of design documentation facilitates the development of the finite element model and provides insight into the thinking of the original engineers. Fortunately, the oldest segments in the system have excellent documentation in the form of design drawings and a published article describing design methodology (Mast and Dolan 1972).

Objective ratings are assigned to various segments based on the above criteria and these ratings are summed to obtain an overall rating to determine the preferred segment. This is an iterative process with much feedback from the owner. Twenty possible points are assigned to the primary criteria and ten possible points to the secondary criteria (see Table 2).

Table 2: Objective Rating of Bridge Segment Candidates

Location	Maximum Nominal Height	Subjective Score on Study-Related Criteria						Total Score
		Significant Segment	Representative Segment	Minimizes Visibility	Boundary Conditions	Access, Communication + Electricity	Existing Documentation	
<b>Segment 1</b>	27'	20	20	5	10	10	10	<b>75</b>
<b>Segment 2</b>	28'	20	20	15	8	5	10	<b>78</b>
<b>Segment 3</b>	29'	5	20	20	10	10	8	<b>73</b>

Segment 2 is chosen for the study. It is recognized that the ratings are somewhat arbitrary. There will always be some difficulty in making an objective decision based on subjective criteria. However, it was useful to develop the objective ratings as a catalyst for discussions with the owner. Feedback was used to modify the ratings and to build consensus regarding which segment to study. Certain factors emerged as controlling factors, especially

visibility and age. Visibility became a key concern as described above. Age was considered important, as studying a segment in the original 1971 loop provides the most useful information with respect to service life and decisions for maintenance and operations.

The exercise of determining the most significant and representative segment in the population may be developed into an exhaustive and rigorous statistical study. This would be beyond the scope of the present study.

### **Software Considerations**

Finite element software was chosen by considering a variety of constraints and objectives. The first requirement was the ability of the software to accurately represent structural behavior, especially geometric and material nonlinearity, post-tensioning including time-dependent effects, and moving load analysis and bridge response. The writers considered usability in practice and attempted to balance this consideration with advanced analysis capabilities (usability in research). These two goals conflict in some ways; more advanced analysis capabilities may be provided by software that is prohibitively difficult to learn such that it would never be implemented in professional practice. The writers intend to establish a benchmark for condition assessment such that this approach may be adopted by practicing engineers using conventional software under conventional constraints of project schedules and limited budgets. Consequently the software should not be prohibitively complicated. However, many conventional FEA software packages used in design offices are limited to predefined frame elements, linear analysis, or other simplifications that would not provide sufficient analysis capabilities for meaningful research. The goal was to find software that strikes a

reasonable balance between robust engineering capabilities, wide use, and ease-of-use in practice.

The writers chose SAP2000 v.9 from Computers and Structures, Inc. (Berkeley, CA). SAP2000 meets the previously defined goals and objectives; it is widely used in practice and has robust analysis capabilities (Computers and Structures Inc. 2004). The specified version also introduces a new *Bridge Design Module* with tools to facilitate model development including parametric variation in section geometry (applicable to the haunched beam profile), post-tensioning modeled as loads or elements with time-dependent effects, material and geometric nonlinearity, and bridge analysis tools to quickly define moving loads and facilitate simulations. Additional advantages to SAP2000 are its long-standing use in the professional practice, its reasonable cost, and the writers' use of the software in the past for a number of different applications. The main disadvantage apparent to the writers is the fact that many of the bridge modeling and analysis tools are new to the current version which was released in late 2004. However, it is possible to test the product by means of benchmark studies. An opportunity exists to use the software in a cutting-edge application.

SAP2000 will be run on a PC notebook with a Pentium M 1.7 GHz processor, 512 MB RAM, and a 60 GB hard drive. Fortunately PC computing power is not the critical issue in choosing software that it was in past years. Gendron (1997) studied four popular finite element packages and evaluated each one for CPU performance and disk space requirements to solve a number of typical civil engineering benchmark problems. The author determined that the software packages were all sufficiently reliable, robust (Gendron 1997). Gendron used a PC with a Pentium 166 MHz processor, 32 MB RAM, and a 2.1 GB hard drive in the study. It is clear that the present study can take advantage of significantly more computing power.

## **Model Visualization**

### **Information Sources**

Model visualization is the process by which the mechanical, physical, and geometric features of the beamway structural system are understood on a detailed, element-by-element level. There are many sources of information to feed the visualization process. These include: (1) review of existing design drawings; (2) interviews with the original designers and engineers, engineers and technicians who take care of the beamway presently, and other experts in the field; (3) review of the original structural calculations (some but not all are readily available) and related documentation such as the published article on the beamway design (Mast and Dolan 1972); (4) review of inspection reports and engineering studies as well as other documentation archived in various forms and locations from the time of the original design to the present day; (5) site visits and physical observations.

The synthesis of all this information into a coherent and useful image or concept of the beamway was a significant challenge in and of itself, even before any new analysis was to be accomplished.

### **Visualization Tools**

Synthesis of all the current and historical beamway information was aided by the development of hand sketches, careful notation and archiving of documents, conversations, meetings, photographs, and other information sources. A significant technological tool was the development and use of three-dimensional CAD models for visualization. 3D CAD models

force the user to work out every design detail and geometrical ambiguity or inconsistency. A detailed understanding of the structure is achieved.

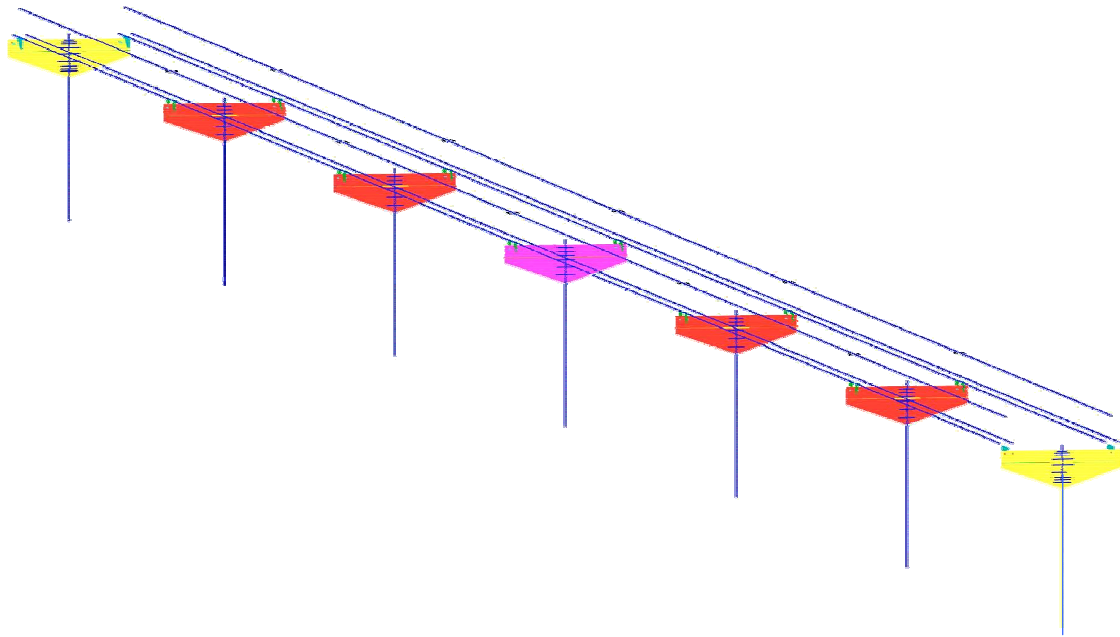


Figure 8: 3D CAD Model of Columns, Crossheads, and Post-tensioning

Figure 8 shows the 3D CAD model of the columns, steel crossheads, and post-tensioning strands. Note the different colors representing the center, typical, and expansion columns. The CAD model also includes features not readily apparent at this resolution, including small lines for link elements at connections and groups of points representing steel studs. Much time was spent on the development of this model and the geometry was imported directly from the CAD software into SAP2000. The geometric CAD elements become finite elements, links, and joint constraints.

The CAD software was used in parallel with SAP2000 for model visualization and development. The bridge modeler in SAP2000 facilitated development of the haunched beam profile of the superstructure, whereas the CAD software was more amenable to development of

more simple and repetitive details including columns, crossheads, and connection elements. The final result is a hybrid (Figure 23) model that incorporates superstructure elements created directly in SAP2000 and columns, crossheads, and connection imported from the CAD software. The full model development process is described in more detail in subsequent sections.

### **Connection Visualization and Analytical Model**

The beam-column connection is perhaps the most complex structural feature of the six-span continuous bridge unit (Figure 9). To understand the connection, one must consider the construction process. First, precast beams were cast with hanger plates stubbed out of the ends. The beams were positioned in the field with the hanger plates supported on steel crossheads. The crossheads were embedded in the precast columns. The beam self-weight travels a load path through the hanger plate to the crosshead, through the crosshead to the column, and through the column to the pile foundation.

After the precast beams were erected and aligned, a concrete connection was cast-in-place (CIP). The concrete cured and the six adjacent beams were post-tensioned together, forming a semi-continuous beamway. Any additional loads (including train loads) are resolved in part through the hanger plates to the top of the crosshead, and in part through the CIP concrete connection to the crosshead and the shear studs welded to its face. The connection is indeterminate because the beam shear may be resolved through the beam hanger plate, through the cast-in-place concrete, or through some combination of the two load paths.

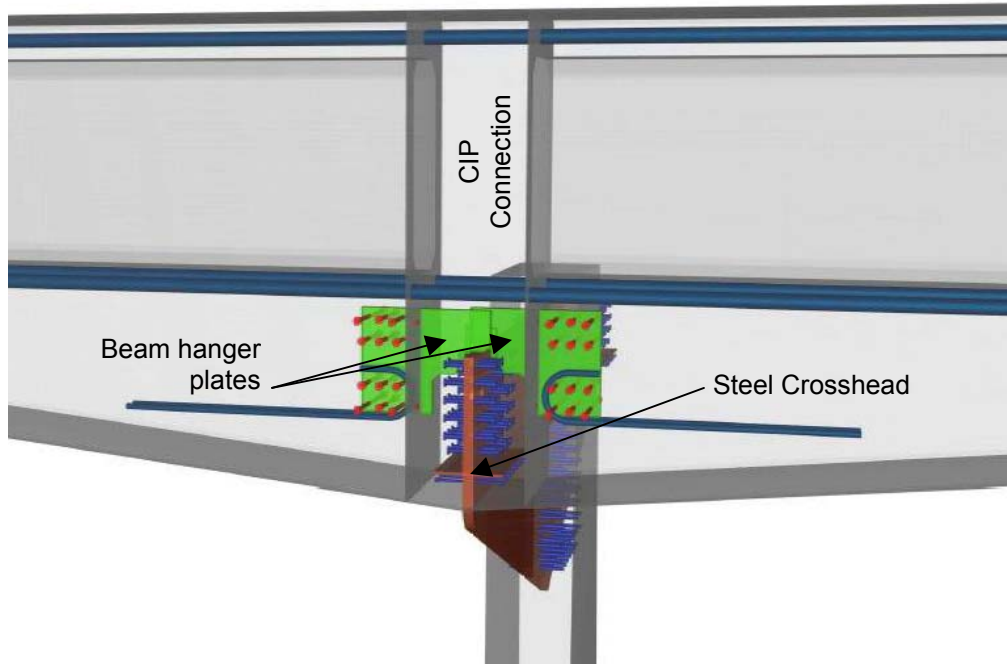


Figure 9: 3D CAD Model of CIP Connection (Perspective View)

Load sharing in the connection will be determined by the relative rigidity of the components. The writers developed a number of benchmark models in SAP2000 to represent the indeterminate condition. The two goals in development were (1) to accurately represent the physical behavior and (2) to use elements with adjustable parameters to control the load sharing.

The solution was to use frame elements with cross-sectional areas representing the cross-sectional area of the CIP concrete. Two frame elements connect the bottom flange of the box beam to the steel crosshead. Two additional frame elements connect the top flange directly to the adjacent beam. The free-body diagram representing these engineering assumptions is shown in Figure 10. The lower left frame element is omitted for clarity.

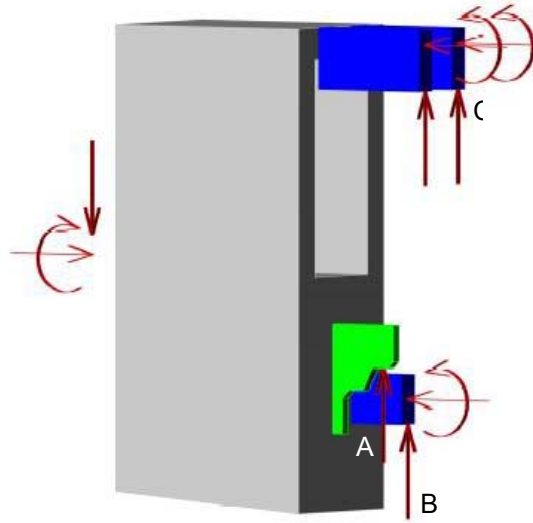


Figure 10: Free-Body Diagram (Precast Beam End)

This configuration mimics the indeterminate connection by dividing beam shear between reaction *A* at the hanger plate and reaction *B* in the CIP concrete. The analyst can adjust the proportion of load passing through paths *A* and *B* by adjusting the material stiffness parameters for steel or concrete. The most straightforward approach is to adjust the modulus of elasticity,  $E_{CIP}$ , for the cast-in-place concrete in the connection.  $E_{CIP}$  represents the modulus of elasticity for the concrete frame elements shown in Figure 10 at locations *B* and *C*. The modulus of elasticity is defined independently in SAP2000 for steel, for the CIP concrete, the beam concrete, and the column concrete. The shear modulus is not directly specified in SAP2000, but instead is defined in terms of Young's modulus and Poisson's ratio (Computers and Structures Inc. 2004).

By increasing  $E_{CIP}$ , the load resisted by the CIP concrete increases, and a greater proportion of the beam load is resolved through paths *B* and *C*. Conversely, by reducing  $E_{CIP}$ , a greater proportion of the beam load is resolved through the beam hanger plate (load path *A*). The frame elements at *C* connect the top corners of adjacent beams. These elements can only transfer

load between the precast beams. All loads must eventually pass through path *A* or path *B* to be resolved into the columns.

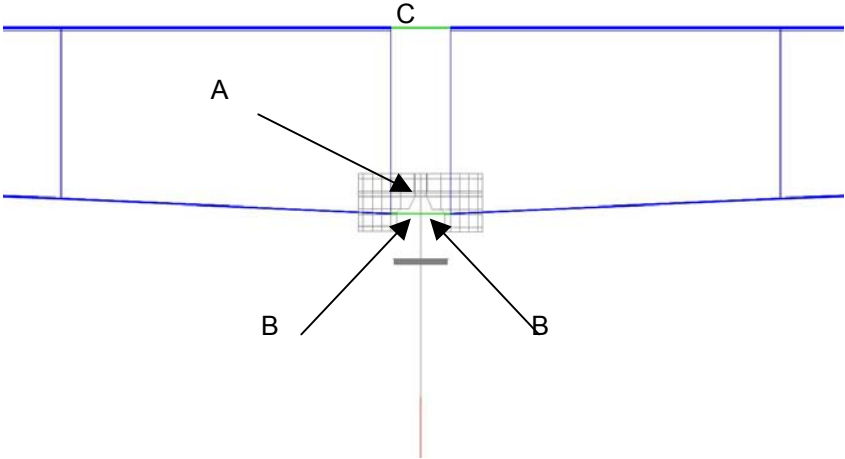


Figure 11: CIP Connection Analytical Model

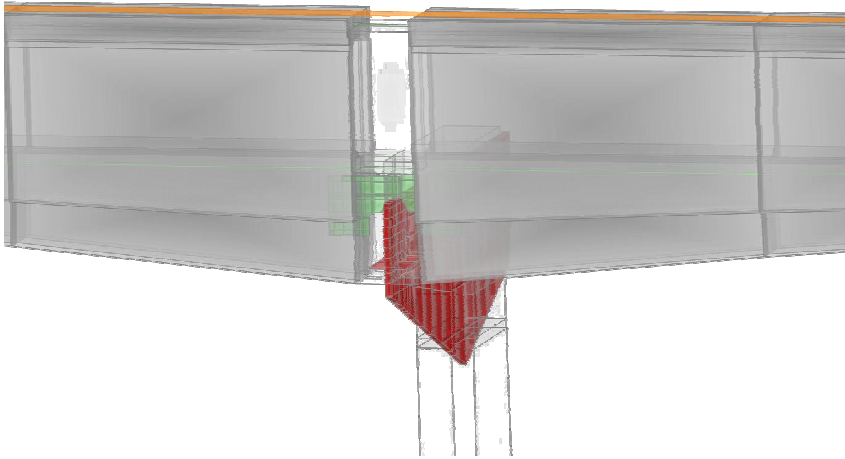


Figure 12: Extruded FEM Perspective

The 3D visualization was accomplished with AutoCAD 2005 (Autodesk, Inc., San Rafael, CA) using solid objects. Parts and dimensions were developed from original construction drawings. Construction methods and the structural concept were inferred from a

magazine article published after construction (Mast and Dolan 1972), as well as from interviews with the owner's engineering staff and original designers.

The connection was developed in SAP2000 using frame elements for the CIP concrete connection. Frame elements are also used for columns. Shell elements represent the concrete box girders, the beam hanger plates, and the steel crossheads. The structural model is shown in Figure 11 with the load paths *A*, *B*, and *C* as previously described. Figure 12 shows an extruded view of the same finite elements.

### **Preliminary Models and Benchmark Studies**

It is useful to develop several models of more simple structural systems before attempting to model an entire six-span continuous beamway segment. Benchmark studies help verify accuracy of the software, acquaint the author with intricacies of the software, and assess the sensitivity of model outputs to various model parameters. Finite element models were developed for structural systems with known experimental results. Special attention was paid to concrete behavior, bridge modeling tools, moving load analysis, and prestressing tools. There is ongoing error evaluation, which consists of quantifying error and identifying its sources. Error sources may include modeling, user, software, discretization, or numerical error. Preliminary model development is a parallel effort with model visualization. Highlights of the model development process are presented in subsequent sections.

#### **Benchmark Study: Simple Reinforced Concrete Beam**

Solid (3D) elements were initially explored for representing concrete because of their ability to represent local behavior (Figure 13).

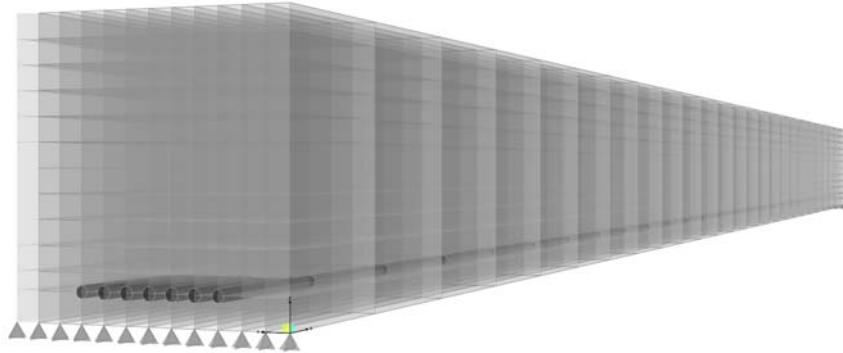


Figure 13: Simple Concrete Beam with Solid Elements

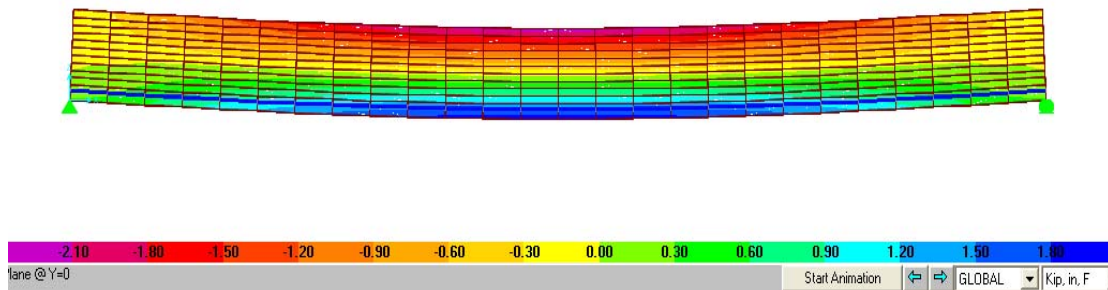


Figure 14: Solid Element Longitudinal Stress Contours in Bending

Solid elements in SAP2000 do not have rotational degrees of freedom activated. The three translational degrees of freedom are activated and the stiffness contributions are only in the translational DOFs (Computers and Structures Inc. 2004). In sharp contrast, shell (2D) and frame (1D) elements activate all six degrees of freedom (translation and rotation) at each connected joint. While a sufficiently refined mesh can approximate rotational behavior, meshing at solid/shell and solid/frame element interfaces would be difficult and development of connections would be significantly limited if solid elements were used for the beams.

Additionally, solid elements are computationally expensive. Consequently, although reasonable results are obtained for a beam in simple elastic bending (Figure 14), solid elements are disqualified from being the best choice to represent the concrete beams in the FEM.

### **Benchmark Study: Concrete Box Girder Bridge**

As the author worked with the finite element software, related documentation, and technical support personnel, an observation was made that shell elements would be a good choice to represent the concrete box girders of the beamway. Shell elements have the advantage over frame elements of representing local behavior. Although bridge models are often developed with frame elements with equivalent cross-sections representing the deck (Banchik and Jasper 2003; Zhang et al. 2001), the goal in this study was to develop additional resolution to capture local behavior at the connections.

A detailed benchmark study was undertaken to understand the details of bridge analysis in SAP2000. Shell elements are chosen for meshing the bridge deck. The benchmark study is presented in detail as Appendix G. For a conceptual understanding of the benchmark problem, three figures are presented. Figure 15 shows the three-span continuous multi-cell box girder. Undulating prestressing tendons are defined within the deck. Appendix G gives the details of parametrically defining the deck section, support conditions, and prestressing.

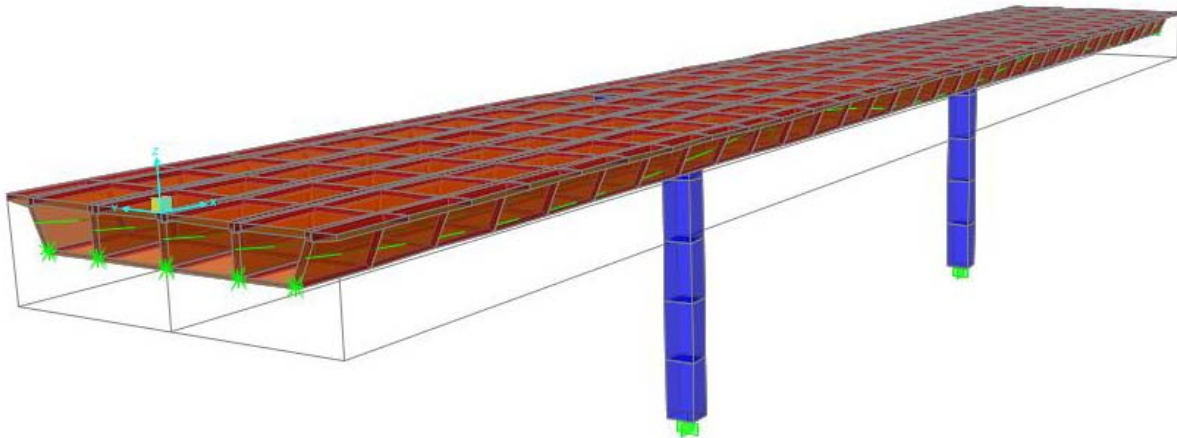


Figure 15: Benchmark Model - Box Girder Bridge

Figure 16 shows the bridge response/force output from SAP2000 for strong-axis bending and the AASHTO Strength I limit state. The bridge object response feature is a powerful tool in SAP2000 that calculates resultant load effects by integrating forces at sections along the length of the bridge object(Computers and Structures Inc. 2004). The moment envelope indicates minimum and maximum values from the moving load analysis. Figure 17 shows the corresponding shear envelope.

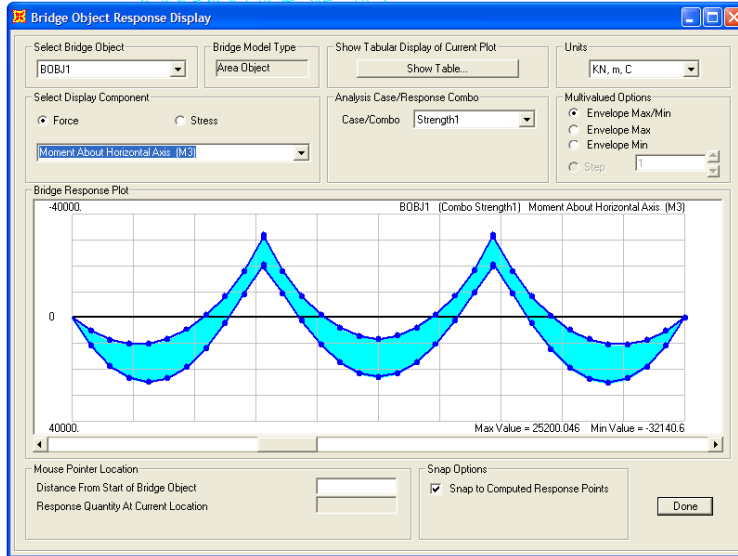


Figure 16: Benchmark Study Moment Envelope

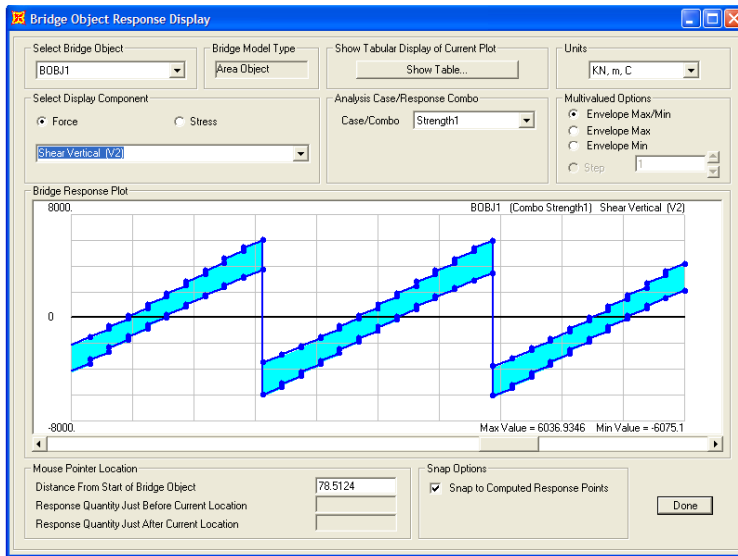


Figure 17: Benchmark Study Shear Envelope

The bridge response calculation is a powerful feature new to SAP2000 version 9. This approach will be used to extract load effects from the beamway model, for use in load rating reliability calculations.

## Steel Crossheads and Concrete Columns

At the same time that methods were being studied for modeling the superstructure, preliminary models were being developed to represent the steel crossheads and columns. An extruded view of one such model is shown as Figure 18. The superstructure is modeled using the SAP2000 bridge modeler, but only with simple frame elements. The parabolic variation of section depth is defined parametrically with the SAP2000 bridge design module. The software automatically generates frame elements with nonprismatic sections(Computers and Structures Inc. 2004).

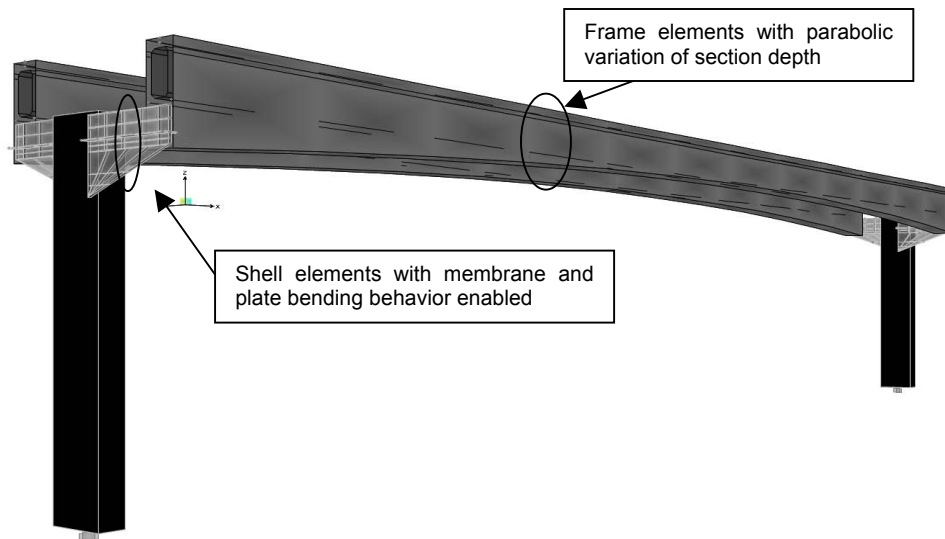


Figure 18: Single-Span Preliminary Model

The single-span preliminary model gives good results for stresses in the steel crossheads under a uniformly distributed live load of 1.2 klf on one span, plus self-weight in both spans, plus post-tensioning. Maximum tensile and compressive stress plots can be generated for the shell elements as in Figure 20. Maximum tensile stress (positive) contours are shown. Stresses in the crossheads approach a maximum value of approximately 15 ksi, discounting high stresses

in the upper left hand corner which are likely due to errors in modeling the beam-crosshead connection with a single rigid link. The values are important to observe in preliminary models, as well as the trends. The trend here is for maximum tension in the upper left side of the cross head, which follows the basic concept of a tension/compression couple, indicating in-plane bending of the shells.

The preliminary model with frame elements was extended to a two-span partial model with shell elements for beams and the fully developed connection (Figure 19). The beams and connection were developed on one side only, later duplicated to the opposite side of the crosshead. This model was used to refine the beam and prestress generation process in SAP2000, as well as to improve the connection details, including the crosshead mesh, defined in AutoCAD. In refining the various meshes, an effort was made to converge on stress patterns that made physical sense, as well as to check reactions and deflected shapes against expected values and trends.

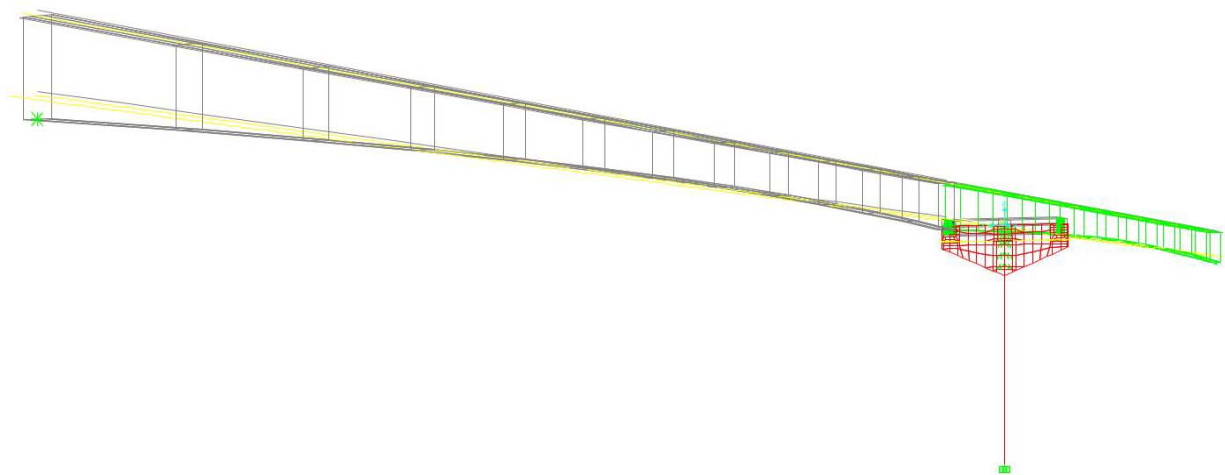


Figure 19: Connection and Adjacent Spans

The final refined mesh for the crosshead is shown in Figure 21, with horizontal in-plane stresses under dead load, and both parallel beamways in-place. Note that maximum tension is at the top fibers and maximum compression is at the bottom fibers, with a gradient in between. This makes physical sense as the plate is bending about its strong axis under symmetric dead load (self-weight). It is interesting to note the effects of the joint constraints (representing shear studs) in concentrating the stress in more flexible regions, between the beams and columns. The nodes of the tight mesh at the beam and column intersection match the shear stud pattern (see also Figure 26). It is also interesting to note the compressive stress concentrations at the small contact areas for the beam hanger plates, seen as four small strips, two resting on each side of the crosshead in Figure 21.

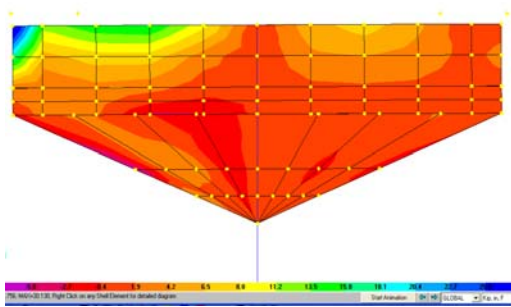


Figure 20: Early Steel Crosshead Mesh with Maximum Tensile Stress Contours

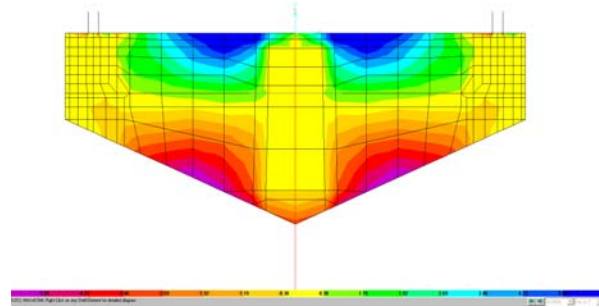


Figure 21: Refined Crosshead Mesh with Horizontal Stress Contours

### Post-Tensioning Tendons

For the preliminary single-span model described above, the post-tensioning load gives the bending moment diagram shown in Figure 22 for the beamway frames. Bending moment is plotted on the tension side of the frame elements. The trend observed in the diagram is

appropriate if we consider that the post-tensioning is designed to balance negative moment over the supports and positive moment at midspan for the six-span continuous bridge segment.

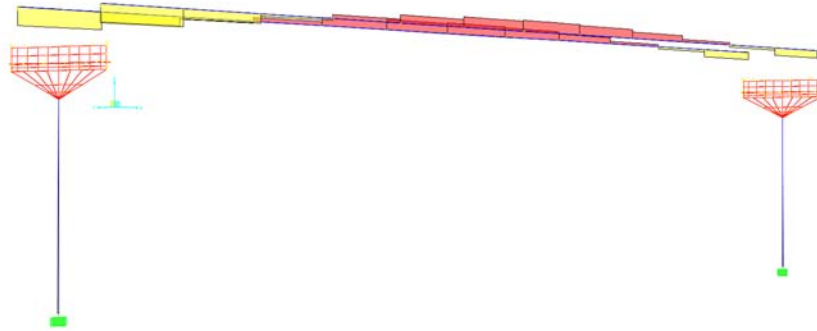


Figure 22: Bridge Frame Bending Moment under Post-Tension Load

As preliminary models and benchmark studies are developed, special attention is paid to identify key model parameters and parameter sensitivity, as convergence is sought to known solutions and expected trends. Model parameters may include element type, aspect ratio, mesh size, material properties, and boundary and continuity conditions. It is important to note how various model parameters affect the outputs. Model outputs include element stresses and bridge forces, deflections, and modal response (natural frequencies and mode shapes). The author considers the sensitivity of the various outputs to the various model parameters. Special attention is paid to modeling the structural connections, continuity, boundary conditions, and supports.

## CHAPTER FOUR: SIX-SPAN FINITE ELEMENT MODEL

A finite element model for the six-span bridge structure is developed as an extension of preliminary models and benchmark studies (Figure 23). Shell elements are used to represent the concrete box girders, steel hanger plates, and steel crossheads. Frame elements with nonprismatic cross-sections represent columns. Rigid links are used to fix the beam hanger plates to the precast beams and the columns to the crossheads. Joint constraints account from the increased rigidity from shear studs. In total, 6680 shell elements, 1450 frame elements, 708 link elements, and 4304 joint constraints are incorporated in the model with a total of 7785 DOFs.

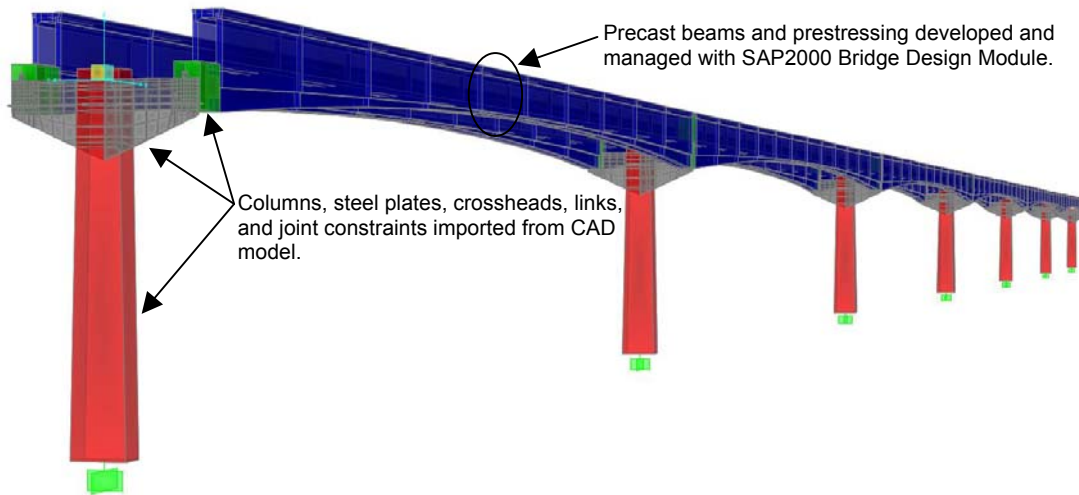


Figure 23: Six-Span Continuous Bridge FEM (Extruded View)

The twelve precast beams and associated pre-tensioning were developed and updated with the SAP2000 Bridge Design Module. Connection elements, including steel hanger plates, crossheads, links, constraints, and the columns were developed and updated in a CAD model, and imported into the finite element model, layer by layer, as required. The complex and repetitive geometry in the connections is easier to produce and maintain in the CAD software.

Geometric properties were calculated from the design drawings. The subsequent sections detail certain assumptions and choices made in developing the full six-span continuous model.

### **Superstructure**

The superstructure refers to the beamway that the trains ride on, principally the precast haunched beams and their associated prestressing elements. While many aspects of developing the beam model have already been discussed, additional items specific to implementation of the full model in SAP2000 are included in subsequent sections.

### **Beams**

The beam geometry and meshing were developed using the SAP2000 version 9.0.8 bridge design module. Shell elements were chosen to represent the beams for reasons discussed in the previous chapter, especially to develop the resolution required to capture local behavior at the connections. Shell elements give results at their neutral axis, which can then be integrated by the software to give resultant forces and moments at a particular section of interest. Extreme fiber stresses and strains are not computed directly, but may be found by additional computation if required.

The box beam section is parametrically defined using geometry from the design drawings. The cross-section is defined at midspan (Figure 24). The haunched beam profile was easily incorporated into the model by defining parabolic variations for overall beam depth and bottom flange thickness (Figure 25).

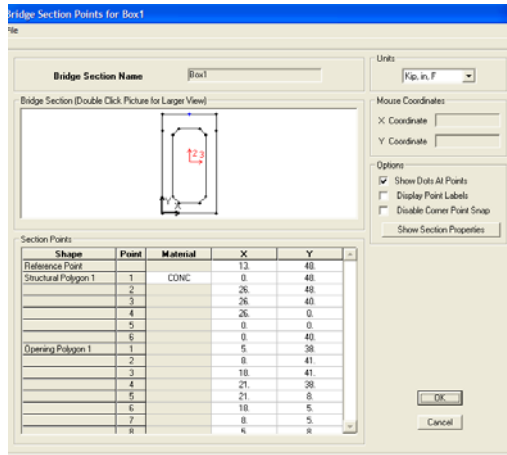


Figure 24: Beam Cross-Section Definition in SAP2000

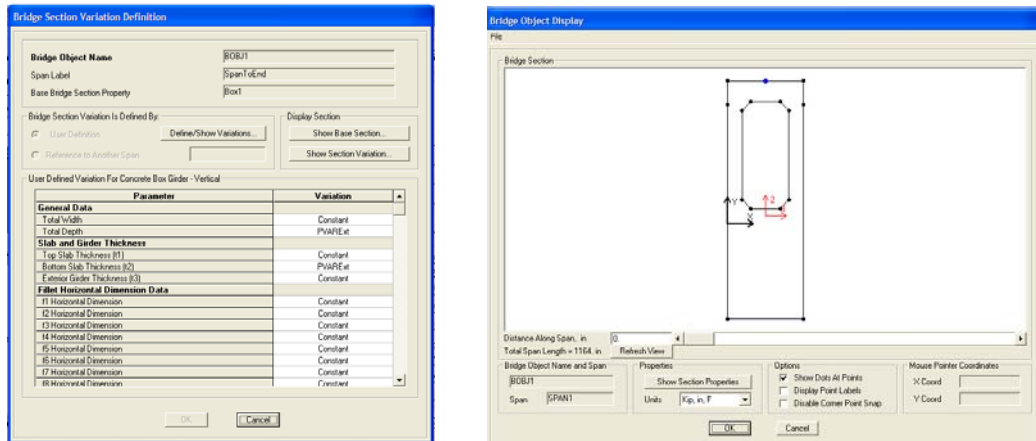


Figure 25: Parametric Variation of Section Depth

The beams are meshed by the bridge design module into segments of a maximum 120 in (10 ft) length. An automatic submesh of 70 in. is also assigned, essentially doubling the resolution of the beam models. No shell is longer than 60 in, which follows the recommended guidelines, to limit the aspect ratio as explained here (Computers and Structures Inc. 2004), analysis.

The aspect ratio of an element should not be too large. For the triangle, this is the ratio of the longest side to the shortest side. For the quadrilateral, this is the ratio

of the longer distance between the midpoints of opposite sides to the shorter such distance. Best results are obtained for aspect ratios near unity, or at least less than four. The aspect ratio should not exceed ten.

The 60 in shell element length provides the adequate aspect ratio, and was tested against finer meshes for convergence. The 60 in value was chosen to balance resolution and computation time.

The concrete unit weight is taken as 160 pcf from the original structural calculations and Poisson's ratio is taken as 0.2. The concrete modulus of elasticity,  $E_c$ , is an important parameter with significant variability. Treatment of  $E_c$  is discussed in subsequent sections.

### **Prestressing**

Twelve bridge objects were defined in the bridge design module, representing the twelve precast beams in a six-span continuous dual beamway. The pre-tensioning geometry was defined based on the design drawings.

The current version of SAP2000 only models bonded post-tensioning tendons (Computers and Structures Inc. 2004). The fundamental difference between the bonded pre-tensioning strands and the bonded post-tensioning tendons in the beamway is that the pre-tensioning strands were pulled and set at the plant before the surrounding concrete cured. To account for this in the SAP2000 model, the bonded pre-tensioning strands are modeled as post-tensioning, but with zero values for friction loss coefficients and anchorage slip.

The post-tensioning is defined independently of the bridge objects. To facilitate rapid model development, the post-tensioning tendons were drawn in the CAD software as lines and imported into SAP2000 as frame elements. Post-tensioning tendons were drawn over the frame elements, and the frame elements were then erased. While this process may seem awkward, it

was faster than trying to draw the tendons directly in SAP2000. Presently SAP2000 has no direct way to import tendons from AutoCAD.

Many researchers and professionals choose to neglect the effect of the prestress force on global structural behavior (Xu et al. 1997). However, because the prestress force is such an integral and important structural feature in the continuous beamway, the present study considers the effect of the prestress force (and, consequently, prestress loss) on static and dynamic structural behavior. This is accomplished by defining a nonlinear load case for prestress and self-weight to act on the structure with P-Delta effects enabled (Computers and Structures Inc. 2004). The resulting stiffness is used as the basis for all static and dynamic analyses. The P-Delta effect of the prestress force (axial compression) has the effect of reducing the effective stiffness of the beams in lateral and vertical bending. The prestress loss parameters are very important to the behavior of the structural model. The prestress loss parameters are defined and discussed in subsequent sections.

### **CIP Connections**

The development of the connection model is discussed previously in detail. The practical implementation of this model in SAP2000 involved the use of frame elements with concrete material properties and a total cross-sectional area equal to the cross-section of the CIP concrete. Rigid link elements are used to connect the ends of the two lower short concrete frames to the steel crosshead. The links are just long enough to span the distance between the end of the frame and the nearest node point in the crosshead mesh. The entire assembly is symmetric and frames into the beams at the shell nodes, so as not to introduce any secondary moments from the connection elements.

### **Steel Crossheads**

The steel crossheads are modeled in SAP2000 with shell elements. The thickness is defined from the design drawings and the material properties are the standard definitions for steel. Both membrane and plate behavior are enabled (Computers and Structures Inc. 2004). The crosshead shell mesh was developed in AutoCAD, imported into SAP2000 and run in simple span models. Initially, odd stress concentrations and other anomalies occurred. The mesh was improved in CAD and the analysis was run again. This process was iterated until convergence was attained. The magnitudes and signs of shell stresses were checked against expected values. The resolution was increased to reduce or eliminate discontinuities in the stress contours.

Edge constraints are generated for shells located at mesh intersections. Edge constraints eliminate the need for transition meshes at mesh discontinuities. The shells behave as if the mesh were continuous (Computers and Structures Inc. 2004).

### **Beam Hanger Plates**

The beam hanger plates were modeled in a similar manner as the steel crossheads. Rigid links were used to connect the hanger plates to the precast beams. In the real structure, the beam hanger plates are imbedded in the precast beam ends with shear studs. For the FEM, rigid links are defined between nodes representing the shear studs and nodes in the bottom flange of the precast beam at the beam face.

## Shear Studs on Crossheads

Shear studs are found on the steel crossheads to transfer shear through the cast-in-place connection as well as the precast columns (Figure 26). The shear studs develop shear in the concrete. They develop a composite section between the concrete and steel with significantly increased rigidity.

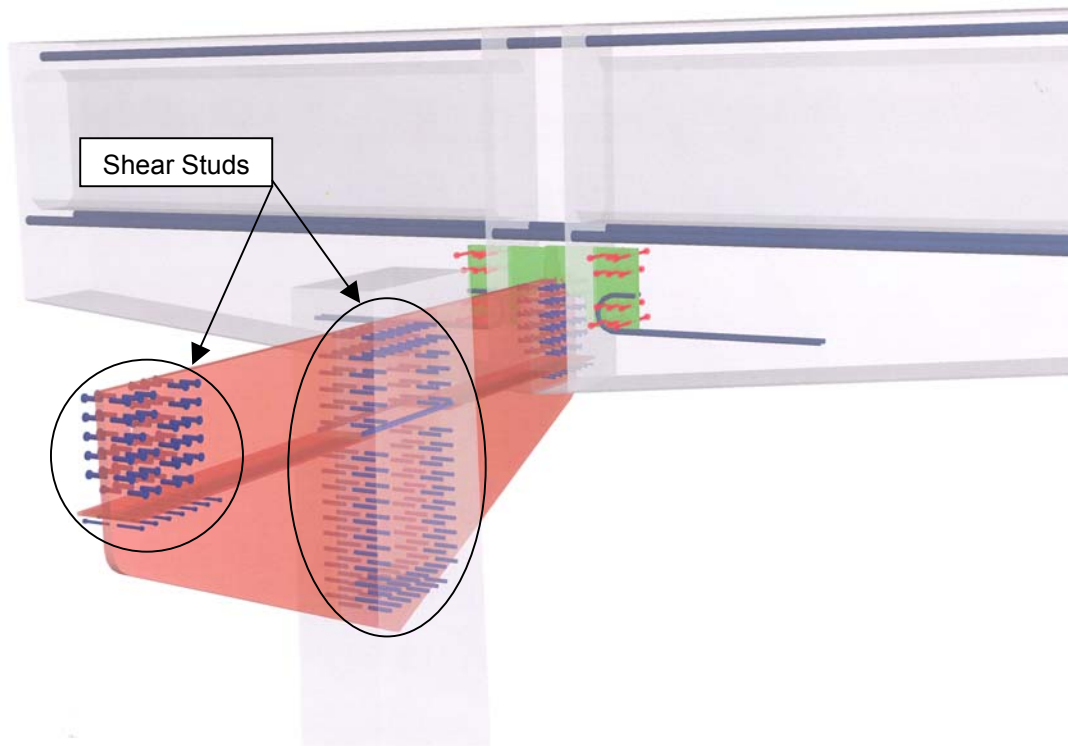


Figure 26: Shear Studs at CIP Connection

In order to represent the increased rigidity induced by the shear studs, rigid constraints were defined to represent each group of shear studs in SAP2000. The process of defining a new set of joint constraints for each group of shear studs for each crosshead was tedious. It was automated somewhat by defining the crosshead mesh and constraint points in AutoCAD. The points are imported and assigned rigid separate joint constraints for each group in SAP2000.

It is clear from Figure 26 that shear studs also exist to develop the connection between the steel hanger plates and precast beams. These shear studs are not represented by joint constraints in SAP2000. Instead, the connection is modeled as explained in the previous section. Rigid links connect the beam hanger shells at the shear stud locations to the precast beam shells at the beam face in the bottom flange.

### **Precast Columns**

The precast columns are modeled in SAP2000 as frame elements with nonprismatic cross-sections. Nonprismatic sections may be defined for which the properties vary along the element length. The variation of bending stiffness may be linear, parabolic, or cubic over each segment. The axial, shear, torsional, mass, and weight properties all vary linearly over each segment (Computers and Structures Inc. 2004). The reason to use the nonprismatic section is to accommodate the tapered column design. The geometry for center, typical, and expansion columns is taken from the design drawings. The concrete unit weight is taken as 160 pcf from the original structural calculations and Poisson's ratio is taken as 0.2. The concrete modulus of elasticity,  $E_c$ , is an important parameter with significant variability. Treatment of  $E_c$  is discussed in subsequent sections.

The column frame elements are discretized to mesh with the crosshead shell elements. Rigid links are used to connect the column frame nodes to the centers of the clusters of shear studs on the crossheads. The rigid links represent the embedment of the steel crossheads in the concrete columns.

The precast columns are rigidly connected to pile caps with grouted pipes. The pile caps develop the rigidity of the steel pile foundations. All the columns are considered fixed at the base for the finite element model.

### **Model Parameters**

Ideally, all possible parameters relating to the geometric, elastic, and inertial properties, as well as the boundary and continuity conditions should be considered for sensitivity studies and model verification (Zhang et al. 2001). However, if too many parameters, as compared to the number of measurements available, are considered, the possibility of obtaining an unreliable updated model may increase (Hjelmstad and Banan 1995).

In the process of developing the benchmark studies and full six-span FEM, the critical model parameters are noted. Special attention is paid to parameters representing material properties, prestressing force/loss, boundary conditions, and the beamway continuity condition over the columns. Some model parameters, such as the length of a beam or the unit weight of concrete, are well-characterized and deterministic. Other parameters, such as the prestress loss or concrete stiffness parameters, have significant uncertainty with their characterization. Different assumptions for these parameters are possible and, in some cases, these assumptions are critical to the behavior of the structural model.

In developing the preliminary models and full six-span model, key parameters were identified that significantly affect the structural response. The finite element model is used for static load analysis including moving loads, as well as eigenvalue modal analysis. The free vibration modes and frequencies depend on global parameters, including material stiffness,

prestress loss, and boundary and continuity conditions. Deflection, moment, and shear from static analysis are sensitive to these parameters as well.

### **Bounding Parameters for Sensitivity Studies**

As part of the present study, key parameters for stiffness, prestress loss, and boundary and continuity conditions were identified and bounded. The critical parameters were divided into one of four categories: (1) material properties; (2) prestress losses; (3) boundary conditions; (4) continuity conditions. A number of technical and academic references were combined with the original structural calculations and engineering judgment to bound parameters key. Nominal, lower-bound, and upper-bound values were determined and used to create eight models for sensitivity studies. The results of the parameter bounding process are presented in Table 3. Details of the parameter bounding process are discussed in subsequent sections.

Table 3: Parameter Bounds

<b>PARAMETERS / INPUTS</b>			
Stiffness Parameters	Nominal Value	Lower-Bound	Upper-Bound
Precast Beams $E_c$ (ksi)	3600	1600	5000
CIP Connection $E_{CIP}$ (ksi)	2600	1500	4500
Columns $E_{COL}$ (ksi)	2600	1500	4500
Prestress Loss Parameters			
Pre-tension loss (ksi)	45000	35000	53000
Post-tension loss (ksi)	30000	25000	35000
Curvature Coefficient $\mu$	0.2	0.15	0.25
Wobble Coefficient $K$ (1/ft)	0.0005	0.0003	0.002
Boundary Condition Parameters			
U1 Stiffness (kip/in)	0	-	326
U2 Stiffness (kip/in)	0	-	160
U3 Stiffness (kip/in)	0	-	979
R1 Stiffness (kip-in/in)	0	-	20026
R2 Stiffness (kip-in/in)	0	-	16840
R3 Stiffness (kip-in/in)	0	-	27743

## Concrete Modulus of Elasticity

The critical material property for analysis is the concrete stiffness, represented by the modulus of elasticity,  $E_c$ . In SAP2000, the concrete stiffness is controlled through the modulus of elasticity. The shear modulus is not directly specified in SAP2000, but instead is defined in terms of Young's modulus and Poisson's ratio (Computers and Structures Inc. 2004).

In some engineering materials, such as steel, strength and the stress-strain relationships are independent of the rate and duration of loading, at least within the usual ranges of rate of stress, temperature, and other variables. In contrast, effect of the rate of loading on the behavior of concrete is significant. The main reason for this is that concrete creeps under load, while steel does not exhibit creep under conditions prevailing in buildings, bridges, and similar structures (Nilson et al. 2004). When calculating deformations, a reduced modulus is used for long-term load (dead load). There is no way to simultaneously represent the reduced stiffness induced by long-term loads and the greater stiffness for live load response in one FEM. Instead, an attempt is made to come up with reasonable values for *effective stiffness*, which adequately represents the dynamic behavior and moving load response, but also considers the dead load influence. It is expected that the appropriate effective concrete modulus for use in the FEM lies somewhere between the instantaneous modulus for live load and the reduced modulus for long-term load.

Many expressions are given for the modulus of elasticity. There are expressions for the instantaneous modulus, as well as expressions that consider long-term loads and curing processes. Many expressions for the concrete modulus were adapted from academic and technical publications (AASHTO 2004; American Concrete Institute 2002; Barker and Puckett 1997; Nawy 2003; Nilson et al. 2004) and used to establish lower- and upper-bound values. A reasonable nominal value was selected using judgment, and based on assumptions in the original

calculations. Expressions for instantaneous and long-term modulus are generally given in terms of the compressive strength,  $f'_c$ . The nominal  $f'_c$  value for the beams (7000 psi), CIP connections (5000 psi), and precast columns (5000 psi) were used in the upper- and lower-bound expressions for  $E_c$  for each of these elements, respectively. The full set of calculations is included as Appendix A. Results are presented in Table 3.

### **Prestress Loss**

It is well-established that the initial prestressing force applied to a concrete element undergoes a progressive process of reduction. The reduction of the prestressing force can be grouped into two categories: (1) immediate elastic loss during fabrication and construction, including elastic shortening of the concrete, anchorage losses, and frictional losses (post-tensioning only); (2) time-dependent losses such as creep, shrinkage, and those due to temperature effects and steel relaxation. An exact determination of these losses is not feasible, because of the many interrelated factors and in imprecise understanding of their values (Nawy 2003).

Empirical methods for estimating losses are adapted from Nawy (2003), including Nawy's presentation of AASHTO and PTI methods. Appendix B gives the full set of prestress loss calculations. The methodology described above is used to generate lower-bound, nominal, and upper-bound values for prestress loss. As with the concrete stiffness, an effective set of loss parameters is developed, although their values may change locally over the length of the beamway, we are interested in their effect on global behavior. The loss parameters are constant over the length of the beamway, with the exception of the wobble coefficient, which influences the prestress loss linearly, from zero effect at the jacking end to full effect at the anchored end.

The prestress loss parameters are given in Table 3. The anchorage set slip of 0.75 in comes for the design assumption in the original structural calculations.

Tendon Load Assignment Data For Line Object 98	
Units: Kip, in, F	
Load Case	PostTen
Load Type	Force
Jack From This Location	I-End (Start)
Tendon End Force (Kip)	244.
Tendon End Stress (Kip/in <sup>2</sup> )	
Curvature Coefficient (Unitless)	0.2
Wobble Coefficient (1/in)	4.200E-05
Anchorage Set Slip (in)	0.75
Loss - Elastic Shortening Stress (Kip/in <sup>2</sup> )	5.
Loss - Creep Stress (Kip/in <sup>2</sup> )	10.
Loss - Shrinkage Stress (Kip/in <sup>2</sup> )	10.
Loss - Steel Relaxation Stress (Kip/in <sup>2</sup> )	5.

Figure 27: Tendon Assignments Including Prestress Loss

The prestress loss parameters are divided into elastic shortening stress, creep stress, shrinkage stress, and steel relaxation stress, in addition to curvature and wobble coefficient for friction, and anchorage set slip. SAP2000 adds the stress losses algebraically (Computers and Structures Inc. 2004), so it makes no difference how we split up the losses among the categories of elastic shortening, creep, shrinkage, and steel relaxation stress loss. For the nominal model, the losses are defined as shown in Figure 27. Note that the stress losses add to 30 ksi, which is the nominal value for post-tension loss given in Table 3.

### Time-Dependent Behavior of Concrete

SAP2000 allows the user to specify time-dependent material properties for creep, shrinkage, and aging effects. However, these properties can only be applied during a nonlinear staged-construction analysis (Computers and Structures Inc. 2004). The staged construction

module is sold as an addition to the SAP2000 Advanced software and we did not have this module available for this study.

The time-dependent properties were accounted for indirectly by two principle means. First, long-term prestress losses were defined explicitly to reduce the prestress force directly, including stress loss from effects of creep, shrinkage, and steel relaxation. Second, the lower-bound value for the modulus of elasticity for concrete accounts for long-term creep (Nawy 2003).

### **Boundary Conditions**

Each six-span continuous unit is connected to an adjacent unit by aluminum expansion joints. The connection ensures compatibility and consistent alignment between adjacent six-span bridge units. The expansion joint boundary condition introduces additional indeterminacy into the system. For one extreme case, the aluminum finger plates may slip freely and provide now significant end restraint. In the other extreme, the expansion joints may fully engage and lock, providing a near-rigid connection. Real behavior is likely in-between these extreme cases, and varies by location, environmental effects including temperature and humidity, and deterioration such as creep or settlement. In any case, the effect of the expansion joint on the boundary condition is reduced by the significant restraint provided by the expansion column and cast-in-place connection.

To approximate the restraint provided by expansion joints, a stiffness matrix is generated at the end of a six-span continuous unit. The direct stiffness method was used by inducing a unit displacement in all six DOFs. The reactions were recorded. The stiffness matrix is generated for

a joint on the crosshead, midway between the two links that connect the precast beam. Figure 28 shows the loading configuration for unit translation in DOF U1 (axial translation).

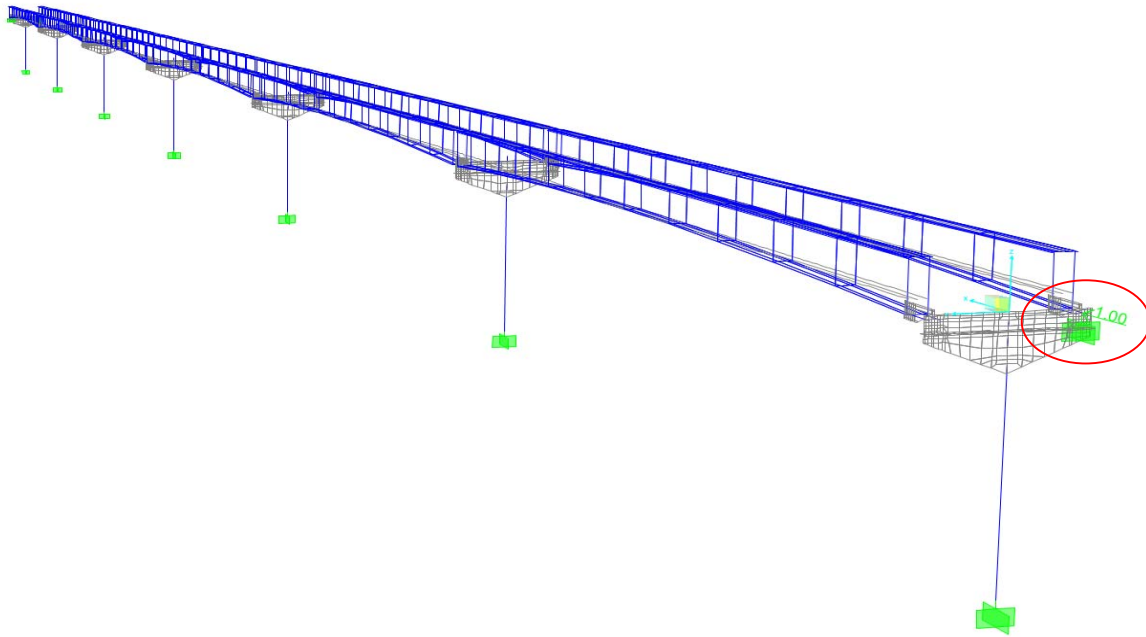


Figure 28: U1 Displacement Loading to Generate Stiffness Matrix

This method to determine equivalent stiffness contributions of an adjacent span was carried out for two cases. The first case is such that the beamway is unrestrained at the opposite end of the six-span continuous structure. The second case is such that the beamway is fully restrained at the opposite end. The results are given in Table 4 and Table 5.

Table 4: Boundary Condition Stiffness Matrix (Opposite End Unrestrained)

Unrestrained						
	U1 (kip)	U2	U3	R1 (kip-in)	R2	R3
Rx	119	1	3	0	8	-19
Ry	1	160	-291	9	0	24
Rz	3	-291	978	229	-15	-7
Mx	0	9	229	20026	-2	3
My	8	0	-15	-2	16839	15
Mz	-19	24	-7	3	15	27739

Table 5: Boundary Condition Stiffness Matrix (Opposite End Restrained)

Restrained						
	U1 (kip)	U2	U3	R1 (kip-in)	R2	R3
Rx	326	3	8	0	24	-44
Ry	3	160	-291	9	0	23
Rz	8	-291	979	229	-15	-8
Mx	0	9	229	20026	-2	3
My	24	0	-15	-2	16840	14
Mz	-44	23	-8	3	14	27743

The only stiffness value to vary significantly from the unrestrained case to the restrained case is axial translation stiffness (U1). The higher value is used, on the basis of choosing the upper-bound case. This value may be adjusted by model calibration in future studies, if determined to be a significant parameter by sensitivity studies.

When defining stiffness in the structural model, the effect of the adjacent six-span continuous beamway unit is approximated by six springs representing the six DOFs. To facilitate model calibration, the stiffness in each DOF is uncoupled (off-diagonal stiffness values are ignored). The stiffness definition in SAP2000 is shown in Figure 29. These stiffness values define the upper bound condition at the expansion joints, assuming the connection is fully continuous. The nominal stiffness values are defined by zero stiffness, corresponding to a free connection with negligible stiffness contributions from the expansion plates. The expansion joint is expected provide negligible restraint in the field.

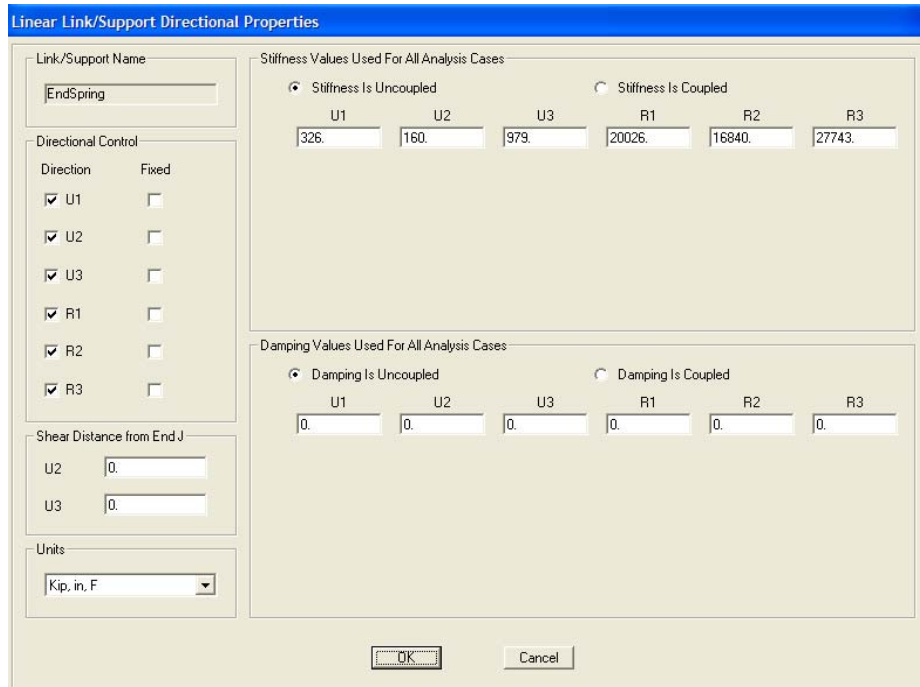


Figure 29: Boundary Condition Definition in SAP2000

### Continuity Condition

Recalling the development of the connection model, frame elements were used to represent the cross-sectional area of the CIP concrete. Two frame elements connect the bottom flange of the box beam to the steel crosshead. Two additional frame elements connect the top flange directly to the adjacent beam. The free-body diagram representing these engineering assumptions is shown in Figure 10. The lower left frame element is omitted for clarity.

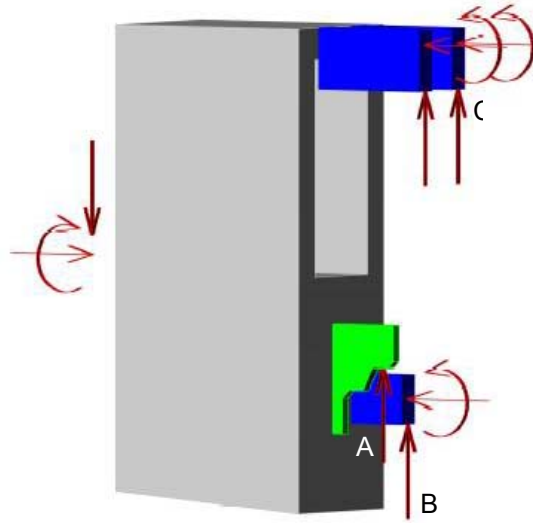


Figure 30: Free-Body Diagram (Precast Beam End)

This configuration mimics the indeterminate connection by dividing beam shear between reaction *A* at the hanger plate and reaction *B* in the CIP concrete. The proportion of load passing through paths *A* and *B* is adjusted by adjusting the stiffness parameters. The most straightforward adjustment is made by changing the modulus of elasticity,  $E_{CIP}$ , for the cast-in-place concrete at the connection. A lower value of  $E_{CIP}$  forces more load through the beam hanger plate and softens the connection overall. Increasing  $E_{CIP}$  increases the load resisted by the CIP concrete and stiffens the connection overall.

The modulus of elasticity is defined independently for the CIP connection, the precast beams, and the columns. For the upper-bound and lower-bound continuity conditions, all the parameters are held at nominal values, while the CIP connection is defined with the upper-bound and lower-bound values for modulus of elasticity, given in Table 3 as  $E_{CIP}$ .

## CHAPTER FIVE: MODAL ANALYSIS AND PARAMETER SENSITIVITY

### Modal Analysis

Eigenvalue analysis (modal analysis) determines the undamped free-vibration mode shapes and frequencies of a given structural system. In SAP2000, eigenvalue analysis involves the solution of the generalized eigenvalue problem:

$$[K - \Omega^2 M] \Phi = 0$$

where  $K$  is the stiffness matrix,  $M$  is the diagonal mass matrix,  $\Omega^2$  is the diagonal matrix of eigenvalues, and  $\Phi$  is the matrix of corresponding eigenvectors, or mode shapes (Computers and Structures Inc. 2004).

The modal analysis case for the beamway is defined such that it uses the stiffness at the end of a nonlinear case accounting for the P-delta effects of the prestress force. This approach was recommended by technicians at Computers and Structures, Inc. as the best way to account for the prestress force effects on the stiffness and, consequently, the frequencies and mode shapes. Eight models defined with the parameter bounds described in the previous chapter are analyzed to determine trends, critical parameters, and modal sensitivity to those parameters.

Modal analysis is used to measure the impact of parameter variations on the frequency characteristics of a bridge by incrementally changing one parameter at a time, neglecting any cross sensitivities. The frequencies and mode shape vectors provide the best global indications of structural condition and structural behavior (Catbas and Aktan 2002). Results of the modal analysis may be used to plan a field verification plan or long-term monitoring program. A flowchart that shows a procedure for manual FEM calibration using modal analysis is given in Aktan et al. (1998).

### **Selection of Modes**

Zhang et al. (2001) gives practical recommendations for selection of relevant modes. For the case of long-span bridge response to wind excitation, inclusion of the lowest few vertical-dominant, horizontal-dominant, and torsional-dominant deck modes recommended. The response of the bridge can be quite accurately spanned by the lower modes. For seismic response prediction, those modes dominated by motions of the towers or piers should also be taken into account. The in the areas of structural health monitoring and damage detection, it is found that higher modes are more sensitive to local damage. Indeed, it would be ideal to match as many modes as possible between the measurement and FEM prediction. However, it does not seem logical to include higher modes that cannot be obtained reliably from either the measurement or the FEM analysis.

For the present study, a sufficient number of modes will be reported such that all the characteristic responses are represented. For the six-span continuous beamway, the following characteristic responses are identified: (1) vertical beam bending; (2) lateral beam bending; (3) weak-axis column bending/longitudinal oscillation of beamways; and (4) strong-axis column bending.

### **Preliminary Moving Load Analysis**

In addition to the modal analysis, a moving load analysis was conducted using empty Mark IV trains. The moving load analysis was performed to give deflections under the empty train, for use in planning field tests, to verify the order of magnitude of results, and to add to the understanding of critical parameters and parameter sensitivity. Both the modal analysis and the

moving load analysis were conducted for all eight parametric models, with goal of capturing lower-bound and upper-bound behaviors.

### **Parameter Sensitivity Studies**

Eight parametric models were developed based on the parameter bounding process described previously. The goal of all the studies presented is to gain an understanding of lower-bounds and upper-bounds for structural behavior and response to load.

The first model has all nominal parameters. The second and third models are defined with lower-bound and upper-bound values for concrete stiffness ( $E_c$ ,  $E_{CIP}$ , and  $E_{COL}$ ). The fourth and fifth models are defined with the lower-bound and upper-bound prestress loss parameters. The sixth model is defined with the upper-bound boundary condition. The seventh and eighth models represent the lower-bound and upper-bound continuity conditions at the supports, with lower-bound and upper-bound values used for  $E_{CIP}$ . The specific parameter values are given in Table 3.

### **Results**

Eigenvalue analysis of the beamway in SAP2000 gives natural frequencies in the range from 0.73 Hz to 2.99 Hz for the first 20 modes of the nominal model. In general, the mode shapes of the bridge could be classified as exhibiting lateral beam bending, vertical beam bending, longitudinal bridge oscillation, and transverse bridge sway. Examples of these behaviors are shown graphically in Figure 31.

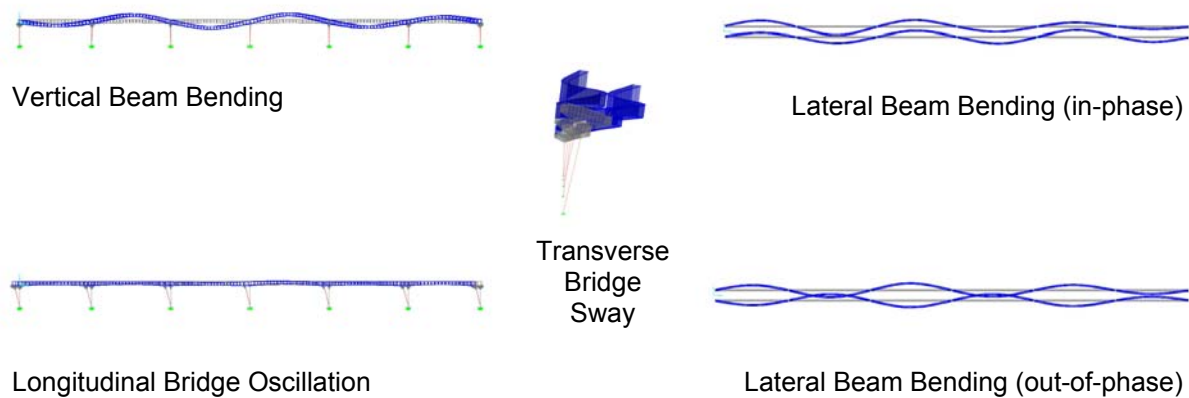


Figure 31: Distinct Modal Behaviors

Appendix C gives tables with frequencies along with graphical representations and text descriptions of mode shapes for all eight parametric models. The tables have certain colors highlighted to indicate the emergence of pure modal behaviors at their lowest frequency. For example, longitudinal modes may be classified as pure longitudinal modes and modes associated with other vibrations (Xu et al. 1997). The pure longitudinal modes mean that they have distinct frequencies and modal configurations, while the other modes participate in lateral, torsional, and vertical modes only. The first pure longitudinal mode was found to occur at a natural frequency of 1.037 Hz.

The results of the modal analysis as well as the moving load analysis for each of the eight models are summarized in Table 6. The first occurrences of the pure modes are included the table, including lateral beam bending, longitudinal bridge oscillation, transverse bridge sway and vertical beam bending.

Table 6: Modal and Static Analysis Results

OUTPUTS / RESULTS					
Model and Description	First Mode Free Vibration Frequency (Hz)	First Longitudinal Oscillation Frequency (Hz)	First Vertical Bending Frequency (Hz)	First Transverse Bridge Sway Frequency (Hz)	Maximum Deflection Under Train Load (in)
Nominal	0.735	1.037	2.340	1.684	-0.919
Ec Lower-Bound	0.114	0.805	1.434	1.104	-2.464
Ec Upper-Bound	0.998	1.328	2.809	2.074	-0.642
Prestress Loss Lower-Bound	0.680	1.031	2.322	1.675	-0.927
Prestress Loss Upper-Bound	0.877	1.038	2.397	1.716	-0.899
Boundary Condition Upper-Bound	0.816	2.216	2.377	1.700	-0.905
Continuity Condition Lower-Bound	0.734	1.035	2.339	1.637	-0.934
Continuity Condition Upper-Bound	0.736	1.039	2.341	1.714	-0.910

The modal analysis results are presented graphically in Figure 32. Each colored bar represents the free vibration frequency at the first occurrence of the four distinct modes shown in Figure 31. Maximum deflection under the empty Mark VI train load is given in Figure 33 for the eight parametric models. The tabulated deflection values correspond to a joint at midspan of the third precast beam.

Deflection data was provided by the owner for three test runs with empty Mark VI trains on a segment of the beamway built in 1982. The 1982 beamway is very similar to the 1971 beamway modeled in the present study. A few design details are different, most notably the solid beam ends (void is not continuous throughout). This was the best data available for this study and is useful to consider because the two beamway designs are so similar. The three graphs of data provided by the owner are included as *Appendix D: Static Deflection Results*. The three test runs give a maximum deflection of approximately 0.65 in, 0.8 in, and 0.75 in,

respectively. Taking an average of these results, we obtain a maximum deflection of approximately 0.7 in.

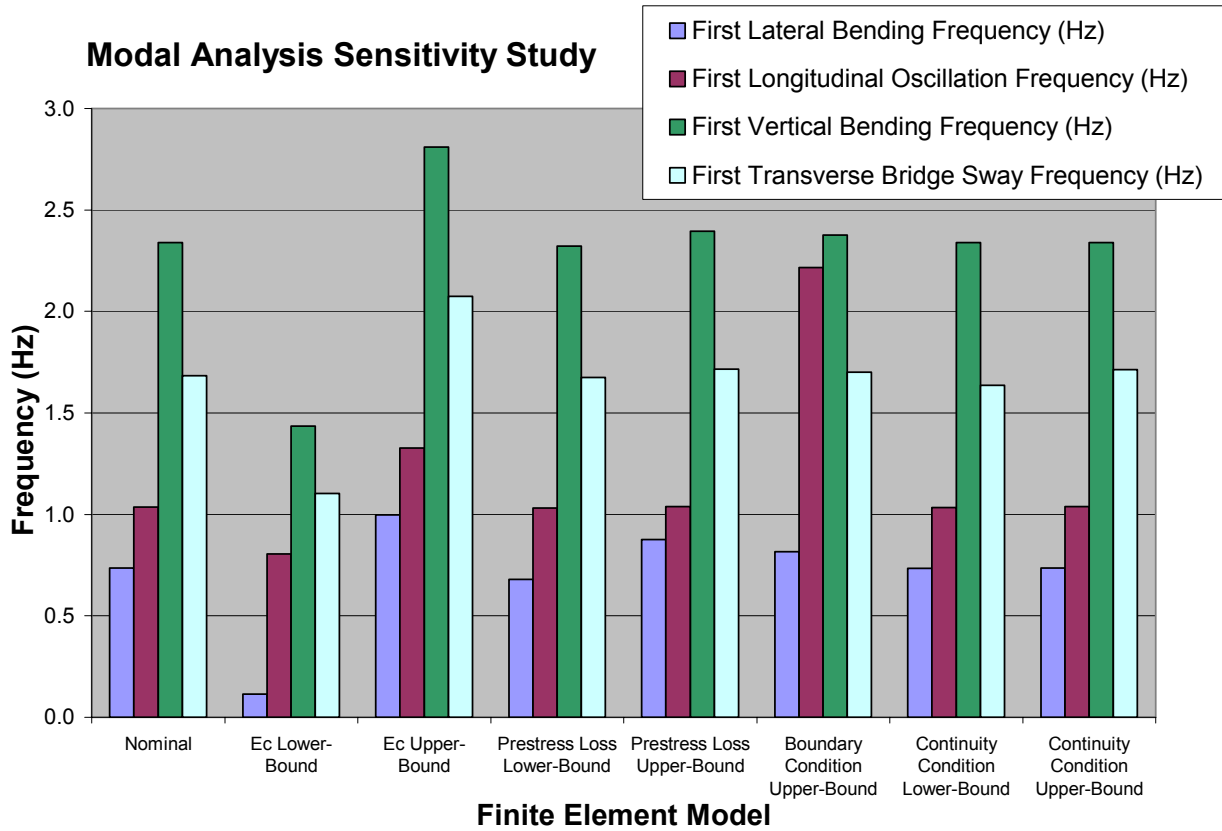


Figure 32: Modal Analysis Sensitivity Study

### Discussion

The results demonstrate significant sensitivity of the outputs to the concrete modulus,  $E_c$ . The deflection under train load varies by more than 1.5 inches for different values of the modulus. The first mode frequency varies by more than 0.5 Hz. The upper-bound boundary condition also has significant effect on the dynamic response. It requires much more energy to overcome the longitudinal resistance, so we see the first longitudinal mode occur at a much higher frequency when the boundary condition is enforced. The effect of the upper-bound

boundary condition results in *modal switching*; whereby the longitudinal oscillation and transverse sway modes switch in order of appearance (in terms of lowest to highest frequency). The static and dynamic outputs are less sensitive to the prestress loss and continuity condition parameters.

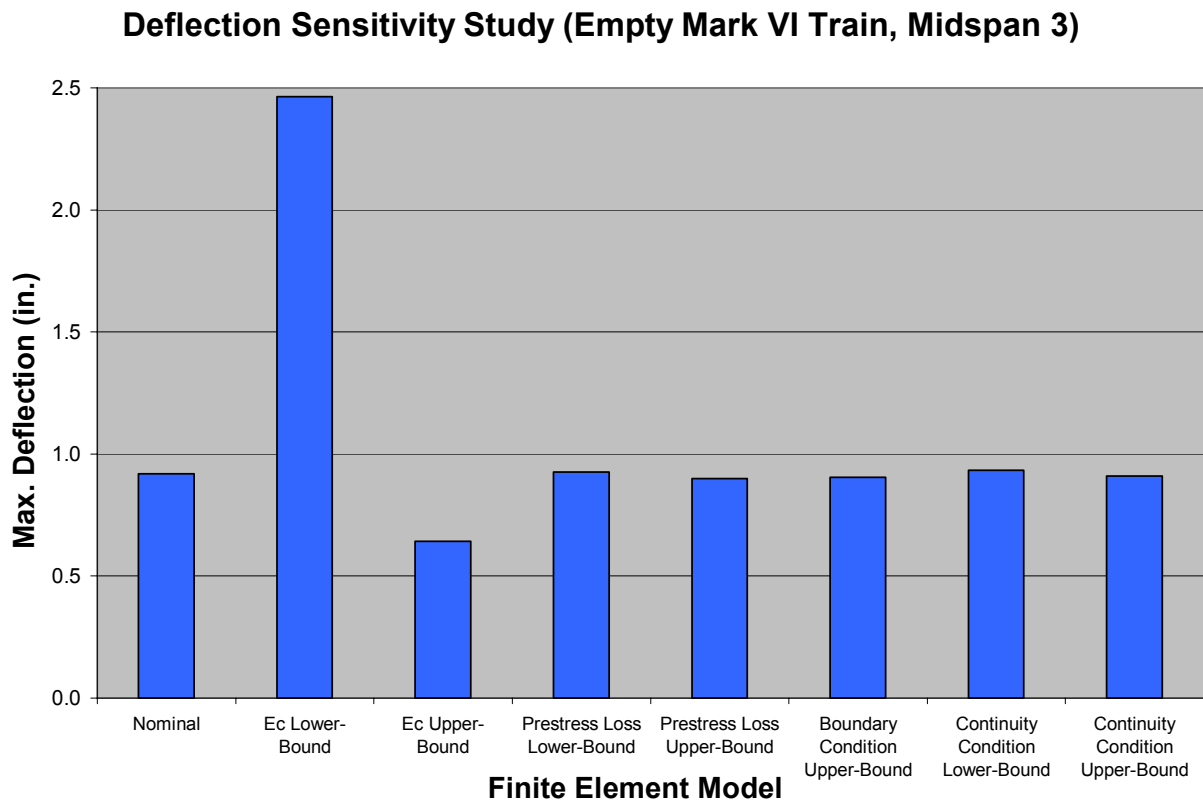


Figure 33: Moving Load Sensitivity Study Results

It is interesting to note that the 0.7 in. deflection measured by the owner falls between the deflection results for the nominal model (0.64 in) and the upper-bound stiffness model (0.92 in). The experimental result is closest to the upper-bound stiffness model. The upper-bound stiffness model may represent the most realistic response to live load as it uses the instantaneous value for

$E_c$ . It is well-established that concrete beams have a higher effective modulus of elasticity for live load deflection than dead load deflection. This is because of the influence of creep strain under long-term dead loads. Consequently, the lower-bound stiffness model is not realistic for deflection under live load. The excessive deflections represented in the lower-bound stiffness model probably do not occur in the real structure. The upper-bound value for  $E_c$  is based on the nominal compressive strength. The in-situ concrete is likely stronger and, consequently, even stiffer than the upper-bound stiffness case considered in this sensitivity study.

Although the 0.7 in. deflection result is measured on a different beam and the results are limited, it is reassuring to know that the experimental deflection is of the same order-of-magnitude as the FEM prediction. The close correspondence to the upper-bound stiffness model makes sense for live load deflections, and the knowledge of the 0.7 in. deflection provides limited validation of the FEM with upper-bound stiffness for live load deflections. It is recommended that comprehensive modal testing be pursued for a more objective and comprehensive model calibration and validation.

## CHAPTER SIX: SIMULATIONS, LOAD RATING AND RELIABILITY

Results are presented for the load rating and reliability analysis, following the AASHTO LRFR methodology and structural reliability theory. Resistance calculations are based on the AASHTO LRFD methods, including the Modified Compression Field Theory for shear capacity. Simulations are conducted using the eight parametric models. Load effects are derived from the FEM output. Critical limit states are identified as well as trends in the data and the physical meaning of the results.

### **Reliability Index and Probability of Failure**

Calibration of the current *AASHTO LRFD Bridge Design Specifications* (LRFD Code) is based on a reliability analysis procedure (Nowak 1995; Nowak and Collins 2000). Structural performance is measured in terms of the reliability or probability of failure. In the context of reliability analysis, failure is defined as the realization of one of a number of predefined limit states (Barker and Puckett 1997). An alternative method for expressing probability of failure is to use the reliability index,  $\beta$ . For normally distributed random variables  $R$  and  $Q$ , it can be shown that the probability of failure is related to the reliability index as follows,  $P_f = \Phi(-\beta)$ . If the random variables are all normally distributed and uncorrelated, then this relationship between  $\beta$  and  $P_f$  is exact. Otherwise, this expression provides only an approximate means of relating the probability of failure to the reliability index,  $\beta$ . The reliability index is a common metric used to quantify how close a design code or specification is in achieving its objective (Nowak and Collins 2000).

The LRFD Code provisions are formulated such that new structures will have a consistent and uniform safety level. The basic design formula is:

$$\sum \gamma_i \cdot Q_i < \Phi \cdot R_n$$

where  $Q_i$  = nominal load effect i  
 $\gamma_i$  = load factor i  
 $R_n$  = nominal resistance  
 $\Phi$  = resistance factor

In the LRFD Code calibration, load and resistance are treated as random variables and are described by bias factors ( $\lambda$ ) and coefficients of variation ( $V$ ). Resistance factors,  $\phi$ , are calculated so that the structural reliability is close to the target value  $\beta_T = 3.5$  (Nowak 1995).

An expression for the reliability index,  $\beta$ , is developed for the present study. A linear limit state function is assumed, following Eq. (5.18) (Nowak and Collins 2000):

$$\beta := \frac{a_0 + \sum_{i=1}^n (a_i \cdot \mu_{X_i})}{\sqrt{\sum_{i=1}^n (a_i \cdot \sigma_{X_i})^2}} \quad \text{for the linear limit state function of the form,}$$

$$g(X_1, X_2, \dots, X_n) = a_0 + a_1 \cdot X_1 + a_2 \cdot X_2 + \dots + a_n \cdot X_n$$

This expression must be adapted for the current study, considering load effects and resistance in bending and shear. The limit state function is developed in terms of resistance and load effects for the AASHTO Strength I limit state:

$$g(M_{Res}, M_{DL}, M_L) = M_{Res} - M_{DL} - M_L$$

where  $M_{Res}$  = nominal moment resistance  
 $M_{DL}$  = dead load effect  
 $M_L$  = live load effect

The corresponding reliability index is:

$$\beta := \frac{\mu_R - \mu_{DL} - \mu_L}{\sqrt{\sigma_R^2 + \sigma_{DL}^2 + \sigma_L^2}}$$

A similar expression is developed for shear:

$$g(V_n, V_{DC}, V_{LL\_IM}) = V_n - V_{DC} - V_{LL\_IM}$$

where  $V_n$  = nominal shear resistance  
 $V_{DC}$  = dead load effect  
 $V_L$  = live load effect

The limit state functions are valid as long as each load effect can be stated in terms of only one random variable. Statistical parameters for load and resistance tend to be given in terms of load effects (Nowak 1995; Nowak and Collins 2000) and are available for the present study. Subscripts may seem inconsistent between moment and shear. This is only to accommodate the need for unique subscripts in the MathCAD files. A full set of reliability analysis calculations can be found in *Appendix F: Load Rating and Reliability Analyses*.

### **Load Rating**

The AASHTO LRFR Manual prescribes three methods for evaluating the safe maximum live-load capacity of bridges (LRFR 6.1.6): (1) load and resistance factor rating of bridges; (2) load rating by load testing; (3) safety evaluation using structural reliability methods for special cases. The load and resistance factor rating is given generally as LRFR Eq. (6-1):

$$RF = \frac{C - \gamma_{DC} \cdot DC - \gamma_{DW} \cdot DW - \gamma_P \cdot P}{\gamma_L \cdot (LL + IM)} \quad \text{Eq. (6-1)}$$

where  $C$  = capacity  
 $\gamma_x$  = load where x represents  
the particular load or load effect  
 $DC$  = dead-load effect due to structural components and attachments  
 $DW$  = dead-load effect due to wearing surface and utilities  
 $LL$  = live-load effect  
 $IM$  = dynamic load allowance  
 $P$  = permanent loads other than dead loads  
(P term is added or subtracted for maximum effect)

This rating factor indicates reserve live load capacity. It may be simplified conceptually as the *capacity minus dead-load demand, all over live-load demand*. If there is no reserve live-load capacity, then the rating factor is 1.0. Additional live-load capacity is indicated by rating factors greater than 1.0. The AASHTO load rating is a global expression of capacity, limited by the critical behavior (Cai and Shahawy 2003).

Load rating will be developed according to the AAHSTO LRFR methodology. For design load rating of concrete structures, the LRFR Manual prescribes the following limit states for load rating (LRFR 6.5.4.1), “The Strength I load combinations shall be checked for reinforced concrete components. The Strength I and Service III load combinations shall be checked for prestressed components.” With regard to fatigue, the commentary (C6.5.4.1) states, “Fatigue is not a concern until cracking is initiated. Hence, prestressed components need not be routinely checked for fatigue.”

A choice is made to check only the Strength I limit state in the present study. The Service III limit state is intended to limit cracking due to exclusion vehicles (LRFD C3.4.1), which are not a concern on the beamway because the monorail train loading is well-characterized. The beamway is not subject to any other significant loads or overloads analogous to exclusion vehicles on highway bridges. Adapting the Service III limit state to the beamway to consider cracking would make for an interesting future study.

### **Live Load Factor**

A special load factor was developed for the monorail train live load. Conventional live load factors for AASHTO LRFD/LRFR were determined for HL-93 loading. The inventory and operating design load rating factors ( $g = 1.75$  and  $g = 1.35$ , respectively) seemed overly

conservative for the beamway application. There is substantial uncertainty involved with developing one model (HL-93) to represent the wide array of highway truck loading. It is believed that the scatter in monorail train loads is significantly less, and there must be a rational basis to compute a more appropriate load factor for design and rating. The calculation that follows is excerpted from Appendix F:

Assume the following expression for load factor (Nowak, 1993):

$$\gamma := \lambda \cdot (1 + k \cdot \text{COV})^2$$

Where  $\gamma$  = load factor

$\lambda$  = bias factor

COV = coefficient of variation

k = constant

From Barker (1997):

$$\lambda := \frac{x_m}{x_n}$$

Information from the owner gives the following:

$x_m := 122753\text{lb}$  mean value of Mark VI empty train weight (based on weight data collected in 2000 for all 12 trains)

$x_n := 122753\text{lb}$  nominal or design value used in SAP2000 will be the mean axle weights from the measured data

Bias factor:

$$\lambda_{LL} := \frac{x_m}{x_n} \quad \lambda_{LL} = 1 \quad \text{Note: There is no bias because the analysis values are equivalent to the measured values.}$$

Coefficient of variation:

From weight data provided by owner (2000 adjusted weight data), we assume the highest (most conservative) COV associated with the twelve train axles, and apply to the maximum load effect,

$$\text{COV}_{LL} := 0.0251698$$

Assume  $k := 2.5$  This is the upper-bound (conservative) value for LRFD Code calibration (Nowak, 1993)  
 Then the appropriate load factor for Mark VI train loads:

$$\gamma_{LL} := \lambda_{LL} (1 + k \cdot COV_{LL}) \quad \gamma_{LL} = 1.06$$

However, the lowest live load factor given in AASHTO LRFR for permit vehicles is 1.10. As a conservative assumption, assume 1.10 as a lower-bound value to account for additional uncertainties,

$$\gamma_{LL} := 1.10 \quad \text{lower-bound for permit vehicles} \quad \text{LRFR Table 6-6}$$

### **Design vs. Load Rating**

Bridge design and rating, though similar in overall approach, differ in important aspects. Bridge ratings generally require the engineer to consider a wider range of variables than is typical in bridge design. Design may adopt a conservative reliability index and require comprehensive serviceability and durability checks. In rating, the target reliability is reduced and application of the serviceability limit states is done on a more selective basis. The added costs of overly conservative evaluation standards can be prohibitive as load restrictions, rehabilitation, and replacement become increasingly necessary (AASHTO 2003).

The rating procedures presented in the *AASHTO Manual for Condition Evaluation and Load and Resistance Factor Rating (LRFR) of Highway Bridges* (AASHTO 2003) are intended to reflect a balance between safety and economics. As such, a lower target reliability than design has been chosen for load rating at the strength limit state. While the LRFD Code calibration reported  $\beta_T = 3.5$ , the LRFR Manual adopts a reduced target reliability index,  $\beta_T$  of approximately 2.5, calibrated to past AASHTO operating level load rating. This value was chosen to reflect the reduced exposure period, consideration of site realities, and the economic considerations of rating vs. design (AASHTO 2003). The reduced target reliability is reflected in the reduced live load factor for Design-Load Rating at the Operating Level for the Strength I

Limit State,  $\gamma_{LL} = 1.35$  [LRFR 6.4.3.2.2],  $\beta_T = 2.5$ . This may be compared with the LRFD Code Strength I live load factor,  $\gamma_{LL} = 1.75$  [LRFD Table 3.4.1-1],  $\beta_T = 3.5$ .

### **Relationship between Load Rating and Reliability**

For probabilistic design specifications such as the LRFD Code, the rating factor and reliability should be highly correlated, because a target reliability index,  $\beta_T$ , is used to calibrate the design and rating factors. While it is clear that relationships between reliability and rating form the basis of load and resistance factors for bridge components (elements), very good correlation has also been demonstrated between rating factors and reliability indices for bridge systems (Akgul and Frangopol 2003). In order to compare ratings against predicted reliability over the life of the bridges in a network, Akgul and Frangopol (2003) calculated rating values and reliabilities over the lifetime, in a continuous manner, based on deterioration and live load models. Resulting relationships between ratings and reliabilities of existing bridges in a network can be used to determine optimum maintenance strategies at the network level.

### **Simulations, Load Rating and Reliability**

Once sufficient reliability is demonstrated for the resistance calculations and FEM outputs, loading simulations are performed with the eight parametric FEMs developed and described in previous chapters. The critical load effects for dead load and live (train) load were extracted from the finite element analysis results at the locations shown in Figure 34. The load effects were compared against moment and shear capacities calculated following the methods of the AASHTO LRFD Bridge Design Specifications (AASHTO 2004). Load ratings following the AASHTO LRFR (AASHTO 2003) methodology were calculated. A reliability analysis was

performed. The reliability index,  $\beta$ , was calculated and, assuming normal distribution of random variables, the equivalent probability of failure,  $P_f$  was found.

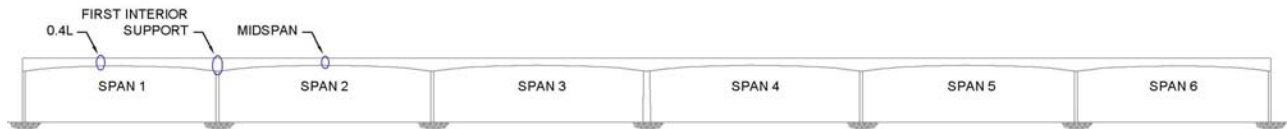


Figure 34: Critical Locations for Moment and Shear

The present study considers two train loads, in addition to dead load (self-weight of structural components) and prestress loads. The two train loading configurations represent the original Mark IV train and the current Mark VI train. A vertical point load is defined for each axle in the SAP2000 moving load analysis.

The Mark IV train axle loads are all 10.6 kip axle loads, as assumed in the original design calculations held by the owner. Mark VI train axle loads are based on mean values for axle loads determined by weighing all twelve trains in the year 2000. Fifty-five passengers at 155 lb each are assumed for each train car. This is the design loading used to evaluate the beamway for new trains purchased in 1989. The fifty-five passenger load is divided evenly among each of the two axles in each car. Additionally, five passenger-weights are added to the first and last axle of the Mark VI trains to simulate a full cab (pilot plus four passengers).

Appendix E includes the two tables that SAP2000 uses to define the Mark IV and Mark VI train loads and axle spacing. These tables are extracted from SAP2000 and may be quickly modified using the *Interactive Database Editing* feature. SAP2000 sends the vehicle load table to Excel, the user enters or pastes new values into the spreadsheet, and SAP2000 applies the new values to the model. The values shown in the bottom portion of Table 18 reflect the Mark VI loading assumptions described above.

## **Load Distribution**

The finite element models developed in this study are intended to represent the current or in-situ structural condition. The distribution of live load is modeled directly by the FEM. However, the dead load (self-weight) distribution in the beams is more complicated. The dead load distribution is a function of changing continuity conditions associated with the construction sequence.

Consider the construction sequence described in previous chapters; the beams were precast and pre-tensioned in a manufacturing plant and then simply-supported on the steel crossheads. Consequently, the initial moment distribution in the beams for dead load may be represented by a simply-supported model in which maximum moment occurs at midspan and zero moment occurs at the supports. After initial erection of the precast beams, the cast-in-place connections are placed and the post-tensioning strands are jacked to create the six-span continuous beamways. Over time, significant creep and shrinkage are presumed to have occurred, causing some dead load moment redistribution from midspan to the supports. The actual dead load distribution is likely somewhere between the simply-supported and continuous cases.

SAP2000 has the ability to account for structural changes during the course of the analysis by means of the staged construction nonlinear static analysis (Computers and Structures Inc. 2004). However, the staged construction module is an add-on feature that was not available for this study. It is recommended that this option be explored in future studies.

In a previous study conducted on the beamway in 1987, the following assumption was made for dead load distribution,

Due to the beam erection sequence, an adjustment was appropriate in the design factors. The individual precast beams are erected in place and supported in

position at each end. As a result the beam is initially self supporting (simple beam) prior to developing continuity by post tensioning the beams together. When establishing the most severe design condition, the vertical dead load bending moment, (considering continuity) from each load combination was removed and replaced by a simple beam moment. At some joints this is the governing design criteria.

With this assumption, the critical location for bending is at midspan of the first span. This assumption gives a conservative result for moment at midspan and a non-conservative result at the support.

For the present study, without the staged construction module available in SAP2000, we cannot directly account for the nonlinear time history of dead load and load effects. The dead load and live load are applied to the continuous structure. As will be seen in subsequent sections, the critical location for bending in the present study is at the first interior support. In comparing the 1987 study to the present study, it should be noted that the two different analytical assumptions for dead load distribution give two different critical locations for bending. The real behavior is likely somewhere in-between the simply-supported and continuous cases. The dead load assumption in the present study is conservative for bending at the support (which controls) and non-conservative for bending at the midspan. Future studies may consider alternate ways to model the structure for dead load effects.

### **Verification**

Before proceeding with the full set of rating and reliability calculations for eight parametric models, there was an attempt to verify the results of the calculations for critical load effects and resistance in the nominal model. The most effective way to verify the calculations was to compare them to the original calculations. This comparison is summarized in Table 7.

Table 7: Capacities and Load Effect Comparison

	*1970 CALCULATIONS		CURRENT RESULTS (Loads from SAP 2000, Capacities from AASHTO LRFR/LRFD)			
BEAM LENGTH						
<b>MOMENT</b>				Difference from Calcs		Difference from Calcs
Beam End	100'	110'	100'		110'	
(-) $M_n$ (kip-ft)	3733	3733	3567	-4%	3567	-4%
$M_{LL}$ (kip-ft)	991	978	916	-8%	917	-6%
Midspan						
(+) $M_n$ (kip-ft)	4676	4861	4435	-5%	4665	-4%
$M_{LL}$ (kip-ft)	636	488	546	-14%	508	4%
<b>SHEAR</b>						
Beam End						
Critical Distance from Beam Face / Shear Depth (in)	64	64	58		58	
** $V_c$ (kip)	275	288	181	-34%	181	-37%
** $V_s$ (kip)	128	128	268	109%	268	109%
** $V_n$ (kip)	404	416	449	11%	449	8%
$V_{LL}$ (kip)	53	52	47	-13%	45	-13%
*1970 capacities are divided (increased) by $\Phi = 0.90$ for flexure and $\Phi = 0.85$ for shear to compare with nominal capacities calculated from AASHTO LRFR/LRFD.						
**The shear capacities calculated presently use the MCFT method and Mark VI train loads.						

Table 7 shows that the present results are of the same order of magnitude as the 1970 calculations. The comparison for moment capacity is quite good, showing a difference of only 4-5% between present and historical values. The shear capacity shows a greater difference of 8-11%. A significant difference in shear capacity is to be expected as the modified compression field theory (MCFT) method in the AASHTO LRFD Code is very different from the 1970 approach. The MCFT method is also dependent on applied load. The Mark VI train load effects were used to calculate the shear capacity as this is the conservative case.

The load effects for the Mark IV train show a greater difference from the 1970 assumptions than the capacities. The end moments are underestimated by 6-8% by the SAP2000 model and the midspan moments are overestimated by 4% for the 110' interior span and underestimated by 14% for the 100' exterior span. One possible explanation of the redistribution

of midspan moments in the FEM would be the boundary and continuity conditions. The 1970 calculations may have assumed a pin support at the end of the six-span continuous bridge, whereas there is some flexural resistance offered by the column and crosshead in the FEM. This would explain a reduction of the exterior midspan moment in the FEM. The live-load shear is underestimated by 13%. It is not clear exactly why this is the case, but a possible explanation is that the 1970 calculations used rigid beams whereas the nominal FEM has more flexible CIP connections over the columns. Other reasons for the discrepancies may be related to the model. Sources of error in finite element analysis can include modeling error, user error, software bugs, discretization error, or numerical error (Cook et al. 2002). Additional sources of error may be numerical or modeling error in the current resistance calculations and the 1970 load and resistance calculations. Considering the large number of assumptions and variables that go into these calculations, as well as the thirty-five year difference in time, it is believed that the results in Table 7 are promising, and that the comparison demonstrates sufficient reliability in the FEM and the resistance calculations to proceed with the study.

## **Results**

A full set of calculations, using the nominal model to find load rating, structural reliability, and probability of failure, is given in Appendix F. The calculations are performed using Mathcad version 12.1 (Mathsoft Engineering and Education Inc. 2004). Once the calculations are laid out for the nominal model, the software facilitates rapid adaptation of the calculations for the seven additional parametric models by changing the appropriate inputs. Calculations for the seven additional parametric models can be assumed to be the same as for the

nominal model, with the appropriate changes in load effects from SAP2000. Results for all eight models are summarized in Table 8.

### **Discussion**

Table 8 contains three condition indices: (1) rating factor RF indicating reserve live load capacity; (2) reliability index,  $\beta$ , indicating structural reliability; and (3) probability of failure, also indicating structural reliability. For normally distributed random variables R and Q, it can be shown that the probability of failure is related to the reliability index as follows,  $P_f = \Phi(-\beta)$ . If the random variables are all normally distributed and uncorrelated, then this relationship between  $\beta$  and  $P_f$  is exact. Otherwise, this expression provides only an approximate means of relating the probability of failure to  $\beta$  (Nowak and Collins 2000).

Table 8: Load Rating and Reliability Analysis Results

Condition Index	Limit State	Train	Finite Element Model			
			Nominal	E <sub>c</sub> Lower-Bound	E <sub>c</sub> Upper-Bound	Prestress Loss Lower-Bound
Rating Factor	Bending, First Interior Support	Mark IV	1.53	1.45	1.53	1.52
	Bending, Span 1, 0.4L	Mark IV	4.85	4.03	4.98	4.82
	Bending, Span 2, 0.5L	Mark IV	6.41	5.21	6.61	6.36
	Shear, First Interior Support	Mark IV	5.56	5.53	5.57	5.56
	Bending, First Interior Support	Mark VI	1.02	0.97	1.03	1.02
	Bending, Span 1, 0.4L	Mark VI	3.57	2.96	3.66	3.55
	Bending, Span 2, 0.5L	Mark VI	4.71	3.83	4.86	4.68
	Shear, First Interior Support	Mark VI	3.96	3.93	3.96	3.96
Reliability Index, $\beta$	Bending, First Interior Support	Mark IV	4.23	4.04	4.24	4.22
	Bending, Span 1, 0.4L	Mark IV	9.68	9.30	9.73	9.67
	Bending, Span 2, 0.5L	Mark IV	11.00	10.64	11.05	10.99
	Shear, First Interior Support	Mark IV	4.83	4.82	4.83	4.82
	Bending, First Interior Support	Mark VI	2.56	2.27	2.58	2.55
	Bending, Span 1, 0.4L	Mark VI	9.00	8.47	9.06	8.98
	Bending, Span 2, 0.5L	Mark VI	10.42	9.92	10.49	10.40
	Shear, First Interior Support	Mark VI	4.57	4.56	4.57	4.57
Probability of Failure	Bending, First Interior Support	Mark IV	1.16E-05	2.70E-05	1.14E-05	1.20E-05
	Bending, Span 1, 0.4L	Mark IV	0	0	0	0
	Bending, Span 2, 0.5L	Mark IV	0	0	0	0
	Shear, First Interior Support	Mark IV	6.99E-07	7.15E-07	6.99E-07	7.00E-07
	Bending, First Interior Support	Mark VI	5.23E-03	1.16E-02	4.95E-03	5.42E-03
	Bending, Span 1, 0.4L	Mark VI	0	0	0	0
	Bending, Span 2, 0.5L	Mark VI	0	0	0	0
	Shear, First Interior Support	Mark VI	2.48E-06	2.57E-06	2.47E-06	2.48E-06

Condition Index	Limit State	Train	Finite Element Model (Continued)			
			Prestress Loss Upper-Bound	Boundary Condition Upper-Bound	Continuity Condition Lower-Bound	Continuity Condition Upper-Bound
Rating Factor	Bending, First Interior Support	Mark IV	1.54	1.60	1.56	1.51
	Bending, Span 1, 0.4L	Mark IV	4.91	5.05	4.83	4.87
	Bending, Span 2, 0.5L	Mark IV	6.55	6.51	6.34	6.45
	Shear, First Interior Support	Mark IV	5.57	5.61	5.58	5.56
	Bending, First Interior Support	Mark VI	1.03	1.07	1.04	1.01
	Bending, Span 1, 0.4L	Mark VI	3.61	3.71	3.55	3.58
	Bending, Span 2, 0.5L	Mark VI	4.81	4.79	4.66	4.74
	Shear, First Interior Support	Mark VI	3.97	3.99	3.97	3.95
Reliability Index, $\beta$	Bending, First Interior Support	Mark IV	4.25	4.44	4.33	4.18
	Bending, Span 1, 0.4L	Mark IV	9.70	9.82	9.66	9.69
	Bending, Span 2, 0.5L	Mark IV	11.03	11.03	10.96	11.02
	Shear, First Interior Support	Mark IV	4.83	4.84	4.83	4.82
	Bending, First Interior Support	Mark VI	2.59	2.79	2.67	2.50
	Bending, Span 1, 0.4L	Mark VI	9.03	9.15	8.97	9.01
	Bending, Span 2, 0.5L	Mark VI	10.47	10.46	10.38	10.44
	Shear, First Interior Support	Mark VI	4.57	4.58	4.57	4.56
Probability of Failure	Bending, First Interior Support	Mark IV	1.07E-05	4.42E-06	7.60E-06	1.48E-05
	Bending, Span 1, 0.4L	Mark IV	0	0	0	0
	Bending, Span 2, 0.5L	Mark IV	0	0	0	0
	Shear, First Interior Support	Mark IV	6.97E-07	6.60E-07	6.89E-07	7.05E-07
	Bending, First Interior Support	Mark VI	4.74E-03	2.62E-03	3.85E-03	6.20E-03
	Bending, Span 1, 0.4L	Mark VI	0	0	0	0
	Bending, Span 2, 0.5L	Mark VI	0	0	0	0
	Shear, First Interior Support	Mark VI	2.46E-06	2.33E-06	2.43E-06	2.50E-06

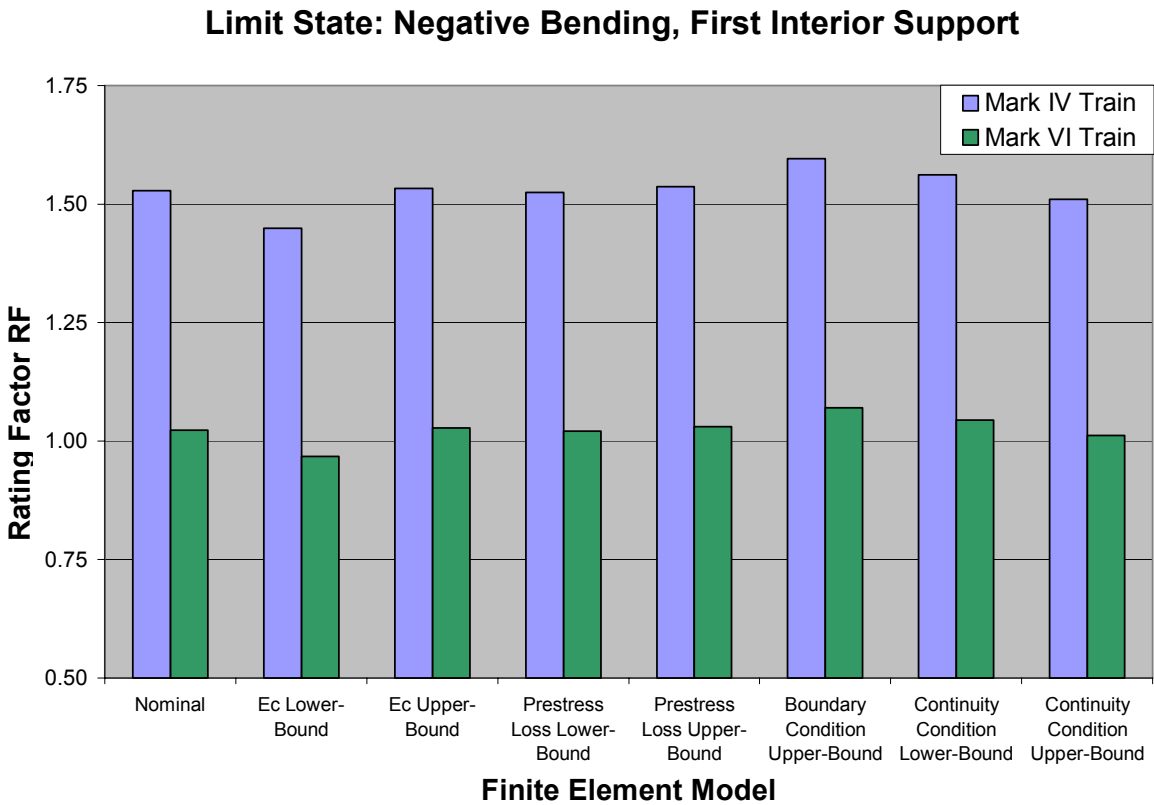


Figure 35: Rating Factor, Negative Bending at First Interior Support

It is useful to plot the simulation results for the eight parametric models to visualize trends among the models. The most critical limit state observed is negative bending at the first interior support. Figure 35 shows the results for Mark IV and Mark VI trains, for all eight parametric finite element models. The rating factor is an indication of reserve live load capacity. For the Mark IV (1971) trains, simulations conducted with all eight models give a rating factor of approximately 1.5. This implies that the live load effect may be increased by approximately 1.5 without violating the AASHTO LRFR Strength I limit state.

For probabilistic design specifications such as the LRFD Code, the rating factor and reliability should be highly correlated, because a target reliability index,  $\beta_T$ , is used to calibrate the design and rating factors. Relationships between reliability and rating form the basis of load

and resistance factors for bridge components (Akgul and Frangopol 2003). Considering the same probabilistic weight data was used to develop the monorail train load factor as well as the reliability index,  $\beta$ , we may expect the rating factor and reliability index to be highly correlated. The reliability index for negative bending at the first interior support is plotted as Figure 36.

The nominal model gives a reliability index just over 2.5 for Mark VI trains and approximately 4.25 for Mark IV trains. In the LRFD Code calibration, load and resistance factors are treated as random variables and are described by bias factors ( $\lambda$ ) and coefficients of variation ( $V$ ). Resistance factors,  $\phi$ , are calculated so that the structural reliability is close to the target value  $\beta_T = 3.5$  (Nowak 1995). The rating procedures presented in the AASHTO LRFR Manual are intended to reflect a balance between safety and economics. As such, a lower target reliability than design was chosen for load rating at the strength limit state. The LRFR Manual adopts a reduced target reliability index,  $\beta_T$  of approximately 2.5, calibrated to past AASHTO operating level load rating. This value was chosen to reflect the reduced exposure period, consideration of site realities, and the economic considerations of rating vs. design (AASHTO 2003). *ACI 358.1R-92: Analysis and Design of Reinforced and Prestressed-Concrete Guideway Structures* uses a target reliability index,  $\beta_T$  of 4.0. “The reliability index is higher than the value generally used for highway bridges, in order to provide a lower probability of failure due to the consequences of a guideway structure in a public transit system (American Concrete Institute 1992).”

The present study indicates that the beamway structural reliability under the Mark VI train load, for the strength limit state, is comparable to the target reliability for operating highway bridges (LRFR Manual,  $\beta_T = 2.5$ ). Restating this finding in terms of probability of failure, the nominal model gives  $P_f = 5.23 \times 10^{-3}$  for  $\beta = 2.56$  (Mark VI trains), which is

comparable to  $P_f = 6.21 \times 10^{-3}$  for  $\beta = 2.5$  (LRFR Manual). The present study indicates that beamway performance under the Mark IV train load, for the strength limit state, exceeds the target reliability for new guideway structures (ACI 358,  $\beta_T = 4.0$ ,  $P_f = 3.17 \times 10^{-5}$ ), as well as the target reliability for new highway bridges (AASHTO LRFD,  $\beta_T = 3.5$ ,  $P_f = 2.33 \times 10^{-4}$ ).

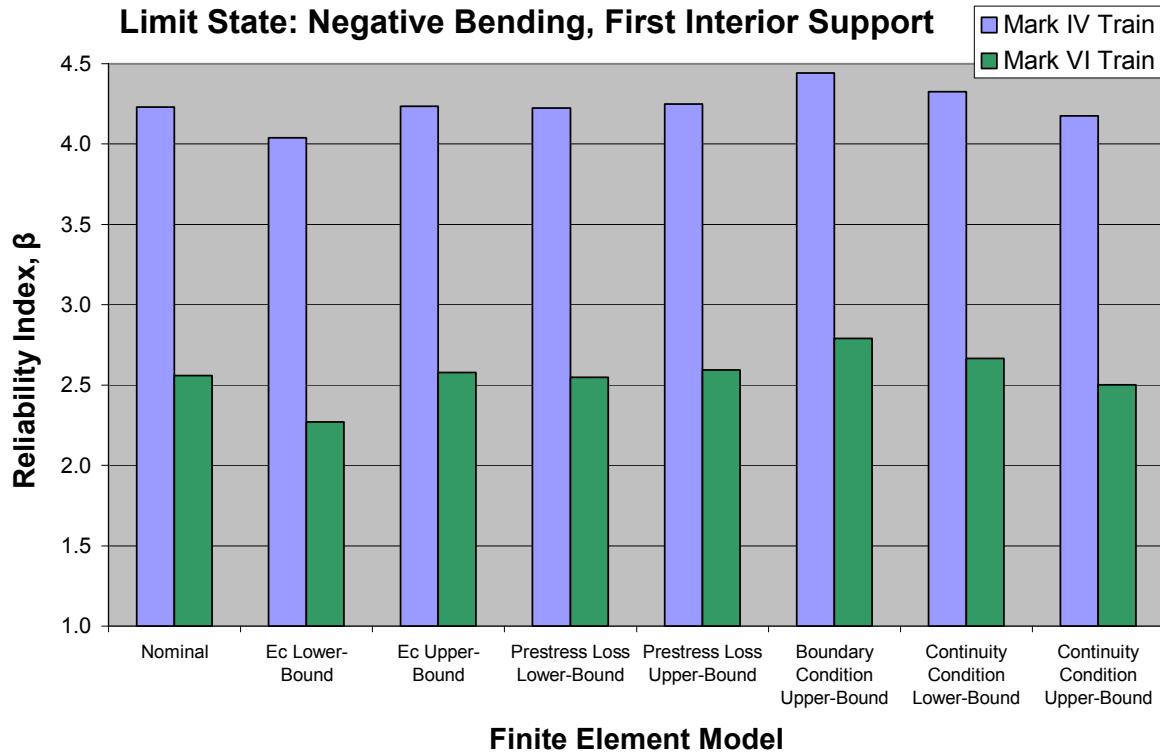


Figure 36: Reliability Index, Negative Bending at First Interior Support

Similar trends are observed in the results for load rating factor and reliability index, confirming the assumption that these indices are highly correlated. The lower-bound concrete stiffness model gives the lowest rating factor (0.97) and lowest reliability index (2.27), below prescribed values in the AASHTO LRFR Manual. It should be noted that highway bridges, as constructed systems, have a wide variation in loading, material resistance, and other factors that influence reliability. Constructed systems may be contrasted with manufactured systems, in

which the relevant parameters are more deterministic (less probabilistic) and more narrowly defined (Catbas and Aktan 2002). Although it is a constructed facility, the beamway was constructed and is maintained to exacting standards. The train loads are well-understood and the concept of exception vehicles, (heavy trucks and overloads) does not apply. Consequently, a slightly lower reliability index for the beamway may not carry the same concern as it would for a highway bridge. Finally, it is important to note that some conservative assumptions were made in this analysis, and that a more refined and give different results.

The highest load rating factor (1.07) and reliability index (2.79) for negative bending under Mark VI load is found for the boundary condition upper-bound model. This model assumes that the expansion joints fully transfer loads to adjacent six-span segments. It makes sense that moment distribution, from the first interior support to the exterior support, would occur under these conditions. The difference between the highest (2.79) and lowest (2.27) reliability indices for the eight models, Mark VI trains, and the negative bending limit state is approximately 20%.

The reliability indices are plotted for the remaining limit states considered in the simulations, load rating, and reliability analyses. Figure 37 shows the reliability index for positive bending at 0.4 L in the first span. Note the high values for reliability index, indicating reserve capacity at midspan, should some capacity be lost at the support and moment redistribution occur. The reliability index is most sensitive to stiffness of the concrete and the boundary condition at expansion joints.

It is interesting to note the redistribution of moments from supports to midspan depending on the continuity condition. When the stiffness of the connection is reduced (lower-bound model), the reliability increases for negative bending at the supports (Figure 36), whereas

the reliability decreases for positive bending at the midspans (Figure 37, Figure 38), where compared to the nominal value. Put another way, with the softening of the connection, less moment is resisted at the support. The opposite trend is observed for the upper-bound connection model, in which case the increased stiffness of the connection attracts more moment at the supports (reliability reduced) and reduces moment demand for the midspans (reliability increases).

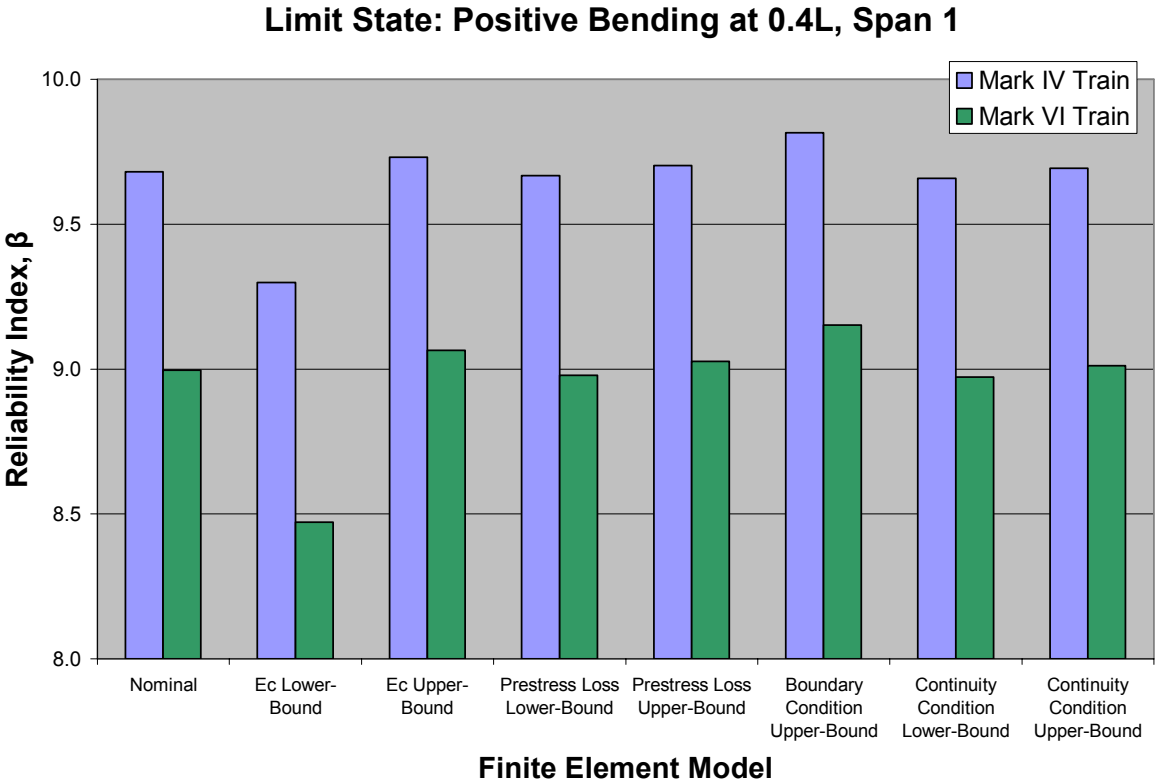


Figure 37: Reliability Index, Positive Bending at 0.4L, Span 1

Excess capacity is also indicated for positive bending at midspan of the second span, as shown in Figure 38. This confirms interviews with one of the original designers who said that, if the ultimate bending limit state is reached at the supports, there is reserve capacity at midspan to accommodate moment redistribution. However, the significant cracking and deformation

associated with reaching the bending limit state at the supports would probably be unacceptable from a serviceability point of view.

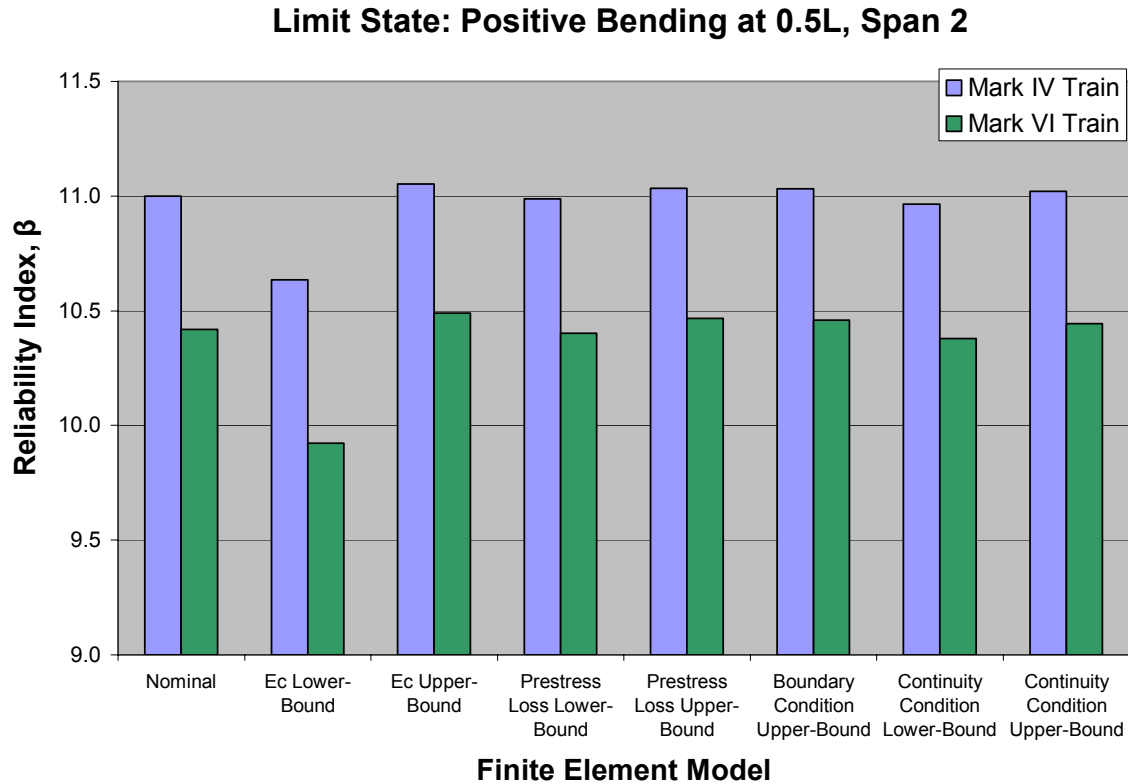


Figure 38: Reliability Index, Positive Bending at 0.5L, Span 2

Figure 39 shows the sensitivity analysis for the reliability index for shear at the critical section (exterior face of first interior support). The reliability for shear seems less sensitive to the model parameters than reliability for moment limit states. Even as the moment redistributes in the beamway, the shear values are less affected. There is also less of a difference between the reliability associated with the Mark IV train and Mark VI trains. This may be because a higher proportion of the total shear comes from dead load (constant among the different trains) than live load, whereas a higher proportion of the total moment comes from the live load portion, resulting in larger scatter in reliability between the two trains. The reliability exceeds 4.5 ( $P_f = 3.40 \times 10^{-7}$ )

6) for shear with all parametric models, whereas the target reliability for the AASHTO LRFD Design Specifications is 3.5 ( $P_f = 2.33 \times 10^{-4}$ ) as described previously. The reliability for the shear limit is significantly higher than for the critical limit state in bending for all models.

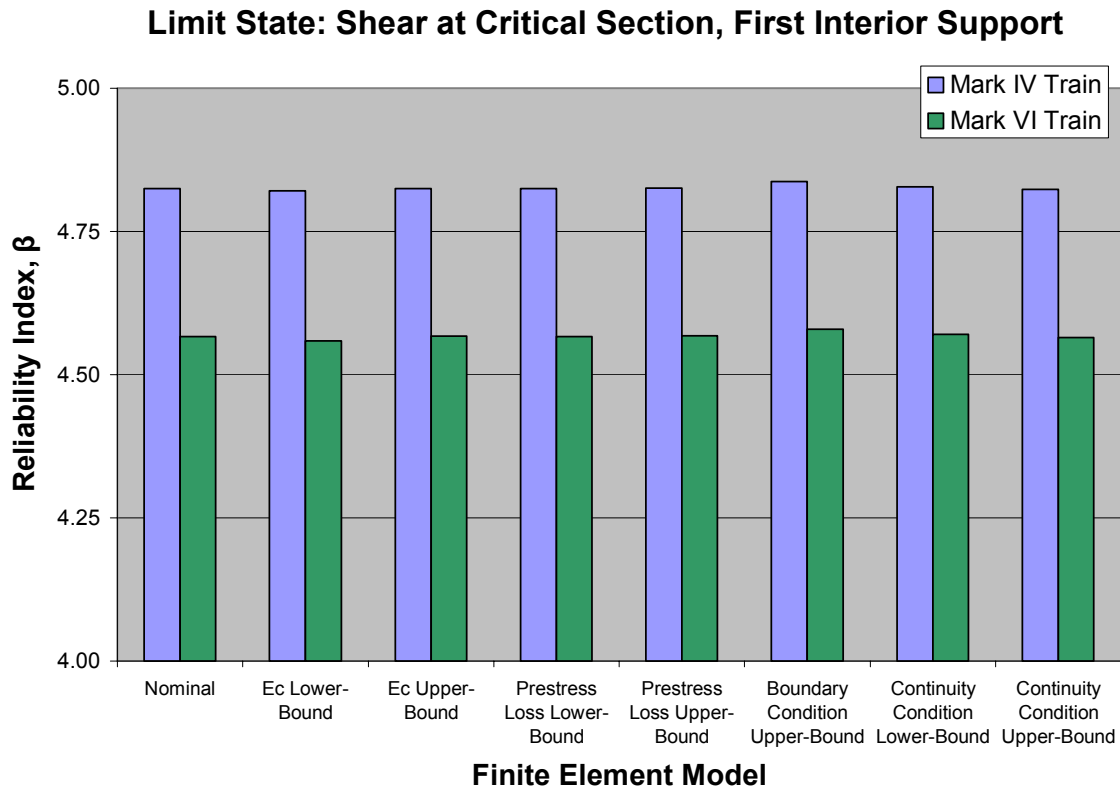


Figure 39: Reliability Index, Shear at Critical Section, First Interior Support

## CONCLUSIONS AND RECOMMENDATIONS

A detailed finite element model has been developed to represent the six-span continuous beamway bridge structure. Sensitivity studies were conducted using eight parametric models for modal analysis and simulations with moving loads. Load rating and reliability calculations were performed and a concept of lower-bound and upper-bound structural behavior was established.

It was important to develop procedures for verification and validation of the analysis. Benchmark studies were conducted to validate finite element models with well-established solutions. Critical modeling features were incorporated in a number of simpler benchmark studies before the full six-span model was developed. Legacy data were obtained for the Mark IV trains and compared with the load effects and resistance evaluated in the present study. It is encouraging that the FEM-predicted load effects and AASHTO-based resistances were close to those found in the original structural calculations for the Mark IV trains. This verifies the model and accompanying analysis in a qualitative sense. Another qualitative indication of the accuracy of the FEM comes from the fact that the 1982 beamway has been observed to deflect approximately 0.7 in. under train loads. This is close to the deflection predicted by the upper-bound stiffness model developed in the present study for the 1971 beamway, and the two beamway designs are similar. A comprehensive test plan or monitoring program to capture frequencies, mode shapes, and deflections is recommended for objective validation of the FEM. This can lead to model calibration using experimental data and an objective understanding of the measured structural behavior.

The dynamic behavior was evaluated with respect to changes in structural parameters and configurations including concrete stiffness, prestress loss, boundary conditions, and continuity conditions. Eigenvalue analysis of the beamway in SAP2000 gives natural frequencies in the

range from 0.73 Hz to 2.99 Hz for the first 20 modes of the nominal model. The mode shapes of the bridge were categorized in terms of pure modal behaviors including lateral beam bending, vertical beam bending, longitudinal bridge oscillation, and transverse bridge sway. The lowest frequency appearance of any pure mode is recorded and compared in the sensitivity studies. There is significant sensitivity across all modes to variation in the concrete stiffness, as expressed by the modulus of elasticity,  $E_c$ . The boundary condition has significant effect on the longitudinal modes and dramatically increases the energy required to achieve the first longitudinal mode. There is a general reduction in stiffness as the prestress loss is decreased (prestressing force is increased). The dynamic response is less sensitive to the continuity conditions. The frequencies and mode shapes may be captured experimentally for model calibration. A sufficient spatial resolution of sensors is required for meaningful characterization of mode shapes. Advanced data processing methods may be applied to generate mode shapes from ambient vibration inputs.

Simulations were performed with the eight parametric finite element models and critical load effects were extracted from the results. These load effects were combined with AASHTO-based resistance calculations to determine load rating factors and reliability indices for the various models and limit states, all under Mark IV and Mark VI train loads. The nominal model gives a reliability index,  $\beta$ , just over 2.5 for Mark VI trains and approximately 4.0 for Mark IV trains. The critical limit state is negative bending at the supports. There is significant reserve capacity for bending at midspan, should moment redistribution occur with plastic moment at supports. The continuity condition (CIP connection) controls the moment distribution. The stiffness of the CIP connection is controlled by varying the concrete modulus of elasticity in the lower- and upper-bound FEMs. A stiffer connection attracts more moment at the support and

reduces the midspan moment. A softer connection redistributes moment from the support to the midspan. The reliability index varies between 2.27 and 2.79 (approximately 20%) for the eight parametric models studied. A multi-channel modal test or monitoring program can provide additional insight into the actual behavior.

The beamway system has exhibited excellent strength behavior during its thirty-five years of service. It is expected to last without major repair or replacement for a long but unspecified period of time. The present study found the structural reliability for a representative straight dual beamway reduced from the high value of  $\beta = 4.0$  for Mark IV trains to  $\beta = 2.5$  for Mark VI trains. The value  $\beta = 2.5$  says the beamway reliability is comparable to the target reliability of operating highway bridges as defined in the AASHTO LRFR Manual ( $\beta_T = 2.5$ ).

There is a significant difference in the structural reliability for the Mark IV trains and Mark VI trains. The difference in reliability values is much greater than the scatter in those values among the eight parametric models. This indicates a real difference in structural reliability for the two train configurations. The low scatter among the eight models indicate that the effect of the chosen, critical parameters for the FEM is not drastically changing the reliability. In future studies, additional parameters can be added, the parameter ranges can further be varied and more rigorous, non-linear finite element and reliability models can be used to evaluate the structural behavior and reliability.

Concrete stiffness (expressed in the FEM as modulus of elasticity,  $E_c$ ) emerged as the critical parameter to affect the dynamic and static response. It would be very useful to know the in-situ concrete strength and modulus. Even if field tests gave a value for strength or modulus, it should be noted that these properties can vary widely as concrete is not a homogeneous material. It should also be recognized that, due to the effects of long-term creep, the effective modulus for

long-term dead load given by various design specifications is much less than the effective modulus for live load. Investigating the actual material behavior to determine stress-strain behavior, and choosing a proper value for  $E_c$  would make for an interesting research project of its own. An alternative to seeking one effective modulus value might be to develop separate models for dead load and live load analysis with different values, and then to superimpose the results. Future studies may consider the concrete compressive strength,  $f'_c$  as an additional parameter for sensitivity studies. If the in-situ strength were greater than the nominal value, the upper-bound range of  $E_c$  would be increased, as expressions for  $E_c$  depend on  $f'_c$ . In any case, the author finds that there is considerable uncertainty associated with  $E_c$ , that this parameter had the single greatest effect on dynamic and static response, and that it deserves further study.

The FEM developed in this study has the ability to predict load effects from any train axle configuration, but only in the vertical plane. The next logical step would be to develop a model for curved beams, to consider torsion and the influence of side tires. Another way to use the information in the current study would be to incorporate material deterioration models and begin to make service life predictions based on a probabilistic approach and the structural reliability.

## **APPENDIX A: BOUNDING CONCRETE STIFFNESS**

FIND NOMINAL, LOWER-BOUND, AND UPPER-BOUND VALUES FOR THE IMMEDIATE AND LONG-TERM MODULUS OF ELASTICITY FOR CONCRETE

The approach to this problem will be to find expressions for the immediate (upper-bound) modulus and the long-term, ultimate modulus (lower-bound), considering effects of creep under long-term dead load. This approach is repeated for the beams, columns, and CIP connections. The values for  $E_c$  are based on the nominal concrete strength,  $f_c$ .

PRECAST BEAMS  $f_c := 7000\text{psi}$   $w_c := 160\text{pcf}$

UPPER-BOUND MODULUS

For upper-bound behavior, we look at the immediate modulus without any reductions for long-term creep.

Nawy gives expressions for high-strength concrete modulus (Nawy 2003, p. 38), where high-strength concrete is defined as concrete with compressive strength between 6,000 and 12,000psi,

$$E_c := \left[ 40000 \left( \frac{f_c}{\text{psi}} \right)^{0.5} + 10^6 \right] \cdot \left( \frac{w_c}{145\text{pcf}} \right)^{1.5} \text{ psi} \quad E_c = 5038\text{ksi}$$

For normal-weight concrete, ACI 318-02 gives the following expression (Section 8.5.1),

$$E_{cNWC} := 57000 \sqrt{\frac{f_c}{\text{psi}}} \text{ psi} \quad E_{cNWC} = 4769\text{ksi}$$

LOWER-BOUND MODULUS

For lower-bound behavior, consider the effects of long-term creep with expressions from Nawy (2003) and Barker (1997)

The following expression is given for ultimate effective modulus (Nawy 2003, p. 42),

$$E_{cn} := \frac{E_c}{1 + \gamma_t}$$

This is bound by upper and lower values, based on relative humidity,

Assume  $RH := 72.5$  (Southeast Regional Climate Center, 2004)

$$\gamma_{tu} := 1.75 + 2.25 \left( \frac{100 - RH}{65} \right) \quad \gamma_{tu} = 3$$

$$\gamma_{tl} := 0.75 + 0.75 \left( \frac{100 - RH}{50} \right) \quad \gamma_{tl} = 1$$

Use these variables to carry values forward in the worksheet.

$$E_{cnupper} := \frac{E_c}{1 + \gamma_{tu}} \quad E_{cnupper} = 1361\text{ksi} \quad E_{cLT1} := E_{cnupper}$$

$$E_{cnlower} := \frac{E_c}{1 + \gamma_{tl}} \quad E_{cnlower} = 2330\text{ksi} \quad E_{cLT2} := E_{cnlower}$$

To account for the increase in strain due to creep under permanent loads, Barker (1997) gives an expression for a reduced long-term modulus of elasticity that considers humidity, time to permanent load, and volume-to-surface ratio,

$$E_{cLT} := \frac{E_c}{1 + \Psi(t, t_i)}$$

Assume the following for permanent loading,,

$$\begin{aligned} t &:= 40\text{yr} & t_i &:= 1\text{day} & t_i &\text{ is age of concrete in days when the permanent} \\ & & & & & \text{load is applied} \\ t &= 14610\text{day} \end{aligned}$$

Volume to surface area (conservative at minimum value, max  $k_c$ , max  $\Psi$ , in  $E_c$ )

$$VS := \frac{26\text{in} \cdot 48\text{in} - 16\text{in} \cdot 36\text{in}}{26\text{in} \cdot 2 + 48\text{in} \cdot 2}$$

$$VS = 115\text{mm}$$

$$k_c := 0.75 \quad (\text{Barker Figure 7.13})$$

$$f'_c = 48\text{MPa} \quad H := \text{RH}$$

$$k_f := \frac{62\text{MPa}}{42\text{MPa} + f'_c} \quad k_f = 1$$

$$\Psi := 3.5 \cdot k_c \cdot k_f \left( 1.58 - \frac{H}{120} \right) \cdot \left( \frac{t_i}{\text{day}} \right)^{-0.118} \cdot \frac{(t - t_i)^{0.6}}{10\text{day}^{.6} + (t - t_i)^{0.6}} \quad \Psi = 1.71$$

$$E_{cLT3} := \frac{E_c}{1 + \Psi} \quad E_{cLT3} = 1862\text{ksi}$$

Try the Barker method with a much longer  $t_i$ , to get a higher  $E_c$ ,

$$t := 40\text{yr} \quad t_i := 60\text{day}$$

$$\Psi_2 := 3.5 \cdot k_c \cdot k_f \left( 1.58 - \frac{H}{120} \right) \cdot \left( \frac{t_i}{\text{day}} \right)^{-0.118} \cdot \frac{(t - t_i)^{0.6}}{10\text{day}^{.6} + (t - t_i)^{0.6}} \quad \Psi_2 = 1.05$$

$$E_{cLT4} := \frac{E_c}{1 + \Psi_2} \quad E_{cLT4} = 2455\text{ksi}$$

Finally, AASHTO recommends the following simple expression for the modulus of elasticity for permanent loads (Barker 1997),

$$E_{cLT5} := \frac{E_c}{3} \quad E_{cLT5} = 1679\text{ksi}$$

Summary,

UPPER-BOUND

$$E_c = 5038 \text{ksi}$$

LOWER-BOUND

$$E_{cLT1} = 1361 \text{ksi}$$

$$E_{cLT2} = 2330 \text{ksi}$$

$$E_{cLT3} = 1862 \text{ksi}$$

$$E_{cLT4} = 2455 \text{ksi}$$

Compares with  $E_{cLT3}$ , but much longer time to permanent load.

$$E_{cLT5} = 1679 \text{ksi}$$

By engineering judgment, we can ignore the result 1 for long-term modulus. Expression 3 accounts for time to permanent load and RH, whereas expression 1 is not as precise.

Additionally, design calculations give this criteria:

$$E_c := 5187 \text{ksi}$$

$$E_{cLT6} := 0.7E_c$$

$$E_{cLT6} = 3631 \text{ksi}$$

Based on the information above and engineering judgment, assume the following values for the parameter sensitivity study, for the precast beams:

Nominal	$E_c := 3600 \text{ksi}$
---------	--------------------------

Lower-Bound	$E_c := 1600 \text{ksi}$
-------------	--------------------------

Upper-Bound	$E_c := 5000 \text{ksi}$
-------------	--------------------------

CIP CONCRETE CONNECTIONS AND CONCRETE COLUMNS

$f_c := 5000\text{psi} \quad w_c := 155\text{pcf}$

The calculations above are repeated, this time with new inputs for  $f_c$  and  $w_c$  (nominal values for the CIP connections and concrete columns):

UPPER-BOUND

$$E_c := 33 \left( \frac{w_c}{\text{pcf}} \right)^{1.5} \cdot \sqrt{\frac{f_c}{\text{psi}}} \text{psi} \quad E_c = 4503\text{ksi}$$

LOWER-BOUND

$$E_{cnu} := \frac{E_c}{1 + \gamma_{tu}} \quad E_{cnu} = 1216\text{ksi}$$

$$E_{cni} := \frac{E_c}{1 + \gamma_{tl}} \quad E_{cni} = 2082\text{ksi}$$

$$E_{cLT3} := \frac{E_c}{1 + \Psi} \quad E_{cLT3} = 1664\text{ksi}$$

$$E_{cLT4} := \frac{E_c}{1 + \Psi^2} \quad E_{cLT4} = 2195\text{ksi}$$

Compares with  $E_{cLT3}$ , but much longer time to permanent load.

$$E_{cLT5} := \frac{E_c}{3} \quad E_{cLT5} = 1501\text{ksi}$$

Additionally, the design calculations give this criteria:

$$E_c := 4384\text{ksi}$$

$$E_{cLT6} := 0.6E_c \quad E_{cLT6} = 2630\text{ksi}$$

Based on the information above and engineering judgment, assume the following values for the parameter sensitivity study, for the CIP connections and columns:

Nominal  $E_c := 2600\text{ksi}$

Lower-Bound  $E_c := 1500\text{ksi}$

Upper-Bound  $E_c := 4500\text{ksi}$

## **APPENDIX B: BOUNDING PRESTRESS LOSS**

TIME-DEPENDENT LOSSES FOR THE PRECAST/PRE-TENSIONED BEAMS  
(STEP-BY-STEP APPROACH)

This method follows Example 3.9 (Nawy, 2003).

Compute the prestress loss at midspan due to dead load at:

- (a) stage I at transfer
- (b) stage II at 40 years

Assume the prestress transfer occurred 12 hours after tensioning the strands. This assumption is conservative, considering 24-hour fabrication cycle (Mast, 1972). Assume the following properties:

$$f'_c := 7000\text{psi} \quad w_c := 160\text{pcf} \quad \text{span} := 110\text{ft}$$

$$f'_{ci} := 4000\text{psi} \quad \text{Lower-bound as given in original structural calculations.}$$

Section properties at precast beam midspan. These are confirmed by values given in the original calculations:

$$h := 48\text{in}$$

$$b_1 := 26\text{in} \quad h_1 := 7\text{in} \quad A_1 := b_1 \cdot h_1 \quad A_1 = 182\text{in}^2$$

$$b_2 := 5\text{in} \quad h_2 := 36\text{in} \quad A_2 := b_2 \cdot h_2 \quad A_2 = 180\text{in}^2$$

$$b_3 := 26\text{in} \quad h_3 := 5\text{in} \quad A_3 := b_3 \cdot h_3 \quad A_3 = 130\text{in}^2$$

$$A_c := A_1 + 2 \cdot A_2 + A_3 \quad A_c = 672\text{in}^2$$

$$c_t := \frac{A_1 \cdot 3.5\text{in} + 2 \cdot A_2 \cdot 25\text{in} + A_3 \cdot 45.5\text{in}}{A_c} \quad c_t = 23.14\text{in}$$

$$c_b := h - c_t \quad c_b = 24.86\text{in}$$

$$I_c := \frac{b_1 \cdot h_1^3}{12} + \frac{2 \cdot b_2 \cdot h_2^3}{12} + \frac{b_3 \cdot h_3^3}{12} + A_1 \cdot \left( c_t - \frac{h_1}{2} \right)^2 + 2 \cdot A_2 \cdot (25\text{in} - c_t)^2 + A_3 \cdot \left( c_b - \frac{h_3}{2} \right)^2$$

$$I_c = 176338\text{in}^4$$

$$S_t := \frac{I_c}{c_t} \quad S_t = 7620\text{in}^3$$

$$S_b := \frac{I_c}{c_b} \quad S_b = 7094\text{in}^3$$

Dead load,

$$W_D := w_c \cdot A_c \quad W_D = 747 \text{ plf}$$

Prestressing tendons are given as 1/2" diameter, Type 270K strands in the original calculations. Assume the following properties:

$$A_{ps} := 28 \cdot 0.153 \text{ in}^2 \rightarrow 4.284 \text{ in}^2$$

$$f_{pu} := 270000 \text{ psi} \quad E_{ps} := 28 \cdot 10^6 \text{ psi}$$

$$f_{py} := 0.85 \cdot f_{pu} \quad f_{py} = 229500 \text{ psi}$$

$$f_{piN} := 0.70 \cdot f_{pu} \quad f_{piN} = 189000 \text{ psi}$$

Nawy gives expressions for high-strength concrete modulus (Nawy, 2003, p. 38), where high-strength concrete as defined as concrete with compressive strength between 6,000 and 12,000psi,

$$E_{ci} := \left[ 40000 \left( \frac{f_{ci}}{\text{psi}} \right)^{0.5} + 10^6 \right] \cdot \left( \frac{w_c}{145 \text{ pcf}} \right)^{1.5} \quad E_{ci} = 4091.5 \text{ ksi}$$

$$E_c := \left[ 40000 \left( \frac{f_c}{\text{psi}} \right)^{0.5} + 10^6 \right] \cdot \left( \frac{w_c}{145 \text{ pcf}} \right)^{1.5} \quad E_c = 5038.3 \text{ ksi}$$

### Stage 1: Stress Transfer

(a) *Elastic shortening.* Given critical section distance from support  $L := 0.50 \text{ span}$

$$e_c := 45.5 \text{ in} - c_t \quad \text{at the critical section.} \quad e_c = 22.36 \text{ in}$$

$$M_D := \frac{W_D \cdot \text{span}^2}{8} \quad \text{at the critical section} \quad M_D = 1129.3 \text{ kip} \cdot \text{ft}$$

**ASSUME**  $\Delta f_{pES} := 10519.6 \text{ psi}$  or about 10% of  $f_{pi}$

$$f_{pi} := f_{piN} - \Delta f_{pES} \quad f_{pi} = 178480.4 \text{ psi}$$

$$P_1 := A_{ps} \cdot f_{pi} \quad P_1 = 764610 \text{ lbf}$$

$$r := \left( \frac{I_c}{A_c} \right)^{0.5} \quad r^2 = 262.4 \text{ in}^2$$

$$f_{cs} := \left| \frac{-P_1}{A_c} \cdot \left( 1 + \frac{e_c^2}{r^2} \right) + M_D \cdot \frac{e_c}{I_c} \right| \quad f_{cs} = 1586.9 \text{ psi}$$

$$n := \frac{E_{ps}}{E_{ci}} \quad n = 6.84$$

$$\Delta f_{pES} := n \cdot f_{cs} \quad \Delta f_{pES} = 10860 \text{ psi}$$

**CHECK WITH ASSUMPTION  
ABOVE AND ITERATE UNTIL THEY  
CONVERGE.**

(b) *Steel-Stress Relaxation.* Calculate the steel relaxation at transfer.

$$f_{pi} = 178480.4 \text{ psi} \quad \text{However, original } f_{bi} \text{ assumption may also be used (189,000 psi)}$$

$$t := 12 \text{ hr}$$

$$\Delta f_{pR} := f_{pi} \cdot \frac{\log(t \cdot \text{hr}^{-1})}{10} \cdot \left( \frac{f_{pi}}{f_{py}} - 0.55 \right) \quad \Delta f_{pR} = 4386 \text{ psi}$$

$$\Delta f_{pES} + \Delta f_{pR} = 15246 \text{ psi}$$

(c) *Creep Loss*

$$\Delta f_{pCR} := 0$$

(d) *Shrinkage Loss*

$$\Delta f_{pSH} := 0$$

The stage-I total losses are

$$\Delta f_{pT} := \Delta f_{pES} + \Delta f_{pR} + \Delta f_{pCR} + \Delta f_{pSH} \quad \Delta f_{pT} = 15246 \text{ psi}$$

$$f_{pi} := f_{piN} - \Delta f_{pT} \quad f_{pi} = 173754 \text{ psi}$$

$$P_1 := f_{pi} \cdot A_{ps} \quad P_1 = 744363 \text{ lbf}$$

**Stage II: Transfer to Current Day (40 years)**

Assume beam pre-tensioning only resists beam dead load as permanent load.

(a) Creep Loss

$$E_c = 5.04 \times 10^6 \text{ psi}$$

$$E_{ps} = 28 \times 10^6 \text{ psi}$$

$$n := \frac{E_{ps}}{E_c} \quad n = 5.56$$

$$f_{cs} := \left| \frac{-P_i}{A_c} \cdot \left( 1 + \frac{e_c^2}{r^2} \right) + M_D \cdot \frac{e_c}{I_c} \right| \quad f_{cs} = 1499.4 \text{ psi}$$

Following Nawy (2003), Eq. 3.11, p. 82 for creep loss

$$K_{CR} := 2.0 \quad K_{CR} = 2 \quad \text{Nawy, p.82 from ACI-ASCE, pre-tensioned members}$$

$$f_{csd} := 0 \text{ psi}$$

ACI-ASCE Committee for evaluating creep as presented by Nawy (2003)

$$\Delta f_{pCR} := n \cdot K_{CR} \cdot (f_{cs} - f_{csd}) \quad \Delta f_{pCR} = 16666 \text{ psi}$$

(b) Shrinkage Loss. Assume relative humidity RH := 72.5%

PCI expression for prestress loss due to long-term shrinkage,

$$\Delta f_{pSH} := 8.2 \cdot 10^{-6} \cdot K_{SH} \cdot E_{ps} \cdot \left( 1 - 0.06 \frac{V}{S} \right) \cdot (100 - RH)$$

$$K_{SH} := 1.0 \quad \text{for pre-tensioned members}$$

$$V := A_c \quad S := (26 \text{ in} \cdot 2 + 48 \text{ in} \cdot 2 + 16 \text{ in} \cdot 2 + 36 \text{ in} \cdot 2) \cdot \text{in}$$

$$\frac{V}{S} = 2.7 \quad \text{volume-to-surface ratio}$$

$$\Delta f_{pSH} := 8.2 \cdot 10^{-6} \cdot K_{SH} \cdot E_{ps} \cdot \left( 1 - 0.06 \frac{V}{S} \right) \cdot (100 - RH) \quad \Delta f_{pSH} = 5304 \text{ psi}$$

(c) *Steel Relaxation Loss at 40 Years*

$$t_1 := t \quad t_1 = 12 \text{ hr}$$

$$t_2 := 40 \text{ yr}$$

$$f_{ps} := f_{pi} \quad f_{ps} = 173754 \text{ psi}$$

$$\Delta f_{pR} := f_{ps} \cdot \frac{\log(t_2 \cdot \text{hr}^{-1}) - \log(t_1 \cdot \text{hr}^{-1})}{10} \cdot \left( \frac{f_{ps}}{f_{py}} - 0.55 \right)$$

$$\Delta f_{pR} = 16069 \text{ psi}$$

Stage-II total loss is,

$$\Delta f_{pT} := \Delta f_{pCR} + \Delta f_{pSH} + \Delta f_{pR} \quad \Delta f_{pT} = 38039 \text{ psi}$$

Increase in stress in the strands due to the addition of topping is,

$$f_{SD} := n \cdot f_{csd} \quad f_{SD} = 0$$

$$f_{pe} := f_{ps} - \Delta f_{pT} + f_{SD} \quad f_{pe} = 135715 \text{ psi}$$

Total losses, all stages,

$$\Delta f_{pT} := f_{piN} - f_{pe} \quad \Delta f_{pT} = 53285 \text{ psi}$$

Alternatively, using the lump-sum approach, we obtain the following value,

$$\Delta f_{pT} := 45000 \text{ psi} \quad \text{Nawy (2003) from AASHTO specifications}$$

Additionally, the original structural calculations give the following for assumed total losses:

$$\Delta f_{pT} := 35000 \text{ psi}$$

By engineering judgment, assume these values in the parameter sensitivity study for total pre-tensioning losses:

Nominal, 45000psi

Lower Bound, 35000 psi

Upper Bound, 53000 psi

## LUMP-SUM LOSSES FOR POST-TENSIONING SYSTEM

The post-tension tendons are in a complicated stress state that varies throughout the six-span continuous unit. There is no straightforward way to apply the step-by-step method as in the pre-tension (simply-supported for dead load) case.

Nawy (2003, p. 74) says, "A very high degree of refinement of loss estimation is neither desirable nor warranted, because of the multiplicity of factors affecting the estimate. Consequently, lump-sum estimates of losses are more realistic..." Consequently, a lump-sum approach is chosen for post-tensioning losses.

From AASHTO (Nawy Table 3.1),

$$\Delta f_{pT} := 3300 \text{psi} \quad \text{for PT wire or strand, } f_c = 5000 \text{ psi}$$

From PTI (Nawy Table 3.2),

$$\Delta f_{pT} := 3500 \text{psi} \quad \text{for stress-relieved 270-K strands in beams and joists}$$

Assumption given in original structural calculations,

$$\Delta f_{pT} := 2500 \text{psi}$$

These values do not consider anchorage or friction losses,

For tendons in a rigid metal duct (7-wire strand), Nawy Table 3.7 from PCI,

$$K := 0.0002 \text{ft}^{-1} \quad \mu = 0.15 - 0.25$$

If tendons are in flexible metal sheathing,

$$K = 0.0005 - 0.0020$$

Assumption given in original structural calculations,

$$K := 0.0005 \text{ft}^{-1} \quad \mu = 0.2$$

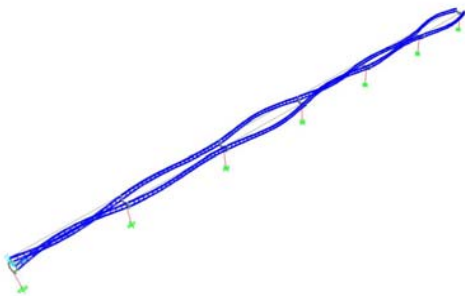
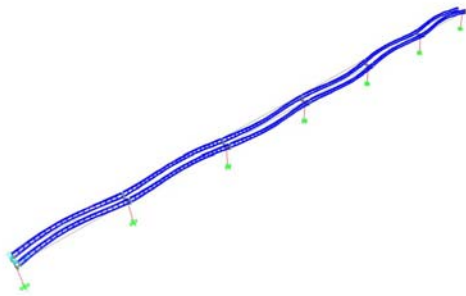
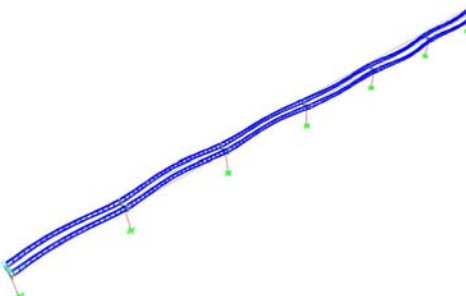
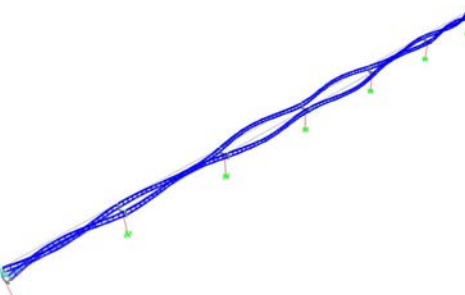
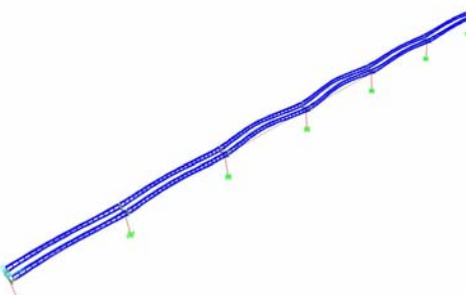
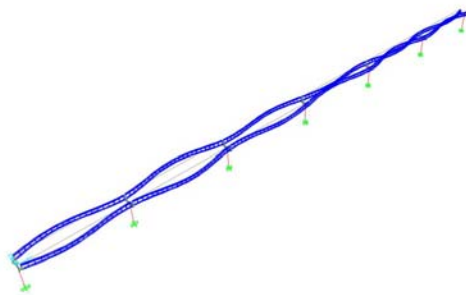
By engineering judgment, we use the following values for the parameter sensitivity study,

Nominal	$K := 0.0005 \text{ft}^{-1}$	$\mu := 0.2$
Lower-Bound	$K := 0.0002 \text{ft}^{-1}$	$\mu := 0.15$
Upper-Bound	$K := 0.0020 \text{ft}^{-1}$	$\mu := 0.25$

## **APPENDIX C: FREQUENCIES AND MODE SHAPES**

Table 9: Nominal Model Frequencies and Mode Shapes

Mode 1	0.7349 Hz	Mode 2	0.8765 Hz	Mode 3	0.9171 Hz
Lateral beam bending		Lateral beam bending, column torsion		Lateral beam bending	
Mode 4	0.9864 Hz	Mode 5	1.0370 Hz	Mode 6	1.2217 Hz
Lateral beam bending, column torsion		Longitudinal bridge oscillation, lateral beam bending		Lateral beam bending, strong-axis column bending	

					
Mode 7	1.2613 Hz	Mode 8	1.4159 Hz	Mode 9	1.5512 Hz
Lateral beam bending, longitudinal bridge oscillation		Strong-axis column bending, lateral beam bending		Transverse bridge oscillation, lateral beam bending, center column torsion	
					
Mode 10	1.5781 Hz	Mode 11	1.6843 Hz	Mode 12	1.9522 Hz
Lateral beam bending		Transverse bridge sway, lateral beam bending, strong-axis column bending		Lateral beam bending	

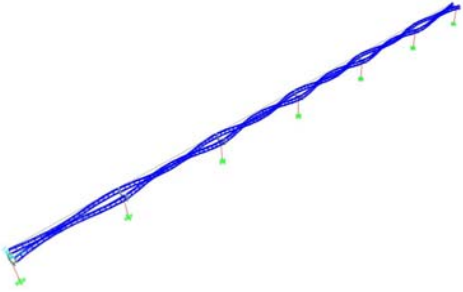
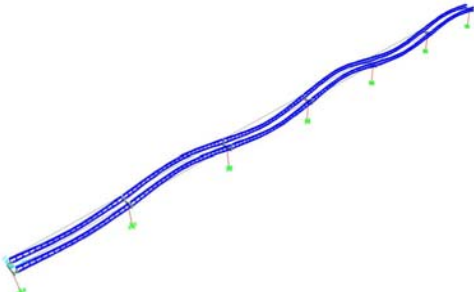
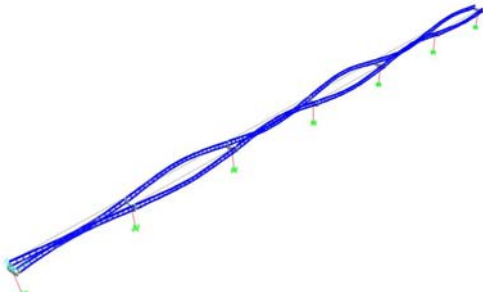
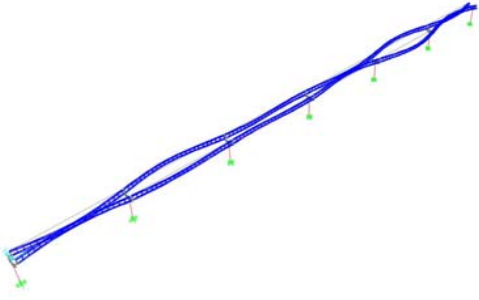
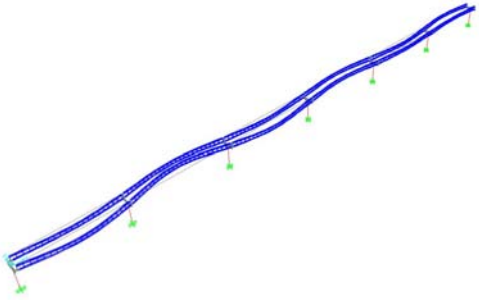
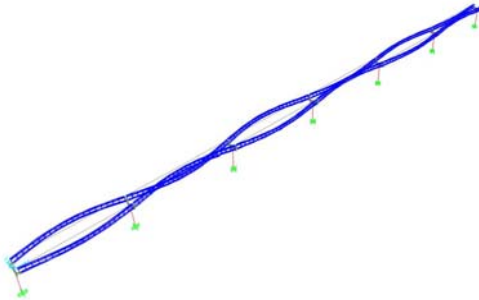
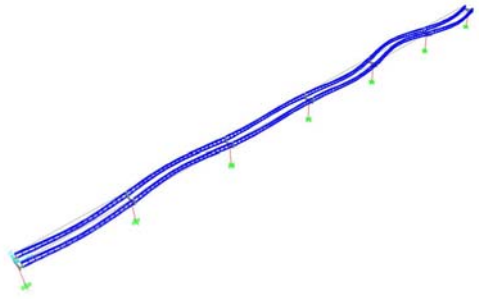
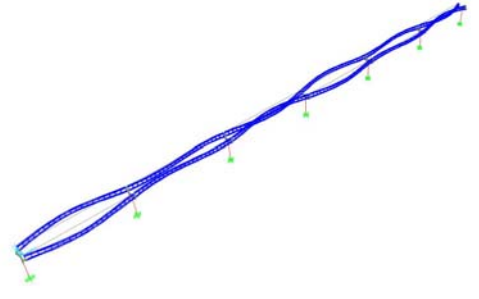
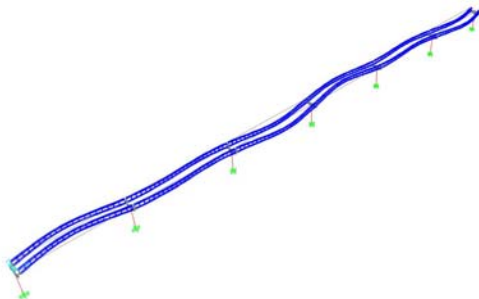
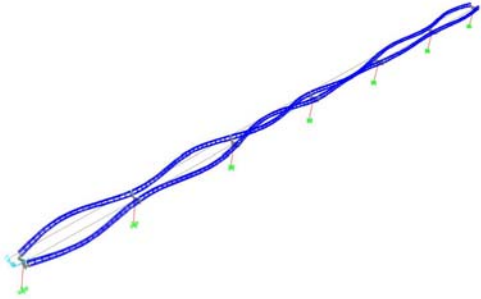
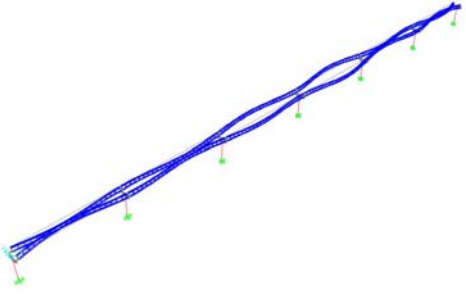
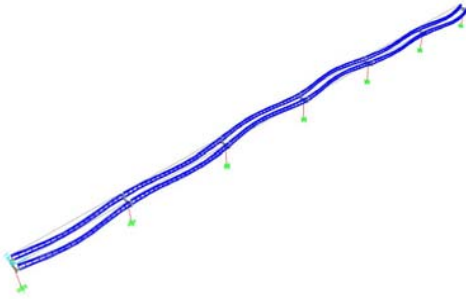
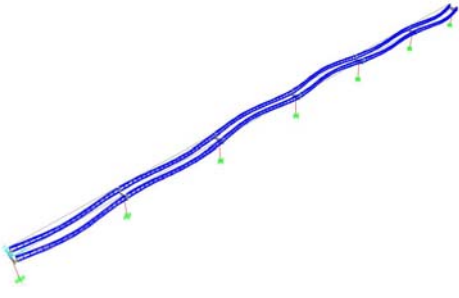
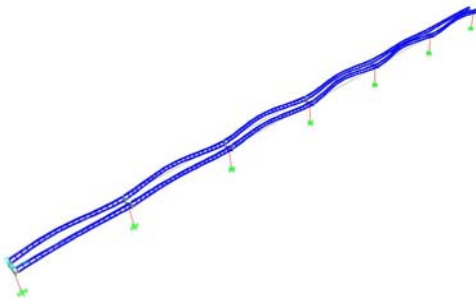
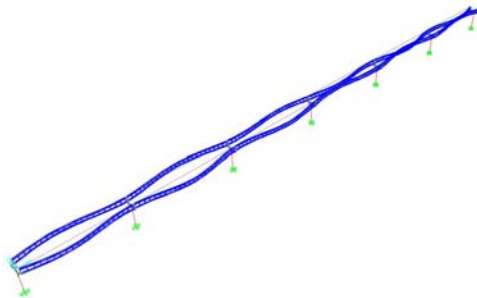
					
Mode 13	2.2348 Hz	Mode 14	2.3399 Hz	Mode 15	2.3775 Hz
Lateral beam bending		Symmetric vertical beam bending, weak-axis column bending		Anti-symmetric vertical beam bending, crosshead torsion, transverse bridge sway	

Table 10: Lower-Bound Stiffness Model Frequencies and Mode Shapes

					
Mode 1	-0.1136 Hz	Mode 2	0.2336 Hz	Mode 3	-0.3428 Hz
Lateral beam bending		Lateral beam bending, column torsion		Lateral beam bending	
					
Mode 4	0.3818 Hz	Mode 5	0.5342 Hz	Mode 6	0.6664 Hz
Lateral beam bending, column torsion		Lateral beam bending, slight longitudinal bridge oscillation		Lateral beam bending, slight strong-axis column bending	

					
Mode 7	0.8045 Hz	Mode 8	0.81458 Hz	Mode 9	0.8333 Hz
Longitudinal bridge oscillation, lateral beam bending		Longitudinal bridge oscillation, lateral beam bending		Strong-axis column bending, lateral beam bending	
					
Mode 10	1.0006 Hz	Mode 11	1.1039 Hz	Mode 12	1.1179 Hz
Transverse bridge oscillation, lateral beam bending, center column torsion		Transverse bridge sway, lateral beam bending, strong-axis column bending		Lateral beam bending	

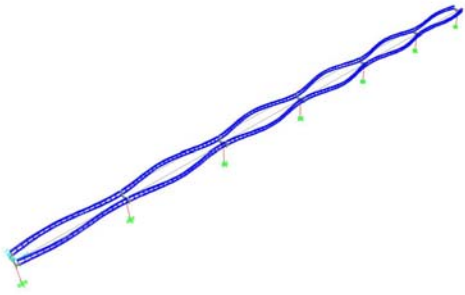
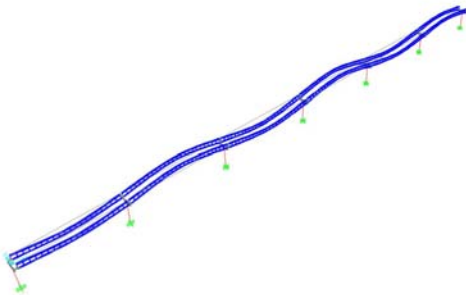
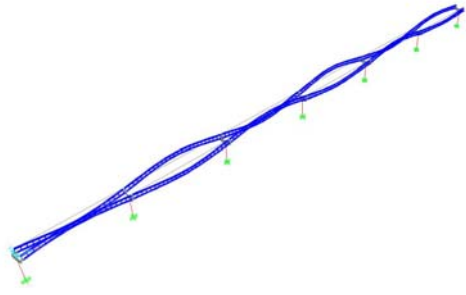
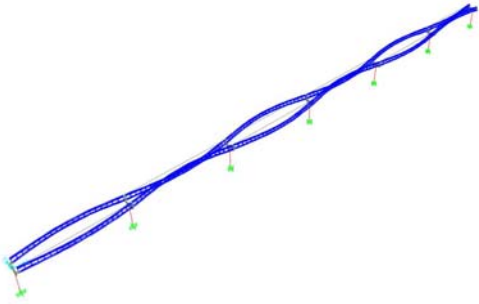
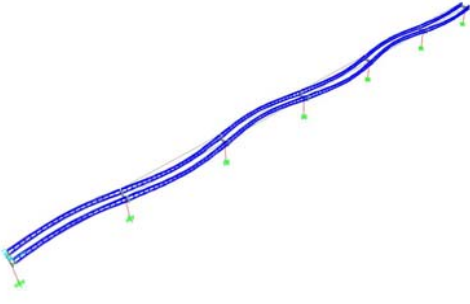
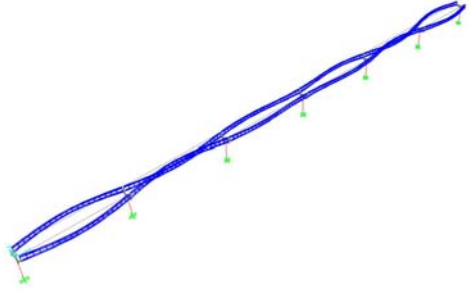
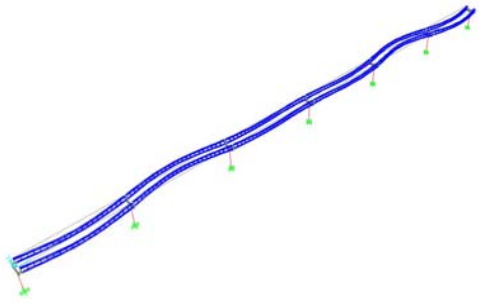
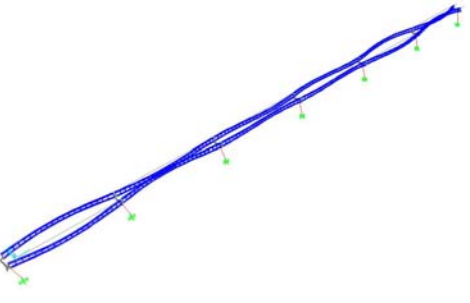
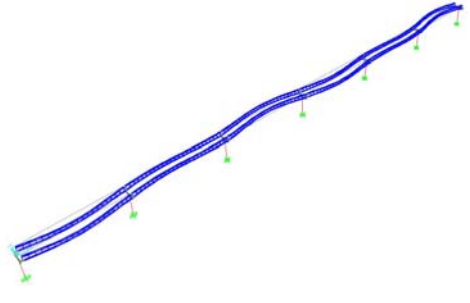
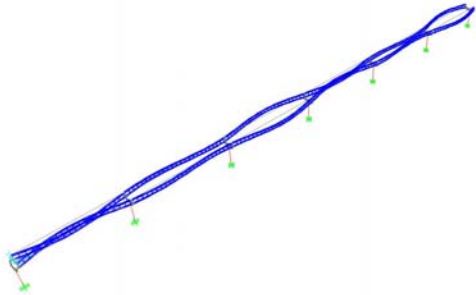
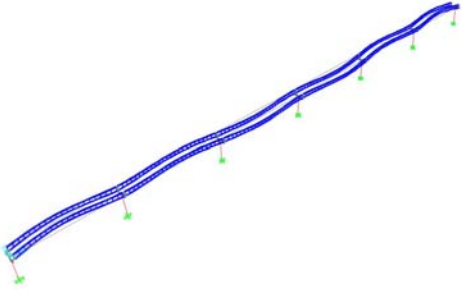
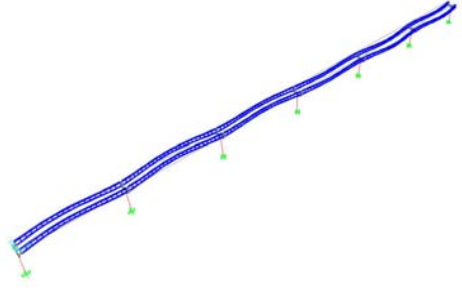
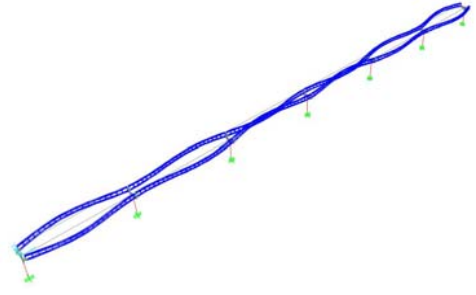
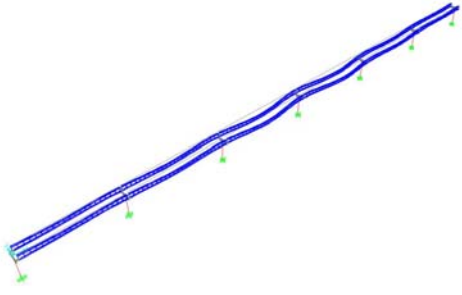
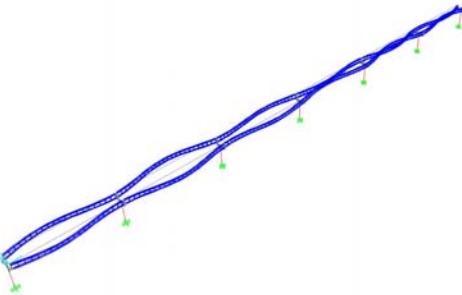
					
Mode 13	1.3232 Hz	Mode 14	1.4344 Hz	Mode 15	1.5019 Hz
Lateral beam bending		Symmetric vertical beam bending, weak-axis column bending		Anti-symmetric vertical beam bending, crosshead torsion, transverse bridge sway	

Table 11: Upper-Bound Stiffness Model Frequencies and Mode Shapes

					
Mode 1	0.9981 Hz	Mode 2	1.1250 Hz	Mode 3	1.2020 Hz
Lateral beam bending, longitudinal bridge oscillation		Lateral beam bending, column torsion		Lateral beam bending	
					
Mode 4	1.2522 Hz	Mode 5	1.3284 Hz	Mode 6	1.5112 Hz
Lateral beam bending, column torsion		Longitudinal bridge oscillation, lateral beam bending		Lateral beam bending, strong-axis column bending, slight longitudinal bridge oscillation	

					
Mode 7	1.5901 Hz	Mode 8	1.7476 Hz	Mode 9	1.9066 Hz
Lateral beam bending, longitudinal bridge oscillation		Strong-axis column bending, lateral beam bending		Transverse bridge oscillation, lateral beam bending, center column torsion	
					
Mode 10	1.9538 Hz	Mode 11	2.0735 Hz	Mode 12	2.3888 Hz
Lateral beam bending		Transverse bridge sway, lateral beam bending, strong-axis column bending		Lateral beam bending	

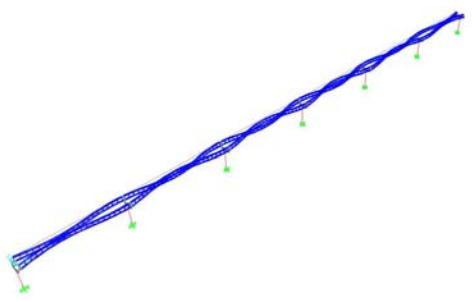
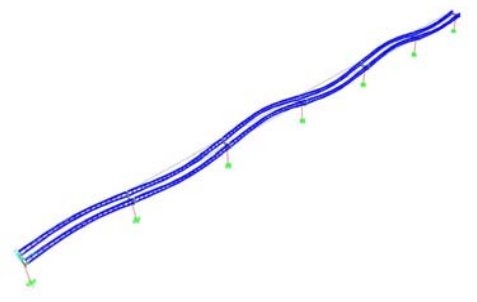
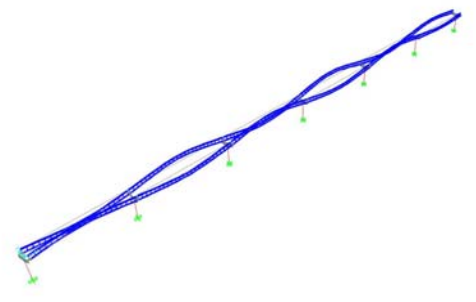
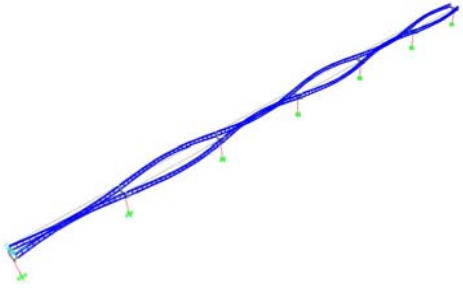
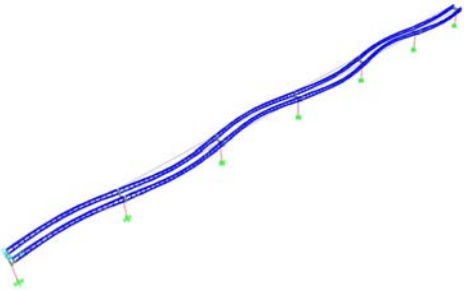
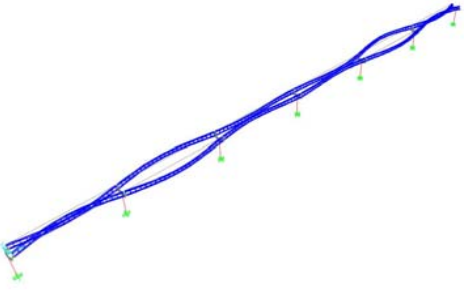
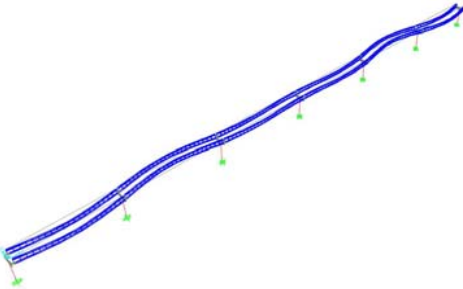
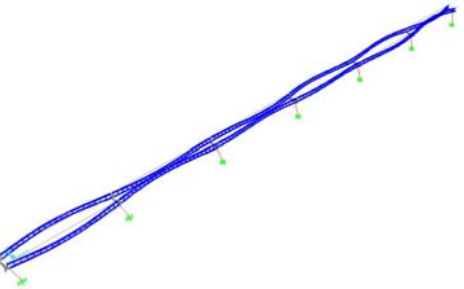
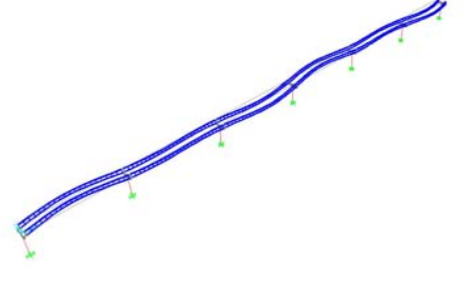
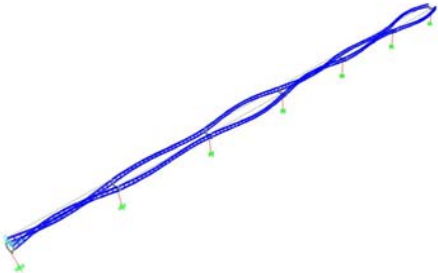
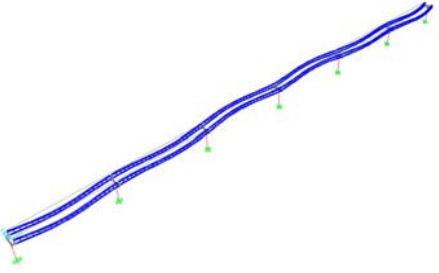
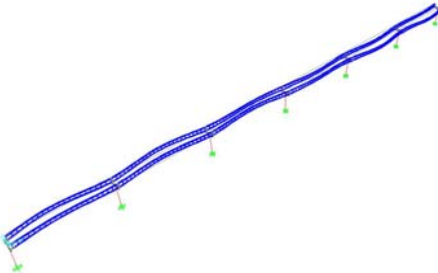
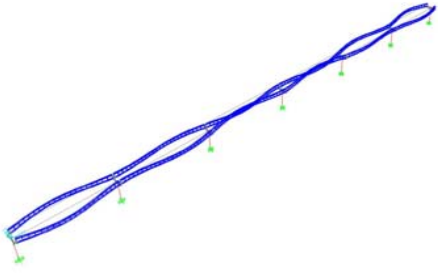
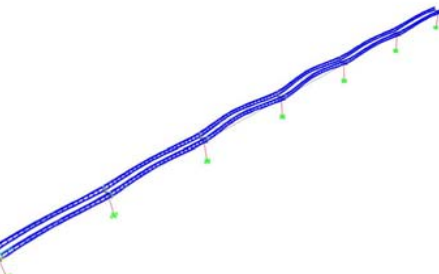
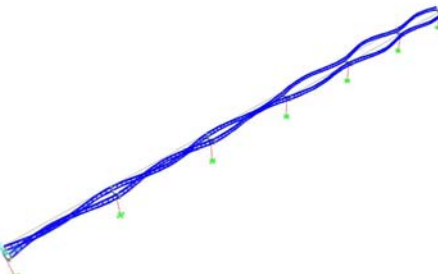
					
Mode 13	2.7233 Hz	Mode 14	2.8093 Hz	Mode 15	2.8396 Hz
Lateral beam bending		Symmetric vertical beam bending, weak-axis column bending		Anti-symmetric vertical beam bending, crosshead torsion, slight transverse bridge sway	

Table 12: Lower-Bound Prestress Loss Model Frequencies and Mode Shapes

					
Mode 1	0.6802 Hz	Mode 2	0.8318 Hz	Mode 3	0.8668 Hz
Lateral beam bending		Lateral beam bending, column torsion		Lateral beam bending	
					
Mode 4	0.9444 Hz	Mode 5	1.0314 Hz	Mode 6	1.1926 Hz
Lateral beam bending, column torsion		Longitudinal bridge oscillation, lateral beam bending		Lateral beam bending, strong-axis column bending	

					
Mode 7	1.2260 Hz	Mode 8	1.3948 Hz	Mode 9	1.5392 Hz
Lateral beam bending, longitudinal bridge oscillation		Strong-axis column bending, lateral beam bending		Transverse bridge oscillation, lateral beam bending, center column torsion	
					
Mode 10	1.5451 Hz	Mode 11	1.6750 Hz	Mode 12	1.9249 Hz
Lateral beam bending		Transverse bridge sway, lateral beam bending, strong-axis column bending		Lateral beam bending	

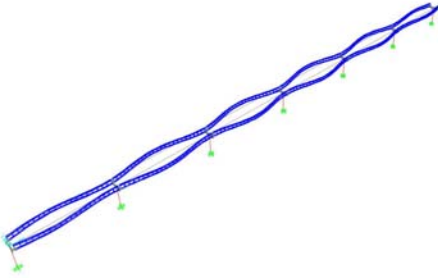
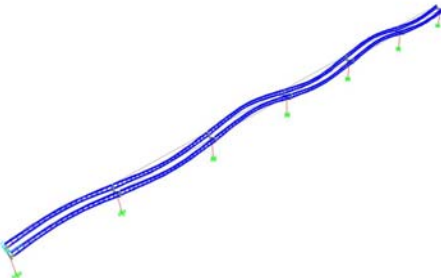
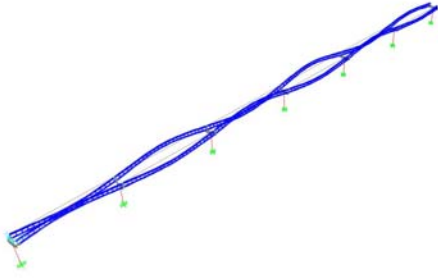
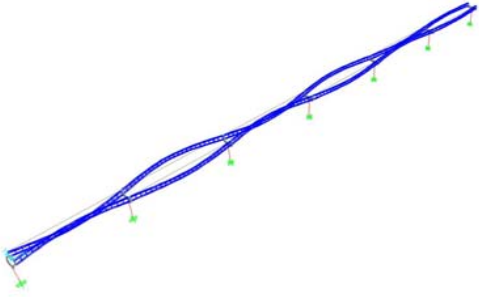
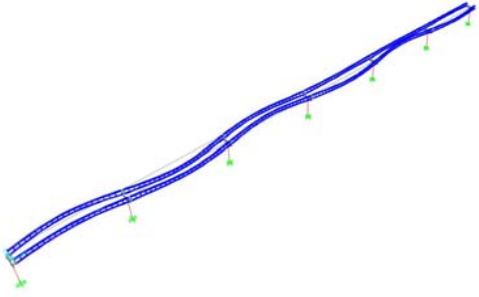
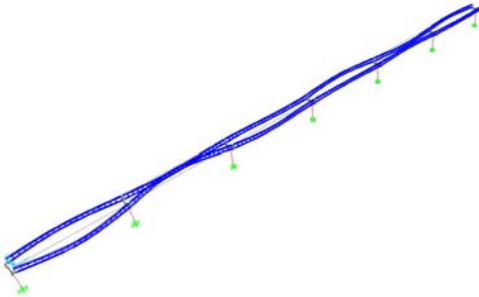
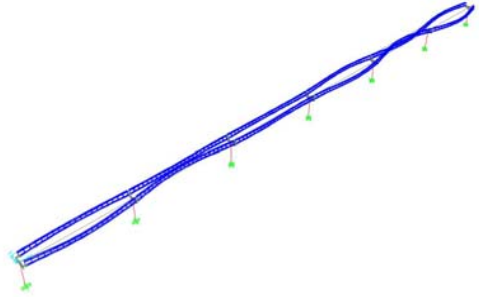
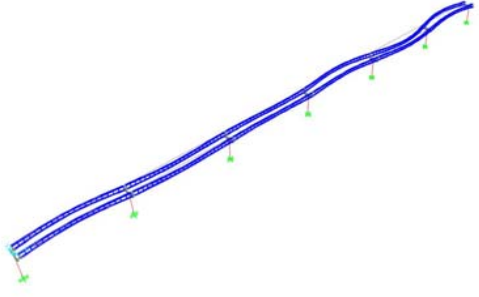
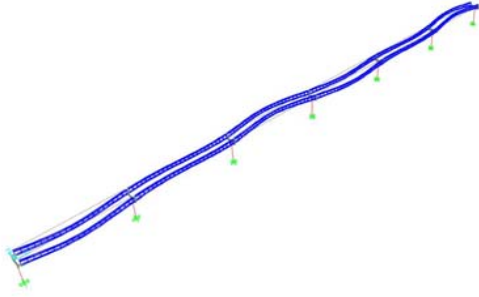
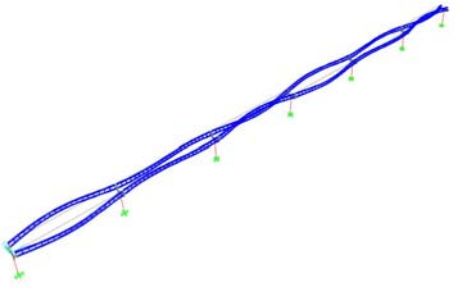
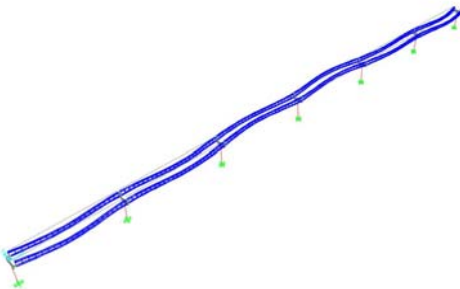
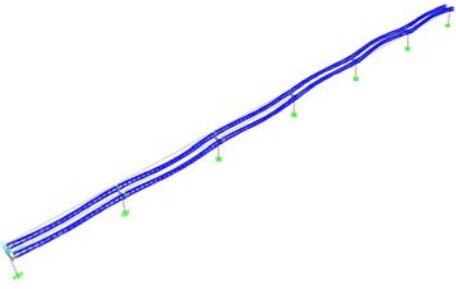
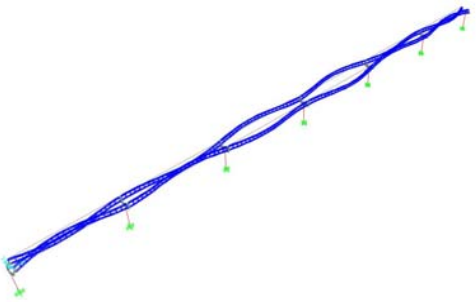
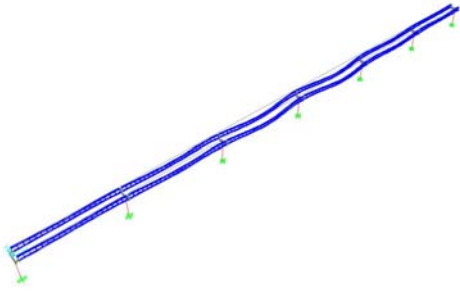
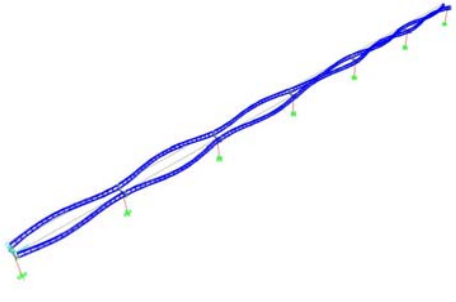
					
Mode 13	2.2109 Hz	Mode 14	2.3223 Hz	Mode 15	2.3607 Hz
Lateral beam bending		Symmetric vertical beam bending, weak-axis column bending		Anti-symmetric vertical beam bending, crosshead torsion, transverse bridge sway	

Table 13: Upper-Bound Prestress Loss Model Frequencies and Mode Shapes

					
Mode 1	0.8769 Hz	Mode 2	0.9928 Hz	Mode 3	1.0376 Hz
Lateral beam bending, longitudinal bridge oscillation		Lateral beam bending, column torsion, slight longitudinal bridge oscillation		Lateral beam bending, longitudinal bridge oscillation	
					
Mode 4	1.0697 Hz	Mode 5	1.1134 Hz	Mode 6	1.3035 Hz
Lateral beam bending, longitudinal bridge oscillation		Lateral beam bending, column torsion		Lateral beam bending, strong-axis column bending	

					
Mode 7	1.3652 Hz	Mode 8	1.4749 Hz	Mode 9	1.5855 Hz
Lateral beam bending, longitudinal bridge oscillation		Strong-axis column bending, lateral beam bending		Transverse bridge oscillation, lateral beam bending, center column torsion	
					
Mode 10	1.6750 Hz	Mode 11	1.7159 Hz	Mode 12	2.0329 Hz
Lateral beam bending		Transverse bridge sway, lateral beam bending, strong-axis column bending		Lateral beam bending	

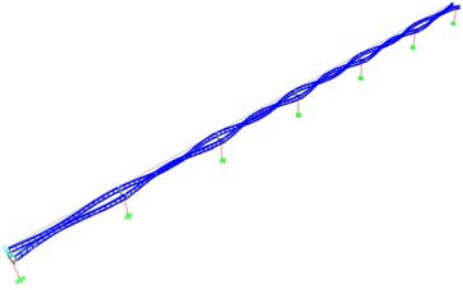
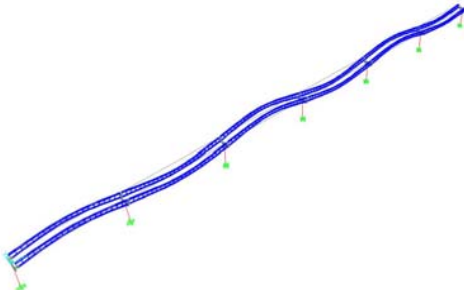
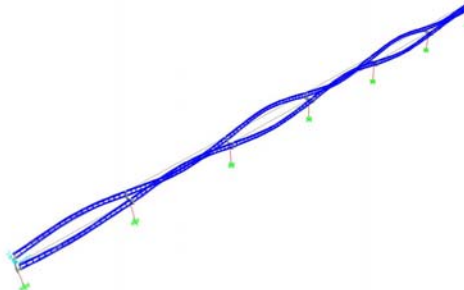
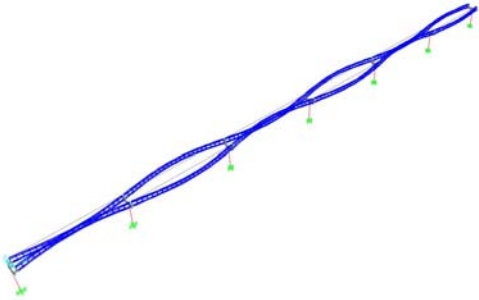
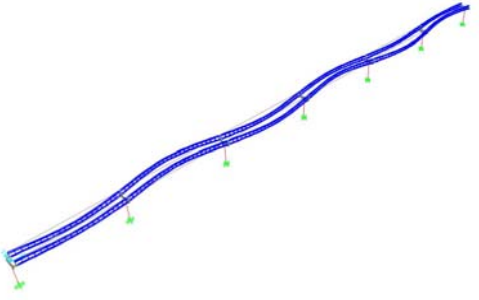
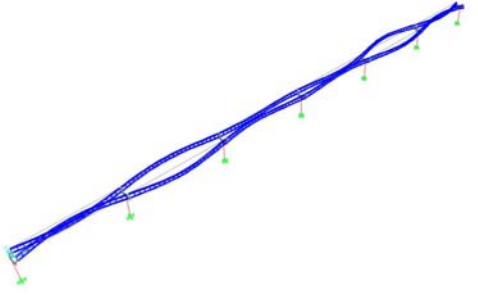
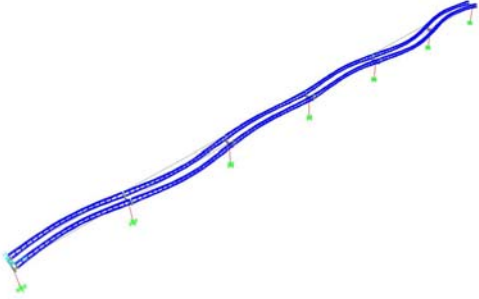
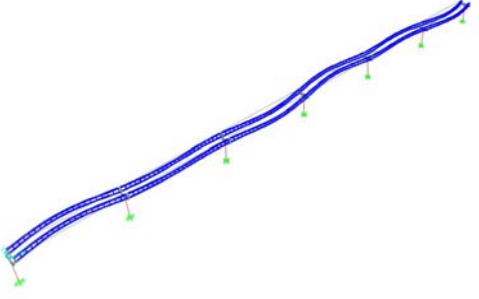
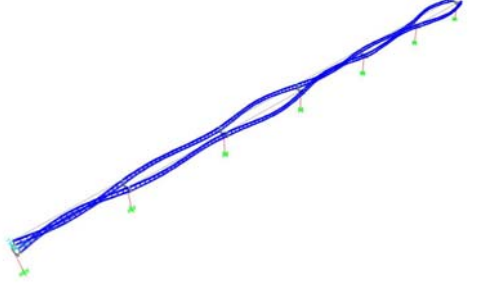
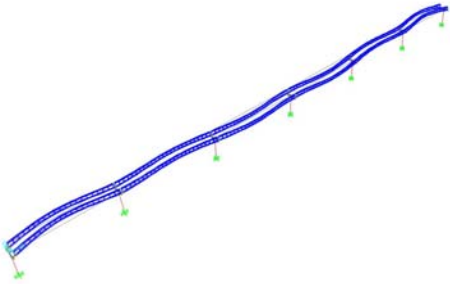
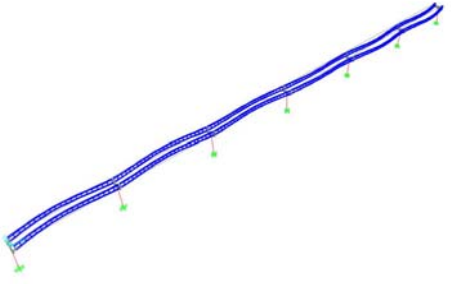
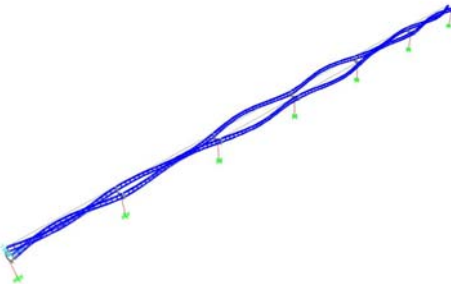
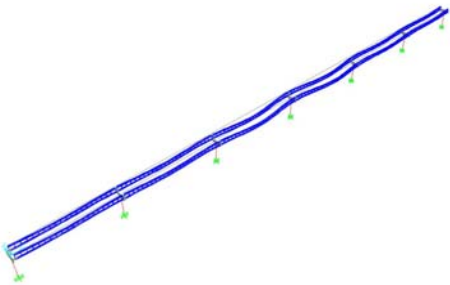
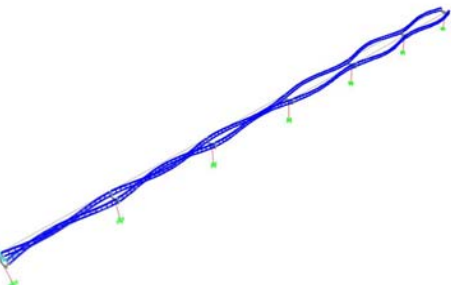
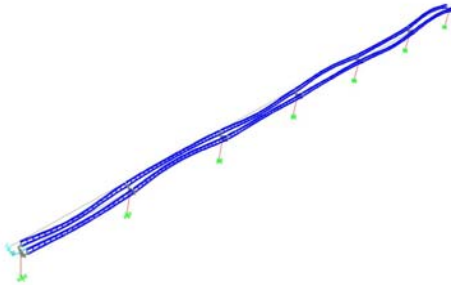
					
Mode 13	2.3127 Hz	Mode 14	2.3965 Hz	Mode 15	2.4313 Hz
Lateral beam bending		Symmetric vertical beam bending, weak-axis column bending		Anti-symmetric vertical beam bending, crosshead torsion, transverse bridge sway	

Table 14: Upper-Bound Boundary Condition Model Frequencies and Mode Shapes

					
Mode 1	0.8155 Hz	Mode 2	0.9434 Hz	Mode 3	0.9797 Hz
Lateral beam bending		Lateral beam bending, column torsion		Lateral beam bending	
					
Mode 4	1.0551 Hz	Mode 5	1.2917 Hz	Mode 6	1.2966 Hz
Lateral beam bending, column torsion, slight center column transverse sway		Lateral beam bending, slight transverse bridge oscillation		Lateral beam bending	

					
Mode 7	1.4802 Hz	Mode 8	1.5908 Hz	Mode 9	1.6222 Hz
Strong-axis column bending, lateral beam bending		Transverse bridge oscillation, lateral beam bending, center column torsion		Lateral beam bending	
					
Mode 10	1.7004 Hz	Mode 11	1.9848 Hz	Mode 12	2.2155 Hz
Transverse bridge sway, lateral beam bending, strong-axis column bending		Lateral beam bending		Longitudinal bridge oscillation, vertical beam bending, lateral beam bending	

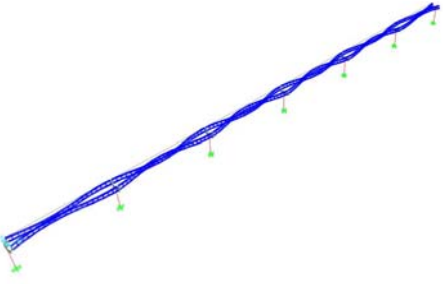
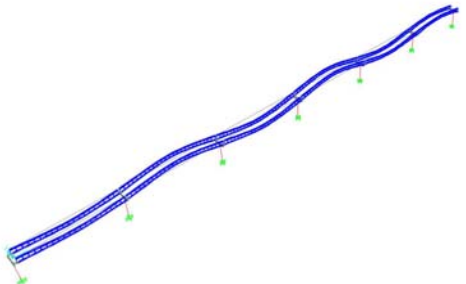
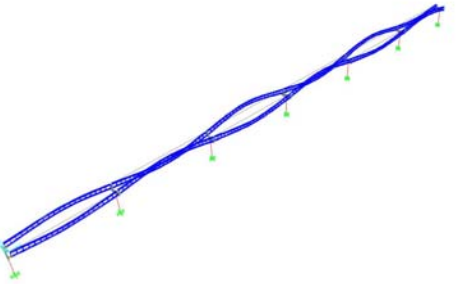
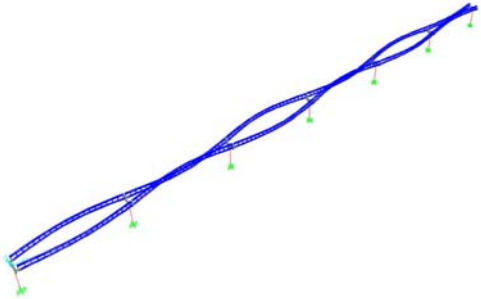
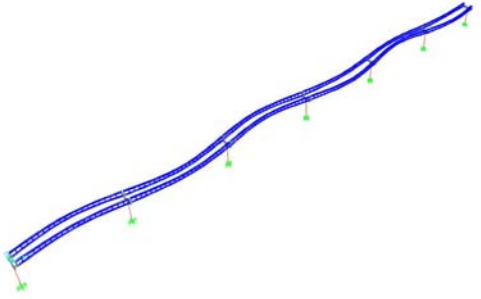
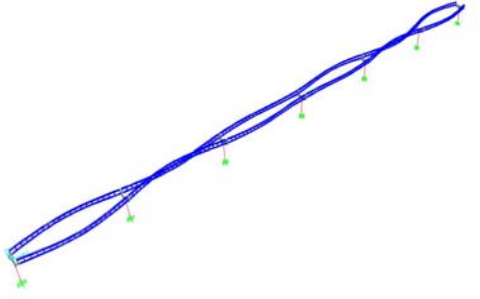
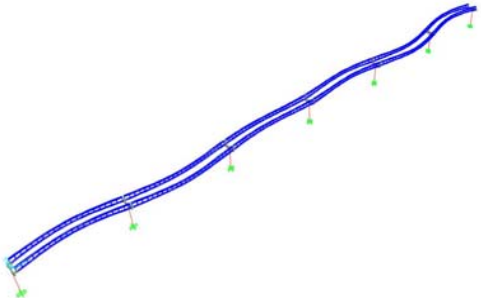
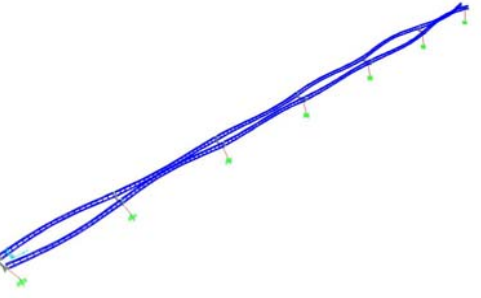
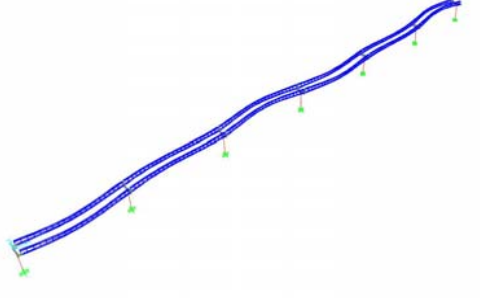
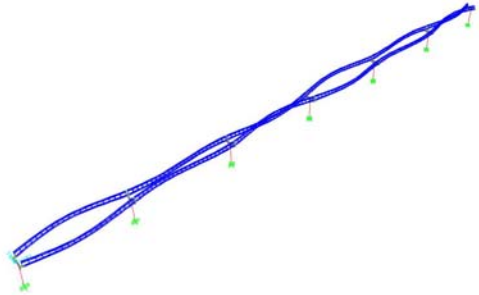
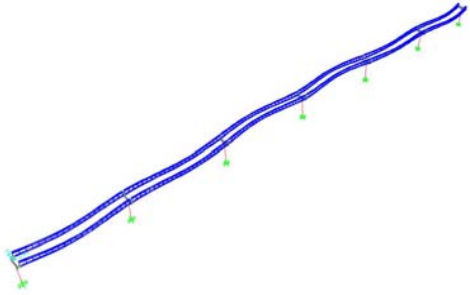
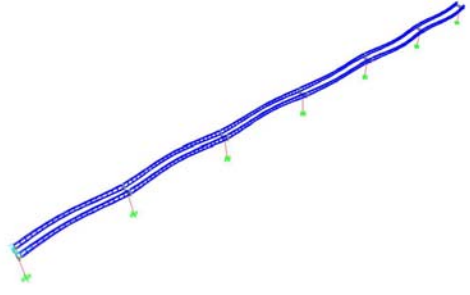
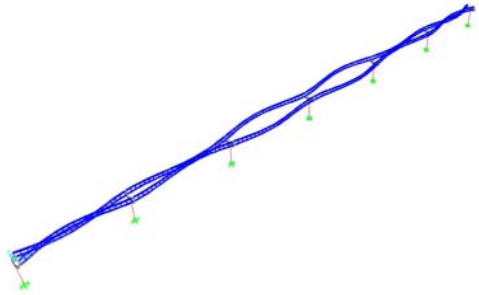
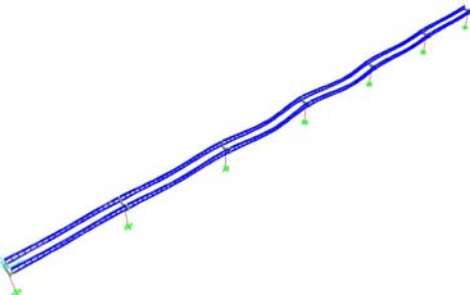
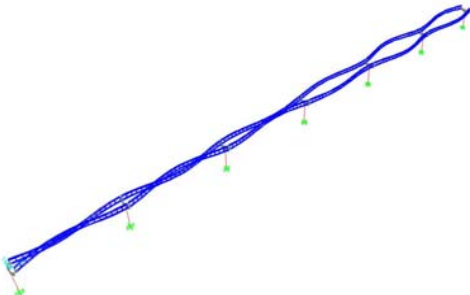
					
Mode 13	2.2656 Hz	Mode 14	2.3771 Hz	Mode 15	2.4302 Hz
Lateral beam bending		Symmetric vertical beam bending, weak-axis column bending, slight longitudinal bridge oscillation		Anti-symmetric vertical beam bending, crosshead torsion, slight transverse bridge sway	

Table 15: Lower-Bound Continuity Condition Model Frequencies and Mode Shapes

					
Mode 1	0.7336 Hz	Mode 2	0.8709 Hz	Mode 3	0.9109 Hz
Lateral beam bending		Lateral beam bending, column torsion		Lateral beam bending	
					
Mode 4	0.9772 Hz	Mode 5	1.0346 Hz	Mode 6	1.2016 Hz
Lateral beam bending, column torsion		Longitudinal bridge oscillation, lateral beam bending		Lateral beam bending, strong-axis column bending	

					
Mode 7	1.2454 Hz	Mode 8	1.3850 Hz	Mode 9	1.5103 Hz
Lateral beam bending, longitudinal bridge oscillation		Strong-axis column bending, lateral beam bending		Transverse bridge oscillation, lateral beam bending, center column torsion	
					
Mode 10	1.5481 Hz	Mode 11	1.6368 Hz	Mode 12	1.9027 Hz
Lateral beam bending		Transverse bridge sway, lateral beam bending, strong-axis column bending		Lateral beam bending	

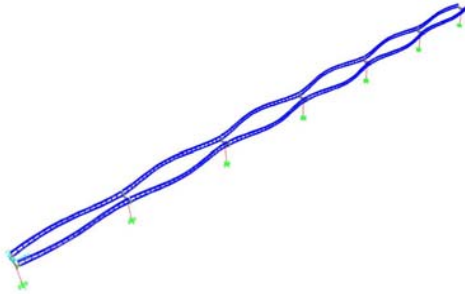
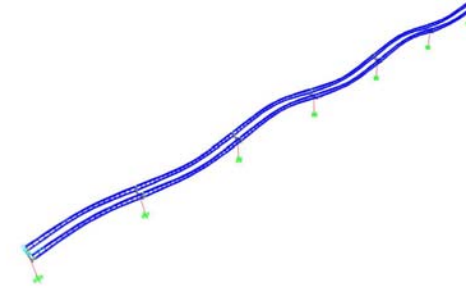
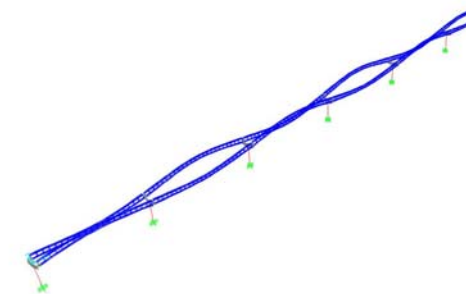
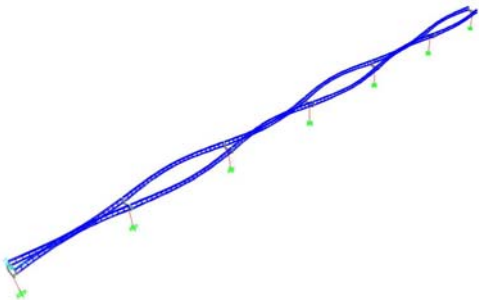
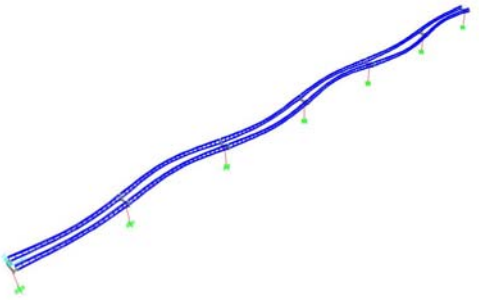
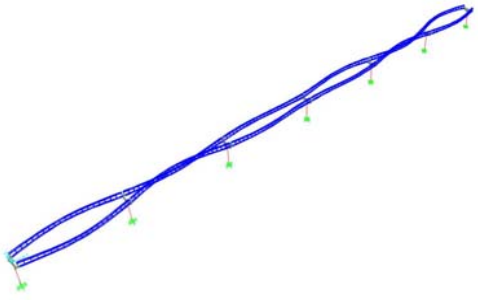
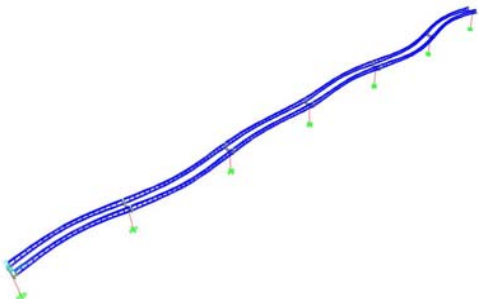
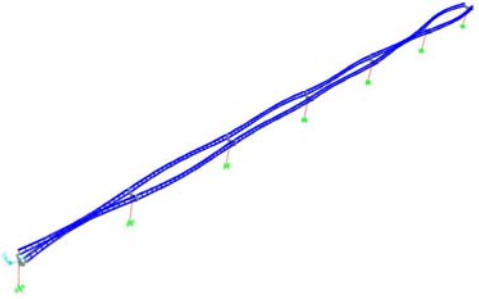
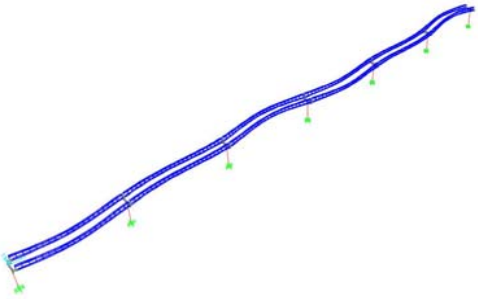
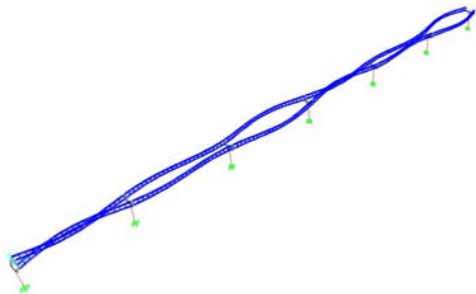
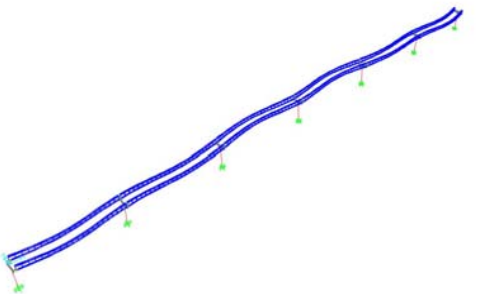
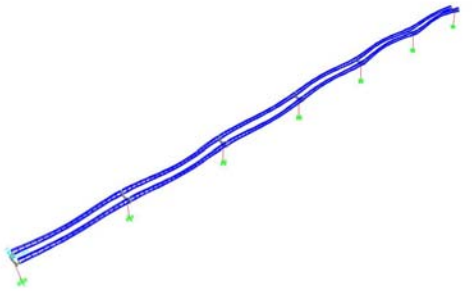
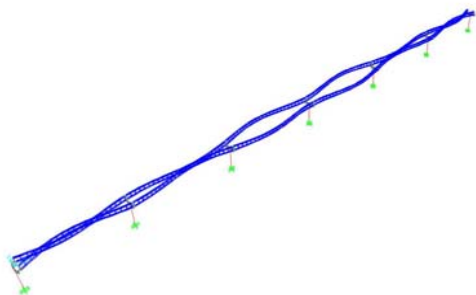
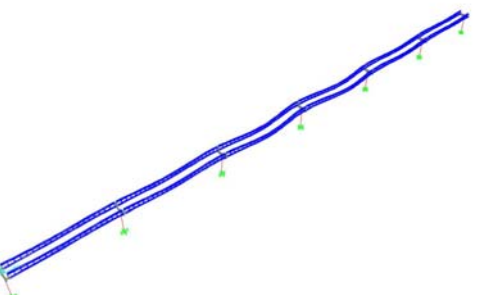
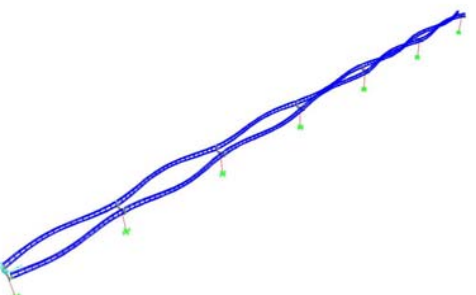
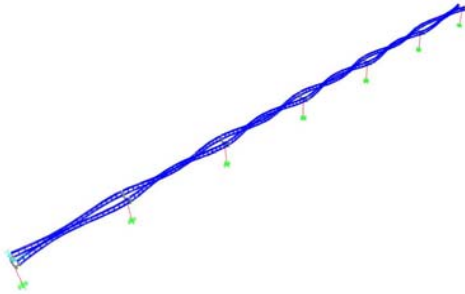
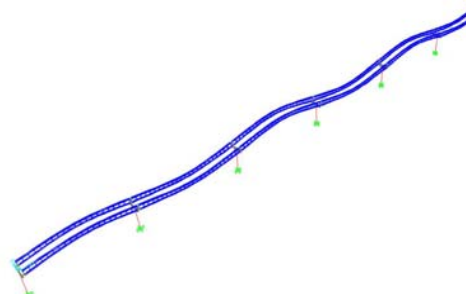
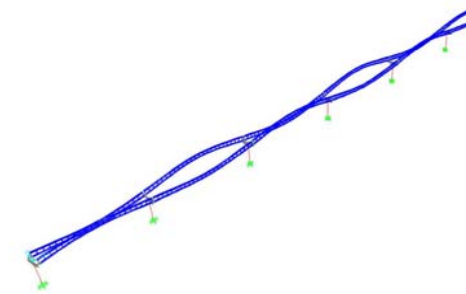
					
Mode 13	2.1636 Hz	Mode 14	2.3389 Hz	Mode 15	2.3705 Hz
Lateral beam bending		Symmetric vertical beam bending, weak-axis column bending		Anti-symmetric vertical beam bending, crosshead torsion, transverse bridge sway	

Table 16: Upper-Bound Continuity Condition Model Frequencies and Mode Shapes

					
Mode 1	0.7357 Hz	Mode 2	0.8798 Hz	Mode 3	0.9208 Hz
Lateral beam bending		Lateral beam bending, column torsion		Lateral beam bending	
					
Mode 4	0.9920 Hz	Mode 5	1.0385 Hz	Mode 6	1.234 Hz
Lateral beam bending, column torsion		Longitudinal bridge oscillation, lateral beam bending		Lateral beam bending, strong-axis column bending	

					
Mode 7	1.2711 Hz	Mode 8	1.4354 Hz	Mode 9	1.5770 Hz
Lateral beam bending, longitudinal bridge oscillation		Strong-axis column bending, lateral beam bending		Transverse bridge oscillation, lateral beam bending, center column torsion	
					
Mode 10	1.5965 Hz	Mode 11	1.7144 Hz	Mode 12	1.9827 Hz
Lateral beam bending		Transverse bridge sway, lateral beam bending, strong-axis column bending		Lateral beam bending	

					
Mode 13	2.2794 Hz	Mode 14	2.3405 Hz	Mode 15	2.3815 Hz
Lateral beam bending		Symmetric vertical beam bending, weak-axis column bending		Anti-symmetric vertical beam bending, crosshead torsion, transverse bridge sway	

## **APPENDIX D: STATIC DEFLECTION RESULTS**

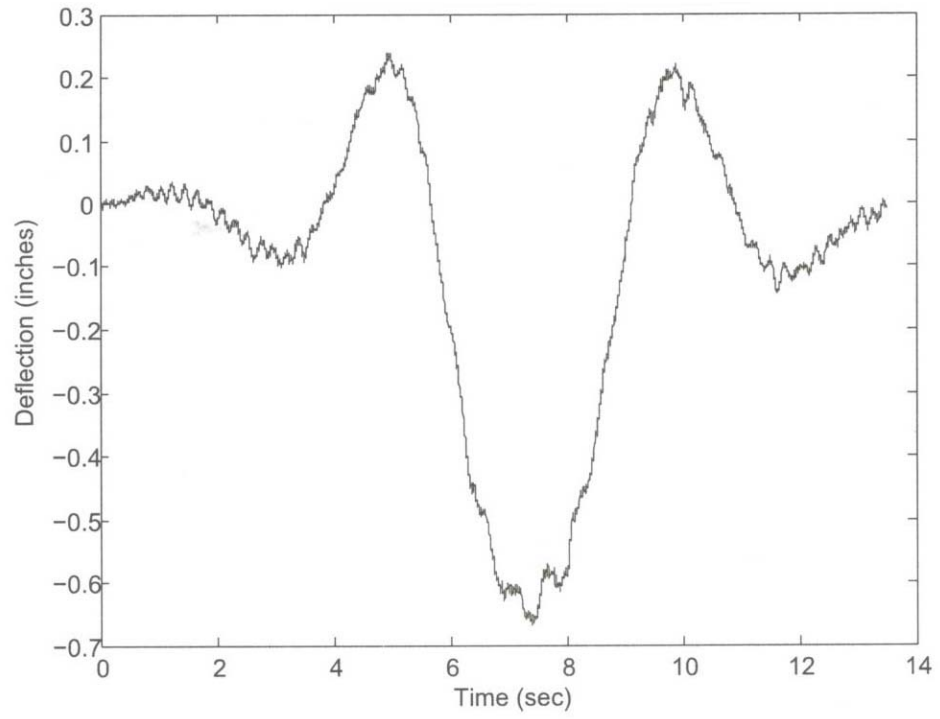


Figure 40: Run #1 Static Deflection Results

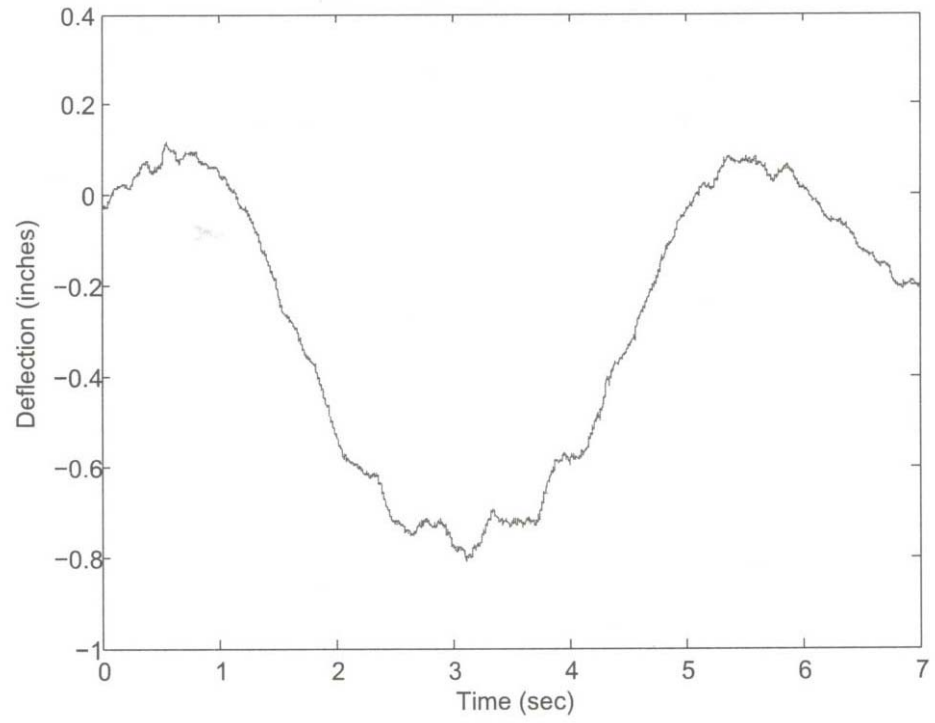


Figure 41: Run #2 Static Deflection Results

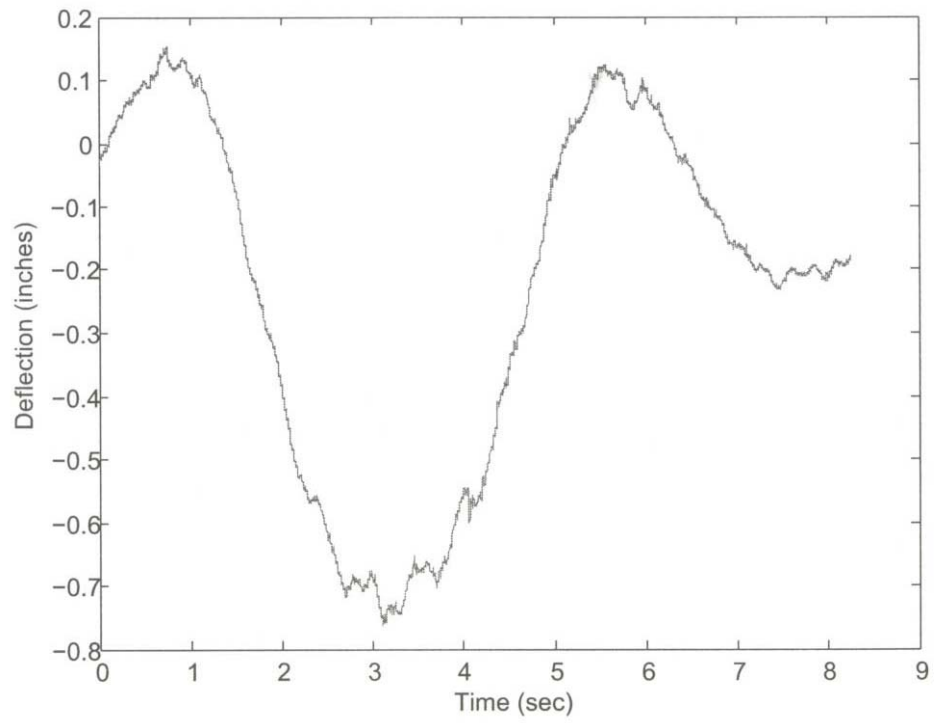


Figure 42: Run #3 Static Deflection Results

## **APPENDIX E: TRAIN LOAD ASSUMPTIONS**

Table 17: Mark IV Train Loads

<b>TABLE: Vehicles 3 - General Vehicles 2 - Loads</b>									
<b>VehName</b>	<b>LoadType</b>	<b>UnifLoad</b>	<b>UnifType</b>	<b>UnifWidth</b>	<b>AxleLoad</b>	<b>AxleType</b>	<b>AxleWidth</b>	<b>MinDist</b>	<b>MaxDist</b>
Text	Text	Kip/in	Text	in	Kip	Text	in	in	in
MarkIV	Fixed Length	0	Zero Width		10.6	One Point		1	
MarkIV	Fixed Length	0	Zero Width		10.6	One Point		306.5	
MarkIV	Fixed Length	0	Zero Width		10.6	One Point		51	
MarkIV	Fixed Length	0	Zero Width		10.6	One Point		306.5	
MarkIV	Fixed Length	0	Zero Width		10.6	One Point		51	
MarkIV	Fixed Length	0	Zero Width		10.6	One Point		306.5	
MarkIV	Fixed Length	0	Zero Width		10.6	One Point		51	
MarkIV	Fixed Length	0	Zero Width		10.6	One Point		306.5	
MarkIV	Fixed Length	0	Zero Width		10.6	One Point		51	
MarkIV	Fixed Length	0	Zero Width		10.6	One Point		306.5	

Table 18: Mark VI Train Loads and Loading Assumptions

VehName	LoadType	UnifLoad	UnifType	UnifWidth	AxleLoad	AxleType	AxleWidth	MinDist	MaxDist
Text	Text	Kip/in	Text	in	Kip	Text	in	in	in
MarkVI	Fixed Leng	0	Zero Width		16.18221	One Point		1	
MarkVI	Fixed Leng	0	Zero Width		13.51308	One Point		308.5	
MarkVI	Fixed Leng	0	Zero Width		14.23413	One Point		54.5	
MarkVI	Fixed Leng	0	Zero Width		14.80810	One Point		308.5	
MarkVI	Fixed Leng	0	Zero Width		14.88679	One Point		54.5	
MarkVI	Fixed Leng	0	Zero Width		14.47308	One Point		308.5	
MarkVI	Fixed Leng	0	Zero Width		14.53410	One Point		54.5	
MarkVI	Fixed Leng	0	Zero Width		14.56456	One Point		308.5	
MarkVI	Fixed Leng	0	Zero Width		14.58254	One Point		54.5	
MarkVI	Fixed Leng	0	Zero Width		13.90858	One Point		308.5	
MarkVI	Fixed Leng	0	Zero Width		13.48183	One Point		54.5	
MarkVI	Fixed Leng	0	Zero Width		16.28627	One Point		308.5	
					175.45529				

**Assumptions**

	Axle1	Axle 2	Axle 3	Axle 4	Axle 5	Axle 6	Axle 7	Axle 8	Axle 9	Axle 10	Axle 11	Axle 12
Passengers/ Car	55	55	55	55	55	55	55	55	55	55	55	55
Cab Passengers	5	0	0	0	0	0	0	0	0	0	0	5
Passengers/ Axle	32.5	27.5	27.5	27.5	27.5	27.5	27.5	27.5	27.5	27.5	27.5	32.5
Passenger Weight (lb)	155	155	155	155	155	155	155	155	155	155	155	155
Passenger Weight/Axle (lb)	5038	4263	4263	4263	4263	4263	4263	4263	4263	4263	4263	5038
Vehicle Self-Weight (lb)	11145	9251	9972	10546	10624	10211	10272	10302	10320	9646	9219	11249
Axle Load (lb)	16182	13513	14234	14808	14887	14473	14534	14565	14583	13909	13482	16286
Axle Load (kip)	16	14	14	15	15	14	15	15	15	14	13	16

## **APPENDIX F: LOAD RATING AND RELIABILITY ANALYSES**

AASHTO LRFR LOAD RATING (USING NOMINAL BEAMWAY FINITE ELEMENT MODEL)

This evaluation is based on *AASHTO Manual for Condition Evaluation and Load and Resistance Factor Rating (LRFR) of Highway Bridges, October 2003* with references to *AASHTO LRFD Bridge Design Specifications, 3rd. Edition, 2004*.

ASSUMPTIONS:

Load factors,

Inventory Level		LRFR Table 6-1
$\gamma_{DC} := 1.25$	$\gamma_{DW} := 1.50$	
$\gamma_{LL}$	To be determined by special calculation below.	
IM := 15%	measured by owner in previous study	

Resistance Factors

LRFD 5.5.4.2.1

$\phi_M := 1.00$	flexure and tension of prestressed concrete
$\phi_V := 0.90$	shear and torsion of normal weight concrete
$\phi_N := 0.75$	axial compression with spirals or ties

Condition Factor  $\phi_c$

LRFR 6.4.2.3

$\phi_c := 1.00$	for "good or satisfactory condition"
------------------	--------------------------------------

System Factor  $\phi_s$

LRFR 6.4.2.4

$\phi_{sM} := \frac{1}{1.05}$	For nonredundant members (LRFD 1.3.4 following LRFR C6.4.2.4). Assume beamway box girders are nonredundant.
$\phi_{sV} := 1.00$	System factors not appropriate for shear (LRFR C6.4.2.4)

Prestressing tendons,

$f_{pu} := 27000\text{psi}$	$E_p := 28500\text{ksi}$
$f_{py} := 0.85 \cdot f_{pu}$	$f_{py} = 22950\text{psi}$

Reinforcing Steel

$E_s := 29000\text{ksi}$
--------------------------

ENTER ALL LOAD EFFECTS (MOMENT AND SHEAR VALUES) FROM SAP2000:

MAXIMUM SHEAR AND MOMENT AT CRITICAL SECTION NEAR INTERIOR SUPPORT

The maximum shear is interpolated from SAP2000 results. Maximum shear is at critical distance (found below as  $dv = 57.6$  in), exterior-facing side of first interior support.

$$V_{LLIV} := 46.477 \text{kip}$$

$$V_{LLVI} := 65.290 \text{kip}$$

$$V_{DC} := 61.403 \text{kip}$$

$$V_{DW} := 0 \text{kip} \quad (\text{no bituminous overlay})$$

Moments (Mark VI Train). Linear interpolation from SAP2000 response:

$$M_{LLMCFT} := 1126.7 \text{kip}\cdot\text{ft}$$

$$M_{DCMCFT} := 1022.9 \text{kip}\cdot\text{ft}$$

$$M_{DW} := 0 \text{kip}\cdot\text{ft}$$

MAX. MOMENTS AT FACE OF FIRST INT. SUPPORT, SPAN 1 @ 0.4L, AND SPAN 2 @ MIDSPAN.

Absolute value for negative bending taken directly from SAP2000 output (Mark IV train):

$$M_{DCAIV} := 1300.093 \text{kip}\cdot\text{ft}$$

$$M_{LLAIV} := 916.684 \text{kip}\cdot\text{ft}$$

Absolute value for positive bending (Span 1, 0.4L) taken directly from SAP2000 output (Mark IV train):

$$M_{DCBIV} := 535.89 \text{kip}\cdot\text{ft}$$

$$M_{LLBIV} := 578.876 \text{kip}\cdot\text{ft}$$

Absolute value for positive bending (Span 2, 0.5L) taken directly from SAP2000 output (Mark IV train):

$$M_{DCCIV} := 245.148 \text{kip}\cdot\text{ft}$$

$$M_{LLCIV} := 509.997 \text{kip}\cdot\text{ft}$$

Absolute value for negative bending taken directly from SAP2000 output (Mark VI train):

$$M_{DCAVI} := M_{DCAIV}$$

$$M_{DCAVI} = 1300.1 \text{kip}\cdot\text{ft}$$

$$M_{LLAVI} := 1368.918 \text{kip}\cdot\text{ft}$$

Absolute value for positive bending (Span 1, 0.4L) taken directly from SAP2000 output (Mark VI train):

$$M_{DCBVI} := M_{DCBIV}$$

$$M_{DCBVI} = 535.9 \text{ kip}\cdot\text{ft}$$

$$M_{LLBVI} := 786.937 \text{ kip}\cdot\text{ft}$$

Absolute value for positive bending (Span 2, 0.5L) taken directly from SAP2000 output (Mark VI train):

$$M_{DCCVI} := M_{DCCIV}$$

$$M_{DCCVI} = 245.1 \text{ kip}\cdot\text{ft}$$

$$M_{LLCVI} := 693.733 \text{ kip}\cdot\text{ft}$$

CUSTOM LOAD FACTOR DETERMINATION (MARK VI TRAINS)

Conventional live load factors for AASHTO LRFD/LRFR were determined for HL-93 loading. The inventory and operating design load rating factors ( $\gamma = 1.75$  and  $\gamma = 1.35$ , respectively) seem overly conservative for the beamway application. Whereas the highway loads have substantial uncertainty, it is believed that the scatter in monorail train loads is significantly less, and there must be a rational basis to compute a more appropriate load factor for design and rating.

Assume the following expression for load factor (Nowak, 1993):

$$\gamma := \lambda \cdot (1 + k \cdot \text{COV})$$

Where  $\gamma$  = load factor  
 $\lambda$  = bias factor  
 COV = coefficient of variation  
 k = constant

From Barker (1997):

$$\lambda := \frac{x_m}{x_n}$$

Information from the owner gives the following:

$x_m := 122755\text{lb}$  mean value of Mark VI empty train weight (based on weight data collected in 2000 for all 12 trains)

$x_n := 122755\text{lb}$  nominal or design value used in SAP2000 will be the mean axle weights from the measured data

Bias factor:

$$\lambda_{LL} := \frac{x_m}{x_n} \quad \lambda_{LL} = 1 \quad \text{Note: There is no bias because the analysis values are equivalent to the measured values.}$$

Coefficient of variation:

From weight data provided by owner (2000 adjusted weight data), we assume the highest (most conservative) COV associated with the twelve train axles, and apply to the maximum load effect,

$$\text{COV}_{LL} := 0.0251698$$

Assume  $k := 2.5$  This is the upper-bound (conservative) value for LRFD Code calibration (Nowak, 1993)

Then the appropriate load factor for Mark VI train loads:

$$\gamma_{LL} := \lambda_{LL} \cdot (1 + k \cdot \text{COV}_{LL}) \quad \gamma_{LL} = 1.06$$

However, the lowest live load factor given in AASHTO LRFR for permit vehicles is 1.10. As a conservative assumption, assume 1.10 as a lower-bound value to account for additional uncertainties,

$$\gamma_{LL} := 1.10 \quad \text{lower-bound for permit vehicles} \quad \text{LRFR Table 6-6}$$

COMPUTE NOMINAL FLEXURAL RESISTANCE AT SUPPORTS (NEGATIVE BENDING)

We will neglect pre-stressing strands because they are acting almost exactly at the c.g.c. (c.g.c = 45.75" from the top, pre-tension c.g. = 45.5" from the top)

Average stress in the prestressing (bonded tendons) steel may be taken as,

$$f_{ps} := f_{pu} \cdot \left(1 - k \cdot \frac{c}{d_p}\right) \quad \text{LRFD Eq. (5.7.3.1-1)}$$

$$k := 0.28 \quad \text{for low-relaxation strands} \quad \text{Table C5.7.3.1.1-1}$$

$$f_{pu} = 270 \text{ksi}$$

$d_p$  = distance from extreme compression fiber to the centroid of the prestressing tendons

$$d_p := 48.5 \text{in} \quad \text{from the bottom of the beam for negative bending}$$

To compute  $c$ , assume rectangular section behavior. (Neglect pre-tensioning and non-prestressed reinforcement.)

$$c := \frac{A_{ps} \cdot f_{pu}}{0.85 f_c \cdot \beta_1 \cdot b + k \cdot A_{ps} \cdot \frac{f_{pu}}{d_p}} \quad \text{LRFD Eq. (5.7.3.1.1-4)}$$

$$A_{ps} := 3 \cdot 8 \cdot 0.153 \text{in}^2 \quad A_{ps} = 3.672 \text{in}^2$$

$$b := 26 \text{in} \quad \text{(Beam Width)}$$

$$f_c := 7.0 \text{ksi} \quad \text{(Beam Concrete Nominal Strength)}$$

$$\beta_1 := 0.85 - 0.05 \left( \frac{f_c - 4 \text{ksi}}{\text{ksi}} \right) \quad \beta_1 = 0.7 > 0.65 \quad \text{LRFD 5.7.2.2}$$

$$c := \frac{A_{ps} \cdot f_{pu}}{0.85 f_c \cdot \beta_1 \cdot b + k \cdot A_{ps} \cdot \frac{f_{pu}}{d_p}} \quad c = 8.696 \text{in}$$

$$a := \beta_1 \cdot c \quad a = 6.09 \text{in} < t_{\text{flange}} = 37 \text{in} \quad \text{LRFD 5.7.2.2}$$

Therefore, the rectangular section behavior assumption is valid.

$$f_{ps} := f_{pu} \cdot \left(1 - k \cdot \frac{c}{d_p}\right) \quad f_{ps} = 256.4 \text{ksi} \quad a_1 := a \quad \text{for use in MCFT calculations below}$$

Nominal Flexural Resistance (Beam End):

$$M_n := A_{ps} \cdot f_{ps} \cdot \left(d_p - \frac{a}{2}\right) \quad M_n = 3567.1 \text{kip-ft} \quad \text{LRFD Eq. (5-7.3.2.2-1)}$$

COMPUTE NOMINAL FLEXURAL RESISTANCE AT MIDSPAN 100' Beam (POSITIVE BENDING)

We consider pre-tensioning in addition to post-tensioning:

Average stress in the prestressing (bonded tendons) steel may be taken as,

$$f_{ps} := f_{pu} \cdot \left( 1 - k \cdot \frac{c}{d_p} \right) \quad \text{LRFD Eq. (5.7.3.1-1)}$$

$$k := 0.28 \quad \text{for low-relaxation strands} \quad \text{Table C5.7.3.1.1-1}$$

$$f_{pu} = 270 \text{ksi}$$

$d_p$  = distance from extreme compression fiber to the centroid of the prestressing tendons

For 100' spans, there are 24 1/2"  $\phi$  pre-tension strands [Drawing S-502]

$$A_{Pre} := 24 \cdot 0.153 \text{in}^2 \quad A_{Pre} = 3.7 \text{in}^2$$

$$d_{pPre} := 45.5 \text{in} \quad \text{from the top of the beam}$$

Neglect top post-tension duct contribution, as it is well above the neutral axis:

$$A_{Post} := 2 \cdot 8 \cdot 0.153 \text{in}^2 \quad A_{Post} = 2.45 \text{in}^2$$

$$d_{pPost} := 45.5 \text{in} \quad \text{Post-tensioning, from the top of the beam for positive bending}$$

Find depth from top of beam to c.g. of pre- and post-tension strands combined:

$$A_{Pre} \cdot d_{pPre} + A_{Post} \cdot d_{pPost} = (A_{Pre} + A_{Post}) \cdot d_p$$

$$d_p := \frac{A_{Pre} \cdot d_{pPre} + A_{Post} \cdot d_{pPost}}{A_{Pre} + A_{Post}} \quad d_p = 45.5 \text{in}$$

To compute  $c$ , assume rectangular section behavior. (Neglect non-prestressed reinforcement.)

$$c := \frac{A_{ps} \cdot f_{pu}}{0.85 f'_c \cdot \beta_1 \cdot b + k \cdot A_{ps} \cdot \frac{f_{pu}}{d_p}} \quad \text{LRFD Eq. (5.7.3.1.1-4)}$$

$$A_{ps} := A_{Pre} + A_{Post} \quad A_{ps} = 6.12 \text{in}^2$$

$$b := 26 \text{in} \quad \text{(Beam Width)}$$

$$f'_c := 7.0 \text{ksi} \quad \text{(Beam Concrete Nominal Strength)}$$

$$\beta_1 := 0.85 - 0.05(f_c - 4\text{ksi}) \cdot \frac{1}{\text{ksi}} \quad \beta_1 = 0.7 > 0.65 \quad \text{LRFD 5.7.2.2}$$

$$c := \frac{A_{ps} \cdot f_{pu}}{0.85 f_c \cdot \beta_1 \cdot b + k \cdot A_{ps} \cdot \frac{f_{pu}}{d_p}} \quad c = 13.949\text{in}$$

$$a := \beta_1 \cdot c \quad a = 9.76\text{in} > t_{\text{flange}} = 7\text{in} \quad \text{LRFD 5.7.2.2}$$

Therefore, the rectangular section behavior assumption is not valid.

We have "T-section" behavior. However, we have a box section with two webs. Assume each 5-in. web contributes a net 10-in. web,  $b_w := 10\text{in}$ . The depth of the compression flange is,  $h_f := 7\text{in}$

$$c := \frac{A_{ps} \cdot f_{pu} - 0.85 \beta_1 f_c (b - b_w) \cdot h_f}{0.85 f_c \cdot \beta_1 \cdot b_w + k \cdot A_{ps} \cdot \frac{f_{pu}}{d_p}} \quad c = 22.9\text{in} \quad \text{LRFD Eq. (5.7.3.1.1-3)}$$

$$a := \beta_1 \cdot c \quad a = 16.02\text{in} \quad \text{LRFD 5.7.2.2}$$

$$f_{ps} := f_{pu} \cdot \left(1 - k \cdot \frac{c}{d_p}\right) \quad f_{ps} = 232\text{ksi}$$

Nominal Flexural Resistance (Midspan):

$$M_{n\text{Midspan100}} := A_{ps} \cdot f_{ps} \cdot \left(d_p - \frac{a}{2}\right) \quad \text{LRFD Eq. (5-7.3.2.2-1)}$$

$$M_{n\text{Midspan100}} = 4435.3\text{kip}\cdot\text{ft}$$

COMPUTE NOMINAL FLEXURAL RESISTANCE AT MIDSPAN 110' Beam (POSITIVE BENDING)

We consider pre-tensioning in addition to post-tensioning:

Average stress in the prestressing (bonded tendons) steel may be taken as,

$$f_{ps} := f_{pu} \cdot \left(1 - k \cdot \frac{c}{d_p}\right) \quad \text{LRFD Eq. (5.7.3.1-1)}$$

$$k := 0.28 \quad \text{for low-relaxation strands} \quad \text{Table C5.7.3.1.1-1}$$

$$f_{pu} = 270 \text{ksi}$$

$d_p$  = distance from extreme compression fiber to the centroid of the prestressing tendons

For 110' spans, there are 28 1/2"  $\phi$  pre-tension strands [Drawing S-502]

$$A_{Pre} := 28 \cdot 0.153 \text{in}^2 \quad A_{Pre} = 4.3 \text{in}^2$$

$$d_{pPre} := 45.5 \text{in} \quad \text{from the top of the beam}$$

Neglect top post-tension duct contribution, as it is well above the neutral axis:

$$A_{Post} := 2 \cdot 8 \cdot 0.153 \text{in}^2 \quad A_{Post} = 2.45 \text{in}^2$$

$$d_{pPost} := 45.5 \text{in} \quad \text{Post-tensioning, from the top of the beam for positive bending}$$

Find depth from top of beam to c.g. of pre- and post-tension strands combined:

$$A_{Pre} \cdot d_{pPre} + A_{Post} \cdot d_{pPost} = (A_{Pre} + A_{Post}) \cdot d_p$$

$$d_p := \frac{A_{Pre} \cdot d_{pPre} + A_{Post} \cdot d_{pPost}}{A_{Pre} + A_{Post}} \quad d_p = 45.5 \text{in}$$

To compute  $c$ , assume rectangular section behavior. (Neglect non-prestressed reinforcement.)

$$c := \frac{A_{ps} \cdot f_{pu}}{0.85 f'_c \cdot \beta_1 \cdot b + k \cdot A_{ps} \cdot \frac{f_{pu}}{d_p}} \quad \text{LRFD Eq. (5.7.3.1.1-4)}$$

$$A_{ps} := A_{Pre} + A_{Post} \quad A_{ps} = 6.732 \text{in}^2$$

$$b := 26 \text{in} \quad \text{(Beam Width)}$$

$$f'_c := 7.0 \text{ksi} \quad \text{(Beam Concrete Nominal Strength)}$$

$$\beta_1 := 0.85 - 0.05(f_c - 4\text{ksi}) \cdot \frac{1}{\text{ksi}} \quad \beta_1 = 0.7 > 0.65 \quad \text{LRFD 5.7.2.2}$$

$$c := \frac{A_{ps} \cdot f_{pu}}{0.85 f_c \cdot \beta_1 \cdot b + k \cdot A_{ps} \cdot \frac{f_{pu}}{d_p}} \quad c = 15.213\text{in}$$

$$a := \beta_1 \cdot c \quad a = 10.65\text{in} > t_{\text{flange}} = 7\text{in} \quad \text{LRFD 5.7.2.2}$$

Therefore, the rectangular section behavior assumption is not valid.

We have "T-section" behavior. However, we have a box section with two webs. Assume each 5-in. web contributes a net 10-in. web,  $b_w := 10\text{in}$ . The depth of the compression flange is,  $h_f := 7\text{in}$

$$c := \frac{A_{ps} \cdot f_{pu} - 0.85 \beta_1 \cdot f_c \cdot (b - b_w) \cdot h_f}{0.85 f_c \cdot \beta_1 \cdot b_w + k \cdot A_{ps} \cdot \frac{f_{pu}}{d_p}} \quad c = 25.6\text{in} \quad \text{LRFD Eq. (5.7.3.1.1-3)}$$

$$a := \beta_1 \cdot c \quad a = 17.9\text{in} \quad \text{LRFD 5.7.2.2}$$

$$f_{ps} := f_{pu} \cdot \left(1 - k \cdot \frac{c}{d_p}\right) \quad f_{ps} = 227.5\text{ksi}$$

Nominal Flexural Resistance (Midspan):

$$M_{n\text{Midspan110}} := A_{ps} \cdot f_{ps} \cdot \left(d_p - \frac{a}{2}\right) \quad \text{LRFD Eq. (5-7.3.2.2-1)}$$

$$M_{n\text{Midspan110}} = 4664.9\text{kip}\cdot\text{ft}$$

## COMPUTE NOMINAL SHEAR RESISTANCE AT CRITICAL SECTION

LRFR 6.5.9 does not require a shear evaluation for the design load and legal loads if the bridge shows no visible sign of shear distress. Shear will be investigated for academic purposes, and because of the unique nature of the beamway structure.

### Shear Location

Critical section for shear near supports is the distance  $d_v$  from the face of the support [LRFD 5.8.3.2]

At this location, gross height of section is approximately,  $h := 80\text{in}$

Effective Shear Depth  $d_v$  is the maximum of:

LRFD 5.8.2.9

a) distance between resultants of the tensile and compressive forces

$$d_{v1} := d_p - \frac{a_1}{2} \quad d_{v1} = 42.5\text{in}$$

b)  $0.9d_e$

$$d_{v2} := 0.9 \cdot d_p \quad d_{v2} = 41\text{in}$$

c)  $0.72h$

$$d_{v3} := 0.72 \cdot h \quad d_{v3} = 57.6\text{in}$$

$$d_v := \max(d_{v1}, d_{v2}, d_{v3}) \quad d_v = 57.6\text{in}$$

### MAXIMUM SHEAR AT CRITICAL SECTION NEAR INTERIOR SUPPORT

The maximum shear at  $d_v = 57.6\text{in}$  is interpolated from SAP2000 results. Maximum shear is at critical distance, exterior-facing side of first interior support (Mark VI Train).

$$V_{LL} := V_{LLVI} \quad V_{LL} = 65.3\text{kip}$$

IM := 15%      measured by owner in previous studies

$$V_{LL\_IM} := V_{LL} \cdot (1 + IM) \quad V_{LL\_IM} = 75.1\text{kip}$$

$$V_{DC} = 61.4\text{kip}$$

$$V_{DW} = 0\text{kip}$$

COMPUTE NOMINAL SHEAR RESISTANCE

Shear resistance,  $V_n$  is given as the lesser of:

$$V_n := V_s + V_c + V_p \quad \text{LRFD Eq. (5.8.3.3-1)}$$

$$V_n := 0.25f'_c \cdot b_v \cdot d_v + V_p \quad \text{LRFD Eq. (5.8.3.3-2)}$$

$$V_p := 0.0 \text{kip} \quad (\text{straight tendons})$$

Critical section for shear is at distance  $d_v = 57.6 \text{in}$  from the face of the support. Assuming interior beam end, the transverse reinforcement at the critical section is: #4 "Type 1 Ties" at 12-in. spacing [see drawings S-508, S-501]

$$A_v := 2 \cdot 0.196 \text{in}^2 \quad A_v = 0.39 \text{in}^2 \quad s := 12 \text{in}$$

Minimum Transverse Reinforcement

LRFD 5.8.2.5

$$A_{vreq} := 0.0316 \sqrt{f'_c} \cdot \frac{b_v \cdot s}{f_y}$$

Counting two 5-in. webs for the beam from drawing S-501,  $f_y := 57 \text{ksi}$   
box beam,

$$b_v := 10 \text{in}$$

$$f'_c = 7 \text{ksi}$$

$$s = 12 \text{in}$$

$$A_{vreq} := 0.0316 \sqrt{f'_c} \cdot \frac{b_v \cdot s}{f_y} \cdot \sqrt{\text{ksi}} \quad A_{vreq} = 0.176 \text{in}^2$$

$$\text{Area provided } A_v = 0.4 \text{in}^2$$

$$\text{Check} := \text{if}(A_{vreq} > A_v, \text{"No Good"}, \text{"OK"})$$

Check = "OK"

$$V_c := 0.0316 \beta \cdot \sqrt{f'_c} \cdot b_v \cdot d_v \quad \text{LRFD Eq. (5.8.3.3-3)}$$

$$V_s := \frac{A_v \cdot f_y \cdot d_v \cdot \cot(\theta)}{s} \quad \text{for } \alpha = 90 \text{ degrees} \quad \text{LRFD Eq. (5.8.3.3-4)}$$

These equations are based on the Modified Compression Field Theory (MCFT) and require the determination of  $\beta$  and  $\theta$  by detailed analysis. A simplified analysis using  $\theta = 45$  degrees and  $\beta = 2.0$  may be used for an initial evaluation before resorting to the MCFT, if necessary, for likely improved shear capacity. NOTE: THE SIMPLIFIED APPROACH MAY GIVE A NONCONSERVATIVE RESULT [C6.5.9]

(a) Simplified Approach       $\theta := 45\text{deg}$        $\beta := 2.0$

Concrete Contribution:

$$V_c := 0.0316\beta \cdot \sqrt{f_c} \cdot b_v \cdot d_v^{\frac{3}{2}}$$

Effective Web Width

$$b_v = 10\text{in}$$

Effective Shear Depth

$$d_v = 57.6\text{in}$$

$$V_c := 0.0316\beta \cdot \sqrt{f_c} \cdot b_v \cdot d_v \cdot \sqrt{\text{ksi}} \quad V_c = 96.3\text{kip}$$

Steel Contribution:

$$V_s := \frac{A_v \cdot f_y \cdot d_v \cdot \cot(\theta)}{s}$$

$$A_v = 0.39\text{in}^2 \quad s = 12\text{in} \quad d_v = 57.6\text{in} \quad f_y = 57\text{ksi}$$

$$V_s := \frac{A_v \cdot f_y \cdot d_v \cdot \cot(\theta)}{s} \quad V_s = 107.3\text{kip}$$

Total Nominal Shear Resistance:

$$V_{n1} := V_s + V_c + V_p \quad V_{n1} = 203.6\text{kip}$$

$$V_{n2} := 0.25f_c \cdot b_v \cdot d_v + V_p \quad V_{n2} = 1008\text{kip}$$

$$V_n := \min(V_{n1}, V_{n2}) \quad V_n = 203.6\text{kip}$$

Load effects from above:

$$V_{LL\_IM} = 75.1\text{kip} \quad V_{DC} = 61.4\text{kip} \quad V_{DW} = 0\text{kip}$$

Factored Shear  $V_u$

$$V_u := \gamma_{LL} \cdot V_{LL\_IM} + \gamma_{DC} \cdot V_{DC} + \gamma_{DW} \cdot V_{DW} \quad V_u = 159.3\text{kip}$$

$$V_u = 159.3\text{kip} \quad V_n = 203.6\text{kip}$$

$$\text{Check} := \text{if}(V_u > V_n, \text{"No Good"}, \text{"OK"}) \quad \text{Check} = \text{"OK"}$$

(b) Modified Compression Field Theory Approach

LRFD 5.8.3.4.2

Does the transverse reinforcement meet minimum specified in LRFD 5.8.2.5? From above, yes. Therefore, use Table 1 to determine  $\theta$  and  $\beta$ .

Shear stress on the concrete

$$v_u := \frac{V_u - \phi_V V_p}{\phi_V b_V \cdot d_V} \quad v_u = 0.3074 \text{ksi} \quad \text{LRFD Eq. (5.8.2.9-1)}$$

$$\frac{v_u}{f_c} = 0.0439 \quad \text{Check} := \text{if} \left( \frac{v_u}{f_c} > 0.25, \text{"No Good"} , \text{"OK"} \right) \quad \text{Check} = \text{"OK"}$$

At Critical Section for Shear ( $d_v = 57.6 \text{in}$ )

Live load moments (Mark VI Train). Linear interpolation from SAP2000 response:

$$M_{LL} := M_{LLMCFT} \quad M_{LL} = 1126.7 \text{kip}\cdot\text{ft}$$

$$IM = 15\%$$

$$M_{LL\_IM} := M_{LL} \cdot (1 + IM) \quad M_{LL\_IM} = 1295.7 \text{kip}\cdot\text{ft}$$

Dead load moments at critical section from SAP2000:

$$M_{DC} := M_{DCMCFT} \quad M_{DC} = 1022.9 \text{kip}\cdot\text{ft}$$

Factored Moment:

$$M_u := \gamma_{LL} \cdot M_{LL\_IM} + \gamma_{DC} \cdot M_{DC} + \gamma_{DW} \cdot M_{DW} \quad M_u = 2703.9 \text{kip}\cdot\text{ft}$$

Following the approach in the LRFD Shear Design Flowchart and Table 1:

LRFD 5.8.3.4.2

$$\frac{v_u}{f_c} = 0.0439 \quad (< 0.075, \text{row 1 of Table 1})$$

LRFD Fig. C5.8.3.4.2-5 & LRFD Table 5.8.3.4.2-1

$$\text{Assume } \epsilon_x < -0.20 \times 10^{-3} \quad ( \quad \epsilon_x \times 1000 < -0.20)$$

$$\text{From Table 1: (row 1, column 2) } \theta := 22.3 \text{deg} \quad \beta := 6.32$$

Calculate  $\epsilon_x$ :

$$\epsilon_x := \frac{\frac{M_u}{d_v} + 0.5 \cdot N_u + (0.5) \cdot (V_u - V_p) \cdot \cot(\theta) - A_{ps} \cdot f_{po}}{2 \cdot (E_s \cdot A_s + E_p \cdot A_{ps})} \quad \text{LRFD Eq. (5.8.3.4.2-1)}$$

LRFD 5.8.3.4.2

$$\epsilon_x := \min(\epsilon_x, 0.001)$$

$$A_{ps} = 6.732 \text{in}^2$$

Assume  $E_p = 28500 \text{ksi}$

Assume  $f_{po} := 0.7 \cdot f_{pu}$        $f_{po} = 189 \text{ksi}$       LRFD Figure C5.8.3.4.2-5

$N_u := 0 \text{kip}$       (factored axial force)

$A_s := 2 \cdot \pi \cdot (0.5 \text{in})^2$        $A_s = 1.57 \text{in}^2$       2 #8 in beam per Drawing S-502

$E_s = 29000 \text{ksi}$

$$\varepsilon_x := \frac{\frac{M_u}{d_v} + 0.5 \cdot N_u + (0.5) \cdot (V_u - V_p) \cdot \cot(\theta) - A_{ps} \cdot f_{po}}{2 \cdot (E_s \cdot A_s + E_p \cdot A_{ps})} \quad \text{LRFD Eq. (5.8.3.4.2-1)}$$

$$\varepsilon_x := \min(\varepsilon_x, 0.001) \quad \varepsilon_x = -1.084 \times 10^{-3}$$

If  $\varepsilon_x$  is negative, it must be recalculated including concrete stiffness:

$E_c := 3600 \text{ksi}$       nominal value for precast beams used in SAP2000 models

$A_c := 1504 \text{in}^2$       at beam end section

$$\varepsilon_x := \frac{\frac{M_u}{d_v} + 0.5 \cdot N_u + (0.5) \cdot (V_u - V_p) \cdot \cot(\theta) - A_{ps} \cdot f_{po}}{2 \cdot (E_c \cdot A_c + E_s \cdot A_s + E_p \cdot A_{ps})} \quad \text{LRFD Eq. (5.8.3.4.2-3)}$$

$$\varepsilon_x := \min(\varepsilon_x, 0.002) \quad \varepsilon_x = -45.5 \times 10^{-6}$$

This value is greater than the assumed  $\varepsilon_x$ . Assume  $\varepsilon_x < 0$ .

From Table 1: (row 1, column 4)       $\theta := 21.8 \text{deg}$        $\beta := 3.75$

Re-calculate  $\varepsilon_x$ :

$$\varepsilon_x := \frac{\frac{M_u}{d_v} + 0.5 \cdot N_u + (0.5) \cdot (V_u - V_p) \cdot \cot(\theta) - A_{ps} \cdot f_{po}}{2 \cdot (E_c \cdot A_c + E_s \cdot A_s + E_p \cdot A_{ps})} \quad \text{LRFD Eq. (5.8.3.4.2-3)}$$

$$\varepsilon_x := \min(\varepsilon_x, 0.002) \quad \varepsilon_x = -45.1 \times 10^{-6}$$

$\varepsilon_x$  assumed is less than next larger value, 0      OK

$\theta = 21.8 \text{deg}$        $\beta = 3.75$

Calculate  $V_n$ . Concrete contribution:

$$V_c := 0.0316\beta \cdot \sqrt{f'_c} \cdot b_v \cdot d_v \cdot \sqrt{\text{ksi}} \quad V_c = 180.59\text{kip}$$

Steel Contribution:

$$V_s := \frac{A_v \cdot f_y \cdot d_v \cdot \cot(\theta)}{s} \quad V_s = 268.1\text{kip}$$

Total Nominal Shear Resistance:

$$V_{n\text{Simple}} := V_n \quad (\text{retain value from simplified method above})$$

$$V_n := V_s + V_c + V_p \quad V_n = 448.7\text{kip}$$

$$V_u = 159.3\text{kip}$$

$$\text{Check} := \text{if}(V_u > V_n, \text{"No Good"}, \text{"OK"}) \quad \text{Check} = \text{"OK"}$$

$$V_n = 448.7\text{kip} \quad \text{from MCFT method}$$

$$V_{n\text{Simple}} = 203.6\text{kip} \quad \text{from simplified method}$$

Check Longitudinal Reinforcement

LRFD 5.8.3.5

$$T_n := A_s \cdot f_y + A_{ps} \cdot f_{ps} \quad T_n = 1621.1\text{kip}$$

$$A_s = 1.57\text{in}^2 \quad f_y = 57\text{ksi} \quad A_{ps} = 6.732\text{in}^2 \quad f_{ps} = 227.5\text{ksi}$$

$$T_u := \frac{M_u}{d_v \cdot \phi_M} + 0.5 \cdot \frac{N_u}{\phi_N} + \left( \frac{V_u}{\phi_V} - 0.5 \cdot V_{st} - V_p \right) \cdot \cot(\theta) \quad \blacksquare \quad \text{LRFD Eq. (5.8.3.5-1)}$$

$$V_s = 268.1\text{kip} \quad \frac{V_u}{\phi_V} = 177.1\text{kip}$$

$$V_{st} := \min\left(V_s, \frac{V_u}{\phi_V}\right)$$

$$T_u := \frac{M_u}{d_v \cdot \phi_M} + 0.5 \cdot \frac{N_u}{\phi_N} + \left( \frac{V_u}{\phi_V} - 0.5 \cdot V_{st} - V_p \right) \cdot \cot(\theta) \quad T_u = 784.6\text{kip}$$

$$\text{Check} := \text{if}(T_u > T_n, \text{"No Good"}, \text{"OK"}) \quad \text{Check} = \text{"OK"}$$

GENERAL LOAD RATING EQUATION

LRFR 6.4.2

$$RF := \frac{C - \gamma_{DC} \cdot DC - \gamma_{DW} \cdot DW + \gamma_P \cdot P}{\gamma_L \cdot (LL + IM)} \quad \text{Eq. (6-1)}$$

Note there should be a +/- before the  $\gamma_P$  term (not possible in Mathcad).

EVALUATION FACTORS (for Strength Limit State)

Factors were determined at the beginning of this worksheet. The following list is for review. Changes should be made at top of worksheet:

- a) Resistance Factor  $\phi$   
 $\phi_M = 1.0$  for flexure       $\phi_V = 0.9$  for shear
- b) Condition Factor  $\phi_c$   
 $\phi_c = 1.00$
- c) System Factor  $\phi_s$   
 $\phi_{sM} = 0.95$  for flexure       $\phi_{sV} = 1.00$  for shear

MARK IV TRAIN, FLEXURE AT FIRST INTERIOR SUPPORT (NEGATIVE BENDING)

DESIGN LOAD RATING

LRFR 6.4.3

Strength I Limit State

LRFR 6.5.4.1

$$RF := \frac{\phi_c \cdot \phi_s \cdot \phi \cdot R_n - \gamma_{DC} \cdot DC - \gamma_{DW} \cdot DW}{\gamma_L \cdot (LL + IM)}$$

Load Rating Factors from Above

$$\gamma_{DC} = 1.25 \quad \gamma_{DW} = 1.50$$

$$\gamma_{LL} = 1.10$$

Load effects:

Absolute value for negative bending taken directly from SAP2000 output (Mark IV train):

$$M_{DC} := M_{DCAIV} \quad M_{DC} = 1300.1 \text{ kip}\cdot\text{ft}$$

$$M_{DW} := 0 \text{ kip}\cdot\text{ft}$$

$$M_{LL} := M_{LLAIV} \quad M_{LL} = 916.7 \text{ kip}\cdot\text{ft}$$

$$IM = 15\% \quad \text{measured by owner in previous studies}$$

$$M_{LL\_IM} := M_{LL} \cdot (1 + IM) \quad M_{LL\_IM} = 1054.2 \text{ kip}\cdot\text{ft}$$

Resistance:

$$M_n = 3567.1 \text{ kip}\cdot\text{ft}$$

$$RF := \frac{\phi_c \cdot \phi_s \cdot \phi \cdot M_n - \gamma_{DC} \cdot M_{DC} - \gamma_{DW} \cdot M_{DW}}{\gamma_{LL} \cdot M_{LL\_IM}}$$

$$\boxed{RF = 1.53}$$

$$RF_{AIV} := RF$$

RELIABILITY INDEX,  $\beta$  (TEST CASE)

We assume a linear limit state function for bending, Eq. (5.18) from (Nowak and Collins, 2000) of the general form:

$$\beta := \frac{a_0 + \sum_{i=1}^n (a_i \cdot \mu_{X_i})}{\sqrt{\sum_{i=1}^n (a_i \cdot \sigma_{X_i})^2}} \quad \text{for the linear limit state function of the form,}$$

$$g(X_1, X_2, \dots, X_n) = a_0 + a_1 \cdot X_1 + a_2 \cdot X_2 + \dots + a_n \cdot X_n$$

This expression must be adapted for the current study, considering load effects and resistance in bending. As an exercise, we will restate Example 5.1 (Nowak and Collins, 2000) in terms of load effects, and check that the same result is obtained:

EXAMPLE 5.1: Consider a simply supported beam of length  $l$ , with concentrated live load  $P$  at midspan and distributed dead load  $w$ . The loads are random variables. Assume that  $P$ ,  $w$ , and the yield stress,  $F_y$  are random quantities; the length  $l$  and the plastic section modulus  $Z$  are assumed to be precisely known (deterministic). Calculate the reliability index.

The following values are given:

$P_n := 12 \text{kip}$	$\lambda_P := 0.85$	$\text{COV}_P := 11\%$
$w_n := 0.25 \frac{\text{kip}}{\text{in}}$	$\lambda_w := 1.0$	$\text{COV}_w := 10\%$
$F_y := 36 \text{ksi}$ (nominal)	$\lambda_F := 1.12$	$\text{COV}_F := 11.5\%$
$l := 18 \text{ft}$	$Z := 80 \text{in}^3$	

Nominal (design) value of maximum load effects:

Live load effect:

$$M_L := \frac{P_n \cdot l}{4} \quad M_L = 54 \text{kip}\cdot\text{ft}$$

$$\text{Mean value } \mu_L := \lambda_P \cdot M_L \quad \mu_L = 45.9 \text{kip}\cdot\text{ft}$$

$$\sigma_L := \text{COV}_P \cdot \mu_L \quad \sigma_L = 5 \text{kip}\cdot\text{ft}$$

Dead load effect:

$$M_{DL} := \frac{w_n \cdot l^2}{8} \quad M_{DL} = 121.5 \text{kip}\cdot\text{ft}$$

$$\text{Mean value } \mu_{DL} := \lambda_w \cdot M_{DL} \quad \mu_{DL} = 121.5 \text{kip}\cdot\text{ft}$$

$$\sigma_{DL} := COV_w \cdot \mu_{DL} \quad \sigma_{DL} = 12.1 \text{ kip}\cdot\text{ft}$$

Resistance:

$$M_{Res} := F_y \cdot Z \quad M_{Res} = 240 \text{ kip}\cdot\text{ft}$$

$$\text{Mean value } \mu_R := \lambda_F \cdot M_{Res} \quad \mu_R = 268.8 \text{ kip}\cdot\text{ft}$$

$$\sigma_R := COV_F \cdot \mu_R \quad \sigma_R = 30.9 \text{ kip}\cdot\text{ft}$$

Calculate the reliability index:

$$g(M_{Res}, M_{DL}, M_L) = M_{Res} - M_{DL} - M_L$$

$$\beta := \frac{a_0 + \sum_{i=1}^n (a_i \cdot \mu_{X_i})}{\sqrt{\sum_{i=1}^n (a_i \cdot \sigma_{X_i})^2}}$$

for the linear limit state function of the form,

$$g(X_1, X_2, \dots, X_n) = a_0 + a_1 \cdot X_1 + a_2 \cdot X_2 + \dots + a_n \cdot X_n$$

$$\beta := \frac{\mu_R - \mu_{DL} - \mu_L}{\sqrt{\sigma_R^2 + \sigma_{DL}^2 + \sigma_L^2}}$$

$$\beta = 3.02$$

The textbook result is  $\beta = 3.01$ . The difference of 0.01 results from rounding errors in the textbook.

We have restated the limit state function in terms of load effects (instead of components of the load effects as presented in the textbook). As long as each load effect can be stated in terms of only one random variable, this method is valid. In fact, statistical parameters for load and resistance tend to be given in terms of load effects (Nowak 1993, Nowak and Collins 2000) rather than components of load effects.

RELIABILITY INDEX,  $\beta$  (MARK IV TRAIN, NEGATIVE BENDING AT FIRST INTERIOR SUPPORT)

We assume a linear limit state function for bending, Eq. (5.18) from (Nowak and Collins, 2000) of the general form:

$$\beta := \frac{a_0 + \sum_{i=1}^n (a_i \cdot \mu_{X_i})}{\sqrt{\sum_{i=1}^n (a_i \cdot \sigma_{X_i})^2}} \quad \text{for the linear limit state function of the form,}$$

$$g(X_1, X_2, \dots, X_n) = a_0 + a_1 \cdot X_1 + a_2 \cdot X_2 + \dots + a_n \cdot X_n$$

Nominal (design) value of maximum load effects:

Live load effect (including impact factor IM = 15%):

$$M_{LL\_IM} = 1054.2 \text{ kip}\cdot\text{ft}$$

$$\text{Bias factor } \lambda_{LL} = 1.00 \quad \text{from above}$$

$$\text{Mean value } \mu_{LL} := \lambda_{LL} \cdot M_{LL\_IM} \quad \mu_{LL} = 1054.2 \text{ kip}\cdot\text{ft}$$

$$\sigma_{LL} := \text{COV}_{LL} \cdot \mu_{LL} \quad \sigma_{LL} = 26.5 \text{ kip}\cdot\text{ft} \quad \text{from above}$$

Dead load effect:

$$M_{DC} = 1300.1 \text{ kip}\cdot\text{ft}$$

Assume the values for bias and COV for dead load of cast-in-place components (conservative choice) from Table 8.4 (Nowak and Collins, 2000). These values are adapted from LRFD Calibration (Nowak, 1993),

$$\text{Bias factor } \lambda_{DC} := 1.05$$

$$\text{Mean value } \mu_{DC} := \lambda_{DC} \cdot M_{DC} \quad \mu_{DC} = 1365.1 \text{ kip}\cdot\text{ft}$$

$$\text{Coefficient of Variation } \text{COV}_{DC} := 0.10 \quad \sigma_{DC} := \text{COV}_{DC} \cdot \mu_{DC} \quad \sigma_{DC} = 136.5 \text{ kip}\cdot\text{ft}$$

Resistance:

$$M_n = 3567.1 \text{ kip}\cdot\text{ft}$$

Assume statistical parameters of resistance from Table 2 (Nowak, 1995). Again, these values are associated with the calibration of the LRFD Code,

$$\lambda_R := 1.05 \quad \text{for moment resistance of prestressed-concrete girders}$$

$$\text{Mean value } \mu_R := \lambda_R \cdot M_n \quad \mu_R = 3745.4 \text{ kip}\cdot\text{ft}$$

$$\text{Coefficient of Variation } \text{COV}_R := 0.075 \quad \sigma_R := \text{COV}_R \cdot \mu_R \quad \sigma_R = 280.9 \text{ kip}\cdot\text{ft}$$

Calculate the reliability index:

$$g(M_n, M_{DC}, M_{LL\_IM}) = M_n - M_{DC} - M_{LL\_IM}$$

$$\beta := \frac{a_0 + \sum_{i=1}^n (a_i \mu_{X_i})}{\sqrt{\sum_{i=1}^n (a_i \sigma_{X_i})^2}}$$

for the linear limit state function of the form,

$$g(X_1, X_2, \dots, X_n) = a_0 + a_1 \cdot X_1 + a_2 \cdot X_2 + \dots + a_n \cdot X_n$$

$$\beta := \frac{\mu_R - \mu_{DC} - \mu_{LL}}{\sqrt{\sigma_R^2 + \sigma_{DC}^2 + \sigma_{LL}^2}}$$

$$\beta = 4.23$$

$$\beta_{AIV} := \beta$$

For normally distributed random variables R and Q, it can be shown that the probability of failure is related to the reliability index as follows,  $P_f = \Phi(-\beta)$ . If the random variables are all normally distributed and uncorrelated, then this relationship between  $\beta$  and  $P_f$  is exact. Otherwise, this expression provides only an approximate means of relating the probability of failure to  $\beta$  (Nowak and Collins, 2000).

The values of the CDF  $\Phi(x)$  for the standard normal probability distribution are embedded in Mathcad and recalled by the function cnorm:

$$P_f := \text{cnorm}(-\beta)$$

$$P_f = 1.16 \times 10^{-5}$$

$$P_{fAIV} := P_f$$

MARK IV TRAIN, FLEXURE AT SPAN 1, 0.4L (POSITIVE BENDING)

DESIGN LOAD RATING

LRFR 6.4.3

Strength I Limit State

LRFR 6.5.4.1

$$RF := \frac{\phi_c \cdot \phi_s \cdot \phi \cdot R_n - \gamma_{DC} \cdot DC - \gamma_{DW} \cdot DW}{\gamma_L \cdot (LL + IM)}$$

Load Rating Factors from Above

$$\gamma_{DC} = 1.25 \quad \gamma_{DW} = 1.50$$

$$\gamma_{LL} = 1.10$$

Load effects:

Absolute value for positive bending (Span 1, 0.4L) taken directly from SAP2000 output (Mark IV train):

$$M_{DC} := M_{DCBIV} \quad M_{DC} = 535.9 \text{ kip}\cdot\text{ft}$$

$$M_{DW} := 0 \text{ kip}\cdot\text{ft}$$

$$M_{LL} := M_{LLBIV} \quad M_{LL} = 578.9 \text{ kip}\cdot\text{ft}$$

IM = 15% measured by owner in previous studies

$$M_{LL\_IM} := M_{LL} \cdot (1 + IM) \quad M_{LL\_IM} = 665.7 \text{ kip}\cdot\text{ft}$$

Resistance:

$$M_{nMidspan100} = 4435.3 \text{ kip}\cdot\text{ft}$$

$$RF := \frac{\phi_c \cdot \phi_s \cdot \phi \cdot M_{nMidspan100} - \gamma_{DC} \cdot M_{DC} - \gamma_{DW} \cdot M_{DW}}{\gamma_{LL} \cdot M_{LL\_IM}}$$

$$RF = 4.85$$

$$RF_{BIV} := RF$$

RELIABILITY INDEX,  $\beta$  (MARK IV TRAIN, POSITIVE BENDING AT SPAN 1, 0.4L)

We assume a linear limit state function for bending, Eq. (5.18) from (Nowak and Collins, 2000) of the general form:

$$\beta := \frac{a_0 + \sum_{i=1}^n (a_i \mu_{X_i})}{\sqrt{\sum_{i=1}^n (a_i \sigma_{X_i})^2}} \quad \blacksquare$$

for the linear limit state function of the form,

$$g(X_1, X_2, \dots, X_n) = a_0 + a_1 \cdot X_1 + a_2 \cdot X_2 + \dots + a_n \cdot X_n$$

Nominal (design) value of maximum load effects:

Live load effect (including impact factor IM = 15%):

$$M_{LL\_IM} = 665.7 \text{ kip}\cdot\text{ft}$$

$$\text{Bias factor } \lambda_{LL} = 1.00 \quad \text{from above}$$

$$\text{Mean value } \mu_{LL} := \lambda_{LL} \cdot M_{LL\_IM} \quad \mu_{LL} = 665.7 \text{ kip}\cdot\text{ft}$$

$$\sigma_{LL} := \text{COV}_{LL} \cdot \mu_{LL} \quad \sigma_{LL} = 16.8 \text{ kip}\cdot\text{ft} \quad \text{from above}$$

Dead load effect:

$$M_{DC} = 535.9 \text{ kip}\cdot\text{ft}$$

Assume the values for bias and COV for dead load of cast-in-place components (conservative choice) from Table 8.4 (Nowak and Collins, 2000). These values are adapted from LRFD Calibration (Nowak, 1993),

$$\text{Bias factor } \lambda_{DC} := 1.05$$

$$\text{Mean value } \mu_{DC} := \lambda_{DC} \cdot M_{DC} \quad \mu_{DC} = 562.7 \text{ kip}\cdot\text{ft}$$

$$\text{Coefficient of Variation } \text{COV}_{DC} := 0.10 \quad \sigma_{DC} := \text{COV}_{DC} \cdot \mu_{DC} \quad \sigma_{DC} = 56.3 \text{ kip}\cdot\text{ft}$$

Resistance:

$$M_{n\text{Midspan}100} = 4435.3 \text{ kip}\cdot\text{ft}$$

Assume statistical parameters of resistance from Table 2 (Nowak, 1995). Again, these values are associated with the calibration of the LRFD Code,

$$\lambda_R := 1.05 \quad \text{for moment resistance of prestressed-concrete girders}$$

$$\text{Mean value } \mu_R := \lambda_R \cdot M_{n\text{Midspan}100} \quad \mu_R = 4657.1 \text{ kip}\cdot\text{ft}$$

$$\text{Coefficient of Variation } \text{COV}_R := 0.075 \quad \sigma_R := \text{COV}_R \cdot \mu_R \quad \sigma_R = 349.3 \text{ kip}\cdot\text{ft}$$

Calculate the reliability index:

$$g(M_{nMidspan100}, M_{DC}, M_{LL\_IM}) = M_{nMidspan100} - M_{DC} - M_{LL\_IM}$$

$$\beta := \frac{a_0 + \sum_{i=1}^n (a_i \mu_{X_i})}{\sqrt{\sum_{i=1}^n (a_i \sigma_{X_i})^2}}$$

for the linear limit state function of the form,

$$g(X_1, X_2, \dots, X_n) = a_0 + a_1 \cdot X_1 + a_2 \cdot X_2 + \dots + a_n \cdot X_n$$

$$\beta := \frac{\mu_R - \mu_{DC} - \mu_{LL}}{\sqrt{\sigma_R^2 + \sigma_{DC}^2 + \sigma_{LL}^2}}$$

$$\beta = 9.68$$

$$\beta_{BIV} := \beta$$

For normally distributed random variables R and Q, it can be shown that the probability of failure is related to the reliability index as follows,  $P_f = \Phi(-\beta)$ . If the random variables are all normally distributed and uncorrelated, then this relationship between  $\beta$  and  $P_f$  is exact. Otherwise, this expression provides only an approximate means of relating the probability of failure to  $\beta$  (Nowak and Collins, 2000).

The values of the CDF  $\Phi(x)$  for the standard normal probability distribution are embedded in Mathcad and recalled by the function cnorm:

$$P_f := \text{cnorm}(-\beta)$$

$$P_f = 0.00 \times 10^0$$

$$P_{fBIV} := P_f$$

MARK IV TRAIN, FLEXURE AT SPAN 2, 05L (POSITIVE BENDING)

DESIGN LOAD RATING

LRFR 6.4.3

Strength I Limit State

LRFR 6.5.4.1

$$RF := \frac{\phi_c \cdot \phi_s \cdot \phi \cdot R_n - \gamma_{DC} \cdot DC - \gamma_{DW} \cdot DW}{\gamma_L \cdot (LL + IM)}$$

Load Rating Factors from Above

$$\gamma_{DC} = 1.25 \quad \gamma_{DW} = 1.50$$

$$\gamma_{LL} = 1.10$$

Load effects:

Absolute value for positive bending (Span 2, 0.5L) taken directly from SAP2000 output (Mark IV train):

$$M_{DC} := M_{DCCIV} \quad M_{DC} = 245.1 \text{ kip}\cdot\text{ft}$$

$$M_{DW} := 0 \text{ kip}\cdot\text{ft}$$

$$M_{LL} := M_{LLCIV} \quad M_{LL} = 510 \text{ kip}\cdot\text{ft}$$

IM = 15% measured by owner in previous studies

$$M_{LL\_IM} := M_{LL} \cdot (1 + IM) \quad M_{LL\_IM} = 586.5 \text{ kip}\cdot\text{ft}$$

Resistance:

$$M_{nMidspan110} = 4664.9 \text{ kip}\cdot\text{ft}$$

$$RF := \frac{\phi_c \cdot \phi_s \cdot \phi \cdot M_{nMidspan110} - \gamma_{DC} \cdot M_{DC} - \gamma_{DW} \cdot M_{DW}}{\gamma_{LL} \cdot M_{LL\_IM}}$$

$$RF = 6.41$$

$$RF_{CIV} := RF$$

RELIABILITY INDEX,  $\beta$  (MARK IV TRAIN, POSITIVE BENDING AT SPAN 2, 0.5L)

We assume a linear limit state function for bending, Eq. (5.18) from (Nowak and Collins, 2000) of the general form:

$$\beta := \frac{a_0 + \sum_{i=1}^n (a_i \cdot \mu_{X_i})}{\sqrt{\sum_{i=1}^n (a_i \cdot \sigma_{X_i})^2}} \quad \blacksquare$$

for the linear limit state function of the form,

$$g(X_1, X_2, \dots, X_n) = a_0 + a_1 \cdot X_1 + a_2 \cdot X_2 + \dots + a_n \cdot X_n$$

Nominal (design) value of maximum load effects:

Live load effect (including impact factor IM = 15%):

$$M_{LL\_IM} = 586.5 \text{kip}\cdot\text{ft}$$

$$\text{Bias factor } \lambda_{LL} = 1.00 \quad \text{from above}$$

$$\text{Mean value } \mu_{LL} := \lambda_{LL} \cdot M_{LL\_IM} \quad \mu_{LL} = 586.5 \text{kip}\cdot\text{ft}$$

$$\sigma_{LL} := \text{COV}_{LL} \cdot \mu_{LL} \quad \sigma_{LL} = 14.8 \text{kip}\cdot\text{ft} \quad \text{from above}$$

Dead load effect:

$$M_{DC} = 245.1 \text{kip}\cdot\text{ft}$$

Assume the values for bias and COV for dead load of cast-in-place components (conservative choice) from Table 8.4 (Nowak and Collins, 2000). These values are adapted from LRFD Calibration (Nowak, 1993),

$$\text{Bias factor } \lambda_{DC} := 1.05$$

$$\text{Mean value } \mu_{DC} := \lambda_{DC} \cdot M_{DC} \quad \mu_{DC} = 257.4 \text{kip}\cdot\text{ft}$$

$$\text{Coefficient of Variation } \text{COV}_{DC} := 0.10 \quad \sigma_{DC} := \text{COV}_{DC} \cdot \mu_{DC} \quad \sigma_{DC} = 25.7 \text{kip}\cdot\text{ft}$$

Resistance:

$$M_{n\text{Midspan110}} = 4664.9 \text{kip}\cdot\text{ft}$$

Assume statistical parameters of resistance from Table 2 (Nowak, 1995). Again, these values are associated with the calibration of the LRFD Code,

$$\lambda_R := 1.05 \quad \text{for moment resistance of prestressed-concrete girders}$$

$$\text{Mean value } \mu_R := \lambda_R \cdot M_{n\text{Midspan110}} \quad \mu_R = 4898.2 \text{kip}\cdot\text{ft}$$

$$\text{Coefficient of Variation } \text{COV}_R := 0.075 \quad \sigma_R := \text{COV}_R \cdot \mu_R \quad \sigma_R = 367.4 \text{kip}\cdot\text{ft}$$

Calculate the reliability index:

$$g(M_{nMidspan110}, M_{DC}, M_{LL\_IM}) = M_{nMidspan110} - M_{DC} - M_{LL\_IM}$$

$$\beta := \frac{a_0 + \sum_{i=1}^n (a_i \mu_{Xi})}{\sqrt{\sum_{i=1}^n (a_i \sigma_{Xi})^2}}$$

for the linear limit state function of the form,

$$g(X_1, X_2, \dots, X_n) = a_0 + a_1 \cdot X_1 + a_2 \cdot X_2 + \dots + a_n \cdot X_n$$

$$\beta := \frac{\mu_R - \mu_{DC} - \mu_{LL}}{\sqrt{\sigma_R^2 + \sigma_{DC}^2 + \sigma_{LL}^2}}$$

$$\beta = 11$$

$$\beta_{CIV} := \beta$$

For normally distributed random variables R and Q, it can be shown that the probability of failure is related to the reliability index as follows,  $P_f = \Phi(-\beta)$ . If the random variables are all normally distributed and uncorrelated, then this relationship between  $\beta$  and  $P_f$  is exact. Otherwise, this expression provides only an approximate means of relating the probability of failure to  $\beta$  (Nowak and Collins, 2000).

The values of the CDF  $\Phi(x)$  for the standard normal probability distribution are embedded in Mathcad and recalled by the function cnorm:

$$P_f := \text{cnorm}(-\beta)$$

$$P_f = 0.00 \times 10^0$$

$$P_{fCIV} := P_f$$

## MARK IV TRAIN, SHEAR AT CRITICAL DISTANCE FROM FIRST INTERIOR SUPPORT

The shear rating factors for Design Load Rating are calculated for academic purposes only. In-service concrete bridges that show no visible signs of shear distress need not be checked for shear during design load or legal load ratings [LRFR 6.5.9]

Shear at Critical Shear Section,  $d_v = 57.6\text{in}$

The maximum shear at  $d_v = 57.6\text{in}$  is interpolated from SAP2000 results. Maximum shear is at critical distance, exterior-facing side of first interior support (Mark IV Train).

$$V_{LL} := V_{LLIV} \quad V_{LL} = 46.5\text{kip}$$

IM := 15%      measured by owner in previous studies

$$V_{LL\_IM} := V_{LL} \cdot (1 + IM) \quad V_{LL\_IM} = 53.4\text{kip}$$

$$V_{DC} = 61.4\text{kip}$$

### 1) Simplified Method

$$V_{n\text{Simple}} = 203.6\text{kip}$$

$$RF := \frac{\phi_c \cdot \phi_s \cdot \phi_V \cdot V_{n\text{Simple}} - \gamma_{DC} \cdot V_{DC} - \gamma_{DW} \cdot V_{DW}}{\gamma_{LL} \cdot V_{LL\_IM}}$$

$$\boxed{RF = 1.81}$$

### 2) MCFT Method

$$V_n = 448.7\text{kip}$$

$$RF := \frac{\phi_c \cdot \phi_s \cdot \phi_V \cdot V_n - \gamma_{DC} \cdot V_{DC} - \gamma_{DW} \cdot V_{DW}}{\gamma_{LL} \cdot V_{LL\_IM}}$$

$$\boxed{RF = 5.56}$$

$$RF_{\text{ShearIV}} := RF$$

RELIABILITY INDEX,  $\beta$  (MARK IV TRAIN, SHEAR AT CRIT. DIST. FROM FIRST INT. SUPPORT)

We assume a linear limit state function for bending, Eq. (5.18) from (Nowak and Collins, 2000) of the general form:

$$\beta := \frac{a_0 + \sum_{i=1}^n (a_i \cdot \mu_{X_i})}{\sqrt{\sum_{i=1}^n (a_i \cdot \sigma_{X_i})^2}} \quad \blacksquare$$

for the linear limit state function of the form,

$$g(X_1, X_2, \dots, X_n) = a_0 + a_1 \cdot X_1 + a_2 \cdot X_2 + \dots + a_n \cdot X_n$$

Nominal (design) value of maximum load effects:

Live load effect (including impact factor IM = 15%):

$$V_{LL\_IM} = 53.4 \text{ kip}$$

$$\text{Bias factor } \lambda_{LL} = 1.00 \quad \text{from above}$$

$$\text{Mean value } \mu_{LL} := \lambda_{LL} \cdot V_{LL\_IM} \quad \mu_{LL} = 53.4 \text{ kip}$$

$$\sigma_{LL} := COV_{LL} \cdot \mu_{LL} \quad \sigma_{LL} = 1.3 \text{ kip} \quad \text{from above}$$

Dead load effect:

$$V_{DC} = 61.4 \text{ kip}$$

Assume the values for bias and COV for dead load of cast-in-place components (conservative choice) from Table 8.4 (Nowak and Collins, 2000). These values are adapted from LRFD Calibration (Nowak, 1993),

$$\text{Bias factor } \lambda_{DC} := 1.05$$

$$\text{Mean value } \mu_{DC} := \lambda_{DC} \cdot V_{DC} \quad \mu_{DC} = 64.5 \text{ kip}$$

$$\text{Coefficient of Variation } COV_{DC} := 0.10 \quad \sigma_{DC} := COV_{DC} \cdot \mu_{DC} \quad \sigma_{DC} = 6.4 \text{ kip}$$

Resistance (MCFT Approach):

$$V_n = 448.7 \text{ kip}$$

Assume statistical parameters of resistance from Table 2 (Nowak, 1995). Again, these values are associated with the calibration of the LRFD Code,

$$\lambda_R := 1.165 \quad \text{for shear resistance of prestressed-concrete girders}$$

$$\text{Mean value } \mu_R := \lambda_R \cdot V_n \quad \mu_R = 522.8 \text{ kip}$$

$$\text{Coefficient of Variation } COV_R := 0.16 \quad \sigma_R := COV_R \cdot \mu_R \quad \sigma_R = 83.6 \text{ kip}$$

Calculate the reliability index:

$$g(V_n, V_{DC}, V_{LL\_IM}) = V_n - V_{DC} - V_{LL\_IM}$$

$$\beta := \frac{a_0 + \sum_{i=1}^n (a_i \mu_{X_i})}{\sqrt{\sum_{i=1}^n (a_i \sigma_{X_i})^2}}$$

for the linear limit state function of the form,

$$g(X_1, X_2, \dots, X_n) = a_0 + a_1 \cdot X_1 + a_2 \cdot X_2 + \dots + a_n \cdot X_n$$

$$\beta := \frac{\mu_R - \mu_{DC} - \mu_{LL}}{\sqrt{\sigma_R^2 + \sigma_{DC}^2 + \sigma_{LL}^2}}$$

$$\beta = 4.83$$

$$\beta_{\text{ShearIV}} := \beta$$

For normally distributed random variables R and Q, it can be shown that the probability of failure is related to the reliability index as follows,  $P_f = \Phi(-\beta)$ . If the random variables are all normally distributed and uncorrelated, then this relationship between  $\beta$  and  $P_f$  is exact. Otherwise, this expression provides only an approximate means of relating the probability of failure to  $\beta$  (Nowak and Collins, 2000).

The values of the CDF  $\Phi(x)$  for the standard normal probability distribution are embedded in Mathcad and recalled by the function cnorm:

$$P_f := \text{cnorm}(-\beta)$$

$$P_f = 6.99 \times 10^{-7}$$

$$P_{f\text{ShearIV}} := P_f$$

MARK VI TRAIN, FLEXURE AT FIRST INTERIOR SUPPORT (NEGATIVE BENDING)

DESIGN LOAD RATING

LRFR 6.4.3

Strength I Limit State

LRFR 6.5.4.1

$$RF := \frac{\phi_c \cdot \phi_s \cdot \phi \cdot R_n - \gamma_{DC} \cdot DC - \gamma_{DW} \cdot DW}{\gamma_L \cdot (LL + IM)}$$

Load Rating Factors from Above

$$\gamma_{DC} = 1.25 \quad \gamma_{DW} = 1.50$$

$$\gamma_{LL} = 1.10$$

Load effects:

Absolute value for negative bending taken directly from SAP2000 output (Mark VI train):

$$M_{DC} := M_{DCAVI} \quad M_{DC} = 1300.1 \text{ kip}\cdot\text{ft}$$

$$M_{DW} := 0 \text{ kip}\cdot\text{ft}$$

$$M_{LL} := M_{LLAVI} \quad M_{LL} = 1368.9 \text{ kip}\cdot\text{ft}$$

$$IM = 15\% \quad \text{measured by owner in previous studies}$$

$$M_{LL\_IM} := M_{LL} \cdot (1 + IM) \quad M_{LL\_IM} = 1574.3 \text{ kip}\cdot\text{ft}$$

Resistance:

$$M_n = 3567.1 \text{ kip}\cdot\text{ft}$$

$$RF := \frac{\phi_c \cdot \phi_s \cdot \phi \cdot M \cdot M_n - \gamma_{DC} \cdot M_{DC} - \gamma_{DW} \cdot M_{DW}}{\gamma_{LL} \cdot M_{LL\_IM}}$$

$$RF = 1.02$$

$$RF_{AVI} := RF$$

RELIABILITY INDEX,  $\beta$  (MARK VI TRAIN, NEGATIVE BENDING AT FIRST INTERIOR SUPPORT)

We assume a linear limit state function for bending, Eq. (5.18) from (Nowak and Collins, 2000) of the general form:

$$\beta := \frac{a_0 + \sum_{i=1}^n (a_i \cdot \mu_{X_i})}{\sqrt{\sum_{i=1}^n (a_i \cdot \sigma_{X_i})^2}}$$

for the linear limit state function of the form,

$$g(X_1, X_2, \dots, X_n) = a_0 + a_1 \cdot X_1 + a_2 \cdot X_2 + \dots + a_n \cdot X_n$$

Nominal (design) value of maximum load effects:

Live load effect (including impact factor IM = 15%):

$$M_{LL\_IM} = 1574.3 \text{ kip}\cdot\text{ft}$$

$$\text{Bias factor } \lambda_{LL} = 1.00$$

from above

$$\text{Mean value } \mu_{LL} := \lambda_{LL} \cdot M_{LL\_IM} \quad \mu_{LL} = 1574.3 \text{ kip}\cdot\text{ft}$$

$$\sigma_{LL} := \text{COV}_{LL} \cdot \mu_{LL} \quad \sigma_{LL} = 39.6 \text{ kip}\cdot\text{ft}$$

from above

Dead load effect:

$$M_{DC} = 1300.1 \text{ kip}\cdot\text{ft}$$

Assume the values for bias and COV for dead load of cast-in-place components (conservative choice) from Table 8.4 (Nowak and Collins, 2000). These values are adapted from LRFD Calibration (Nowak, 1993),

$$\text{Bias factor } \lambda_{DC} := 1.05$$

$$\text{Mean value } \mu_{DC} := \lambda_{DC} \cdot M_{DC} \quad \mu_{DC} = 1365.1 \text{ kip}\cdot\text{ft}$$

$$\text{Coefficient of Variation } \text{COV}_{DC} := 0.10 \quad \sigma_{DC} := \text{COV}_{DC} \cdot \mu_{DC} \quad \sigma_{DC} = 136.5 \text{ kip}\cdot\text{ft}$$

Resistance:

$$M_n = 3567.1 \text{ kip}\cdot\text{ft}$$

Assume statistical parameters of resistance from Table 2 (Nowak, 1995). Again, these values are associated with the calibration of the LRFD Code,

$$\lambda_R := 1.05 \quad \text{for moment resistance of prestressed-concrete girders}$$

$$\text{Mean value } \mu_R := \lambda_R \cdot M_n \quad \mu_R = 3745.4 \text{ kip}\cdot\text{ft}$$

$$\text{Coefficient of Variation } \text{COV}_R := 0.075 \quad \sigma_R := \text{COV}_R \cdot \mu_R \quad \sigma_R = 280.9 \text{ kip}\cdot\text{ft}$$

Calculate the reliability index:

$$g(M_n, M_{DC}, M_{LL\_IM}) = M_n - M_{DC} - M_{LL\_IM}$$

$$\beta := \frac{a_0 + \sum_{i=1}^n (a_i \mu_{X_i})}{\sqrt{\sum_{i=1}^n (a_i \sigma_{X_i})^2}}$$

for the linear limit state function of the form,

$$g(X_1, X_2, \dots, X_n) = a_0 + a_1 \cdot X_1 + a_2 \cdot X_2 + \dots + a_n \cdot X_n$$

$$\beta := \frac{\mu_R - \mu_{DC} - \mu_{LL}}{\sqrt{\sigma_R^2 + \sigma_{DC}^2 + \sigma_{LL}^2}}$$

$$\beta = 2.56$$

$$\beta_{AVI} := \beta$$

For normally distributed random variables R and Q, it can be shown that the probability of failure is related to the reliability index as follows,  $P_f = \Phi(-\beta)$ . If the random variables are all normally distributed and uncorrelated, then this relationship between  $\beta$  and  $P_f$  is exact. Otherwise, this expression provides only an approximate means of relating the probability of failure to  $\beta$  (Nowak and Collins, 2000).

The values of the CDF  $\Phi(x)$  for the standard normal probability distribution are embedded in Mathcad and recalled by the function cnorm:

$$P_f := \text{cnorm}(-\beta)$$

$$P_f = 5.23 \times 10^{-3}$$

$$P_{fAVI} := P_f$$

MARK VI TRAIN, FLEXURE AT SPAN 1, 0.4L (POSITIVE BENDING)

DESIGN LOAD RATING

LRFR 6.4.3

Strength I Limit State

LRFR 6.5.4.1

$$RF := \frac{\phi_c \cdot \phi_s \cdot \phi \cdot R_n - \gamma_{DC} \cdot DC - \gamma_{DW} \cdot DW}{\gamma_L \cdot (LL + IM)}$$

Load Rating Factors from Above

$$\gamma_{DC} = 1.25 \quad \gamma_{DW} = 1.50$$

$$\gamma_{LL} = 1.10$$

Load effects:

Absolute value for positive bending (Span 1, 0.4L) taken directly from SAP2000 output (Mark VI train):

$$M_{DC} := M_{DCBVI} \quad M_{DC} = 535.9 \text{ kip}\cdot\text{ft}$$

$$M_{DW} := 0 \text{ kip}\cdot\text{ft}$$

$$M_{LL} := M_{LLBVI} \quad M_{LL} = 786.9 \text{ kip}\cdot\text{ft}$$

IM = 15%      measured by owner in previous studies

$$M_{LL\_IM} := M_{LL} \cdot (1 + IM) \quad M_{LL\_IM} = 905 \text{ kip}\cdot\text{ft}$$

Resistance:

$$M_{nMidspan100} = 4435.3 \text{ kip}\cdot\text{ft}$$

$$RF := \frac{\phi_c \cdot \phi_s \cdot \phi \cdot M_{nMidspan100} - \gamma_{DC} \cdot M_{DC} - \gamma_{DW} \cdot M_{DW}}{\gamma_{LL} \cdot M_{LL\_IM}}$$

$$RF = 3.57$$

$$RF_{BVI} := RF$$

RELIABILITY INDEX,  $\beta$  (MARK VI TRAIN, POSITIVE BENDING AT SPAN 1, 0.4L)

We assume a linear limit state function for bending, Eq. (5.18) from (Nowak and Collins, 2000) of the general form:

$$\beta := \frac{a_0 + \sum_{i=1}^n (a_i \cdot \mu_{X_i})}{\sqrt{\sum_{i=1}^n (a_i \cdot \sigma_{X_i})^2}} \quad \text{for the linear limit state function of the form,}$$

$$g(X_1, X_2, \dots, X_n) = a_0 + a_1 \cdot X_1 + a_2 \cdot X_2 + \dots + a_n \cdot X_n$$

Nominal (design) value of maximum load effects:

Live load effect (including impact factor IM = 15%):

$$M_{LL\_IM} = 905 \text{ kip}\cdot\text{ft}$$

$$\text{Bias factor } \lambda_{LL} = 1.00 \quad \text{from above}$$

$$\text{Mean value } \mu_{LL} := \lambda_{LL} \cdot M_{LL\_IM} \quad \mu_{LL} = 905 \text{ kip}\cdot\text{ft}$$

$$\sigma_{LL} := \text{COV}_{LL} \cdot \mu_{LL} \quad \sigma_{LL} = 22.8 \text{ kip}\cdot\text{ft} \quad \text{from above}$$

Dead load effect:

$$M_{DC} = 535.9 \text{ kip}\cdot\text{ft}$$

Assume the values for bias and COV for dead load of cast-in-place components (conservative choice) from Table 8.4 (Nowak and Collins, 2000). These values are adapted from LRFD Calibration (Nowak, 1993),

$$\text{Bias factor } \lambda_{DC} := 1.05$$

$$\text{Mean value } \mu_{DC} := \lambda_{DC} \cdot M_{DC} \quad \mu_{DC} = 562.7 \text{ kip}\cdot\text{ft}$$

$$\text{Coefficient of Variation } \text{COV}_{DC} := 0.10 \quad \sigma_{DC} := \text{COV}_{DC} \cdot \mu_{DC} \quad \sigma_{DC} = 56.3 \text{ kip}\cdot\text{ft}$$

Resistance:

$$M_{n\text{Midspan}100} = 4435.3 \text{ kip}\cdot\text{ft}$$

Assume statistical parameters of resistance from Table 2 (Nowak, 1995). Again, these values are associated with the calibration of the LRFD Code,

$$\lambda_R := 1.05 \quad \text{for moment resistance of prestressed-concrete girders}$$

$$\text{Mean value } \mu_R := \lambda_R \cdot M_{n\text{Midspan}100} \quad \mu_R = 4657.1 \text{ kip}\cdot\text{ft}$$

$$\text{Coefficient of Variation } \text{COV}_R := 0.075 \quad \sigma_R := \text{COV}_R \cdot \mu_R \quad \sigma_R = 349.3 \text{ kip}\cdot\text{ft}$$

Calculate the reliability index:

$$g(M_{nMidspan100}, M_{DC}, M_{LL\_IM}) = M_{nMidspan100} - M_{DC} - M_{LL\_IM}$$

$$\beta := \frac{a_0 + \sum_{i=1}^n (a_i \mu_{X_i})}{\sqrt{\sum_{i=1}^n (a_i \sigma_{X_i})^2}}$$

for the linear limit state function of the form,

$$g(X_1, X_2, \dots, X_n) = a_0 + a_1 \cdot X_1 + a_2 \cdot X_2 + \dots + a_n \cdot X_n$$

$$\beta := \frac{\mu_R - \mu_{DC} - \mu_{LL}}{\sqrt{\sigma_R^2 + \sigma_{DC}^2 + \sigma_{LL}^2}}$$

$$\beta = 9$$

$$\beta_{BVI} := \beta$$

For normally distributed random variables R and Q, it can be shown that the probability of failure is related to the reliability index as follows,  $P_f = \Phi(-\beta)$ . If the random variables are all normally distributed and uncorrelated, then this relationship between  $\beta$  and  $P_f$  is exact. Otherwise, this expression provides only an approximate means of relating the probability of failure to  $\beta$  (Nowak and Collins, 2000).

The values of the CDF  $\Phi(x)$  for the standard normal probability distribution are embedded in Mathcad and recalled by the function cnorm:

$$P_f := \text{cnorm}(-\beta)$$

$$P_f = 0.00 \times 10^0$$

$$P_{fBVI} := P_f$$

MARK VI TRAIN, FLEXURE AT SPAN 2, 05L (POSITIVE BENDING)

DESIGN LOAD RATING

LRFR 6.4.3

Strength I Limit State

LRFR 6.5.4.1

$$RF := \frac{\phi_c \cdot \phi_s \cdot \phi \cdot R_n - \gamma_{DC} \cdot DC - \gamma_{DW} \cdot DW}{\gamma_L \cdot (LL + IM)}$$

Load Rating Factors from Above

$$\gamma_{DC} = 1.25 \quad \gamma_{DW} = 1.50$$

$$\gamma_{LL} = 1.10$$

Load effects:

Absolute value for positive bending (Span 2, 0.5L) taken directly from SAP2000 output (Mark VI train):

$$M_{DC} := M_{DCCVI} \quad M_{DC} = 245.1 \text{ kip}\cdot\text{ft}$$

$$M_{DW} := 0 \text{ kip}\cdot\text{ft}$$

$$M_{LL} := M_{LLCVI} \quad M_{LL} = 693.7 \text{ kip}\cdot\text{ft}$$

IM = 15% measured by owner in previous studies

$$M_{LL\_IM} := M_{LL} \cdot (1 + IM) \quad M_{LL\_IM} = 797.8 \text{ kip}\cdot\text{ft}$$

Resistance:

$$M_{nMidspan110} = 4664.9 \text{ kip}\cdot\text{ft}$$

$$RF := \frac{\phi_c \cdot \phi_s \cdot \phi \cdot M_{nMidspan110} - \gamma_{DC} \cdot M_{DC} - \gamma_{DW} \cdot M_{DW}}{\gamma_{LL} \cdot M_{LL\_IM}}$$

$$RF = 4.71$$

$$RF_{CVI} := RF$$

RELIABILITY INDEX,  $\beta$  (MARK IV TRAIN, POSITIVE BENDING AT SPAN 2, 0.5L)

We assume a linear limit state function for bending, Eq. (5.18) from (Nowak and Collins, 2000) of the general form:

$$\beta := \frac{a_0 + \sum_{i=1}^n (a_i \cdot \mu_{X_i})}{\sqrt{\sum_{i=1}^n (a_i \cdot \sigma_{X_i})^2}} \quad \blacksquare$$

for the linear limit state function of the form,

$$g(X_1, X_2, \dots, X_n) = a_0 + a_1 \cdot X_1 + a_2 \cdot X_2 + \dots + a_n \cdot X_n$$

Nominal (design) value of maximum load effects:

Live load effect (including impact factor IM = 15%):

$$M_{LL\_IM} = 797.8 \text{ kip}\cdot\text{ft}$$

$$\text{Bias factor } \lambda_{LL} = 1.00 \quad \text{from above}$$

$$\text{Mean value } \mu_{LL} := \lambda_{LL} \cdot M_{LL\_IM} \quad \mu_{LL} = 797.8 \text{ kip}\cdot\text{ft}$$

$$\sigma_{LL} := \text{COV}_{LL} \cdot \mu_{LL} \quad \sigma_{LL} = 20.1 \text{ kip}\cdot\text{ft} \quad \text{from above}$$

Dead load effect:

$$M_{DC} = 245.1 \text{ kip}\cdot\text{ft}$$

Assume the values for bias and COV for dead load of cast-in-place components (conservative choice) from Table 8.4 (Nowak and Collins, 2000). These values are adapted from LRFD Calibration (Nowak, 1993),

$$\text{Bias factor } \lambda_{DC} := 1.05$$

$$\text{Mean value } \mu_{DC} := \lambda_{DC} \cdot M_{DC} \quad \mu_{DC} = 257.4 \text{ kip}\cdot\text{ft}$$

$$\text{Coefficient of Variation } \text{COV}_{DC} := 0.10 \quad \sigma_{DC} := \text{COV}_{DC} \cdot \mu_{DC} \quad \sigma_{DC} = 25.7 \text{ kip}\cdot\text{ft}$$

Resistance:

$$M_{n\text{Midspan110}} = 4664.9 \text{ kip}\cdot\text{ft}$$

Assume statistical parameters of resistance from Table 2 (Nowak, 1995). Again, these values are associated with the calibration of the LRFD Code,

$$\lambda_R := 1.05 \quad \text{for moment resistance of prestressed-concrete girders}$$

$$\text{Mean value } \mu_R := \lambda_R \cdot M_{n\text{Midspan110}} \quad \mu_R = 4898.2 \text{ kip}\cdot\text{ft}$$

$$\text{Coefficient of Variation } \text{COV}_R := 0.075 \quad \sigma_R := \text{COV}_R \cdot \mu_R \quad \sigma_R = 367.4 \text{ kip}\cdot\text{ft}$$

Calculate the reliability index:

$$g(M_{nMidspan110}, M_{DC}, M_{LL\_IM}) = M_{nMidspan110} - M_{DC} - M_{LL\_IM}$$

$$\beta := \frac{a_0 + \sum_{i=1}^n (a_i \cdot \mu_{X_i})}{\sqrt{\sum_{i=1}^n (a_i \cdot \sigma_{X_i})^2}}$$

for the linear limit state function of the form,

$$g(X_1, X_2, \dots, X_n) = a_0 + a_1 \cdot X_1 + a_2 \cdot X_2 + \dots + a_n \cdot X_n$$

$$\beta := \frac{\mu_R - \mu_{DC} - \mu_{LL}}{\sqrt{\sigma_R^2 + \sigma_{DC}^2 + \sigma_{LL}^2}}$$

$$\beta = 10.42$$

$$\beta_{CVI} := \beta$$

For normally distributed random variables R and Q, it can be shown that the probability of failure is related to the reliability index as follows,  $P_f = \Phi(-\beta)$ . If the random variables are all normally distributed and uncorrelated, then this relationship between  $\beta$  and  $P_f$  is exact. Otherwise, this expression provides only an approximate means of relating the probability of failure to  $\beta$  (Nowak and Collins, 2000).

The values of the CDF  $\Phi(x)$  for the standard normal probability distribution are embedded in Mathcad and recalled by the function cnorm:

$$P_f := \text{cnorm}(-\beta)$$

$$P_f = 0.00 \times 10^0$$

$$P_{fCVI} := P_f$$

## MARK VI TRAIN, SHEAR AT CRITICAL DISTANCE FROM FIRST INTERIOR SUPPORT

The shear rating factors for Design Load Rating are calculated for academic purposes only. In-service concrete bridges that show no visible signs of shear distress need not be checked for shear during design load or legal load ratings [LRFR 6.5.9]

Shear at Critical Shear Section,  $d_v = 57.6\text{in}$

The maximum shear at  $d_v = 57.6\text{in}$  is interpolated from SAP2000 results. Maximum shear is at critical distance, exterior-facing side of first interior support (Mark VI Train).

$$V_{LL} := V_{LLVI} \quad V_{LL} = 65.3\text{kip}$$

IM := 15%      measured by owner in previous studies

$$V_{LL\_IM} := V_{LL} \cdot (1 + IM) \quad V_{LL\_IM} = 75.1\text{kip}$$

$$V_{DC} = 61.4\text{kip}$$

### 1) Simplified Method

$$V_{nSimple} = 203.6\text{kip}$$

$$RF := \frac{\phi_c \cdot \phi_s \cdot \phi_V \cdot V_{nSimple} - \gamma_{DC} \cdot V_{DC} - \gamma_{DW} \cdot V_{DW}}{\gamma_{LL} \cdot V_{LL\_IM}}$$

$$\boxed{RF = 1.29}$$

### 2) MCFT Method

$$V_n = 448.7\text{kip}$$

$$RF := \frac{\phi_c \cdot \phi_s \cdot \phi_V \cdot V_n - \gamma_{DC} \cdot V_{DC} - \gamma_{DW} \cdot V_{DW}}{\gamma_{LL} \cdot V_{LL\_IM}}$$

$$\boxed{RF = 3.96}$$

$$RF_{ShearVI} := RF$$

RELIABILITY INDEX,  $\beta$  (MARK VI TRAIN, SHEAR AT CRIT. DIST. FROM FIRST INT. SUPPORT)

We assume a linear limit state function for bending, Eq. (5.18) from (Nowak and Collins, 2000) of the general form:

$$\beta := \frac{a_0 + \sum_{i=1}^n (a_i \cdot \mu_{X_i})}{\sqrt{\sum_{i=1}^n (a_i \cdot \sigma_{X_i})^2}} \quad \text{for the linear limit state function of the form,}$$

$$g(X_1, X_2, \dots, X_n) = a_0 + a_1 \cdot X_1 + a_2 \cdot X_2 + \dots + a_n \cdot X_n$$

Nominal (design) value of maximum load effects:

Live load effect (including impact factor IM = 15%):

$$V_{LL\_IM} = 75.1 \text{ kip}$$

$$\text{Bias factor } \lambda_{LL} = 1.00 \quad \text{from above}$$

$$\text{Mean value } \mu_{LL} := \lambda_{LL} \cdot V_{LL\_IM} \quad \mu_{LL} = 75.1 \text{ kip}$$

$$\sigma_{LL} := COV_{LL} \cdot \mu_{LL} \quad \sigma_{LL} = 1.9 \text{ kip} \quad \text{from above}$$

Dead load effect:

$$V_{DC} = 61.4 \text{ kip}$$

Assume the values for bias and COV for dead load of cast-in-place components (conservative choice) from Table 8.4 (Nowak and Collins, 2000). These values are adapted from LRFD Calibration (Nowak, 1993),

$$\text{Bias factor } \lambda_{DC} := 1.05$$

$$\text{Mean value } \mu_{DC} := \lambda_{DC} \cdot V_{DC} \quad \mu_{DC} = 64.5 \text{ kip}$$

$$\text{Coefficient of Variation } COV_{DC} := 0.10 \quad \sigma_{DC} := COV_{DC} \cdot \mu_{DC} \quad \sigma_{DC} = 6.4 \text{ kip}$$

Resistance (MCFT Approach):

$$V_n = 448.7 \text{ kip}$$

Assume statistical parameters of resistance from Table 2 (Nowak, 1995). Again, these values are associated with the calibration of the LRFD Code,

$$\lambda_R := 1.165 \quad \text{for shear resistance of prestressed-concrete girders}$$

$$\text{Mean value } \mu_R := \lambda_R \cdot V_n \quad \mu_R = 522.8 \text{ kip}$$

$$\text{Coefficient of Variation } COV_R := 0.16 \quad \sigma_R := COV_R \cdot \mu_R \quad \sigma_R = 83.6 \text{ kip}$$

Calculate the reliability index:

$$g(V_n, V_{DC}, V_{LL\_IM}) = V_n - V_{DC} - V_{LL\_IM}$$

$$\beta := \frac{a_0 + \sum_{i=1}^n (a_i \cdot \mu_{X_i})}{\sqrt{\sum_{i=1}^n (a_i \cdot \sigma_{X_i})^2}}$$

for the linear limit state function of the form,

$$g(X_1, X_2, \dots, X_n) = a_0 + a_1 \cdot X_1 + a_2 \cdot X_2 + \dots + a_n \cdot X_n$$

$$\beta := \frac{\mu_R - \mu_{DC} - \mu_{LL}}{\sqrt{\sigma_R^2 + \sigma_{DC}^2 + \sigma_{LL}^2}}$$

$$\beta = 4.57$$

$$\beta_{\text{ShearVI}} := \beta$$

For normally distributed random variables R and Q, it can be shown that the probability of failure is related to the reliability index as follows,  $P_f = \Phi(-\beta)$ . If the random variables are all normally distributed and uncorrelated, then this relationship between  $\beta$  and  $P_f$  is exact. Otherwise, this expression provides only an approximate means of relating the probability of failure to  $\beta$  (Nowak and Collins, 2000).

The values of the CDF  $\Phi(x)$  for the standard normal probability distribution are embedded in Mathcad and recalled by the function cnorm:

$$P_f := \text{cnorm}(-\beta)$$

$$P_f = 2.48 \times 10^{-6}$$

$$P_{f\text{ShearVI}} := P_f$$

Results :=	(	RF <sub>AIV</sub>	β <sub>AIV</sub>	P <sub>fAIV</sub>	)	=	(	1.53 × 10 <sup>0</sup>	4.23 × 10 <sup>0</sup>	1.16 × 10 <sup>-5</sup>	)
		RF <sub>BIV</sub>	β <sub>BIV</sub>	P <sub>fBIV</sub>				4.85 × 10 <sup>0</sup>	9.68 × 10 <sup>0</sup>	0 × 10 <sup>0</sup>	
		RF <sub>CIV</sub>	β <sub>CIV</sub>	P <sub>fCIV</sub>				6.41 × 10 <sup>0</sup>	1.1 × 10 <sup>1</sup>	0 × 10 <sup>0</sup>	
		RF <sub>ShearIV</sub>	β <sub>ShearIV</sub>	P <sub>fShearIV</sub>				5.56 × 10 <sup>0</sup>	4.83 × 10 <sup>0</sup>	6.99 × 10 <sup>-7</sup>	
		RF <sub>AVI</sub>	β <sub>AVI</sub>	P <sub>fAVI</sub>				1.02 × 10 <sup>0</sup>	2.56 × 10 <sup>0</sup>	5.23 × 10 <sup>-3</sup>	
		RF <sub>BVI</sub>	β <sub>BVI</sub>	P <sub>fBVI</sub>				3.57 × 10 <sup>0</sup>	9 × 10 <sup>0</sup>	0 × 10 <sup>0</sup>	
		RF <sub>CVI</sub>	β <sub>CVI</sub>	P <sub>fCVI</sub>				4.71 × 10 <sup>0</sup>	1.04 × 10 <sup>1</sup>	0 × 10 <sup>0</sup>	
		RF <sub>ShearVI</sub>	β <sub>ShearVI</sub>	P <sub>fShearVI</sub>				3.96 × 10 <sup>0</sup>	4.57 × 10 <sup>0</sup>	2.48 × 10 <sup>-6</sup>	



Capture results for use in Excel.

Results

## **APPENDIX G: BOX GIRDER BENCHMARK STUDY**

## **Concrete Box-Girder Bridge Analysis with SAP2000 v. 9.0.8**

### ***Introduction and Problem Statement***

Analyze the concrete box-girder bridge described in example 7.10.5 from *Design of Highway Bridges* (Barker, 1997) using SAP2000 v.9 and the bridge design module. Compare results with those given in the textbook which were determined by conventional hand analysis methods. References are made to [in brackets] to relevant sections of the *AASHTO LRFD Bridge Specifications, 1<sup>st</sup> Edition* (1994).

The post-tensioned box-girder bridge has 30m-36m-30m spans and is designed for the HL-93 live load. The roadway width is 13420 mm curb to curb. Allow for a future wearing surface of 75-mm thick bituminous overlay. The textbook analysis uses the empirical method for deck slabs [A9.7.2] to design the top flange of the box girder. Additional parameters are as follows:

$$f_c = 35 \text{ MPa}$$

$$f_y = 400 \text{ MPa}$$

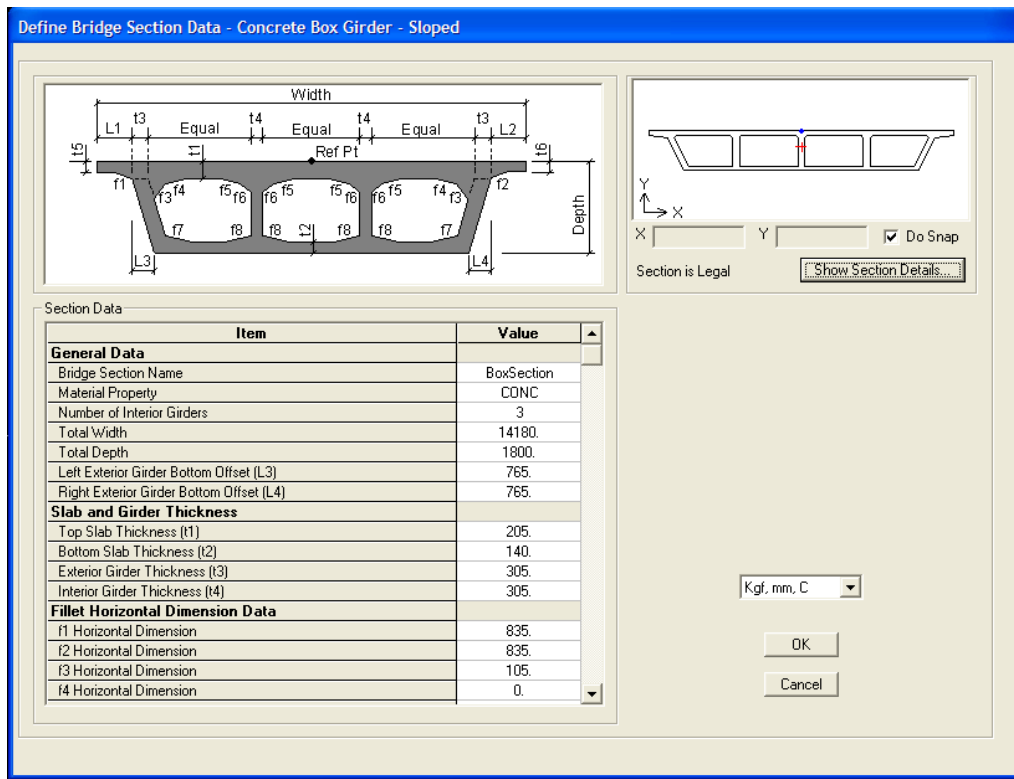
1860 MPa, low-relaxation 12.70 mm, 7-wire strands

## Analytical Methods

The problem is solved using SAP2000 v.9 from Computers and Structures, Inc. (Berkeley, CA), with the bridge design module used to develop the model. The bridge design module facilitates rapid model development through parametric definition of deck sections, layout lines, abutments, bents, and moving load cases. The user-defined properties are assigned to a *bridge object*. The bridge design module links the parametric bridge properties to the structural model and develops the bridge object as finite elements, joints, constraints, and restraints.

The superstructure may be developed as frame, shell, or solid elements. The user controls mesh parameters for the bridge objects. These parameters may be changed. The bridge design module updates the linked model.

The following figure shows the dialog box for parametric definition of the deck section. The concrete box-girder cross-sectional dimensions are quickly copied from the textbook problem to the software.



## Textbook Analysis Model

After defining the deck section, the abutments (end supports) and bents (interior supports) are defined. The textbook assumes a two-dimensional beam analysis with three roller supports and one pin support for the 30m-36m-30m continuous spans. Consequently, the support conditions are statically determinate. The textbook analysis treats the multi-cell box girder as a series of I-shaped interior and exterior cross-sections. This is the AASHTO approach for hand calculations, using empirical distribution factors to distribute the gross moments and shears to the fictitious component I-shaped girders.

## Finite Element Model

The statically determinate support conditions are assumed for the FEM. One support must be a pin to prevent axial translation. It seems arbitrary which support to make a pin. The textbook approach is followed for this benchmark study by making the first interior support a pin. The two abutments are defined as three-dimensional rollers (vertical and transverse translation is fixed, axial translation is free). Rotation about the longitudinal bridge axis is restrained. There is no restraint for the in-plane rotations (major- and minor-axis bending). The second interior support (column bent) is defined with the same restraints. The following figure shows the dialog box for abutment definition. Note the abutment supports are defined at each girder (each box-girder web).

Bridge Abutment Data

Units: KN, m, C

Bridge Abutment Name: ABUT2

Bridge Abutment Is Defined By:

- Link/Support Property
- User Definition

User Abutment

DOF/Direction	Release Type	Stiffness
Translation Parallel To Abutment (U1)	Fixed	
Translation Normal To Abutment (U2)	Free	
Translation Vertical (U3)	Fixed	
Rotation About Abutment (R1)	Free	
Rotation About Line Normal To Abutment (R2)	Fixed	
Rotation About Vertical Line (R3)	Free	

Horizontal Location of Abutment Supports:

- At Reference Line Location
- At Each Girder Location
- Equally Spaced Over Bridge Width

Number of Supports: \_\_\_\_\_

Vertical Diaphragm:

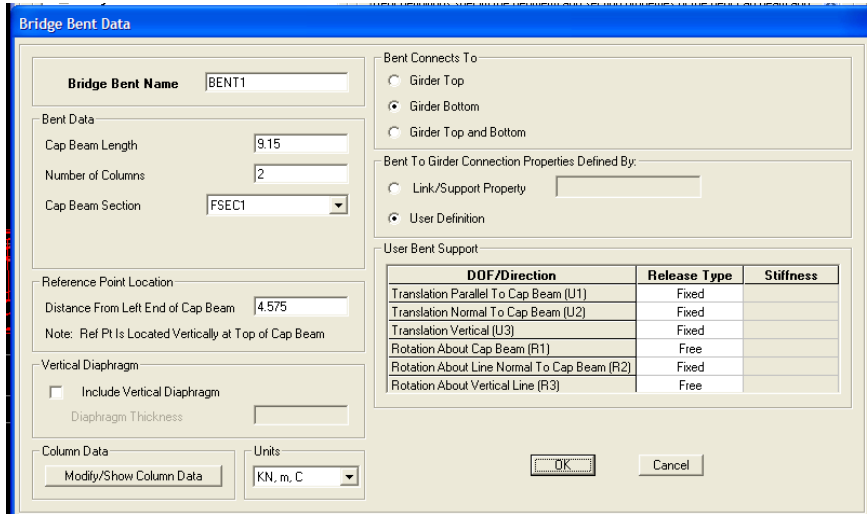
- Include Vertical Diaphragm

Diaphragm Thickness: \_\_\_\_\_

OK Cancel

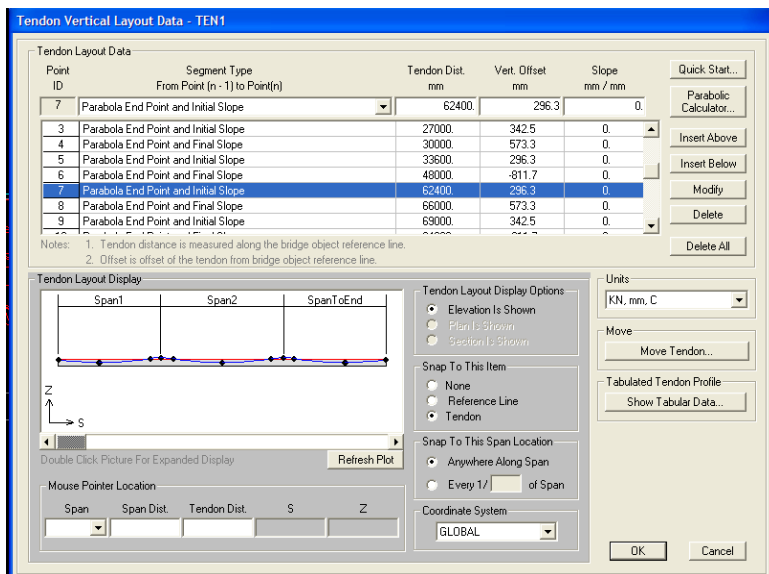
The first interior support is defined as above with the addition of a restraint for longitudinal translation (pin support). In other words, all three translational DOFs are fixed. The two in-plane bending DOFs are released. Torsional rotation is restrained.

The definition for the first interior bent is shown in the following figure. The secondary data for the bent beam and column is left with default values. We are not concerned with the structural behavior of the bent for this problem. We only want it to be strong enough to support the superstructure without significant deformation. If deformation affects results, the bent frame section may be increased.



### Post-tensioning Tendons

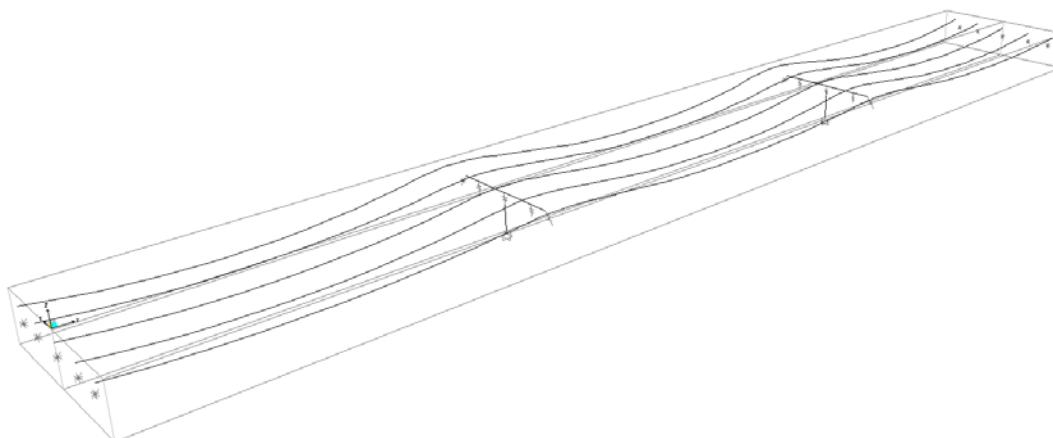
Post-tensioning is defined next. The tendon profile as given in the example problem is applied to the FEM. The tendon layout is easily copied into the software, which calculates the parabolic geometry from the textbook inputs.



The prestress loss parameters on the previous page are quickly copied into the SAP2000 bridge design module data form (below). The textbook problem calculates all long-term losses in one lump sum. We arbitrarily assign this loss as elastic shortening stress with the other three parameters set at zero. SAP2000 adds the losses algebraically so it makes no difference how we split up the losses among the categories of elastic shortening, creep, shrinkage, and steel relaxation stress loss.

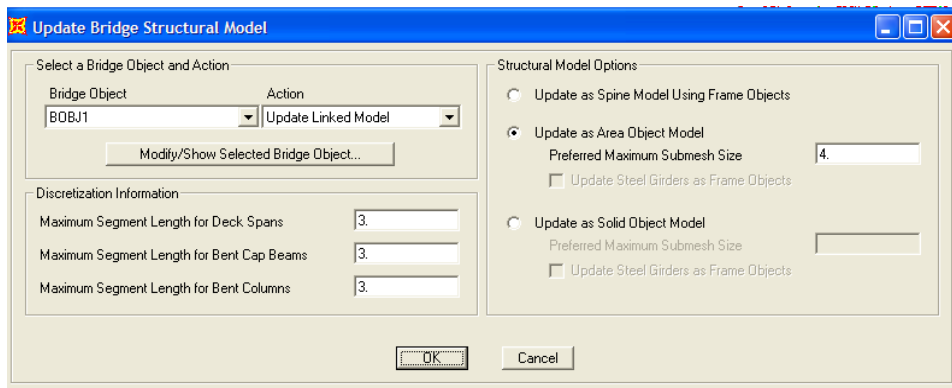
Basic tendon data is added to the Tendon Data dialog box. This information includes jacking fore, whether the tendon is jacked from one or both ends, tendon area, and load case to assign loads. Tendons are modeled as loads to account for loss parameters defined above. If tendons were defined as elements, we would have to conduct a *staged construction analysis* to see time-dependent loss effects. This is unduly complicated. Also, UCF does not own this module.

Prestress tendons are shown graphically in the following figure.

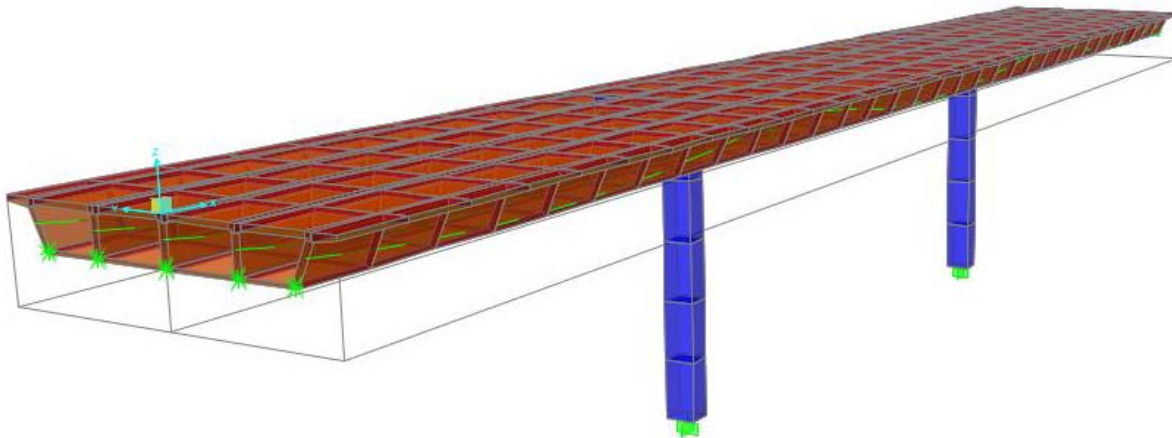


## Model Updating and Meshing

After all the model parameters are defined in the bridge design module, we are given the option to mesh with frame, shell, or solid elements. There are meshing options for superstructure and substructure, as well as submeshing options. A submesh is a further mesh of objects into elements during analysis. Note that a 3m mesh is chosen. This breaks up our 30 m spans into tenth points, a reasonable level of refinement for bridge analysis (Barker, 1997).



The model is shown graphically in the following figure.



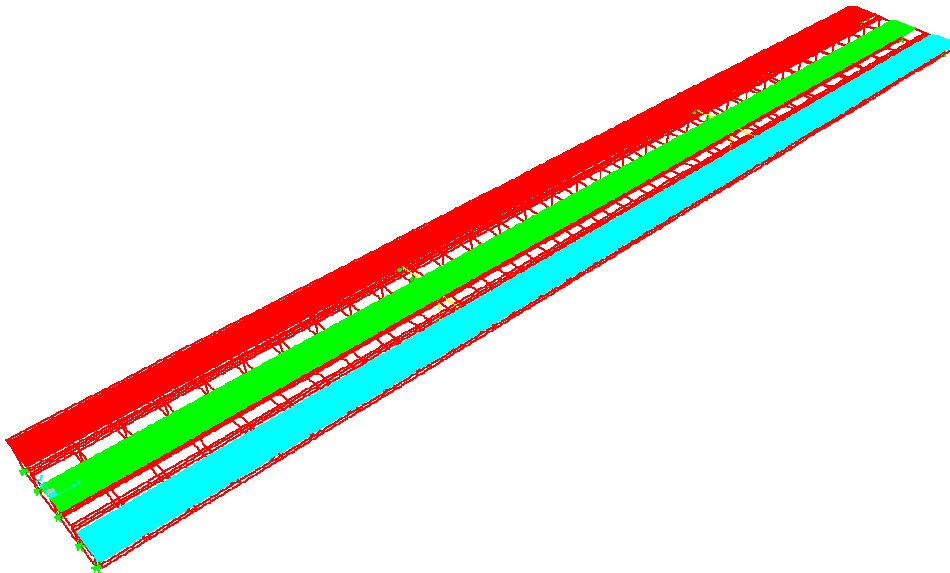
### ***Moving Load Analysis Case***

SAP2000 automates the moving load analysis, breaking it down into the following basic steps:

1. Define lanes.
2. Define vehicles.
3. Define vehicle classes.
4. Define the moving load case.
5. Define bridge responses.

### **Lane Definition**

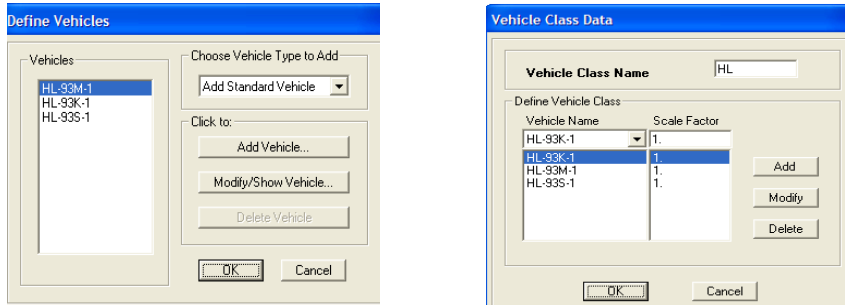
The AASHTO traffic lane is 3600 mm. Dividing the clear roadway width by 3600 mm and taking the next smallest integer [A3.6.1.1.1], we get 3 possible traffic lanes. The AASHTO design lane is 3000 mm with the vehicle placed within that lane for extreme effect. The three design lanes are positioned at the centerline and extreme transverse positions, respectively.



The writer recognizes that this is one of many possible lane placements. Other obvious lane placements for critical effect would be all at the center, or all to one side of the bridge deck. An exhaustive analysis would consider all possible lane placements for maximum effect. This is beyond the scope of this assignment, and the writers chose the placement above as one likely possibility for actual lane placement.

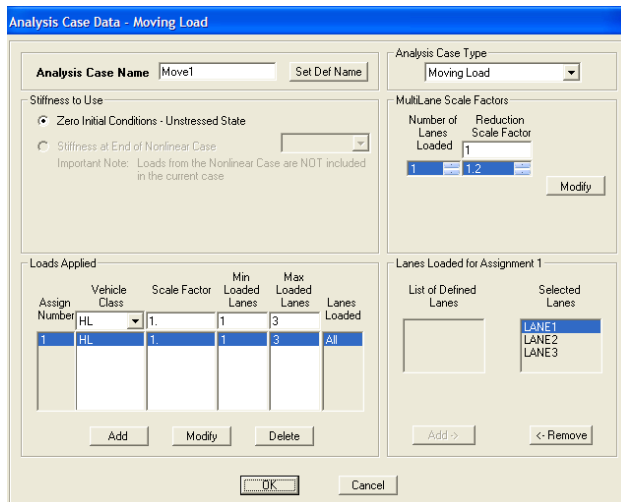
## Vehicle and Vehicle Class Definition

SAP2000 has the required vehicles pre-defined. We simply add the vehicles, which represent AASHTO loading including concentrated truck and tandem loads, as well as uniform lane loads. The vehicles are added to a vehicle class to be applied to the moving load analysis.



## Moving Load Case and Bridge Responses

The moving load analysis case is defined. This brings together vehicles and lanes, and considers multiple presence factors.



We also specify for the software to calculate joint displacement, shell resultant and stresses, and section cut response. It is recommended to specify as few responses as possible, as response calculation increases analysis run-time exponentially.

Additional load cases are defined for the barrier, which is assigned as vertical load assigned at the joints, based on the self-weight, and the bituminous overlay, which is applied as a uniform pressure over the bridge deck.

## ***Load Combinations and Load Factors***

The following limit states are considered:

Strength I  
 Service I  
 Service III  
 Fatigue

From Table 3.1 [AASHTO Table 3.4.1-1]

Live load plus the allowance for dynamic loading,

$$U_{LI} := U_L \cdot \left( 1 + \frac{IM}{100} \right) \quad \begin{array}{l} IM := 33 \\ IM := 15 \end{array} \quad \begin{array}{l} \text{Impact} \\ \text{Fatigue} \end{array}$$

Note that 33% increase for dynamic effects is built into vehicle definition.

Strength I

$$U := 0.95 [1.25DC + 1.50DW + 1.75(LL + IM)]$$

$\eta := 0.95$       strength

$$U := 1.1875DC + 1.425DW + 1.6625(LL + IM)$$

$\eta := 1.0$       service, fatigue

Service I

$$U := 1.0 [DC + DW + (LL + IM)]$$

Service III

$$U := 1.0 [DC + DW + 0.8(LL + IM)]$$

## ***Prestress Parameters***

Prestressing parameters are provided in the textbook example,

Jacking at both ends.

Uncoated seven-wire low-relaxation strands (Grade 270) 1860 MPa

Rigid galvanized ducts

$$P_{\text{jacking}} := 6000\text{kN}$$

Prestress losses,

$$\text{Anchorage} := 186\text{MPa}$$

$$E := 197000\text{MPa} \quad L := 100\text{m} \quad (\text{approx.})$$

$$f_{\text{pu}} := 1860\text{MPa} \quad \sigma := 0.1 \cdot f_{\text{pu}}$$

$$f_{\text{py}} := 0.9f_{\text{pu}} \quad f_{\text{py}} = 1674\text{MPa}$$

$$\Delta L := \frac{L \cdot \sigma}{E} \quad \Delta L = 94.416\text{mm}$$

$$K := 6.6 \cdot 10^{-7} \text{mm}^{-1}$$

$$\mu := 0.2$$

Long-term losses (lump sum approach) from Barker page 672,

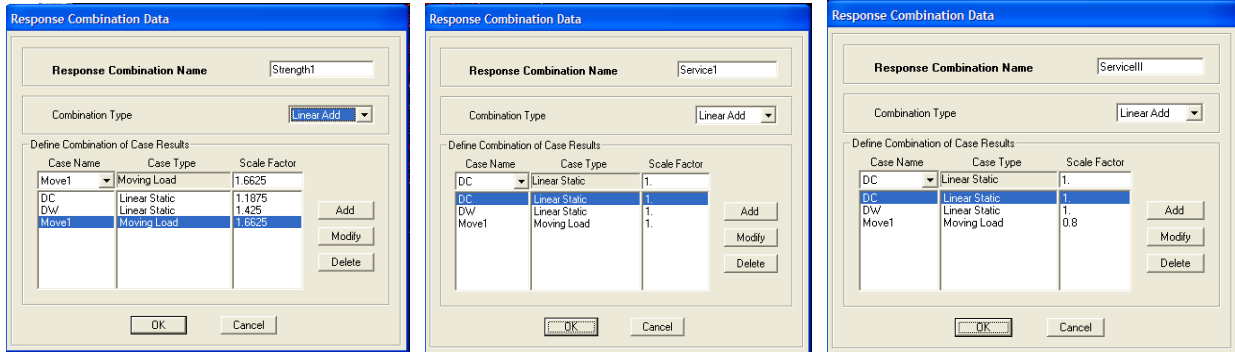
$$\text{Losses} := 0.8f_{\text{py}} - 0.74f_{\text{pu}}$$

From Barker, page 679,

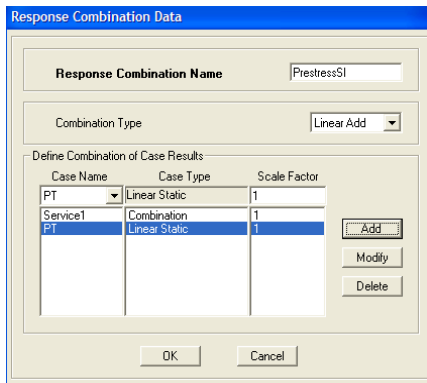
$$P_{\text{jacking}} := 6000\text{kN}$$

$$A_{\text{ps}} := 4032.3\text{mm}^2 \quad \text{per web}$$

Analysis combinations are specified corresponding to the AASHTO combinations shown on the previous page.



An additional combination is defined to consider the prestress force in combination with Service I. Although not explicitly defined as an AASHTO load combination, this combination is required to check stress limits with prestress.



## ***Results***

SAP2000 gives extensive results for all elements and joints including stresses, forces, displacements, and rotation. A challenge in this problem is finding quantities generated from SAP that are useful for comparison to textbook values.

The writer decided to compare bending stress from SAP2000 to the equivalent stress from moments in Table E7.5-1 (Barker, 1997). Additionally, top and bottom fiber stresses are compared with prestress force, given by Barker (1997), pp. 677 to 679. The moments in Table E7.5-1 are converted to bending stress using the section modulus.

All results are for an “interior girder”, as defined in Barker. Stresses are S11 stress (longitudinal stress) from SAP2000, taken at the centerline of the bridge, at locations 104, 200, and 205. Stresses at two joints from two adjacent shells are recorded at these locations. The average value is taken as the stress at that location. The raw data copied from SAP2000 is immediately below the averaged results. This information is found in the chart on the following page.

<b>RESULTS</b>							
Location	104						
	Moment (kN m)	Text	SAP2000	% Change	Text	SAP2000	% Change
Load Combination	M <sub>104</sub>	f <sub>t</sub> (Mpa)	f <sub>t</sub> (Mpa)		f <sub>b</sub> (Mpa)	f <sub>b</sub> (Mpa)	
Strength I (internal webs)	7252	8.72	5.77	-34%	10.54	6.10	-42%
Service I (internal webs)	5097	6.13	4.16	-32%	7.41	4.45	-40%
Service III (internal webs)	4624	5.56	3.81	-31%	6.72	4.11	-39%
Prestress + SI (internal webs)		-5.58	-3.65	-35%	0.00	-2.31	

**SAP2000  
OUTPUTS**

	Shell	Joint	Min	Max	Joint	Shell
Values from Tables						
StrengthI	636	1	-6887.39	6082.73	20	650
	636	121	-4640.19	6167.35	18	650
	669	121	-4885.93	6132.84	18	683
	669	1	-6673.33	6014.11	20	683
ServiceI	636	1	-4918.14	4445.1	20	650
	636	121	-3373.28	4510.75	18	650
	669	121	-3554.71	4468.33	18	683
	669	1	-4802.32	4378.07	20	683
ServiceIII	636	1	-4477.25	4106.49	20	650
	636	121	-3106.16	4169.34	18	650
	669	121	-3274.84	4120.24	18	683
	669	1	-4393.66	4034.85	20	683
PTService	636	1	-4576.25	-2319.06	20	650
	636	121	-2779.01	-2270.73	18	650
	669	121	-2813.58	-2285.32	18	683
	669	1	-4414.87	-2361.42	20	683

Effective Interior Section Properties

I (mm <sup>4</sup> )	6.89E+11
ct (mm)	828.3
cb (mm)	1001.7
St (mm <sup>3</sup> )	8.32E+08
Sb (mm <sup>3</sup> )	6.88E+08

<b>RESULTS</b>							
Location	200						
	Moment (kN m)	Text	SAP2000	% Change	Text	SAP2000	% Change
Load Combination	M <sub>200</sub>	f <sub>t</sub> (Mpa)	f <sub>t</sub> (Mpa)		f <sub>b</sub> (Mpa)	f <sub>b</sub> (Mpa)	
Strength I (internal webs)	-9728	-11.69	7.55	-35%	-14.14	6.14	-57%
Service I (internal webs)	-7107	-8.54	5.47	-36%	-10.33	4.64	-55%
Service III (internal webs)	-6620	-7.96	5.35	-33%	-9.62	4.37	-55%
Prestress + SI (internal webs)		0.00	-1.06		-7.89	-3.84	-51%

### SAP2000 OUTPUTS

	Shell	Joint	Max	Min	Joint	Shell
Values from Tables						
StrengthI	834	290	8055.5	-5740.02	304	848
	834	289	6968.3	-5944.97	303	848
	867	289	7009.65	-6530.93	303	881
	867	290	8170.28	-6329.41	304	881
	867	290	6061.56	-4383.35	304	848
ServiceI	834	289	5267.52	-4538.58	303	848
	867	289	5280.67	-4889.38	303	881
	867	290	5280.67	-4737.43	304	881
	867	290	5700.55	-4158.17	304	848
ServiceIII	834	289	4967.26	-4304.72	303	848
	867	289	4969.57	-4584.21	303	881
	867	290	5742.76	-4441.12	304	881
	867	290	-1395.69	-4518.39	304	848
PTService	834	289	-72.72	-4600.31	303	848
	867	289	-970.92	-3151.93	303	881
	867	290	-1811.95	-3070.77	304	881

### Effective Interior Section Properties

I (mm <sup>4</sup> )	6.89E+11
ct (mm)	828.3
cb (mm)	1001.7
St (mm <sup>3</sup> )	8.32E+08
Sb (mm <sup>3</sup> )	6.88E+08

<b>RESULTS</b>							
Location	205						
	Moment (kN m)	Text	SAP2000	% Change	Text	SAP2000	% Change
Load Combination	M <sub>205</sub>	f <sub>t</sub> (Mpa)	f <sub>t</sub> (Mpa)		f <sub>b</sub> (Mpa)	f <sub>b</sub> (Mpa)	
Strength I (internal webs)	6409	7.70	5.45	-29%	9.32	5.04	-46%
Service I (internal webs)	4455	5.36	3.88	-28%	6.48	3.71	-43%
Service III (internal webs)	4011	4.82	3.52	-27%	5.83	3.44	-41%
Prestress + SI (internal webs)		-6.25	-4.54	-27%	0.00	-0.89	

### SAP2000 OUTPUTS

	Shell	Joint	Min	Max	Joint	Shell
Values from Tables						
StrengthI	1032	458	-6379.69	4993.23	472	1046
	1032	457	-4534.08	5100.82	471	1046
	1065	457	-4532.95	5096.2	471	1079
	1065	458	-6369.58	4988.72	472	1079
ServiceI	1032	458	-4511.54	3673.29	472	1046
	1032	457	3247.67	3755.45	471	1046
	1065	457	-3246.71	3751.56	471	1079
	1065	458	-4503.03	3669.49	472	1079
ServiceIII	1032	458	-4081.13	3407.52	472	1046
	1032	457	-2962.41	3485.46	471	1046
	1065	457	-2961.46	3481.57	471	1079
	1065	458	-4072.61	3403.73	472	1079
PTService	1032	458	-5470	-958.08	472	1046
	1032	457	-3604.94	-890.79	471	1046
	1065	457	-3607.67	-822.87	471	1079
	1065	458	-5463.65	-883.86	472	1079

C Top      Ten Bot

#### Effective Interior Section Properties

I (mm <sup>4</sup> )	6.89E+11
ct (mm)	828.3
cb (mm)	1001.7
St (mm <sup>3</sup> )	8.32E+08
Sb (mm <sup>3</sup> )	6.88E+08

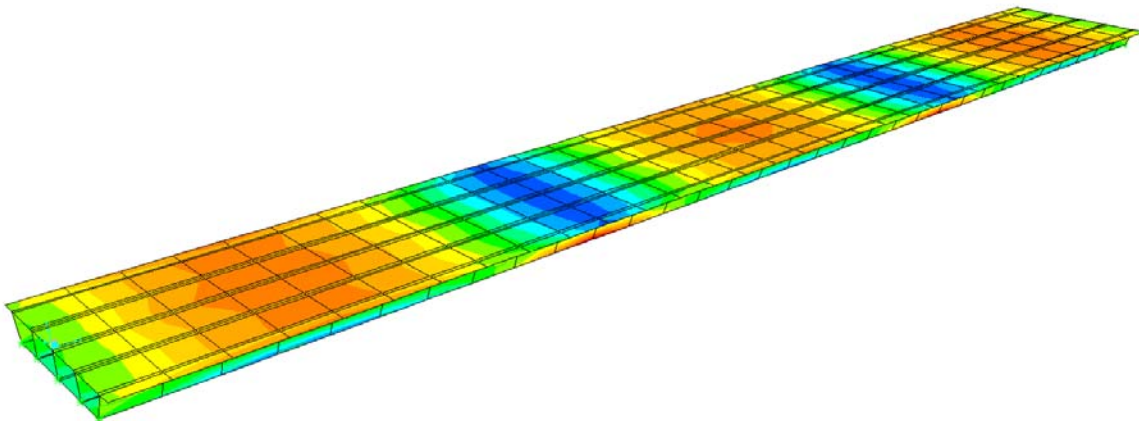
## *Discussion*

The stresses found in SAP2000 are consistently lower than those computed in the textbook analysis. The SAP2000 results are 30% to 50% less than the textbook results. The top stresses are typically 25-35% reduced, whereas the bottom stresses are approximately 40-55% reduced. Note that for the prestress case negative stress indicates compression. Zero stress implies zero tension. SAP2000 always gives compression results in the prestress case.

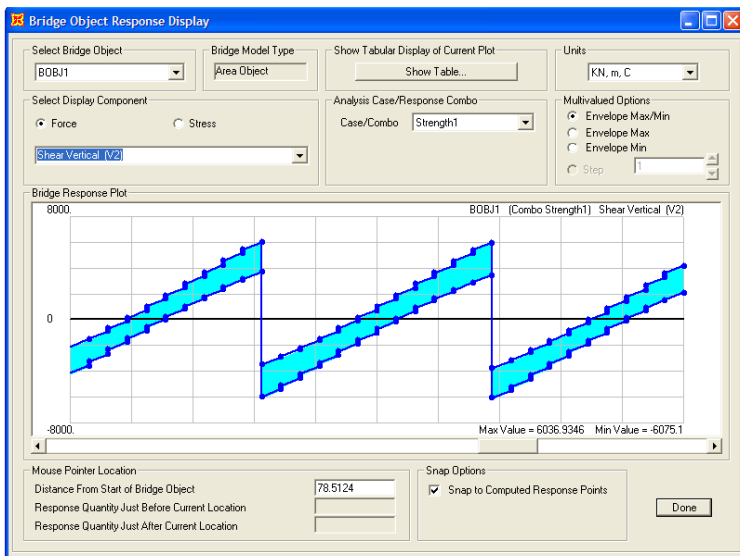
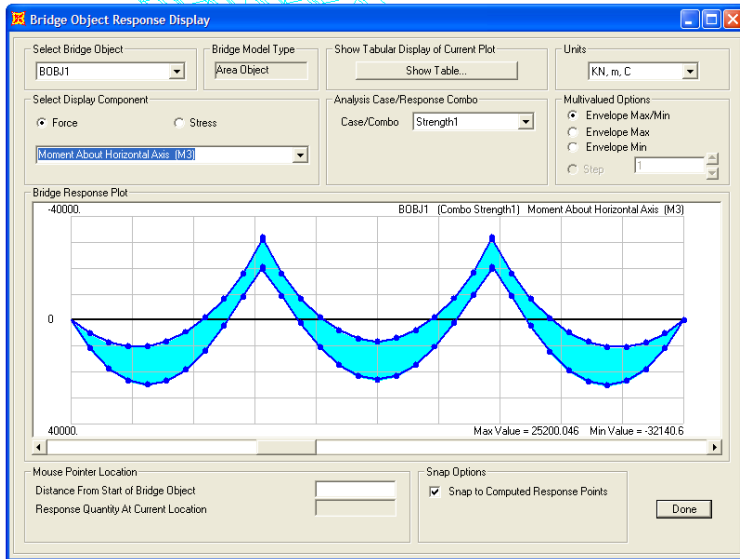
There may be a number of factors leading to the reduced stress magnitudes. One apparent reason is the more exact nature of the analysis and the ability to share load between girders. Because the AASHTO distribution factors are widely applicable, they are imprecise and conservative.

A second reason for reduced stress output in SAP2000 may be lane placement. If the problem were to be solved again, the writer would consider placing all lanes side-by-side in the center for maximum effect. By placing the outside lanes at the deck edges, the maximum effect at the center is reduced. A third reason for reduced stresses in SAP2000 may be that stresses are computed at the centroid of the shell elements, whereas maximum bending stress actually occurs at the extreme fibers.

Despite the reduced magnitude of stress values reported from SAP2000, the trends observed are correct. The following longitudinal stress plot indicates tension in top fibers over supports and compression in top fibers at midspan. This follows the basic concepts of negative and positive bending in continuous beams.



Additionally, SAP2000 can calculate resultant bridge force diagrams by integrating forces at sections along the length of the bridge object. The following figures show the resultant bridge force envelopes for the Strength I limit state, for strong-axis bending and shear.



The diagrams show expected trends for moment and shear. There is no straightforward way to compare these results with the textbook approach, because of the empirical factors and methods applied to analyze the multi-cell box girder as if it were a number of I-shaped component girders. The bridge force/stress resultant approach may be used for the beamway, and will be directly comparable to hand calculations because of the single-cell nature of the beamway box girders.

## *Conclusions*

In general, the stress magnitudes found in SAP2000 were less than those calculated in the textbook analysis. This result is to be expected, as the textbook load distribution approach is broadly applicable, inexact, and conservative. The writer assumed textbook stresses are overestimated and this assumption was confirmed.

The stresses are consistently reduced by 30-50% in SAP2000. The fact that this trend is consistent, and that all results are “in the ballpark” (reasonable order of magnitude) is satisfying to the writer. The stress reduction in SAP2000 may have been exaggerated for reasons explained above. Caution should be used in applying these results as they may be nonconservative. It is not clear why the difference in SAP2000 and textbook values is greater in the bottom flanges than the top flanges.

It is recommended that further analyses consider the error sources theorized above. Lane placement is of immediate concern. An exhaustive analysis would require many different lane configurations.

## LIST OF REFERENCES

- AASHTO. (2003). *Manual for Condition Evaluation and Load and Resistance Factor Rating (LRF) of Highway Bridges*, American Association of State Highway and Transportation Officials, Washington, D.C.
- AASHTO. (2004). *AASHTO LRFD Bridge Design Specifications*, American Association of State Highway and Transportation Officials, Washington, D.C.
- Akgul, F., and Frangopol, D. M. (2003). "Rating and Reliability of Existing Bridges in a Network." *Journal of Bridge Engineering*, 8(6), 383-393.
- Aktan, A. E., Catbas, F. N., Grimmelsman, K. A., and Tsikos, C. J. (2000). "Health Monitoring of Large Infrastructure Systems for Management." *Journal of Engineering Mechanics*, 126(7).
- Aktan, E., Catbas, N., Turer, A., and Zhang, Z. (1998). "Structural Identification: Analytical Aspects." *Journal of Structural Engineering*, 817-829.
- American Concrete Institute. (1992). *Analysis and Design of Reinforced and Prestressed-Concrete Guideway Structures (ACI 358.1R-92)*, American Concrete Institute, Farmington Hills, MI.
- American Concrete Institute. (2002). *Building Code Requirements for Structural Concrete (ACI 318-02)*, American Concrete Institute, Farmington Hills, MI.
- Arafa, M., and Mehlhorn, G. (1998). "Nonlinear Finite Element Analysis of Concrete Structures with a Special Model." *Computational Modeling of Concrete Structures*, Balkema, Rotterdam, 777-786.
- Banchik, C. A., and Jasper, H. (2003). "Riding High in Las Vegas." *Civil Engineering*, 73(3), 68.
- Barker, R. M., and Puckett, J. A. (1997). *Design of Highway Bridges*, John Wiley & Sons Inc., New York.
- Beatty, T. L. (2002). "Life-Cycle Cost Analysis Primer." U.S. Department of Transportation: Federal Highway Administration.
- Berman, A. (1998). "Validity of Improved Mathematical Models: A Commentary." *16th International Modal Analysis Conference*, Union College, Schenectady, N.Y., 681-691.

- Cai, C. S., and Shahawy, M. (2003). "Understanding Capacity Rating of Bridges from Load Tests." *ASCE Practice Periodical on Structural Design and Construction*, 8:4, 209-216.
- Catbas, F. N., and Aktan, A. E. (2002). "Condition and Damage Assessment: Issues and some promising indicies." *Journal of Structural Engineering*, 128(8), 1026-1036.
- Catbas, F. N., Brown, D. L., and Aktan, A. E. (2004a). "Parameter Estimation for Multiple-Input Multiple-Output Modal Analysis of Large Structures." *Journal of Engineering Mechanics*, 130(8), 921-930.
- Catbas, F. N., Shah, M., Burkett, J., and Basharat, A. (2004b). "Challenges in Structural Health Monitoring." *Fourth International Workshop on Structural Control*, New York, NY.
- Computers and Structures Inc. (2004). *CSI Analysis Reference Manual for SAP2000, ETABS, and SAFE*, Computers and Structures, Inc., Berkeley, USA.
- Cook, R. D., Malkus, D. S., Plesha, M. E., and Witt, R. J. (2002). *Concepts and Applications of Finite Element Analysis*, John Wiley & Sons Inc., Hoboken, NJ.
- Dolan, C. W. (2004). "Phone Interview." Laramie, Wyoming.
- El-Mezaini, N., and Citipitioglu, E. (1991). "Finite Element Analysis of Prestressed and Reinforced Concrete Structures." *Journal of Structural Engineering*, 117(10), 2851-2864.
- Farrar, C. R., and James, G. H., III. (1997). "System Identification from Ambient Vibration Measurements of a Bridge." *Journal of Sound and Vibration*, 205(1), 1-18.
- Federal Highway Administration. (2004). "National Bridge Inventory." United States Department of Transportation, Washington, D.C.
- Friswell, M. I., and Mottershead, J. E. (1995). *Finite Element Model Updating in Structural Dynamics*, Kluwer Academic, Boston, MA.
- Gendron, G. (1997). "A Review of Four PC Packages for FE Structural Analysis." *Finite Elements in Analysis and Design*(28), 105-114.
- Hjelmstad, K. D., and Banan, M. R. (1995). "On Building Finite Element Models of Structures from Modal Response." *Earthquake Engineering and Structural Dynamics*, 24(1), 53-67.
- Kompfner, T. (2004). "Phone Interview." San Diego, California.

- Mast, R. F., and Dolan, C. W. (1972). "Walt Disney World Monorail Designed for Smooth Riding." *Civil Engineering Magazine*, 48-51.
- Mathsoft Engineering and Education Inc. (2004). "Mathcad." Cambridge, MA.
- Nawy, E. G. (2003). *Prestressed Concrete: A Fundamental Approach*, Pearson Education, Upper Saddle River, New Jersey.
- Ngo, D., and Scordelis, A. C. (1967). "Finite Element Analysis of Reinforced Concrete Beams." *ACI Journal*, 64(3), 152-163.
- Nilson, A. H., Darwin, D., and Dolan, C. W. (2004). *Design of Concrete Structures*, McGraw-Hill Higher Education, New York.
- Nowak, A. S. (1995). "Calibration of LRFD Bridge Code." *Journal of Structural Engineering*, 121(8), 1245-1251.
- Nowak, A. S., and Collins, K. R. (2000). *Reliability of Structures*, McGraw-Hill Higher Education, New York.
- Pothisiri, T., and Hjelmstad, K. D. (2003). "Structural Damage Detection and Assessment from Modal Response." *Journal of Engineering Mechanics*, 129(2), 135-145.
- Scordelis, A. C. (1984). "Computer Models for Nonlinear Analysis of Reinforced and Prestressed Concrete Structures." *PCI Journal*, November-December, 1984, 116-135.
- Wang, X., Kangas, S., Padur, D., Liu, L., Swanson, J. A., Helmicki, A. J., and Hunt, V. J. (2005). "Overview of a Modal-Based Condition Assessment Procedure." *Journal of Bridge Engineering*, 10(4), 460-467.
- Xu, Y. L., Ko, J. M., and Zhang, W. S. (1997). "Vibration Studies of Tsing Ma Suspension Bridge." *Journal of Bridge Engineering*, 149-156.
- Zhang, Q. W., Chang, T. Y. P., and Chang, C. C. (2001). "Finite-Element Model Updating for the Kap Shui Mun Cable-Stayed Bridge." *Journal of Bridge Engineering*, 6(4), 285-293.